# SEISMIC RETROFITTING OF RC BEAM – COLUMN JOINTS USING COMPOSITE MATERIALS

by

Osman Kaya

B.S. in Civil Engineering, Pamukkale University, 1998

M.Sc. in Civil Engineering, Boğaziçi University, 2003

Submitted to the Institute for Graduate Studies in

Science and Engineering in partial fulfillment of

the requirements for the degree of

Doctor of Philosophy

Graduate Program in Civil Engineering

Boğaziçi University

2010

*to my truelove and wonderful wife Serap,*
*and my little son Emir Efe*

# SPECIAL ACKNOWLEDGEMENTS

The author wishes to express his gratitude to Associate Professor Azadeh Parvin of The University of Toledo for her invaluable co-advising role, motivation and assistance especially providing innovative ideas in the developing of CFRP wrapping techniques during the experimental phases of this thesis.

This thesis work, entitled "*Seismic Retrofitting of RC Beam – Column Joints Using Composite Materials*" was accomplished by a collaborative program of NSF (OISE-0352947) and TUBITAK (İCTAG I 597 NSF 103I026) and co-directed by Dr. Azadeh Parvin and Dr. Cem Yalçın.

# ACKNOWLEDGEMENTS

I would like to express my sincere thanks to my thesis supervisors, Assoc. Prof. Dr. Cem Yalçın and Assoc. Prof. Dr. Azadeh Parvin for their invaluable guidance, continuous support, and helpful suggestions in the preparation of this thesis.

My sincere gratitude is also due to the members of my advisory committee Prof. Dr. Cengiz Karakoç, Assist. Prof. Dr. Kutay Orakçal, Assoc. Prof. Dr. Şevket Özden, Assist. Prof. Dr. Ercan Yüksel, and for their useful suggestions and comments.

Special thanks are due to my friend Selçuk Altay for his continuous support during every phase of this study. I would also like to thank to Dr. Onur Ertaş for his endless help and encouragement and my friends, Erdal, İbrahim, Savaş, Umut, Uğur, Hasan, Tevfik and Denizhan for their help.

I owe special thanks to the technicians of Structures Laboratory, Hasan Şenel and Hamdi Ayar, for their help especially in the experimental phase of this research. Also, Ümit Melep and Mesut Kardaş, the technicians of the Materials Laboratory, are acknowledged.

My special gratitude goes to my lovely wife, Serap, for her patience, suggestions, continuous encouragement and support for every stage of this thesis, and my son, Emir, for making each day more enjoyable.

This research has been financially supported by the U.S. National Science Foundation (NSF) through grant OISE-0352947; the Scientific and Technological Research Council of Turkey (TUBITAK) through grant ICTAG-I597-NSF (103I026) and Boğaziçi University Scientific Research Project, under Grant No. 05A401. I would also like to acknowledge the BASF-YKS, the Chemical Company, for providing support in material supply.

Last, but not least, I would like to dedicate this thesis to my family. My special thanks, of course, go to my father, brothers and sister. They have always supported and encouraged me to do my best in all matters of life.

# ABSTRACT

## SEISMIC RETROFITTING OF RC BEAM – COLUMN JOINTS USING COMPOSITE MATERIALS

Many of the existing reinforced concrete structures built prior to 1999 have deficient design details due to their non-seismic design or construction flaws. These structures are at risk of collapse under severe earthquakes. Especially, the beam-column joints would experience high shear forces during such events due to transverse reinforcements and lap splice inadequate design details resulting in damage or failure of structures. To enhance the seismic performance of such joint systems with insufficient reinforcement details, several strengthening techniques have been proposed by various researchers. In this study, new strengthening techniques were developed using carbon fiber reinforced polymers (CFRP) to retrofit the deficient beam-column joints and the effects were investigated on the specimens having structural deficiencies. One control specimen was constructed according to detailing provisions specified by the 1975 design code of Turkey, whereas the other four control specimens were constructed with deficiencies observed in the real applications. Moreover, three additional specimens were constructed to develop an alternative strengthening technique. The tests were carried out by applying a constant axial load and a reversed cyclic lateral load to the top of the column. The tested control specimens were repaired and/or strengthened by CFRP sheets and retested. Comparative analysis of control and CFRP-strengthened joint specimens' results showed that, significant improvements in the lateral load and the energy dissipation capacities were achieved by using the proposed CFRP-strengthening techniques. Furthermore, an analytical model was proposed to predict the lateral load capacities of the shear critical joint specimens. The predicted results were compared with the experimental results of this research. All the predictions were in good agreement with the experimental results. On the other hand, the proposed model was found to reproduce 11 test results from the literature with reasonable accuracy.

# ÖZET

## BETONARME KOLON-KİRİŞ BİRLEŞİM BÖLGELERİNİN DEPREME KARŞI KOMPOZİT MALZEMELERLE GÜÇLENDİRİLMESİ

1999 öncesi inşa edilmiş betonarme yapılarda, o dönemin mevcut tasarım yönetmeliklerindeki eksikliklerden ve uygulama hatalarından dolayı çeşitli yapısal problemlerin mevcut olduğu bilinmektedir. Bu yapılar olabilecek yıkıcı depremler altında tamamıyla göçme tehlikesi altındadır. Özellikle, kolon-kiriş birleşim bölgeleri, etriye eksikliği ve yetersiz bindirme boyu gibi binanın göçmesine ve hasar görmesine sebep olan detaylandırma eksiklikleri nedeniyle yüksek kayma gerilmelerine maruz kalmaktadır. Bunun gibi eksik detaylandırılmış birleşim bölgelerinin sismik performansını arttırmak için, araştırmacılar tarafından çeşitli güçlendirme yöntemleri geliştirtmiştir. Bu çalışmada, Karbon Fiber Takviyeli Polimer (CFRP) kullanarak yeni güçlendirme yöntemleri geliştirilmiş ve eksik detaylandırılmış numuneler üzerinde etkileri incelenmiştir. 1975 Türk deprem Yönetmeliğine uygun olarak detaylandırılıp üretilmiş, bir adet kontrol numunesi ve uygulamada görülen detaylandırma eksikliklerinin etkilerini incelemek amacıyla bu eksiklikleri bulunduran 4 adet kontrol numunesi üretilmiştir. Ayrıca 3 adet numune üzerinde de farklı güçlendirme metotları geliştirilmiş ve davranış üzerindeki etkileri incelenmiştir. Deneyler kolon üstünden uygulanan sabit eksenel yük ve tersinir tekrarlı yatay yüklemeler altında yapılmıştır. Kontrol numuneleri test edildikten sonra tamir edilerek veya tamir edilip CFRP ile güçlendirilerek tekrar teste tabi tutulmuştur. Test sonuçları, güçlendirilen numunenin yatay yük kapasitesinde ve dolayısıyla enerji tüketme kapasitelerinde önemli bir artış olduğunu göstermiştir. Ayrıca bu çalışmada, birleşim bölgesinde eksik detaylandırılmış numunelerin yatay yük taşıma kapasitelerini hesaplayabilmek içinde analitik bir analiz yöntemi geliştirilmiştir. Analitik olarak bulunan sonuçlar deney sonuçları ile karşılaştırılmış ve sonuçların yakın olduğu görülmüştür. Ayrıca, önerilen analitik model, literatürde yapılmış 11 deneyin sonucunu da yaklaşık olarak doğru tahmin etmiştir.

# TABLE OF CONTENTS

# LIST OF FIGURES

# LIST OF TABLES

# LIST OF SYMBOLS / ABBREVIATIONS

| | |
|---|---|
| $a$ | Unsupported length of greater dimension of transverse reinforcement |
| $a_s$ | Effective depth of the compressive strut |
| $A_{CFRP}$ | Effective cross-sectional area of CFRP sheets |
| $A_{L\text{-}Shape}$ | Effective cross-sectional area of L shaped CFRP sheets |
| $A_b$ | Concrete cross-section area at the joint |
| $A_{diagonal}$ | Diagonal cross-sectional area of joint panel |
| $A_g$ | Gross cross-section area |
| $A_s$ | The longitudinal reinforcement area |
| $A_{str}$ | Effective area of diagonal strut |
| $A_w$ | The area of one leg of transverse reinforcement |
| $A_{w\text{-}min}$ | The minimum transverse reinforcement area in confined region |
| $b$ | Width of the joint panel |
| $b_c$ | Width of the column cross-section |
| $b_{eff}$ | Effective width of CFRP layers |
| $b_s$ | Width of the diagonal strut |
| $B$ | Length of the beam |
| $C_b$ | Compression force of beam |
| $C_{c1}$ | Compression force of top column |
| $C_{c2}$ | Compression force of bottom column |
| $d$ | Greater dimension of column cross-section |
| $d_{1,2}$ | Distance of displacement sensors from the surface of the member in curvature readings |
| $D_{1,2}$ | Gauge lengths of diagonally placed displacement sensors |
| $d_b$ | Effective cross-sectional height |
| $E_c$ | Modulus of Elasticity of concrete |
| $E_s$ | Modulus of Elasticity of steel |
| $F$ | Applied lateral load |
| $F_{1\text{-}6}$ | Internal forces of truss members |
| $f'_c$ | Concrete compressive strength |
| $f_{\text{-}truss}$ | Stresses of truss members |

| | |
|---|---|
| $f_s$ | The stresses of longitudinal reinforcements |
| $f_t$ | The tensile strength of concrete |
| $f_u$ | The ultimate strength of steel, concrete and CFRP |
| $f_y$ | The yield strength of reinforcement |
| $h$ | Height of the joint panel |
| $h_{1,2}$ | Gage length of displacement sensors in curvature readings |
| $h_c$ | Height of column or beam cross-section |
| $h_c'$ | Width of joint panel |
| $h_b$ | Height of beam cross-section |
| $h_b'$ | Height of joint panel |
| $H$ | Height of column in test specimen |
| $l_b$ | Length of beam |
| $l_{c1}$ | Height of top column |
| $l_{c2}$ | Height of bottom column |
| $L$ | Length of the beam in test specimen |
| $L_c$ | Distance between two displacement sensors in curvature readings |
| $L_s$ | Clear height of the column |
| $L'$ | Clear span length of beam |
| $M$ | Moments of the section |
| $n$ | Number of CFRP layers |
| $N$ | Axial force |
| $NA$ | Neutral Axis |
| $N_o$ | Minimum axial force |
| $R_1$ | Vertical reaction at column support |
| $R_2$ | Horizontal reaction at column support |
| $R_3$ | Vertical reaction at beam support |
| $s$ | Spacing of transverse reinforcements |
| $s_1$ | Spacing of transverse reinforcements at the joint region |
| $s_2$ | Spacing of transverse reinforcements at the confined region |
| $s_3$ | Spacing of transverse reinforcements at the unconfined region |
| $t$ | Thickness of one layer of CFRP |
| $T_b$ | Tensile force of beam longitudinal reinforcement |
| $T_{c1}$ | Tensile force of top column longitudinal reinforcement |

| | |
|---|---|
| $T_{c2}$ | Tensile force of bottom column longitudinal reinforcement |
| $V$ | Shear force acting on joint |
| $v_c$ | Shear strength of concrete |
| $v_s$ | Shear strength of transverse reinforcements |
| $V_b$ | Shear force acting on beam |
| $V_{c1}$ | Shear force acting top column |
| $V_{c2}$ | Shear force acting on bottom column |
| $V_{jh}$ | Horizontal joint shear force |
| $V_{jv}$ | Vertical joint shear force |
| $X,Y$ | Dimensions of undeformed joint panel |
| $z$ | Level arm of the beam cross-sections |

| | |
|---|---|
| $\alpha$ | The angel of diagonal cracks occurred at joint region |
| $\beta$ | The ratio of shear strength of transverse reinforcement to that of concrete |
| $\Delta$ | Relative longitudinal displacement reading taken from the displacement sensors |
| $\Delta_{1,2}$ | Readings of displacement sensors in curvature measurements |
| $\varepsilon_o$ | The strain values at the maximum strength of concrete model |
| $\varepsilon_c$ | The compressive strain of extreme fiber of the section |
| $\varepsilon_t$ | The tensile strain of extreme fiber of the section |
| $\varepsilon_{sh}$ | The strain value where the strain hardening initiates |
| $\varepsilon_u$ | The ultimate strain value of concrete and steel |
| $\varepsilon_y$ | The yield strain value of steel |
| $\varepsilon_{1,2}$ | Strains calculated from |
| $\gamma$ | The angel of CFRP fibers to horizontal axis |
| $\gamma_s$ | Shear deformations of the joint |
| $\kappa$ | Curvature |
| $\rho$ | Longitudinal reinforcement ratio |
| $\rho_{l\text{-}min}$ | Minimum longitudinal reinforcement ratio |
| $\rho_s$ | Transverse reinforcement ratio |

# 1. INTRODUCTION

## 1.1. General

Recent earthquakes worldwide in urban areas have illustrated the vulnerability of existing structures to seismic loading. Generally, these structures were designed for gravity loads only, without regard to any significant lateral forces. Also, the strength of the concrete and the amount of reinforcements was often below the minimum values specified in current codes. Therefore, the lateral load resistance of these structures is considered suspect for even moderate earthquakes.

After severe earthquakes, these structures revealed that one of the weakest links in lateral load resisting frame is the beam-column connection region. Poorly detailed joints, especially exterior ones, have been identified as critical structural elements, which appear to fail prematurely in R/C frames. The lessons learned after each earthquake and vast number of parameters affecting the joint behavior has stimulated many researchers to experimentally investigate the connections under simulated earthquake loads [1-13]. Even though some investigation was performed analytical study about the connections to predict the shear strength and the shear deformations of the joint panel [37-42].

Strengthening of R/C joints is a challenging task that poses major practical difficulties. A variety of techniques applicable to concrete elements have also been applied to the joints with the most common ones being the construction of R/C or steel jackets [2]. Reinforced concrete jackets and some forms of steel jackets, namely steel ‘‘cages,’’ require intensive labor and detailing. Plain or corrugated steel plates have also been tried for jacketing the joint region [3-5]. Moreover, concrete jackets increase the dimensions and weight of structural elements. In addition to corrosion protection, these elements require special attachment through the use of either epoxy adhesives combined with bolts or special grouting.

More than a decade ago, a new technique for strengthening structural elements emerged. The technique involves the use of fiber reinforced polymers (FRP) as externally

bonded reinforcement in critical regions of R/C elements. FRP materials, which are available today in the form of strips or in situ resin impregnated sheets, are being used to strengthen a variety of R/C elements, including beams, slabs, columns, and shear walls, to enhance the flexural, shear, and axial (through confinement) capacity of such elements. FRP materials offer advantages over structural steel, reinforced concrete and timber. Some of the advantages are ease of installation; immunity to corrosion; high stiffness-to-weight and strength-to-weight ratios; availability in convenient ‘‘to apply’’ forms, and the ability to control the material’s behavior by selecting the proper orientation of the fibers etc. All of these features make carbon fiber composites a highly engineered material suitable for infrastructure applications, in spite of the fact that the cost of carbon fibers is much higher than the cost of conventional construction materials.

### 1.1.1. Background

In the past, building structures were primarily designed to carry the service loads, including the dead load and live load, which are referred as gravity loads. The dead load results from the weight of the structure and all other permanently attached material, while live load results from expected usage, which may be movable and their intensity varying.

When a R/C frame is subjected to a loading, the beam-column joints are assumed to be rigid and they play an important role in transferring moments and internal forces among adjacent beams and columns. Figure 1.1 shows the deflection shapes and associated bending moment diagram of a frame structure, subjected to gravity and lateral load respectively.

Under the action of gravity loads on beam spans, each beam is subjected to a moment where it frames in to the column. Interior beam-column joints are subjected to no or small shear forces, as the shear effects from the beams on opposite sides of the joint detract from each other. This is not the case for exterior joints where the moment of the beam is balanced by the column moment. The corresponding shear induced is not very significant. On the other hand, to resist the applied lateral load, both beams and columns in a frame will deform in double curvature. Inflection points generally occur near the mid height of each column and the mid span of each beam. The change of moments in the

beams and columns across the joint induces both vertical and horizontal shearing forces, as shown in Figure 1.2.

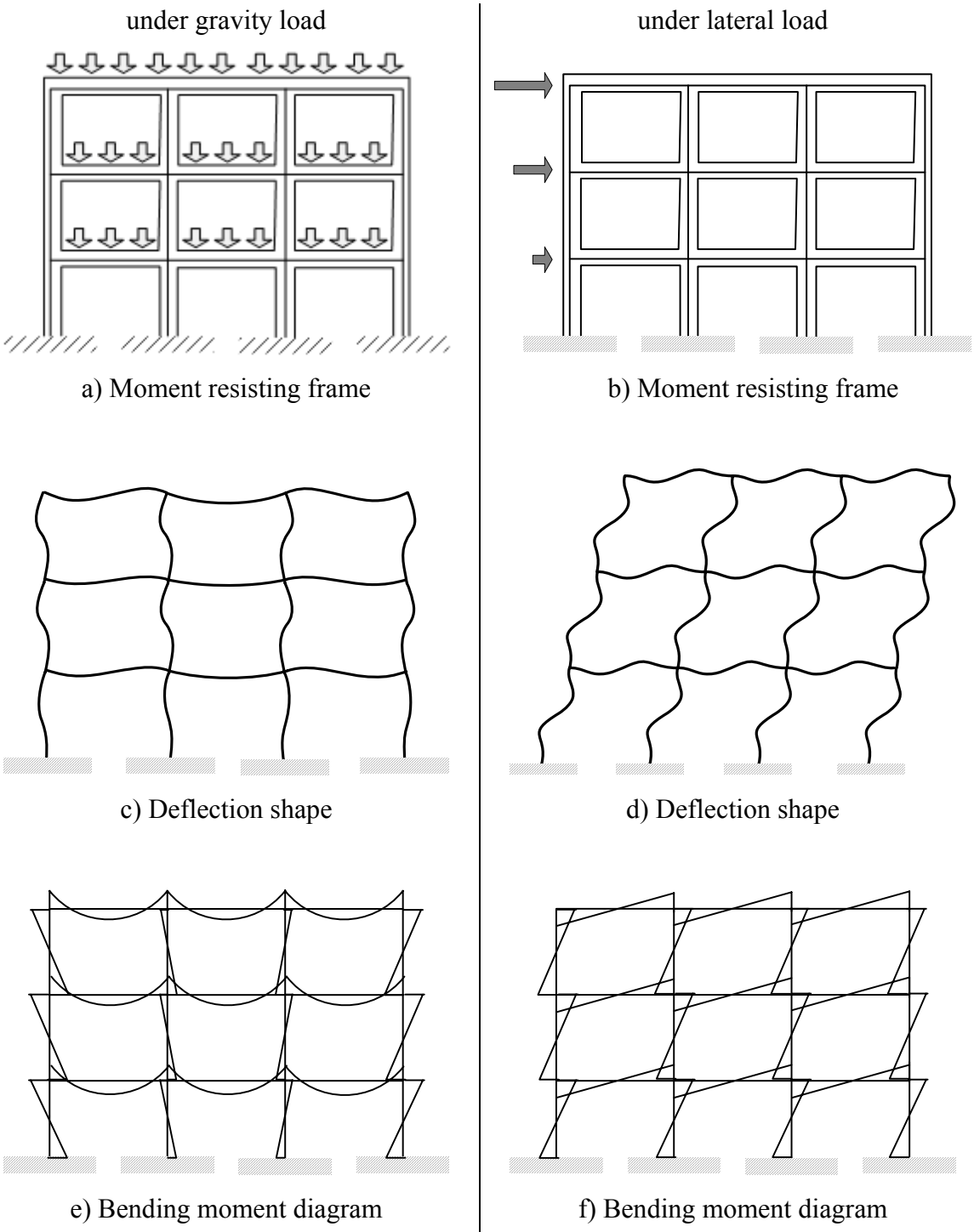


Figure 1.1. Behavior of moment resisting frame under gravity and lateral load

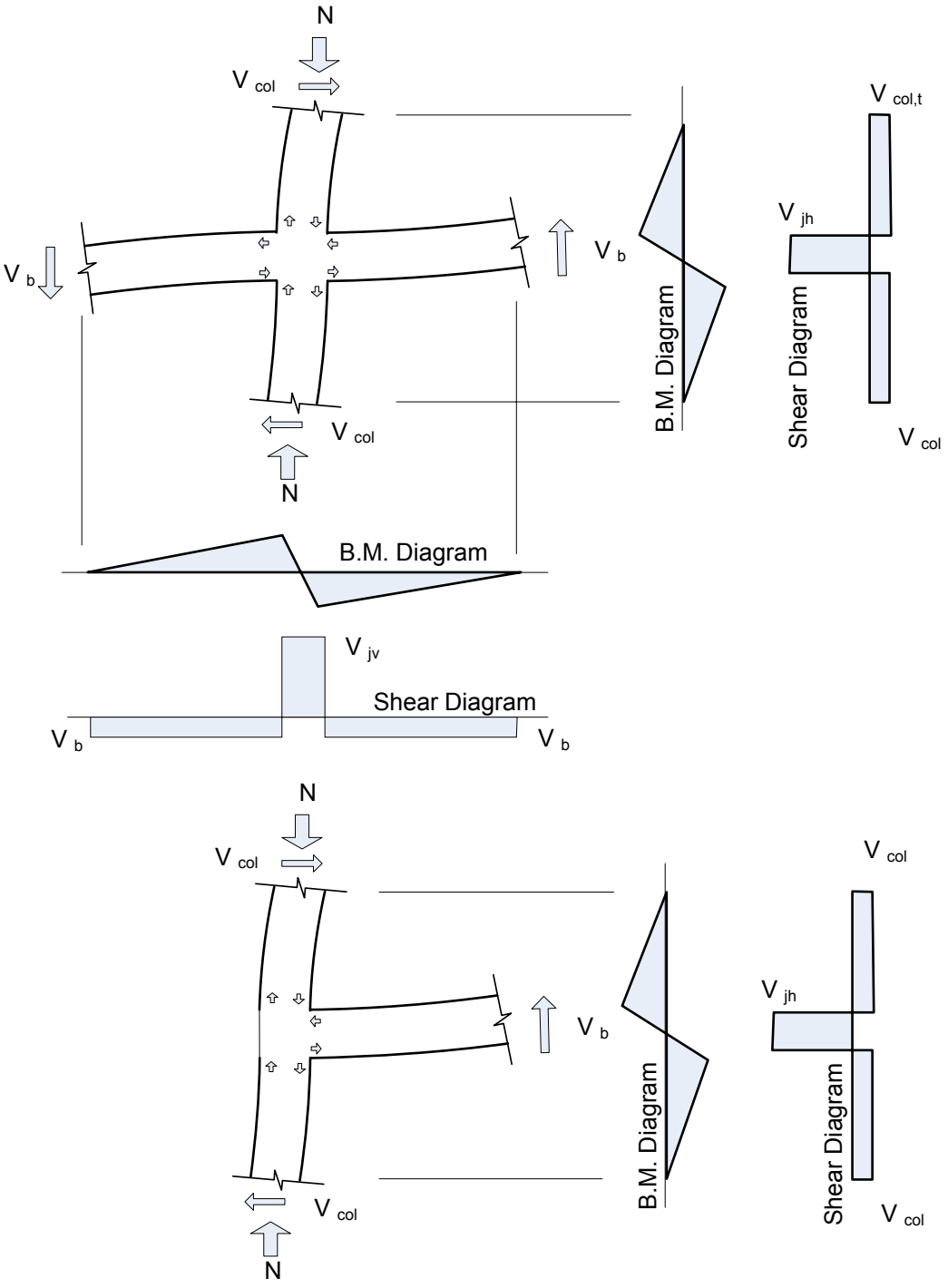


Figure 1.2. Shear at interior and exterior joint region

## 1.2. Problem Statement

A critical region in a R/C frame is the beam-column connection, where different constructive details can originate from local failures, such as the shear collapse of the panel

due to the lack of transverse reinforcement. On interior and exterior connections (a large part of the joints of a building), an experimental study was performed by Beres *et al.* [6].

This study emphasized six critical details that could be potential causes of failure in a non-seismically designed structure subject to an earthquake:

- Lapped splices of the longitudinal reinforcement just above the construction joint,
- Scarce confinement provided by the ties in column and in beam,
- No confinement in the joint region,
- Using plain re-bars for longitudinal and transverse reinforcement,
- Construction joints above and below the beam-column connection,
- Weak column-strong beam condition.

## 1.3. Literature Review

This section presents a review of current knowledge on R/C beam-column joints. Development of joint shear forces and various relevant parameters are mentioned, and previous experiments and analytical studies on beam column joints and the corresponding findings are stated.

### 1.3.1. Beam-Column Joint Behavior

During the strong earthquakes, beam-to-column connections are subjected to severe reversed cyclic loading. If they are not designed and detailed properly, their performance can significantly affect the overall response of the structure. The joints ensure continuity of a structure and transfer the forces from one element to another. Due to this significance, beam-column joint was investigated by many researchers.

The first behavior studies of beam-column joints were conducted at the Portland Cement Association laboratories by Hanson and Connor in 1967 [7]. They concluded that subassemblies containing joints must have in a ductile manner if frame structures are to perform satisfactorily in a major earthquake. Then, the problem has been studied by other researchers in many countries. In 1975, Park and Paulay were investigated the behavior of

beam-column joints [8, 9]. In 1978, Paulay *et al.* carried on experiments, and revealed the force transfer mechanism of the joint including compression mechanism and truss mechanism [10].

In order to determine the effects of the flexural strength ratio, the percentage of transverse reinforcement within the joint and the shear stress within the joint, twelve reinforced concrete beam-to-column subassemblies representing typical exterior beam-to-column connections in the upper levels of a multistory ductile, moment-resisting reinforced concrete space frame were tested under simulated earthquake loadings by Ehsani and Wight [11]. In all control specimens diagonal shear cracks connecting the opposite corners of the joint were observed during the first cycle of loading. In the bare specimens there was a flexural hinging region in the beam portion of the specimen near the joint panel.

Durrani and Wight investigated the effects of the less transverse reinforcement on three interior beam-column sub-assemblages. Also, level of joint shear stress on strength, stiffness and energy dissipation of beam-column joints were examined. As a conclusion, joint shear stresses have a significant effect on the strength and the stiffness. A minimum column-to-beam flexural strength ratio of 1.5 was found to be suitable for designing the beam column joints [12].

Ehsani and Wight carried out experiments on six exterior beam-to-column joints in 1986 in order to verify the existing design recommendation. The ratio of the column-to-beam flexural capacity, the joint shear stress and the effects of transverse reinforcements in the joints were the main parameters investigated. The specimens were subjected to cyclic load reversals at deflection levels intended to represent the levels that could be obtained during a moderate or severe earthquake. It is concluded that in some cases the present design recommendations could be safely relaxed [13].

Fujii and Morita investigated the joint on eight interior and exterior beam-column sub-assemblages. According to the test results, the increase of column axial load level gave no influence on the ultimate shear strength of the interior joints, but this increase in column axial load improved the shear strength of the exterior joints nearly %10 [14].

Effects of existing transverse beam and slab on the behavior of beam-column joints have also been studied by Ehsani and Wight. The ratio of the column flexural capacity to that of the beam and slab, the joint shear stress and presence/absence of the transverse reinforcement in the joint were investigated as parameters. As a results the presence of transverse beams, which are not load directly, considerably improves the joint behavior [15].

In 1992, Tsonos *et al*. carried out an experimental study on the behavior of external beam-column joints with inclined reinforcing bars under seismic loading. The effects of the amount of inclined bars, the ratio of the column-to-beam flexural capacity and the joint shear stress were investigated on 20 full-scale exterior beam-column subassemblies. It was concluded that, the use of crossed inclined bars in the joint region is one of the most effective ways to improve the seismic resistance of exterior R/C beam-column joints [16].

Beres *et al.*made an extensive study on existing exterior and interior beam-column joint to define the behavior of joints [6, 17, 18, 19,]. To determine the effect of using hooked and coated high performance steel fiber reinforced concrete in place of conventional concrete in the joint region.

Clyde *et al.* studied on reinforced concrete buildings that were built in the 1960s behave in a nonductile manner and did not meet current seismic design criteria. Beam-column joints of such nonductile buildings were investigated using several performance-based criteria. Four half-scale R/C exterior joints were tested to investigate their behavior in a shear-critical mode. The joints were subjected to quasi-static cyclic loading, and their performance was examined in terms of lateral load capacity, drift, axial load reduction in the column at high levels of drift, joint shear strength, ductility, shear angle, residual strength. Two levels of axial compression load in the columns were investigated, and their influence on the performance of the joint are discussed. It is concluded that the joint strength coefficient, $\gamma$, changes with the variation of the column compressive axial load [20]. Shannag *et al.* tested beam-column joints containing different amounts of brass-coated or hooked steel fiber. The steel fiber concrete specimens exhibited three times higher load levels, 20 times larger energy dissipation, and two times slower stiffness degradation compared to the reference concrete specimens. Using hooked steel fibers

showed a significant increase three times in the maximum load carrying capacity and in the initial secant stiffness compared to reference specimens. [21].

LaFave and Wight investigated three reinforced concrete exterior wide beam-column-slab sub-assemblages having wide beam flexural steel anchored outside the column core for beams [22]. Shin and LaFave investigated the effects of slabs on the seismic performance of 2/3 scale eccentric beam-column-slab subassemblies. It was concluded that the floor slabs diminished differences between seismic performances of the specimens and increased joint shear strengths of the specimens when compared with other eccentric connections without floor slabs [23]. Hatamoto *et al.* conducted two series of experiments to study the performance of wide beam-to-columns sub-assemblages under lateral loading. As a result the cracking pattern of wide beams changes with the beam-to-column width ratio [24].

The effects of slippage of longitudinal beam reinforcements passing through interior beam-column joints were investigated by Hakuto *et al*. As a result of high bond stresses in joint, the slippage and bond deterioration occurs. Consequently, the loss of compression reinforcement reduces both flexural strength and the ductility of the adjacent beam [25].

Engindeniz *et al.* made a detailed state of the art on beam-column joints. He examined the performance of joints, effectiveness of strengthening and retrofitting techniques including epoxy repair, removal and replacement, concrete jacketing, concrete masonry unit jacketing, steel jacketing and additional external steel elements, and strengthening with fiber reinforced polymeric composite applications, that proposed between 1975 and 2003 [26]. Advantages and disadvantages such as application details, required labor, applicability and the performance of each method were discussed.

### 1.3.2. Jacketing of the Joint Region

The first study on repairing and testing of beam-column joints was conducted in 1975. The specimens were prepared according to the ACI-1971 code. In order to obtain a damaged specimen, they were subjected to lateral loads in varying levels. After than the specimens were repaired by epoxy injection and different removal and replacement

techniques, and tested. The test results indicated that the applied method can restore structural integrity [27, 28].

In 1999, Tsonos conducted a series of tests on two exterior beam-column joint specimens and re-tested them after repaired and strengthened with R/C jacketing technique developed by United Nations Industrial Development Organization (UNIDO). The repaired and strengthened specimens exhibited higher strength, greater stiffness and better energy dissipation capacity than the original specimens [29]. Adin *et al.* carried out similar tests and obtained good improvements on epoxy-injected specimens [30].

Significant research effort has been devoted to developing a variety of techniques for seismic retrofit. The most common retrofitting techniques include reinforced concrete or steel jackets. In the study of Ghobarah *et al.*, the effectiveness of corrugated steel jackets for enhancing the seismic shear strength and ductility of connections were examined on four exterior beam-to-column specimens. The test results indicated that the shear strength of jacketed joints can be estimated using an approach which is similar to design recommendation of ACI for beam column joints [3].

In 2002, Amoury and Ghobarah tried GFRP sheets for rehabilitation of three beam-column joints built in accordance to pre-1970s codes. In the result of tests, the control specimen showed combined brittle joint shear and bond failure modes while rehabilitated specimens showed a more ductile failure mode. Finally they proposed a simple design equation for the rehabilitation scheme [31].

Biddah *et al,* proposed a new seismic upgrading technique (corrugated steel jacketing) for existing structure. They investigated the effects of amount of transverse reinforcement in column an in the joint, corrugated steel thickness and jacketing only or both beam and column on six one third scale beam-column connections. Test results demonstrated that existing reinforced concrete frame connections upgraded using corrugated steel jackets performed satisfactorily when subjected to high cyclic load levels. The corrugated steel jacket was found to be an effective system of upgrading as it increases the joint shear strength and energy dissipation capacity. Also they formulated the design of the thickness and the depth of the corrugation [4].

### 1.3.3. Composite Materials for Strengthening the Beam-Column Joints

The rehabilitation of R/C columns jacketed with carbon fiber-reinforced plastic composites (CFRP) for improving shear strength, confinement, and ductility has received considerable attention for the last few decades. Antonopoulos and Triantafillou carried out comprehensive experimental program, aimed at providing a fundamental understanding of the behavior of shear-critical exterior reinforced concrete R/C joints strengthened with fiber reinforced polymers under simulated seismic load. The strength and dissipated energy increased significantly, but not proportionally to the number of CFRP layers, due to the premature debonding [1]. In the study of Geng *et al.* the effects of CFRP tow sheets wrapped around the column near the joint region for improving the ductility of concrete column-to-beam connection and the capability of connections containing insufficient development length were investigated [32].

The study of Prota *et al.* focuses on a new technique for the seismic upgrade of R/C beam-column connections in gravity load-designed frames by the application (combined or not) of FRP rods and laminates. The FRP rods provide flexural strengthening, whereas the lay-up laminates provide confinement and shear strengthening. Along with the modeling of such upgraded connections to assess the increase of strength and/or ductility provided by the composite reinforcement, an experimental program was conducted. It appears that the proposed upgrade method will have a significant impact of the engineering practice in the near future [33].

Gergely *et al.* tested exterior beam-column joints strengthened with carbon sheets, to investigate the effects of fiber orientation, and the surface preparation [34]. Amoury and Ghobarah proposed techniques for upgrading reinforced concrete beam-column joints by wrapping around the joint to prevent the joint shear failure. The control specimen showed a brittle failure mode whereas rehabilitated specimens showed a more ductile failure mode (Figure 1.3) [31]. Ghobarah and Said developed effective selective rehabilitation schemes for R/C beam-column joints using advanced composite materials [35].

Kaya *et al.* made an experimental study to evaluate the improvements of behavior of shear-damaged RC joint repaired with chemical epoxy injection method. One control

specimen was tested and, repaired and retested under constant axial load and reversed cyclic lateral load. The test results showed that, the lateral load capacities of the repaired specimen increased twice than that of control one [36].

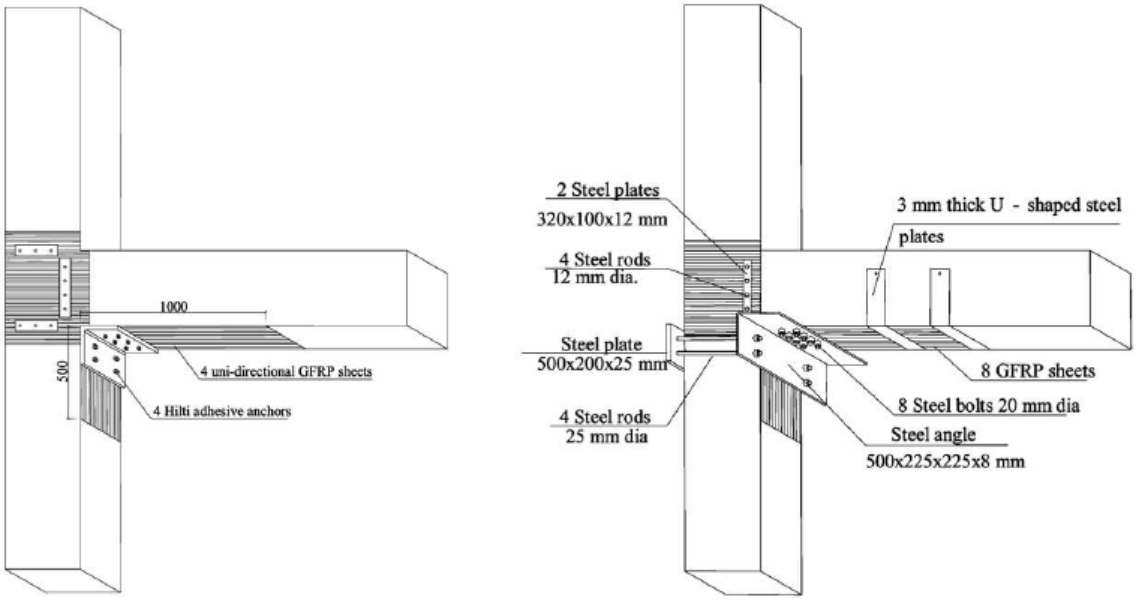


Figure 1.3. Retrofitting schemes of Amoury [31]

### 1.3.4. Joint Shear Modeling

There are several Researchers examine some approaches to modeling of hysteretic behavior of the reinforced concrete structural elements [37-39].

The basic theory relating to the design of reinforced concrete beam-column joints is revised and extended, and the results of a series of tests conducted in the second half of 1976 are reported. It is shown that a joint which contained bond plates to prevent bond failure of the flexural reinforcement in the joint and was proportioned to limit yielding of the steel in this zone had markedly superior performance to specimens designed to comply with the American Concrete Inst. ACI 318-71 code and to specimens designed according to the proposals of May 1976 for the revision of the New Zealand Ministry of Works and Development code of practice for the design of public buildings [40].

Scarpas made a study on the behavior of exterior beam column joints. The results are presented of tests of three reinforced concrete exterior beam-column sub-assemblies under

simulated seismic loading. The main variable studied was the amount of horizontal joint shear reinforcement. A new tentative model for the mechanism of exterior joint shear resistance is proposed [41].

Six full-sized interior beam-column joint specimens were tested under quasi-static loading intended to simulate earthquake input. All specimens were designed following the accepted design philosophy of strong column-weak beam approach. The three variables selected for this investigation included the percentage of transverse hoop reinforcement in the joint, the joint shear stress level, and the presence of transverse beams and slab on half of the specimens. On the basis of test results, it was concluded that the joint shear stress level was critical for the satisfactory performance of beam-to-column connections without transverse beams and slab. For connections with transverse beams and slab, a well-confined joint core was essential for the effective participation of the transverse beams in resisting joint shear. In the analytical part of this study, a hysteretic model for beam-column subassemblies is developed from the hysteretic behavior of specimens observed during testing. The proposed model accounted for pinching of hysteretic loops, stiffness degradation, reduced unloading stiffness, and fixed end rotations due to the slippage of bars through the joint. A simple analytical model for computing the maximum story displacements for regular frames is proposed. The maximum story level displacements were found to be in good agreement with those obtained from models [42].

In 1996, Scot made an experimental work on 17 R/C exterior beam-column joints. Effects of depth of beam, tension steel percentage, reinforcing details of beam, and axial load were examined. He measured the strain distribution along the beam and column reinforcing bars [43]. Gergely *et al.* calculated the contribution of the FRP to the shear capacity of a joint by analogy to steel stirrups, assuming that the FRP crossing a potential shear crack in the beam will exhaust its tensile capacity [44].

Antonopoulous and Triantafillou developed a model from the experimental data obtained from literature. Shear strength prediction gave the good results [45]. Parvin *et al.* indicated that the moment capacity of the beam-column joint capacity was increased by using external FRP wrapping, and also Finite Element analysis were carried out on T-joints to investigate the effect of fiber composites [46, 47, 48].

Hwang and Lee developed a joint model for exterior beam-to-column joint to determine the shear strength. They also investigated the applicability of this model to interior beam-column joint, and obtained good agreement. In exterior one they proposed a method called as “softened strut-and-tie model” which is based on strut-and-tie concept and derived to satisfy equilibrium, compatibility, and the constitutive laws of cracked reinforced concrete. The accuracy of the proposed model was checked by comparing calculated shear strengths with experimental data reported in previous literature, and a satisfactory correlation was found [49, 50]. In Figure 1.4, mechanisms of shear transfers at the exterior joints, taken from the New Zealand design recommendation, were given.

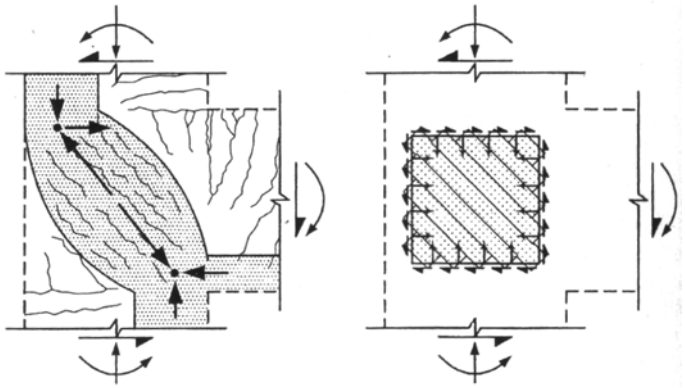

Figure 1.4. Diagonal strut mechanism and truss mechanism [49]

A simplified method, based on softened strut and tie model, for determining the shear strength of discontinuity regions failing in a diagonal compression is proposed by Hwang and Lee. The method incorporates the shear resisting mechanisms as postulated by the softened strut and tie mode, and it is a function of the concrete strength, horizontal shear reinforcement, vertical shear reinforcement and geometrical configuration of the discontinuity regions [51]. Bakır and Boduroğlu presented a new design equation predicting the shear strength of monotonically loaded exterior beam-column joints accurately [52].

Lowes *et al.* developed a model represents the mechanism that may determine inelastic beam-column joint behavior through the combined action of one dimensional shear panel, bar slip, and interface shear components of the model. Comparison of simulated and observed response for a series of beam-column joint buildings sub-assemblages indicates that the model represents well the fundamental characteristic of response for joint subjected to moderate shear demands [39, 53]. Fleury *et al.* proposed a

model, incorporates explicitly the modeling of concrete, steel, and bond, for the beam column connections of R/C frame structures [54].

Shiohara investigated the irrationality in the existing models for shear. Therefore, he examined shear critical 20 R/C beam-column connections. He proposed a new mathematical model [55].

Pantelides *et al*. investigated the seismic performance of beam-column joints with three different details of beam and beam-column joint reinforcement. Six full-scale R/C exterior joints were tested. Lateral load capacity, drift, plastic rotation, joint shear strength, ductility were examined. Also, two levels of axial compression load in the columns were investigated. A strut-and-tie model is developed for verifying the experimental results [56].

Attaalla proposed an analytical expression developed to estimate the shear strength of joint cores in RC beam column connections. Also he verified the model on 130 experiments carried out in different countries, including effects of wide range parameters. The suggested model showed that the joint shear strength depends primarily on the concrete compressive strength $f'_c$ and emphasizes the role of confining the joint core. The results indicated that, the proposed model adequately predict the shear stress of the joint more accurate than the current ACI-318 and New Zealand Code, when compared with test results [57].

Pantazopoulou and Bonacci made a study on mechanics of beam-column joints in laterally loaded frame structures in 1992. The role of axial load and stirrups on the behavior were illustrated. In addition to providing an improved understating of joint behavior, the derivation reflects the relationship between the design limit states and corresponding deformations, giving an opportunity to link joint design to the overall lateral drift [58].

In 2009, Wang and Hsu investigated the interior shear strength of nonductile frames strengthened with reinforced concrete jackets, but no new joint shear hoops and no dowel anchors installed into new and old concrete interface. The results show that the RC jacketed scheme is able to efficiently rehabilitate nonductile frames with very poor joint

details. An empirical equation for calculating the joint shear strength is proposed [59] (Figure 1.5).

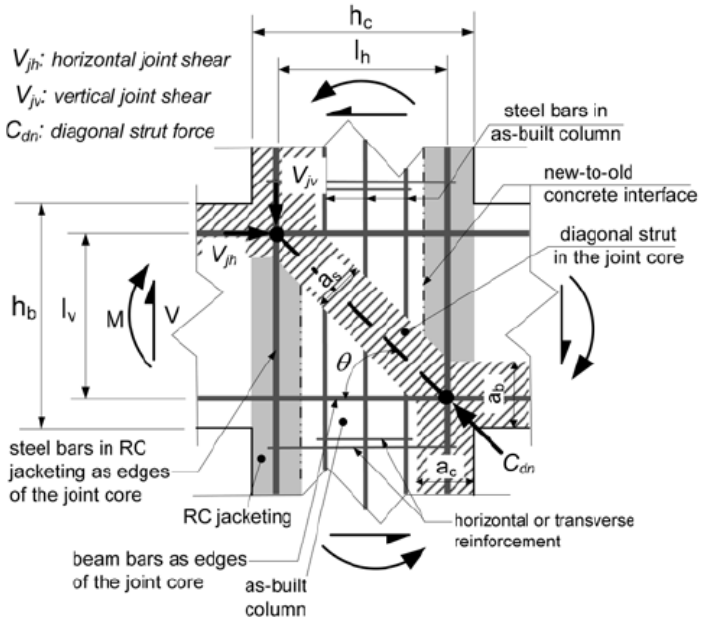


Figure 1.5. Diagonal strut mechanism of interior joints [59]

## 1.4. Factors Effecting Beam-Column Joint Behavior

After reviewing the previous researches and experimental studies, key variable affecting the behavior of beam column joints, in general include: (1) Joint geometry, (2) Compressive strength of concrete, (3) Transverse reinforcement, (4) Bond and anchorage and (5) level of axial loads in column.

## 1.5. Research Objectives and Scope

### 1.5.1. Objectives

The objectives of this study were as follows:

- To understand the behavior of seismic deficient beam-column joints under lateral cyclic loading and constant axial loading,
- To observe the effects of various deficiencies on the joint behavior,

- To propose effective CFRP-strengthening techniques to overcome the joint deficiencies
- To develop a design equation for shear critical reinforced concrete beam-column joints retrofitted with CFRP sheets.

### 1.5.2. Scope

In order to reach the objectives mentioned above, a series of experimental and analytical investigation were carried out on beam-column joint specimens at the Boğaziçi University's Structural Engineering Laboratory. Due to limitations on the experimental set up, this study included only 2D exterior beam-column sub-assemblies without slabs. This research mainly deals with the deficiencies of the structures, constructed before 1999 in Turkey. Three main deficiencies, such as lap-splicing on column reinforcement, inadequate transverse reinforcement in joint region and inadequate anchorage length of beam reinforcements, were selected as key parameters to be investigated throughout the experimental study. Also, plain re-bars and low-quality concrete were used in construction of all specimens as deficiencies. CFRP materials were utilized for strengthening the specimens to decrease the effects of these deficiencies. The influence of slabs, transverse beams and infill walls were not considered in this research.

## 1.6. Research Significance and Rationale for Study

The most crucial part of reinforced concrete structures appears to be the beam-column joints according to failure type of buildings under seismic action. Researchers gave importance to understand the behavior of the joints. During the past 3 decades a great deal of research on beam-column joints subjected to seismic hazards has been conducted. A number of retrofitting strategies were developed and proposed to upgrade the behavior of beam-column joints.

No research was noticed investigating the effects of CFRP retrofitting on beam-column joints with the effects of deficiencies such as plain re-bars, low-quality concrete, lap-splice and inadequate transverse reinforcement. Also, the behavior of

strengthened specimens with CFRP and repaired specimens with epoxy injection were investigated.

In the analytical part of the study, the data obtained from experiments and also from the previous researches were used for developing a design procedure to predict the lateral load capacity of beam-column joint.

## 1.7. Report Outline

This experimental investigation on the seismic behavior of reinforced concrete beam-column connections and retrofitting of these connections by using CFRP sheets and modeling the behavior of joint shear are presented on this thesis.

This thesis is divided into five chapters. Chapter 1 provides brief information about the beam-column joints behaviors, the definition of problems and objectives of the research are provided. Also, the previous researches on beam-column joints including experimental investigation and analytical models are reviewed, and their results are summarized in this chapter.

An experimental program is introduced in Chapter 2, which includes details of the specimens, construction of the specimens, the experimental setup, the instrumentation and testing methodology. Applied strengthening and retrofitting techniques are also explained in this chapter.

The experimental observations of all thirteen large scale specimens are summarized in Chapter 3. The results are presented with graphical data and discussions of the results are also given in this chapter.

Explanation of the suggested shear models are given in Chapter 4. Chapter 5 gives a summary of findings and recommendations for further research in this area.

Finally, for each test specimen, the cracks observed during the testing and load levels for each drift levels were illustrated in tables in the Appendix Section.

# 2. EXPERIMENTAL STUDY

## 2.1. Introduction and Background

To investigate the seismic performance and shear strength of non-seismically designed reinforced concrete beam-column joints tests were carried out on 13 full scale specimens under reversed cyclic loading.

Strengthening of RC frames with CFRP is a noteworthy issue because of ease of application and time-savings. Furthermore, the buildings can remain functional during the strengthening process. In order to find the effective strengthening technique, the deficiencies in the existing reinforced concrete frame elements must be first identified correctly and improvements should be implemented afterwards to mitigate the negative effects of such deficiencies. In this study, the effect of inadequate lap splices on column longitudinal reinforcement at the bottom of the column was investigated, and a methodology was proposed to eliminate the effects of these deficiencies.

For determining the deficiencies of Turkish practice, a survey was conducted on the existing structural building designed between 1957 and 1997 (Table 2.1). The survey revealed that concrete strengths were less than 25 MPa for 90% of the buildings in Turkey and for 50% of those had less than 16 MPa. Besides, St-I type steel, which had 220 MPa yield strength, were used in 70% of buildings. At the end of the survey, common deficiencies such as plain re-bars, low-quality concrete, lacking or insufficient of transverse reinforcement, lap-splice, inadequate anchorage length of beam reinforcements, were determined and implemented in the experimental study.

The experimental study can be explained briefly in three parts. In the first part, for simulating the old practice, beam-column control specimens, designed and detailed according to the provisions of the Turkish Earthquake Code 1975 (TEC 75) including different deficiencies, were produced and tested without any strengthening for determining the effects of deficiencies on the behavior under earthquake loadings. In the second part, a number of identical specimens with the poorest behaved control one were produced.

Table 2.1. Surveying

| Project ID | # of Storey | Height | Year | Concrete Strength | Reinforcement Type | Beam | | | | Column | | | |
|---|---|---|---|---|---|---|---|---|---|---|---|---|---|
| | | | | | | Dimension | Lapsplice | Spacing | Conf. Zone | Dimension | Lapsplice | Spacing | Conf. Zone |
| | | *m* | | *MPa* | | *cm* | | *cm* | | *cm* | | *cm* | |
| Mercan-Tuzla Halim Kumbaracı | 3 | 2,9 | 1990 | 9 | I | 20 x 50 | --- | 10 - 20 | --- | 40 x 25 | --- | 10 - 20 | --- |
| Cemal Tekstil Binası | 6 | 3 | 1988 | 25 | III | --- | --- | --- | --- | 40 x 70<br>40 x 40 | --- | 20 - 30 | --- |
| İşbankası Atatürk cad | 6 | 2,75 | 1997 | 26 | --- | --- | ok | 23 - 32 | not enough | 30 x 75 | --- | 12 - 29 | ok |
| İşbankası Merkez Unkapanı | 8 | 3,1 | 1947 | 25 | I | 40 x 45<br>20 x 60 | --- | --- | --- | 32 x 52 | --- | 12 - 20 | --- |
| EGS Business Park | 4 | 3 | ---- | 25 | --- | 100 x 40 | --- | --- | --- | 25 x 60<br>C70 | --- | --- | --- |
| İşbankası Rıhtım | 8 | 0,15 | 1957 | 23 | I | 40 x 20 | --- | 13 - 21 | ok | 25 x 65 | --- | 14 - 21 | ok |
| İşbankası Karataş | 10 | 2,65 | 1970 | 25 | I | 40 x 20 | ok | 16 - 20 | ok | 25 x 100 | --- | 10 - 25 | ok |
| İşbankası Nişantaşı | 10 | 2,95 | 1980 | 46 | I-II | 48 x 80 | ok | 9 - 18 | ok | 80 x 90 | ok | 13 - 17 | ok |
| İşbankası Beşiktaş | 8 | 2,55 | 1974 | 16 | I | --- | --- | --- | --- | 60 x 60 | --- | 15 - 27 | ok |
| İşbankası Adıyaman | 6 | 2,87 | 1997 | 20 | III | --- | ok | ok | --- | C40 | ok | 20 -<br>not at mid | --- |
| İşbankası Kadıköy | 2 | 3,1 | 1974 | 14 | I | 25 x 35 | ok | --- | --- | 30 x 30 | --- | 19 -28 | ok |
| İşbankası Bayrampaşa | 2 | 4 | 1978 | 12 | I | 20 x 60 | ok | 15 - 20 | ok | 20 x 50 | ok | 10 - 30 | ok |
| İşbakası Küçükyalı | 7 | 2,65 | 1975 | 16 | I | 40 x 15 | ok | 23 - 25 | --- | 35 x 40 | ok | 17 - 20 | --- |
| İşbankası Kavacık | 13 | 3,1 | 1995 | 23 | III | 20 x 100 | ok | --- | --- | 50 x 95 | ok | 18 - 20 | ok |
| İşbankası Mithatpaşa | 9 | 2,64 | 1968 | 8,5 | --- | --- | --- | 15 - 22 | --- | --- | --- | --- | --- |
| İşbankası Kestanepazarı | 4 | 3,12 | 1960 | 14 | I | 23 x 60<br>40 x 30 | --- | 10 - 18 | --- | 25 x 40 | --- | 12 - 28 | --- |

These specimens were planned to be strengthened with different CFRP orientations and number of layers, considering the behavior and cracks pattern of control ones, to find the best technique for decreasing the deficiencies effects. In the final part, the tested and heavily damaged control specimens were repaired by injecting epoxy materials into the cracks and strengthened with CFRP.

The set of experiments can be summarized as:

- Testing of five control specimens designed according to old Turkish design practices which have different reinforcement configuration.

- Testing of three CFRP strengthened specimens which are identical with the poorest control specimen which is TR-5 Control.

- Repairing, strengthening and re-testing the control specimens.

## 2.2. Design of the Test Specimens

In Turkey, most of the buildings were constructed before 1998 according to the provisions of Turkish Earthquake Code (TEC-75). This study aimed to retrofit and improved the behavior of that type of buildings. In this section, the rules applied for the design and detailing of the test specimens are presented, in connection with provisions of the TEC-75. The column and beam members were detailed following the provisions specified by the code. It should be noted that the size of the specimens, member dimensions, and longitudinal reinforcement ratios (influencing capacity) were selected also considering the limitations of the testing facility.

### 2.2.1. Columns

- For rectangular columns cross-sections, the width of the column, $b_c$, was not less than 25 cm, and the ratio of $h_c$ / $b_c$ was not be greater than 3.0.

The column dimensions were selected as 300 x 300 mm and 250 x 250 mm.

- The reinforcement ratio ($\rho$) of the column should not be less than 0.01, and should not be greater than 0.03 for 16 MPa strength- concrete columns. At the lap-spliced region, the reinforcement ratio of the column should not be greater than 0.04 (for C16 type concrete).

  The longitudinal reinforcement ratio of the test specimens were given in Table 2.3.

- The spacing of the transverse reinforcement of the column was considered at three different locations such as (a) at confined region of the column, (b) unconfined region of the column and (c) at beam column joints.

  - Confined Region: The height of the confined region should not be less than (a) greater cross-section dimension of the column, (b) 1/6 of the column height and (c) 45 cm.

    Transverse reinforcement ratio, $\rho_s$, at the confined region of the column should not less than (a) the ratio calculated from Eq (2.1) and (b) 0.01.

$$\rho_s = 0.12 \frac{f'_c}{f_y} \tag{2.1}$$

    where $f'_c$ is concrete compressive strength and $f_y$ reinforcement yield strength. The area of one leg of transverse reinforcement ($A_w$) used in confined region was grater than;

$$A_w = \frac{a \cdot \rho_s \cdot s}{3} \tag{2.2}$$

    where $a$ is the unsupported length of the greater dimension of the transverse reinforcement and $s$ is the spacing of transverse reinforcement.

    At the confined region, less than 8 mm diameter bar should not be used and the spacing of transverse reinforcement should be between 5 cm and 10 cm.

The transverse reinforcements should be hooked with an angle of 135°, and 10 bar diameter in length.

- Unconfined Region: the area of the transverse reinforcements at the mid region should satisfy the maximum shear forces exerted from static and earthquake loading.

  Spacing of transverse reinforcements at this region should not be greater than (a) half of the greater dimension of column cross-section, (b) 20 cm and (c) 12 bar diameter of the smallest longitudinal reinforcement. Column reinforcements should be spliced at the mid region of the column.

- Beam Column Joints: The beam column joint region, as illustrated in Figure (2.1), should be reinforced with transverse reinforcement to satisfy the shear forces at that region. The forces on the internal beam column connections were also indicated in Figure (2.1).

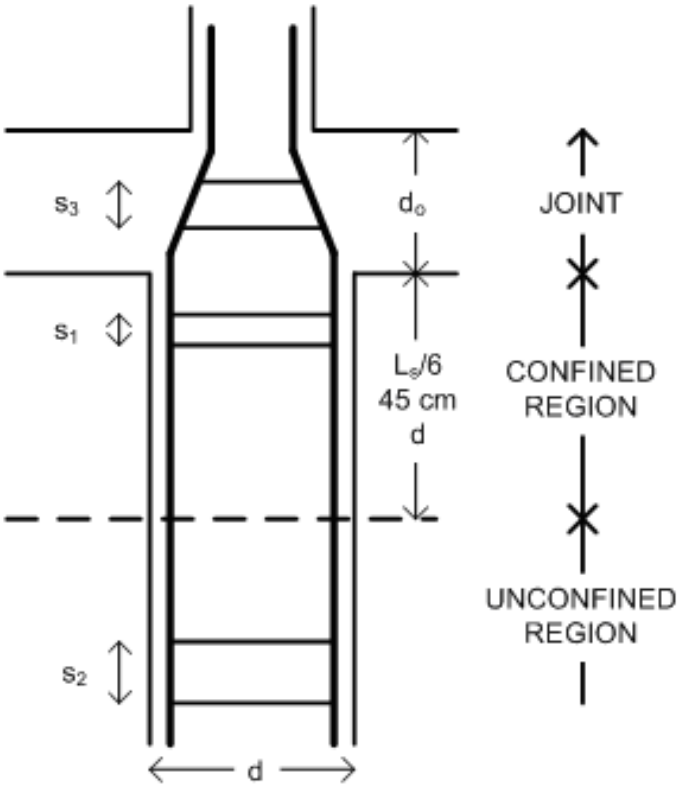


Figure 2.1. Reinforcements and forces at beam column joint

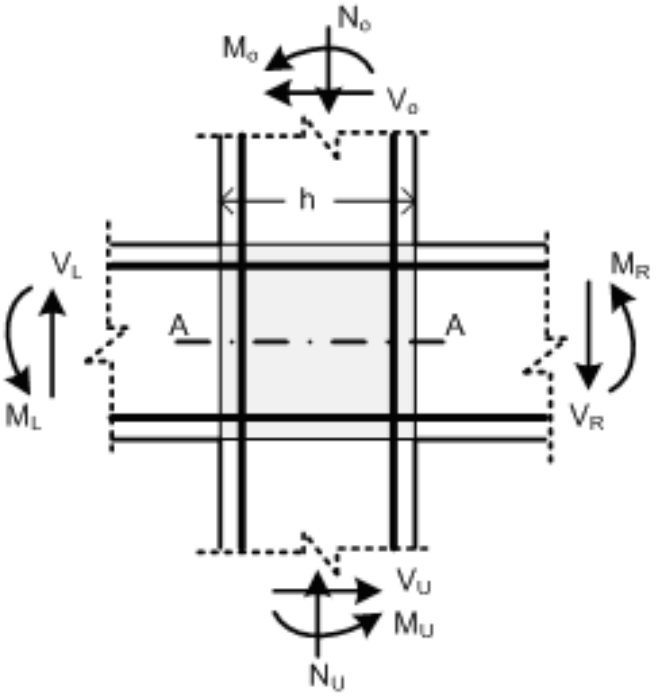


Figure 2.2. Reinforcements and forces at beam column joint

The joint shear forces, $V_j$, can be determined from Eq. (2.3).

$$V_{jh} = -\frac{M_r}{z_r} + \frac{M_l}{z_l} - V_o \tag{2.3}$$

where $M$ values are the beam moments and $z$ values are the level arm of the beams. In exterior beam column joints, one of the $M$ values was zero. From the $V_{jh}$ shear force, the shear strength of the concrete can be calculated as;

$$v_c = \frac{V_{jh}}{b \times z} \tag{2.4}$$

and should satisfy the Eq (2.5).

$$v_c \le 2.5\sqrt{f_c'} \quad (\text{kg/cm}^2) \tag{2.5}$$

$$v_s = \beta \cdot v_c \tag{2.6}$$

where $v_s$ is the shear strength or transverse reinforcements and $\beta$ can be calculated from Eq. (2.7).

$$\beta = \left[ 1 - \frac{0.62}{v_c} \sqrt{\left( 1 + 0.06 \frac{N_o}{A_b} \right) \cdot f_c'} \right] \tag{2.7}$$

where $N_o$ is the minimum axial forces, $A_b$ is the cross-section area of concrete. (unit of the values should be *cm* and *kg* for Eq. (2.7)).

The number of transverse reinforcements per unit length in the joint region should not be less than that of in the unconfined region of the column.

### 2.2.2. Beams

- Minimum cross-sectional dimensions of the beam were 20 x 30 cm.

  In test specimens the dimensions of the beams were 300x500 mm and 250x500 mm.

- Minimum longitudinal reinforcement ratio was given in Table (2.2).

Table 2.2. Minimum longitudinal reinforcement ratio

| | St-I | St-II | St-III |
|---|---|---|---|
| $\rho_{l\text{-}min}$ | 0.005 | 0.004 | 0.003 |

- For doubly reinforced beams, the reinforcement ratio for compression reinforcements should not be greater than (a) 0.01 and (b) half of tensile reinforcement ratio. For single reinforced beams, at least 2ϕ12 rebar should be used in compression region of the beam.

- Longitudinal reinforcements of the beam should not be spliced at tension region or the region with high shear stresses. Otherwise, the spliced region should be confined as defined in Eq. (2.1).

- In exterior beam-column connections, the beam longitudinal reinforcements should be bent with 90° angel and anchored to the columns with an anchorage length as illustrated in Figure (2.3).

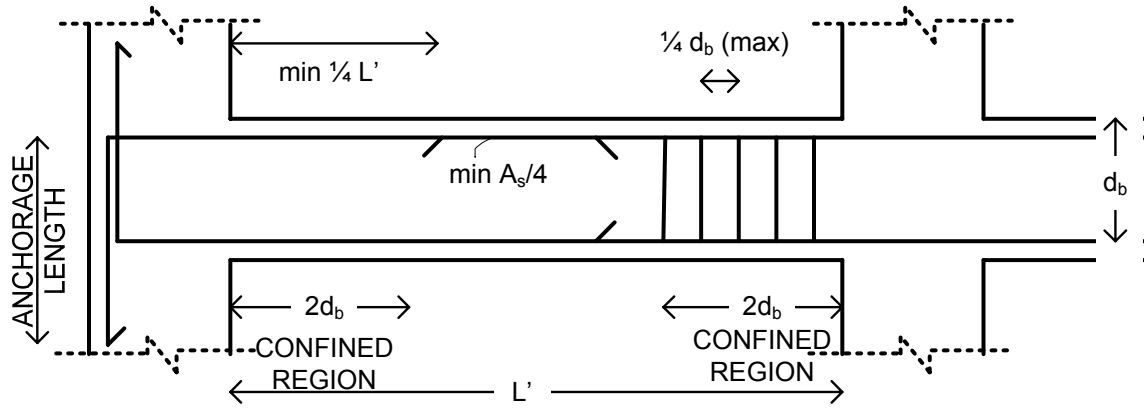


Figure 2.3. Beam reinforcement details

- The diameter of the transverse reinforcements should not be less than 8 mm. Spacing of the transverse reinforcement should not be greater than (a) width of the beam and (b) half of the height of the beam cross-section.

- Transverse reinforcements area should be greater than $A_{w\text{-}min}$ , calculated in Eq (2.8), at the confined region of the beam, which is equal to the two times of height of the beam.

  Moreover, spacing of transverse reinforcement should not be greater than the quarter of the height of the beam. The distance of first transverse reinforcement from the column face should not be greater than 5 cm.

$$A_{w-\min} = 0.15\frac{s}{d_b}A_s \tag{2.8}$$

## 2.3. Properties of Specimens and Test Parameters

Test specimens were designed as an exterior joint of a multi-story building. The specimen was a part of that kind of building extract from the zero moment points. The

height of the column was 2500 mm and the cross-section of the column was 300 mm x 300 mm. The length of the beam from the column face was 1850 mm, and it had 300 mm x 500 mm cross-section. The reinforcement was selected according to the flexural ratio of beam-to-column which is about 1.1. In other words, moment carrying capacity of column was marginally higher than that of beam. The moment distribution of the frame subjected to the lateral load was indicated in Figure 2.4. The dimensional details of the specimen are illustrated in Figure 2.5.

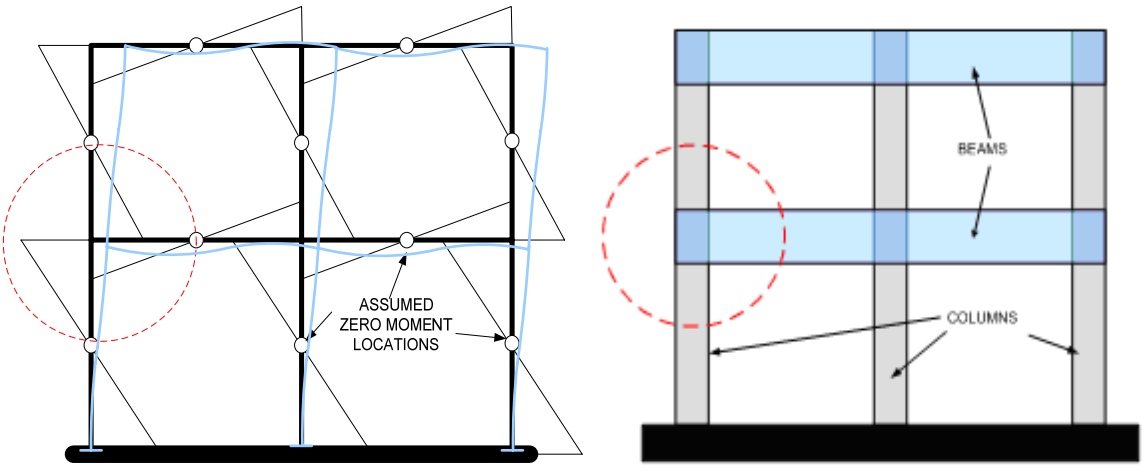


Figure 2.4. Moment diagrams and selecting a specimen

The aim of this study is to investigate the behavior of existing beam-column specimens which have deficiencies such as lacking of transverse reinforcement in joint and beam and column part, insufficient lap-splice length, bond problems of plain re-bars, applied in practice and find the proper technique for strengthening.

In the first part of the study, five control specimens were constructed and tested without any strengthening applied. The first one, which was called Specimen TR-1 Control (Figure 2.6), was the ideal one, detailed to satisfy the requirements of the TEC-75 [60]. In the next specimens (TR-2 Control, TR-3 Control, TR-4 Control and TR-5 Control) the deficiencies got from the survey were implemented one by one to each specimen. These test series shows the effects of the deficiencies on the behavior of beam-column joints under the earthquake loading. According to the test results of the control specimens, one of the worst behaved specimens was selected as a most critical one. Specimen TR-5 Control, including all the deficiencies, behaved worst during the experiments.

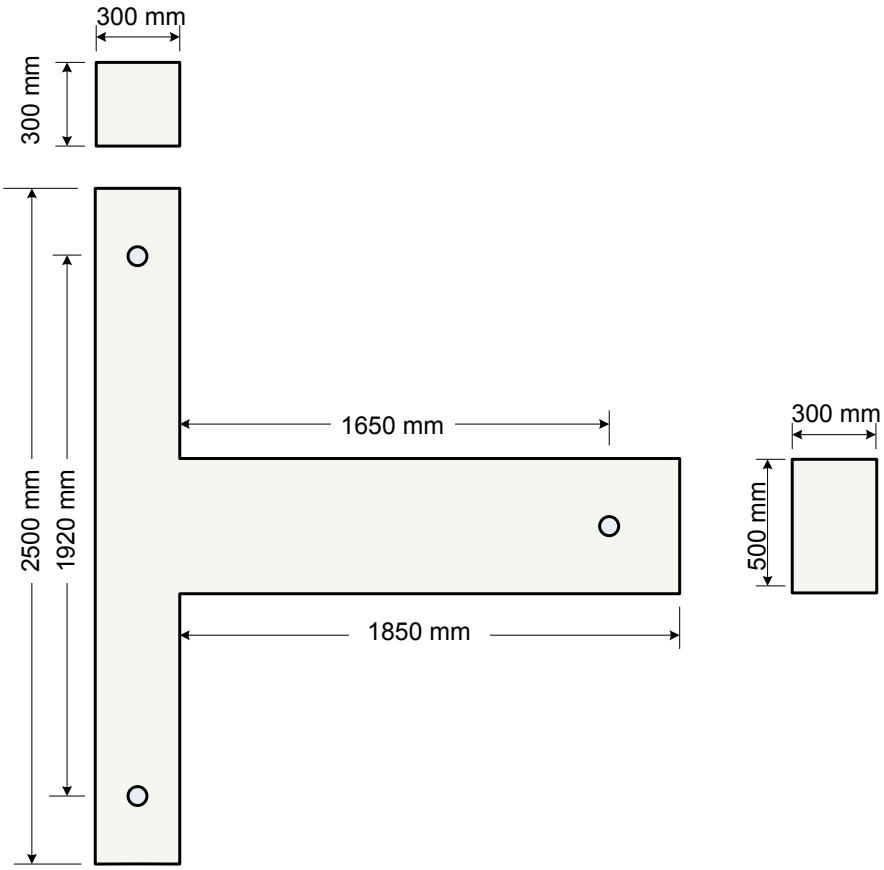


Figure 2.5. Test specimen

Three more specimens were produced identical with the specimen TR-5 Control in the second part of the study. These three new specimens were used for determining the proper CFRP wrapping orientation for strengthening. The first one was strengthened with CFRP considering the crack patterns, damages and failure mechanisms occurred in TR-5 Control specimen test. For the next 2 identical specimens, the strengthening technique was modified step by step considering the test results, damages and failure mechanisms of previous tests. Finally the effective strengthening technique was obtained for deficient beam column joint specimens.

In the last part of the study, the damaged regions were repaired by using chemical epoxy injection method in all of the control specimens. Also, two of the repaired specimen (Specimens TR-2 Control and TR-4 Control) were strengthened with CFRP following the strengthening procedure described in the second part. In Figure 2.6 and Table 2.3, the test parameters investigated for each specimen and the properties of the test specimens were summarized respectively.

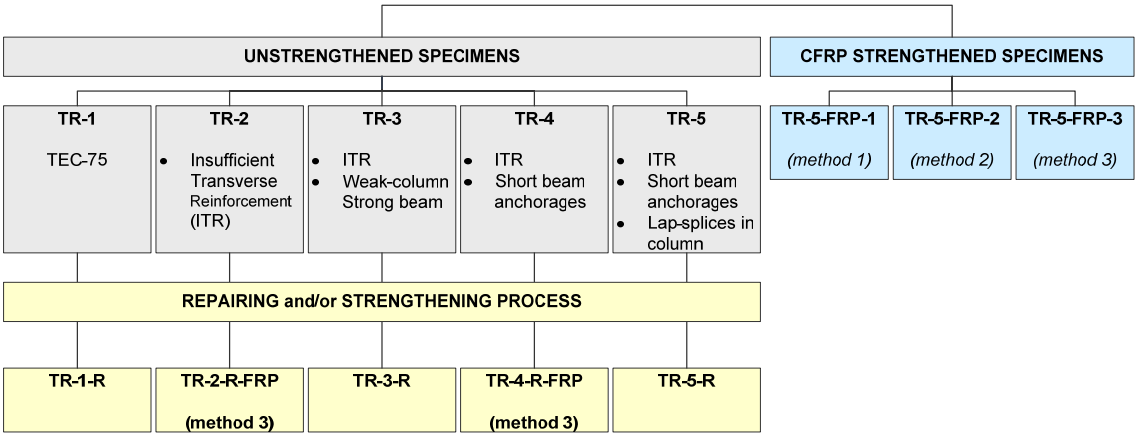


Figure 2.6. Test parameters

Table 2.3. Properties of the test specimens

| Specimen | Strengthening Technique | Column Longitudinal Reinforcement | Beam Longitudinal Reinforcement | $f'_c$ (MPa) | $f_y$ (MPa) |
|---|---|---|---|---|---|
| TR-1 | NA | 4ϕ16 $\rho$=0.01 (For TR-3 $\rho$=0.013) | 9ϕ16 | 15.3 | 280 |
| TR-2 | NA | | 9ϕ16 | 12.8 | |
| TR-3 | NA | | 7ϕ16 | 13.5 | |
| TR-4 | NA | | 9ϕ16 | 14.8 | |
| TR-5 | NA | | 9ϕ16 | 14.2 | |
| TR-5-FRP-1 | Method-1 | | 9ϕ16 | 14.6 | |
| TR-5-FRP-2 | Method-2 | | 9ϕ16 | 16.0 | |
| TR-5-FRP-3 | Method-3 | | 9ϕ16 | 16.0 | |
| TR-1-R | Repairing | | 9ϕ16 | 15.3 | |
| TR-2-R-FRP | Repairing+Method-3 | | 9ϕ16 | 12.8 | |
| TR-3-R | Repairing | | 7ϕ16 | 13.5 | |
| TR-4-R-FRP | Repairing+Method-3 | | 9ϕ16 | 14.8 | |
| TR-5-R | Repairing | | 9ϕ16 | 14.2 | |

### 2.3.1. Flexural Capacity of Members

During the design process of the test specimens, sectional (moment versus curvature) analyses were conducted for the beam and the column (under 30 % $A_g f'_c$ axial load) sections of the test frames, using the software "Response 2000: Reinforced Concrete Sectional Analysis" [61]. The properties of beam and column cross-sections and the results of the sectional analyses were shown in Figure 2.7.

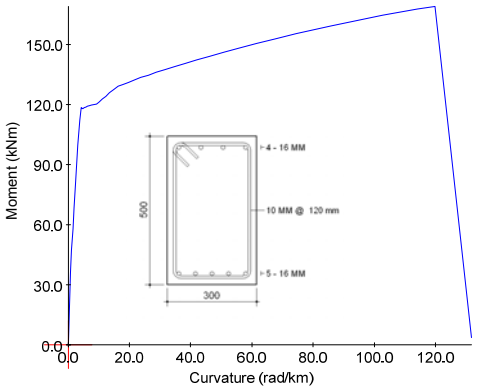


(a) Moment-curvature relationship of beam (dimension 300x500)(pull direction)

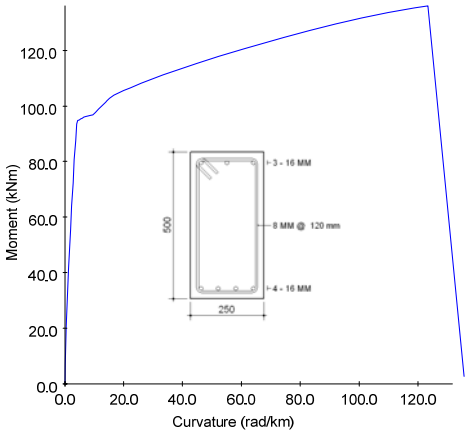


(b) Moment-curvature relationship of beam (dimension 250x500)(pull direction)

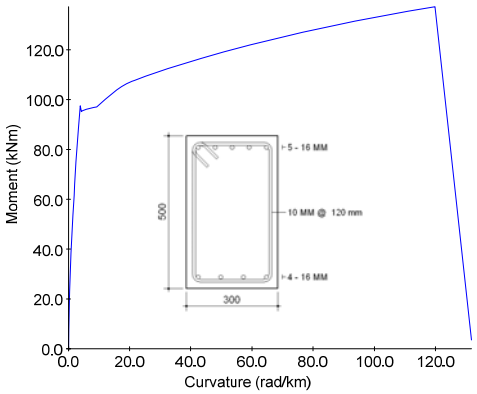


(c) Moment-curvature relationship of beam (dimension 300x500)(push direction)

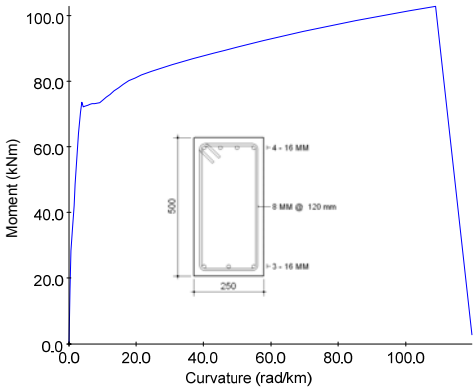


(d) Moment-curvature relationship of beam (dimension 250x500)(push direction)

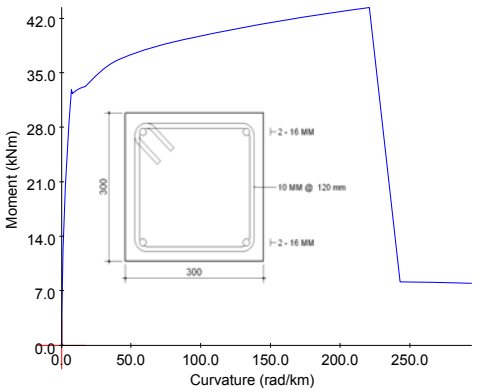


(e) Moment-curvature relationship of column (dimension 300x300)

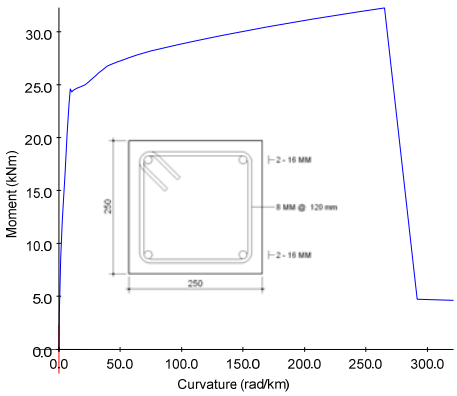


(f) Moment-curvature relationship of column (dimension 250x250)

Figure 2.7. Flexural capacity analysis of beam and column sections

## 2.4. Material Properties

### 2.4.1. Concrete

Since low-quality concrete was intended to use, concrete mix was prepared in laboratory condition. The concrete mix design was given in Table 2.4. Nine samples of concrete cylinders, with a diameter of 150 mm and height of 300 mm, were taken from each specimen. Nominal compressive strengths of cylinder specimens were determined in accordance with ASTM C39-96 [62]. The samples were tested on $7^{th}$ day, $28^{th}$ day and the day that the experiments were conducted (Figure 2.8 ). Out of three cylinder specimens that were tested on the testing day, an average compressive strength was obtained for each beam-column joint specimen.

Table 2.4. Concrete mix design values

| **Materials** | **Weight per $m^3$ ($kg/m^3$)** |
|---|---|
| Cement (PC-32.5) (Akçansa) | 450 |
| Water | 270 |
| Crushed Stone No I (Sandstone) | 535 |
| Crushed Stone No II (Sandstone) | 304 |
| Sand (Crushed Stone) | 384 |
| Sand (Sea Sand) | 294 |

Figure 2.8. Compression tests of concrete cylinders

### 2.4.2. Reinforcing Bars

Plain bars with a diameter of 16 mm were used for longitudinal reinforcements of the columns and the beam. Also, plain bars with a diameter of 10 mm were used as a transverse reinforcement. In addition, stress versus strain relationships the reinforcements were given in Figures 2.9. Table 2.5 indicates the characteristic properties of reinforcement. As seen in Figure 2.10, tensile tests performed in accordance with ASTM A706 / A706M-06a [63] on each reinforcing bars resulted as an average tensile strength of 280 MPa, which is very close to what the steel mill's strength values are.

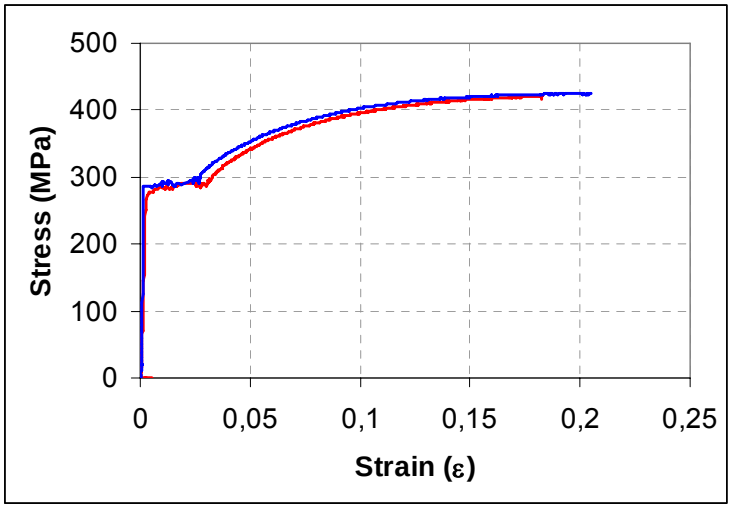


Figure 2.9. Stress-strain relationships for ϕ16 reinforcements

Figure 2.10. Tensile test of plain re-bars

Table 2.5. Characteristic properties of reinforcements

| Bar Diameter | Yield Strength, $f_y$, (MPa) |
|---|---|
| ϕ 16 -plain | 280 |
| ϕ 10 -plain | 280 |

### 2.4.3. Carbon Fiber Reinforced Polymers (MBrace Fiber –C1-30)

Fiber reinforced polymer (FRP) is the composite material that reinforced with fibers. The most common fibers were Glass, Kevlar / Aramid, and Carbon. Carbon fiber reinforced polymer (CFRP) materials are widely used in different areas due to their excellent properties such as low weight, high strength and modulus, resistance to corrosion, ease of application and minimum disturbance to the dwellers. Also, it has some disadvantages such as low fire resistance, weakness to ultraviolet light and some chemicals and moisture. In this research, CFRP materials were used in order to determine contributions to the existing structure. In strengthened specimens, different CFRP wrapping orientation and different number of CFRP layer will be applied considering the damage and crack pattern occurred in control specimens. Properties of CFRP are given in Table 2.6 and stress strain relationship is given in Figure 2.11. Properties of the CFRP sheets were taken from the manufacturer data sheet.

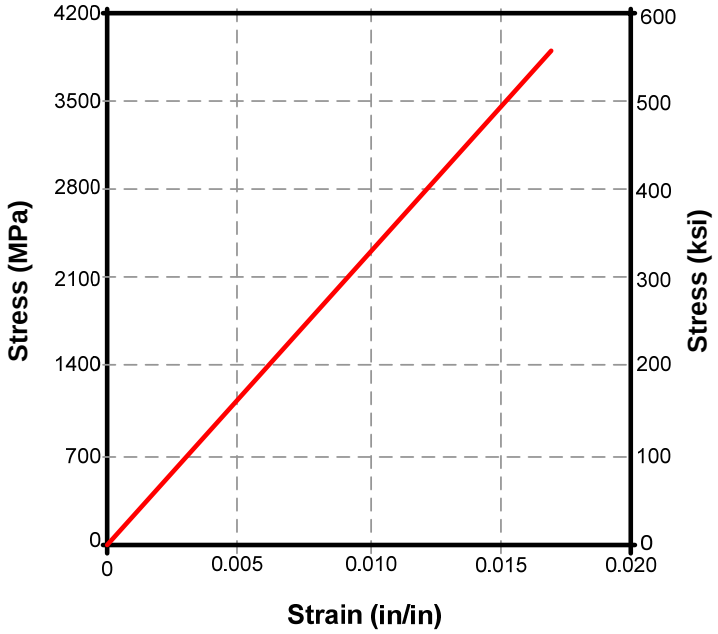


Figure 2.11. Stress-strain relations of CFRP sheets

Table 2.6. Properties of CFRP.

| | |
|---|---|
| Nominal Thickness | 0.176 mm/ply |
| Ultimate Tensile Strength ( 0°) | 3800 MPa |
| Tensile Modulus ( 0°) | 240 GPa |
| Ultimate Rupture Strain ( 0°) | 1.55% |
| Weight | 330 g/m$^2$ |

### 2.4.4. MBT MBrace Primer

Before the application of the CFRP sheets, primer was used for improvement of adherence between the CFRP sheets and the concrete surfaces. It was applied 24 hour before the installation of CFRP wrapping. To obtain a good adherence, the surface must be cleaned of dust before the application of MBrace Primer. And also after the application of primer, it should be kept clean. Table 2.7 illustrates the properties of Primer

Table 2.7. Properties of primers

| | |
|---|---|
| Tensile Strength | >12 MPa |
| Bending Strength | >24 MPa |
| Maximum elongation | 3% |
| Modulus of Elasticity (Tensile) | >700 MPa |
| Modulus of Elasticity (Bending) | >580 MPa |

### 2.4.5. MBT MBrace Adesivo (Saturant)

FRP sheets were applied to the beam-column joint with two-component epoxy based high strength adhesives. Technical properties which are taken from the manufacturer data sheet are given in Table 2.8. The curing time of the mix was about 7 day in room temperature.

### 2.4.6. Repairing Materials

The following repair materials were used to repair damage after the testing of control specimens.

Table 2.8. Properties of adhesives

| | |
|---|---|
| Compressive Strength ( 7 day ) | >60 MPa |
| Flexural Strength ( 7 day ) | >50 MPa |
| Bond Strength( Concrete ) | >3 MPa |
| Modulus of Elasticity ( Tensile ) | 3000 MPa |
| Modulus of Elasticity ( Bending ) | 3500 MPa |

Concresive 1495: This type of epoxy-based repairing material, produced by BASF, was generally used for anchorages but here it was used for filling the wide cracks at the joint region. Also the nipples which will be used for injection were fixed with Concresive 1495.

Concresive 1406: This type of epoxy based repairing material produced by BASF is used for replacing with all loose concrete at the joint region. Before the application of injection, joint core is covered with Concresive 1406. Mechanical properties of Concresive 1406 are given in Table 2.9.

Table 2.9. Properties of Concresive 1406

| | |
|---|---|
| Application Thickness | 2 mm – 30 mm |
| Bending strength | 25 MPa (7 days) |
| Compressive Strength ( 20°) | 75 MPa (7 days) |
| Bond Strength (concrete) | 3.0 MPa |
| (steel) | 3.5 MPa |

Emaco S88C: Cement-based repairing material, produced by BASF, was used for preparing the surface before the application of injection. All the loose concrete was replaced with Emaco S88C at the joint region. Mechanical properties of Emaco S88C are shown in Table 2.10.

Concresive 1302: Used for repairing up to 1 mm width cracks by injecting, produced by BASF. Due to its low viscosity characteristic, it can penetrate into hairline cracks with low pressure. Table 2.11 shows the mechanical properties of Concresive 1302.

Table 2.10. Properties of Emaco S88C

| | | |
|---|---|---|
| Application Thickness | | Min. 10 mm |
| Tensile Strength ( 20°) | | 3.6 MPa (28 day) |
| Compressive Strength ( 28 day, 23°) | | >60 MPa |
| Tensile Strength ( 28 day ) | | >7 MPa |
| Bond Strength ( Steel ) | < | 14 MPa ( smooth bar )<br>30 MPa ( ribbed bar ) |
| Bond strength ( Concrete ) | | >2 MPa |
| Modulus of Elasticity ( 0°) | | >20 GPa |

Table 2.11. Properties of Concresive 1302

| | |
|---|---|
| Viscosity | 200-350 MPa |
| Compressive Strength ( 20°) | >65 MPa ( 7 day ) |
| Flexural Strength | >25 MPa ( 7 day ) |
| Bond Strength ( Concrete ) | >2.0 MPa ( 7 day ) |
| Application Thickness | 0.2 – 1.0 mm |

## 2.5. Testing Methodology

Test will be performed according to ACI T1 [64] document. Minimum requirements of the test procedure can be summarized as follows:

- Test modules shall be subjected to a sequence of displacement-controlled cycles representative of the drifts expected under earthquake motions for that portion of the frame represented by the test module. Cycles shall be to predetermined drift ratios.

- Three fully reversed cycles shall be applied at each drift ratio. (Figure 2.12)

- The initial drift ratio shall be within the essentially linear elastic response range for the module. Subsequent drift ratios shall be to values not less than one and one-quarter times, and not more than one and one-half times, the previous drift ratio.

- Testing shall continue with gradually increasing drift ratios until the drift ratio equals or exceeds 0.035.

- Data shall be recorded from the test such that a quantitative, as opposed to qualitative, interpretation can be made of the performance of the module. A continuous record shall be made of test module drift ratio versus column shear force, and photographs shall be taken that show the condition of the test module at the completion of testing for each sequence of three cycles.

### 2.5.1. Test Setup and Instrumentation

The test specimens were located on strong floor attached by high strength bolts. Lateral and vertical loadings were applied throughout the test. The reversed cyclic lateral load was applied from the top of the column based on the displacement-control criteria with a 250 kN-capacity dynamic actuator, mounted on a steel reaction wall. Three cycles of the same amplitude in every story drift were repeated before displacement amplitude increased. The loading cycles were shown in Figure 2.12. Approximately 35-40 reversed cycles, depending on the behavior of the specimen, were applied throughout the test. All data was collected with a TML 602, 50 Hz. and 60-channel data acquisition system. Observations on cracks on concrete surface, CFRP fractures and debonding, and failure modes were recorded in each of 3-cycle loading set.

The loading set up was shown in Figure 2.14. The specimens were tested in a test setup where beam was placed parallel to the strong floor and they were roller and hinged at the free end of the beam. The column was placed in vertical position and supported by a universal pin at the bottom end. Constant axial load was applied vertically from the top of the column by a load-control loading system with a 900 kN-capacity hydraulic cylinder. The amount of the axial force applied was $40\% f'_c A_g$ where $f'_c$ was the characteristic strength of concrete and $A_g$ was the gross cross-sectional area of column. For preventing the possible out of plane deformations, a steel frame was constructed. The rollers, at the tip of the frame release the movements in plane direction. Simplified free body diagram of the specimens was shown in Figure 2.13.

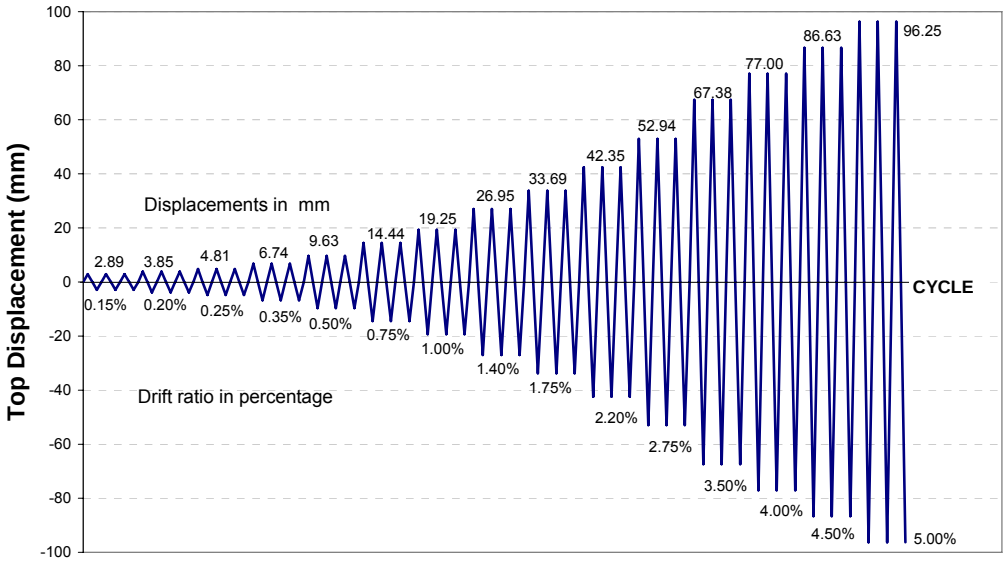


Figure 2.12. Loading protocol

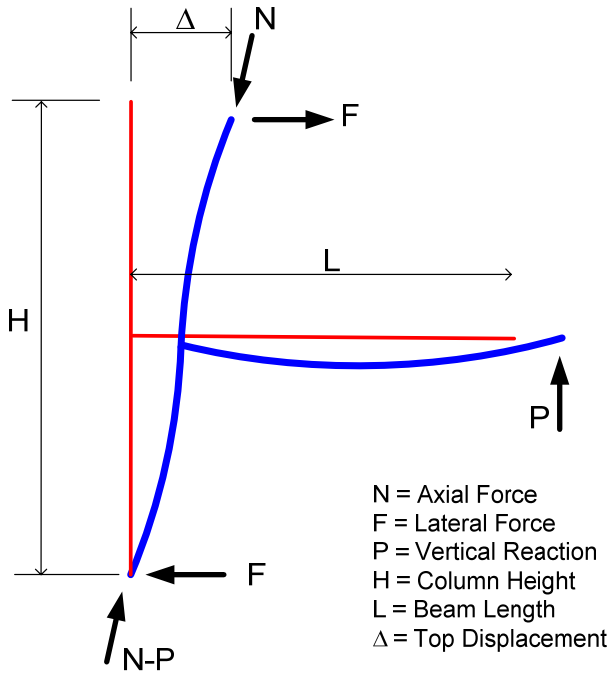


Figure 2.13. Free body diagram of test specimens

A total of 11-strain gauges, which were shown in Figure 2.15, were mounted on the reinforcing bars to gather the strain values during the experiments. All of these strain gauges were connected to the data acquisition system. In addition to the strain gauges, displacement at the tip of the column and the shear deformation in beam-column joint, and curvature readings on the beam and columns at or close to the maximum moment regions

were monitored and measured by Linear Variable Displacement Transducers (LVDT ) and their data was also transferred to the same data acquisition system. To measure the net top displacement value, support movements also monitored. Overall, each data was recorded with 4-second intervals. LVDT locations were shown in Figure 2.15.

Also, for the CFRP strengthened specimens, 10-strain gages which were appropriate for composites, were mounted on the fibers in order to obtain the strain values during the tests.

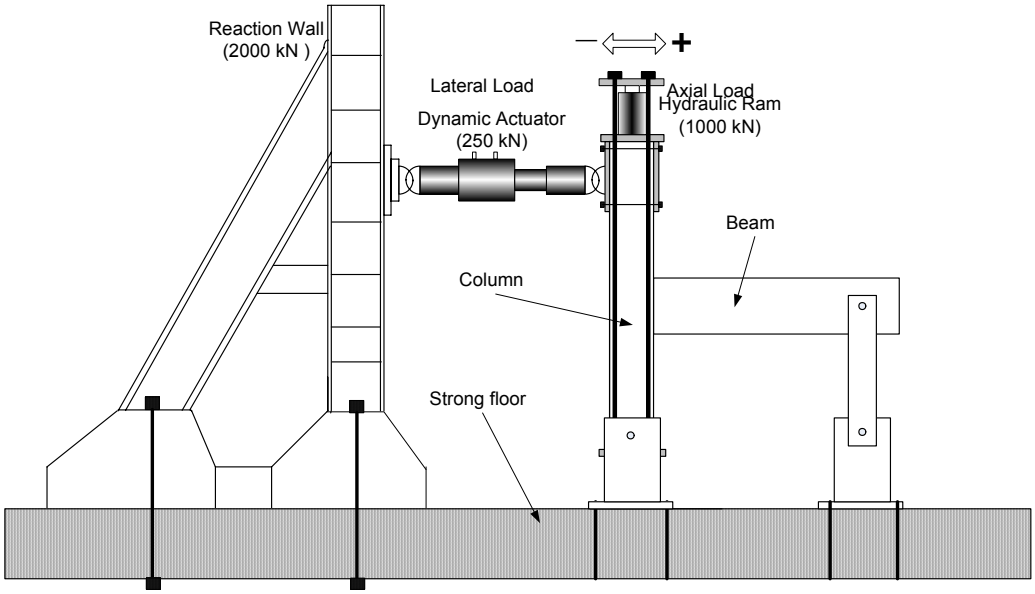


Figure 2.14. Test setup

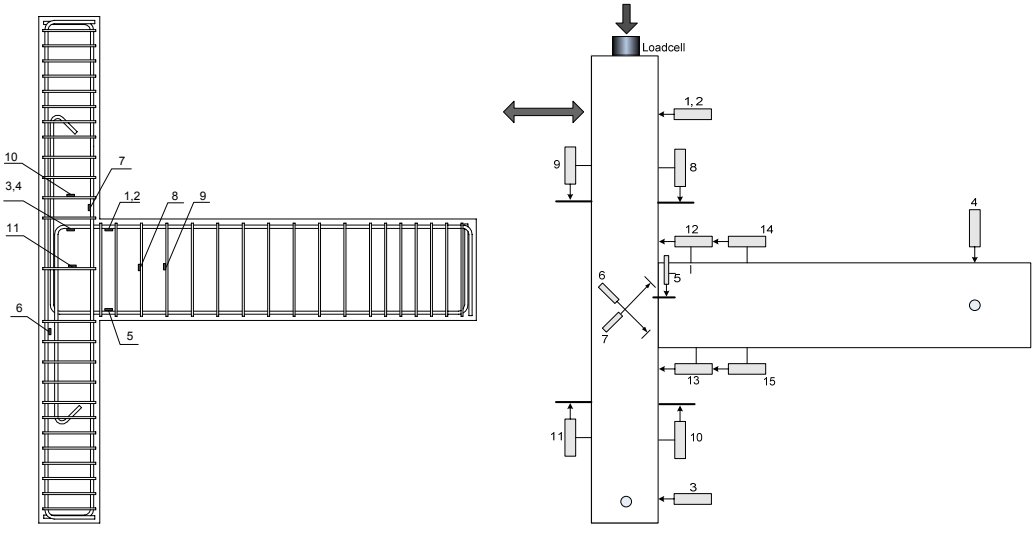


Figure 2.15. Location of strain gages and dial gages

## 2.6. Retrofitting Methodology

Installation of CFRP sheets need special care and can only be carried out by trained technicians. When combined with epoxy, CFRP sheets become very strong in tension. CFRP wrapping provides excellent passive type of confinement effect to the reinforced concrete member [65, 66]. Application of CFRP is illustrated in Figure 2.17. The procedure for installing the CFRP sheets is as follows:

### 2.6.1. Surface Preparation

As a first step, all the faces of beam-column joints beam and column regions were smoothened. The corners were rounded at about 20 mm radius, since increasing the radius of corners increases the confinement effects of CFRP [67]. All large gaps on surface were filled with putty (Concresive 1406), large particles were removed, and the area which was going to be wrapped was cleaned with a wire brush. Finally the surface of the concrete was cleaned up and then vacuumed to obtain a clean surface.

A primer (MBrace Primer) which helps to the adhesion between the CFRP and the concrete was applied to the surface with a roll brush. A 24 hour curing time was passed prior to application of CFRP wrapping, (Figure 2.16).

Figure 2.16. Surface preparation and application of MBrace Primer.

### 2.6.2. CFRP Application

After the primer was cured, two component-epoxy adhesive of CFRP, MBrace Adesivo (Saturant), was prepared and CFRP fabrics were installed on the beam-column joint region. It was made sure that, no air pockets remained under the sheets. It should be noted that the epoxy mixed has about 30 minute working time before it gets hot and dense (Figure 2.17).

The wrapping steps for proposed strengthened methodologies were given in Section 2.8.6 to 2.8.8.

Figure 2.17. CFRP application

## 2.7. Repairing Methodology

After testing of all control specimens, joint region of specimens were heavily damaged. In order to make them re-usable, the joint area should be repaired. The proposed repairing methodology was explained below step by step.

### 2.7.1. Surface Preparation

As a first step, loose concrete was removed from the damaged region of the specimen. The surface of the region that is going to be repaired should be cleaned. All the wide cracks should be free of dusts. Several holes were drilled and check valve nipples were located along the crack on both sides of the specimen. These nipples will be used for injecting fine epoxy into the joint. The big visible cracks were filled with epoxy based high strength repairing material, Concresive 1495. After than, all the surface of the damaged region were covered with Concresive 1406. Once it gets hard, the damaged region was totally covered with cement based repairing material, Emaco S88C (Figure 2.18. ), in order to obtain a smooth surface.

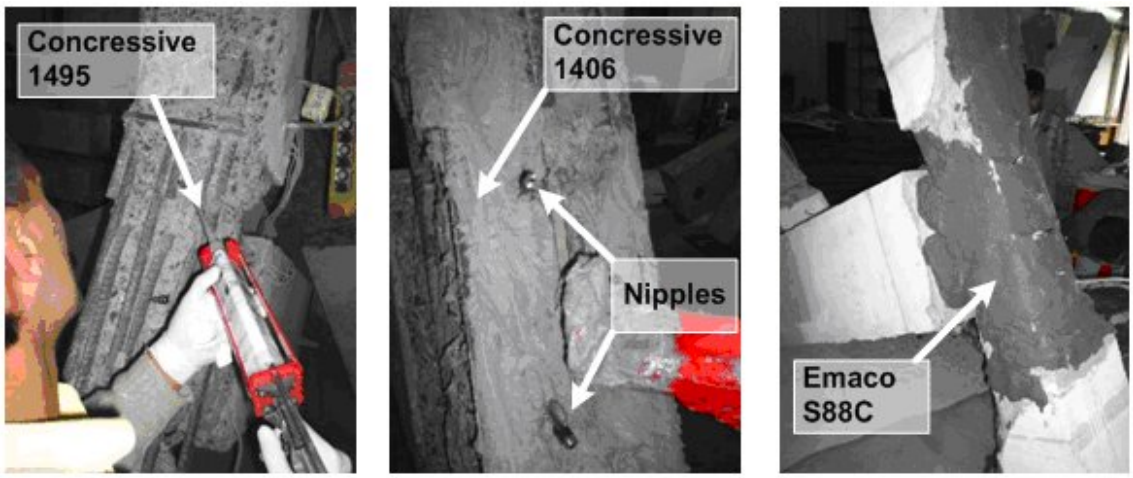


Figure 2.18. Pictures from repairing application

### 2.7.2. Epoxy Injection

After the surface preparation finished and the epoxies were cured, low-viscosity epoxy (Concresive 1302) was injected with 120 bar pressure through the nipples via

special pumps. The pumping procedure was continued until the overflow was observed on the nipples placed on the other sides of the specimen. The photo from repairing technique was illustrated in Figure 2.19.

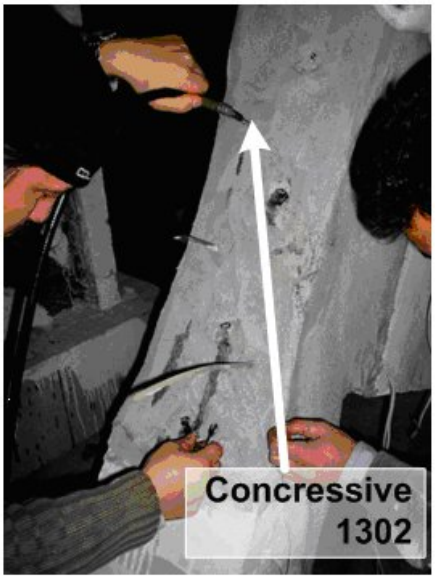


Figure 2.19. Application of epoxy injection

## 2.8. Preparation of Test Specimens

The preparation of the specimen, reinforcement details and repairing and retrofitting methodology of each specimen were explained in this section.

Before the production of the specimens, the surveying about the buildings were carried out. It revealed that the building designed according to the 1975 earthquake code of Turkey, had a lot of deficiencies, such as low quality concrete, plain re-bars and in sufficient transverse reinforcements. In order to apply these deficiencies, all the specimens prepared in Structures Laboratory.

During casting of specimens, vibrators were used to place the concrete. Nine samples of concrete cylinders were taken from each specimen. These samples were tested on $7^{th}$ day, $28^{th}$ day and the day that the experiments were conducted. In order to prevent the failure at the support regions, 7.5 cm spacing of the transverse reinforcements were applied on tip of columns and beam.

### 2.8.1. Specimens TR-1 Control and TR-1-R

Specimen TR-1 Control was produced designed according to detailing provisions of the 1975 Turkish Earthquake Code (TEC-75) [60]. The reinforcement details of TR-1 Control were illustrated in Figures 2.20 and 2.21. 4ϕ16 plain re-bars were used for column longitudinal reinforcement (reinforcement ratio: 1.0%) and 9ϕ16 plain re-bars were used for beam longitudinal reinforcement. Five of them were used on top and remaining four were used at the bottom part. The spacing of transverse reinforcement was selected as 100 mm and 125 mm in column and in beam, respectively. Moreover, two stirrups were used in the joint region to satisfy the requirement in TEC-75. The cylindrical compressive strength of concrete used in TR-1 Control was determined as 15.3 MPa.

Figure 2.20. Picture of Specimen TR-1 Control produced at the laboratory

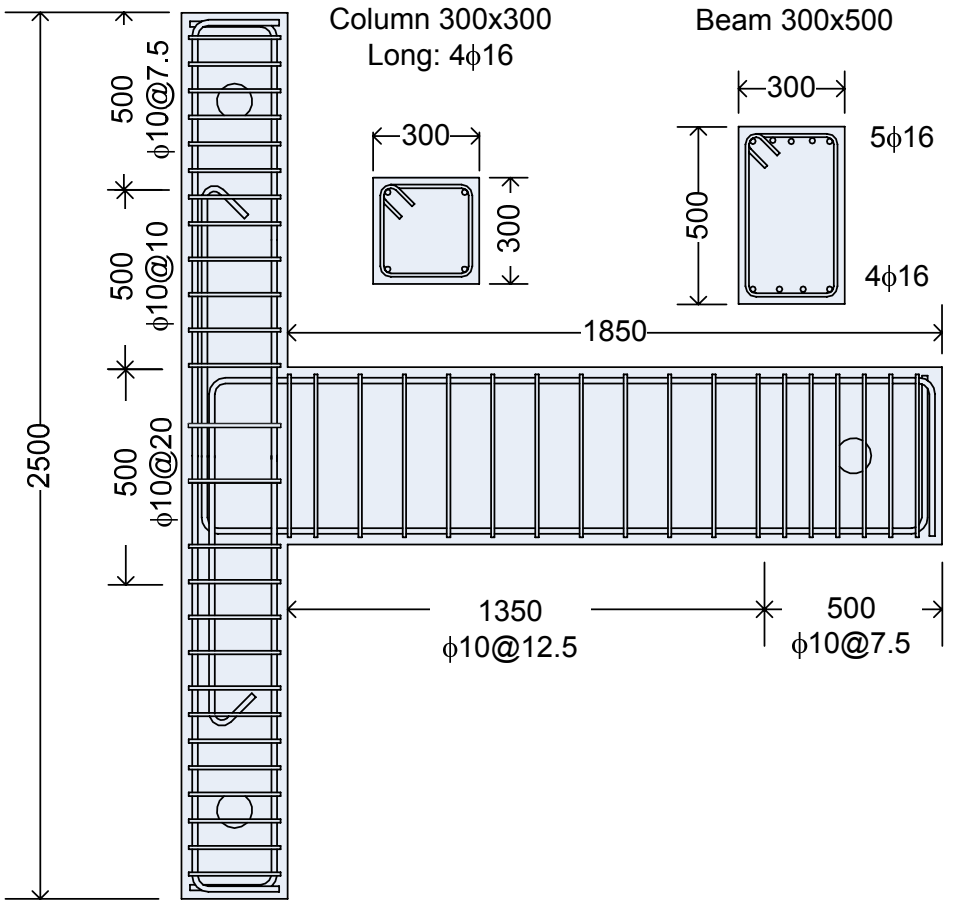


(a)

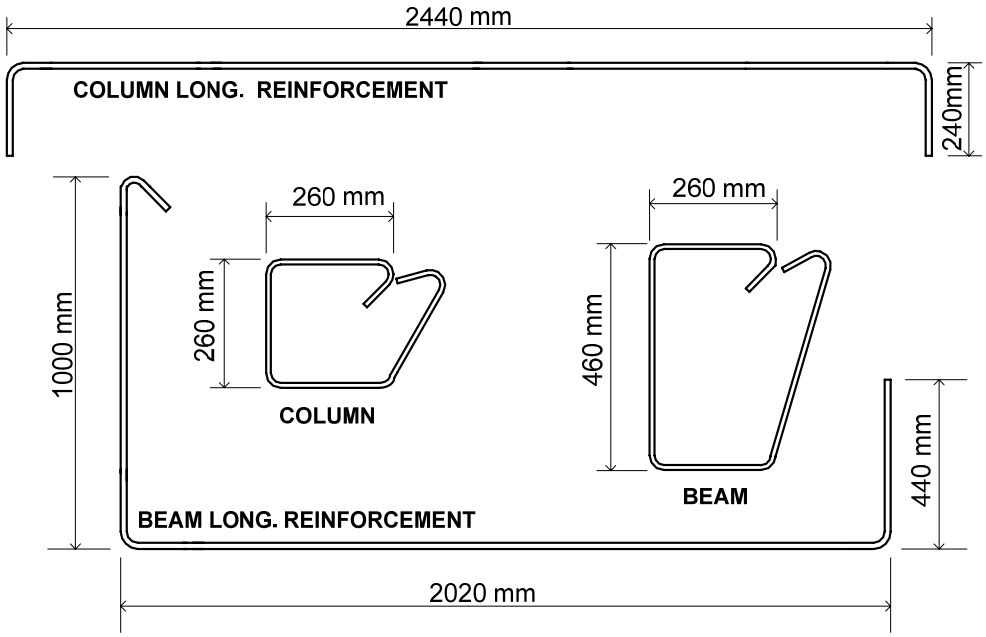


(b)

Figure 2.21. Reinforcement details for Specimen TR-1 Control

After testing of specimen TR-1 Control, the damages were recovered; all the cracks were repaired with chemical epoxy matrix and epoxy injection method as described in Section 2.7 for re-testing. After repairing procedure applied, the specimen was called as specimen TR-1-R.

### 2.8.2. Specimens TR-2 Control and TR-2-R-FRP

Specimen TR-2 Control was also designed according to the requirements of TEC-75 [60] except for amount of transverse reinforcement in beam and column members, also, lacking of stirrups in joint region, which was the most critical deficiency applied in practice. Since there is no room to move hands, it is too hard to put stirrups into the joint region. The dimension and the longitudinal reinforcement details were identical with the TR-1 Control one. In Specimen TR-2 Control, spacing of stirrups was increased to 200 mm in both column and beam. No stirrups were used in joint region. Figures 2.22 and 2.23 clearly show the reinforcement details of specimen TR-2 Control. The cylindrical compressive strength of concrete used in TR-2 Control was determined as 12.8 MPa.


(a)


(b)

Figure 2.22. Pictures from production of Specimen TR-2 Control

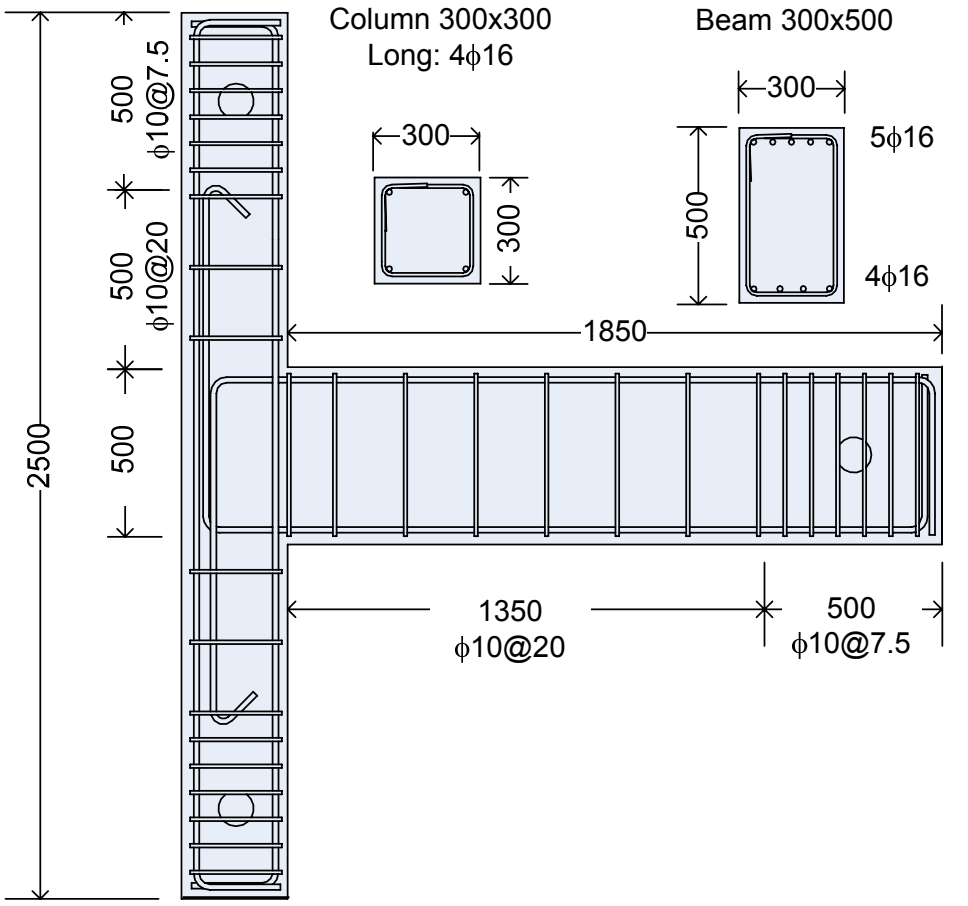


(a)

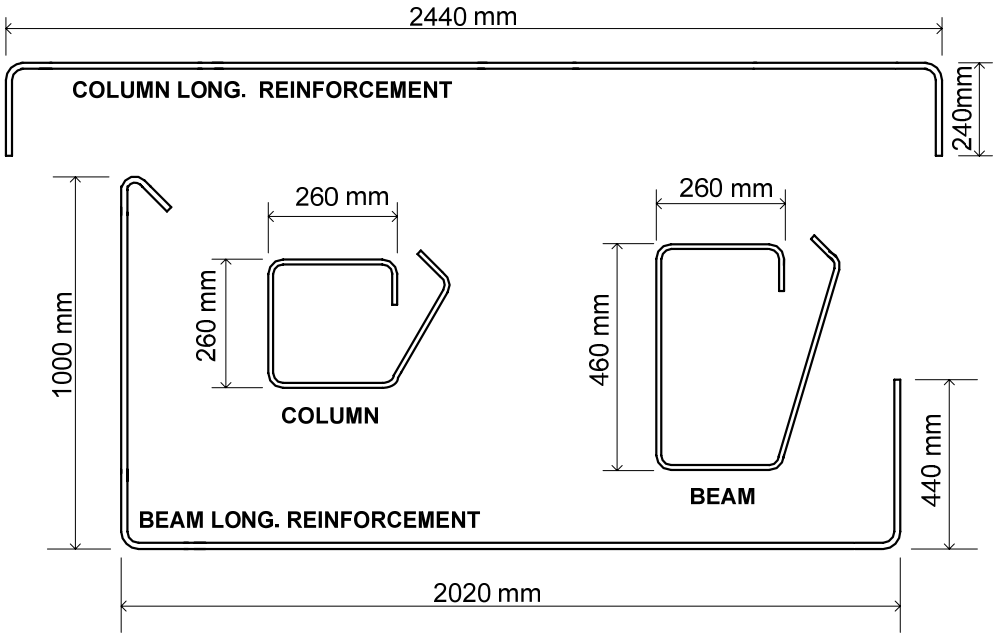


(b)

Figure 2.23. Reinforcement details for Specimen TR-2 Control

After testing of specimen TR-2 Control, all the damages were repaired with chemical epoxy matrix and epoxy injection method described in Section 2.7. And then, it was strengthened with CFRP wrapping described in Section 2.8.8 (Method 3). After repairing and retrofitting procedure, the specimen was called as specimen TR-2-R-FRP.

### 2.8.3. Specimens TR-3 Control and TR-3-R

Specimen TR-3 Control was produced with the same reinforcing detailing of specimen TR-2 Control. In order to obtain different flexural ratio, weaker column and stronger beam, the column dimension was reduced to 250 mm x 250 mm and beam dimension was reduced to 250 mm x 500 mm. All the stirrups were produced from the plain bars with a diameter of 8 mm. Also, 7ϕ16 plain re-bars were used in beam. Figures 2.24 and 2.25 clearly show the internal reinforcement detail of specimen TR-3 Control. The cylindrical compressive strength of concrete used in TR-3 Control was 13.5 MPa.

Figure 2.24. Picture of Specimen TR-3 Control produced at the laboratory

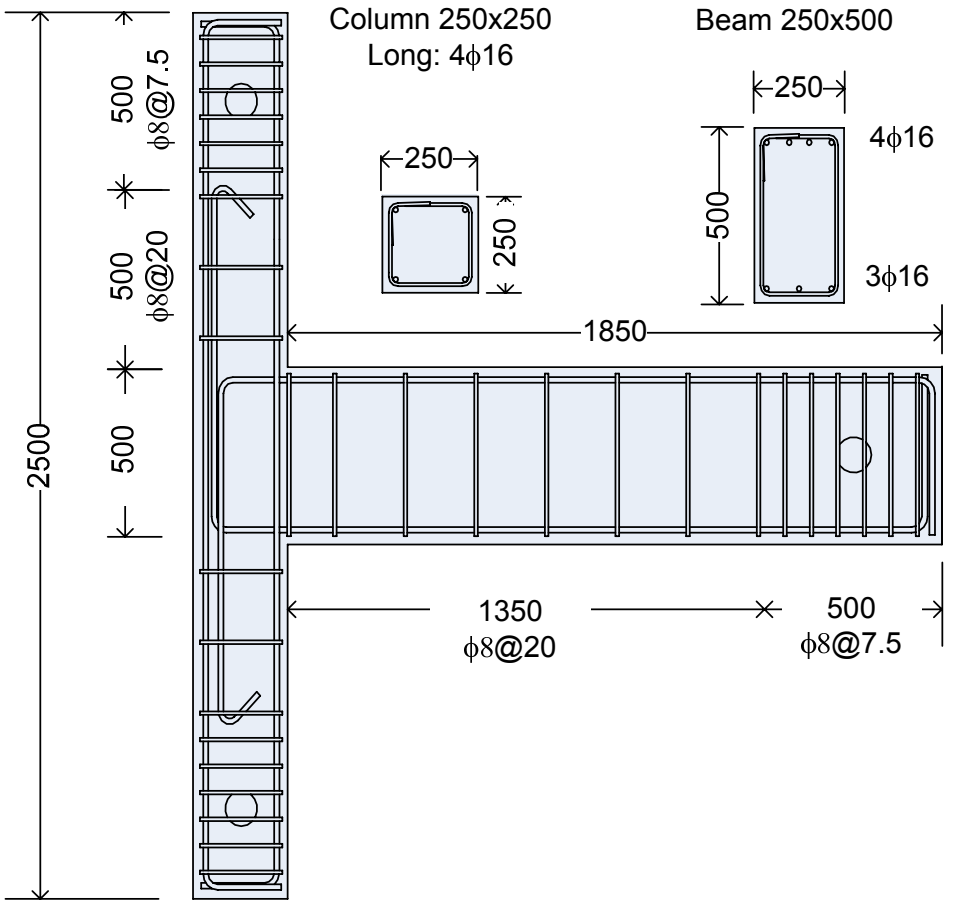


(a)

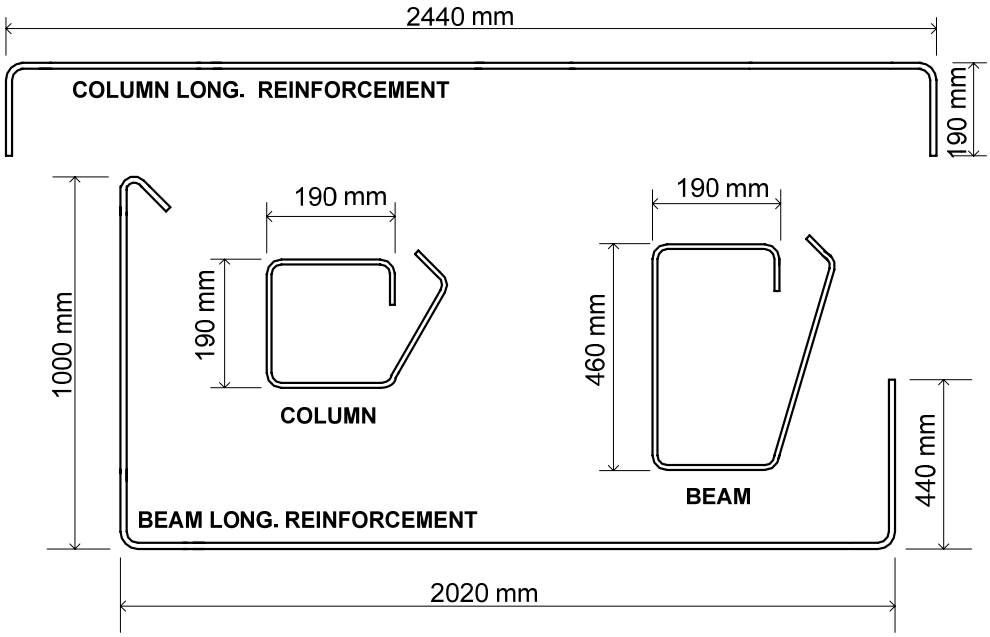


(b)

Figure 2.25. Reinforcement details for Specimen TR-3 Control

After testing of specimen TR-3 Control, all the damages were repaired with chemical epoxy matrix and epoxy injection method described in Section 2.7. After repairing procedure, the specimen was called as specimen TR-3-R.

### 2.8.4. Specimens TR-4 Control and TR-4-R-FRP

Specimen TR-4 Control was produced identical with specimen TR-2 Control except for anchorage length. The parameter investigated in this specimen was the effects of short anchorage length of beam reinforcement. Additional to the deficiencies of sparse transverse reinforcement in column, beam and joint region, the longitudinal reinforcements coming from beam were end up in the joint region. Figures 2.26 and 2.27 clearly show the reinforcement details of specimen TR-4 Control. The cylindrical compressive strength of concrete used in TR-4 Control was determined as 12.7 MPa.

Figure 2.26. Picture of Specimen TR-4 Control produced at the laboratory

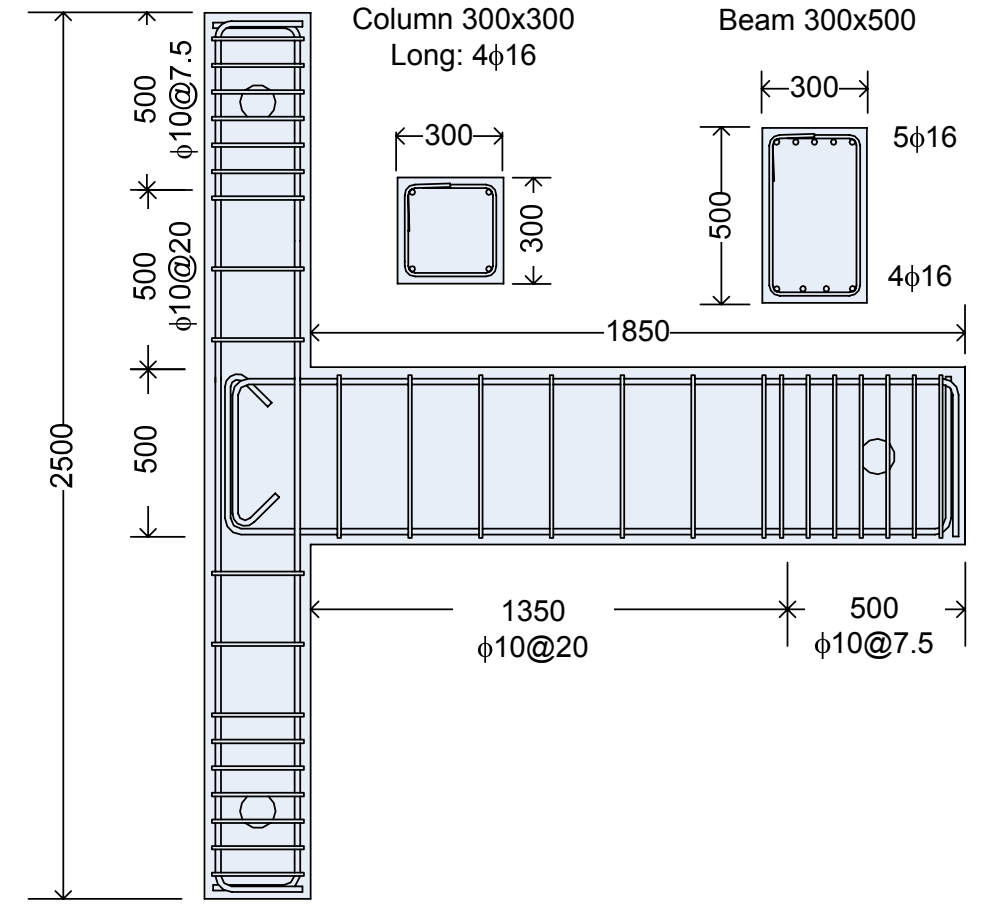


(a)

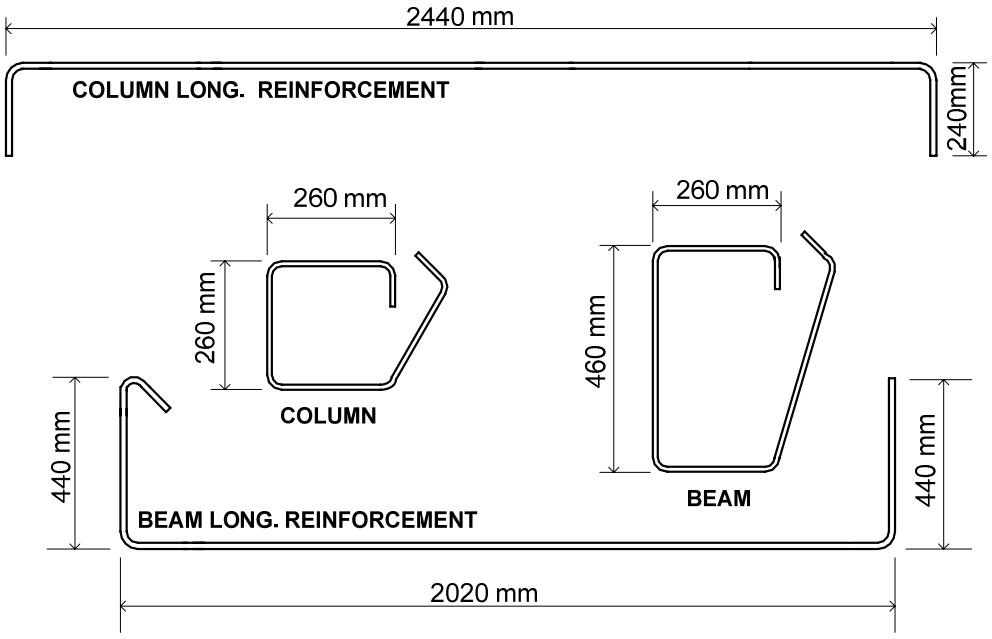


(b)

Figure 2.27. Reinforcement details for Specimen TR-4 Control

After testing of specimen TR-4 Control, all the damages were repaired with chemical epoxy matrix and epoxy injection method described in Section 2.7. And then, it was strengthened with CFRP wrapping described in Section 2.8.8 (Method 3). After repairing and retrofitting procedure, the specimen was called as specimen TR-4-R-FRP.

### 2.8.5. Specimens TR-5 Control and TR-5-R

The main deficiencies, consisted in specimen TR-5 Control, are similar to specimen TR-4 Control, such as widely spaced column and beam ties that provide little confinement to the concrete, no transverse reinforcement in the joint region and short anchorage of beam longitudinal reinforcement except for lap splice length. Main reinforcements were spliced with a length of 500 mm at top column in specimen TR-5 Control. Figures 2.28 and 2.29 clearly show the deficiencies and the reinforcement details of specimen TR-5 Control. Cylindrical compressive strength of concrete was determined as 14.6 MPa.

Figure 2.28. A Picture from Construction of Specimen TR-5 Control

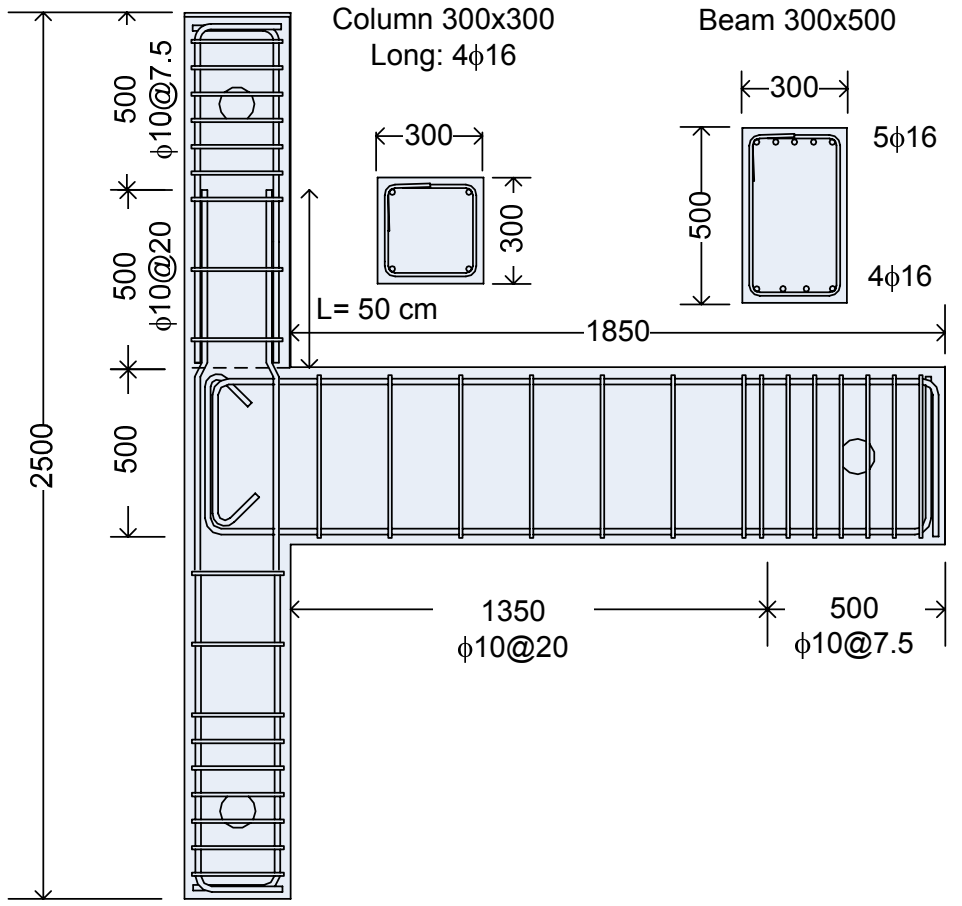


(a)

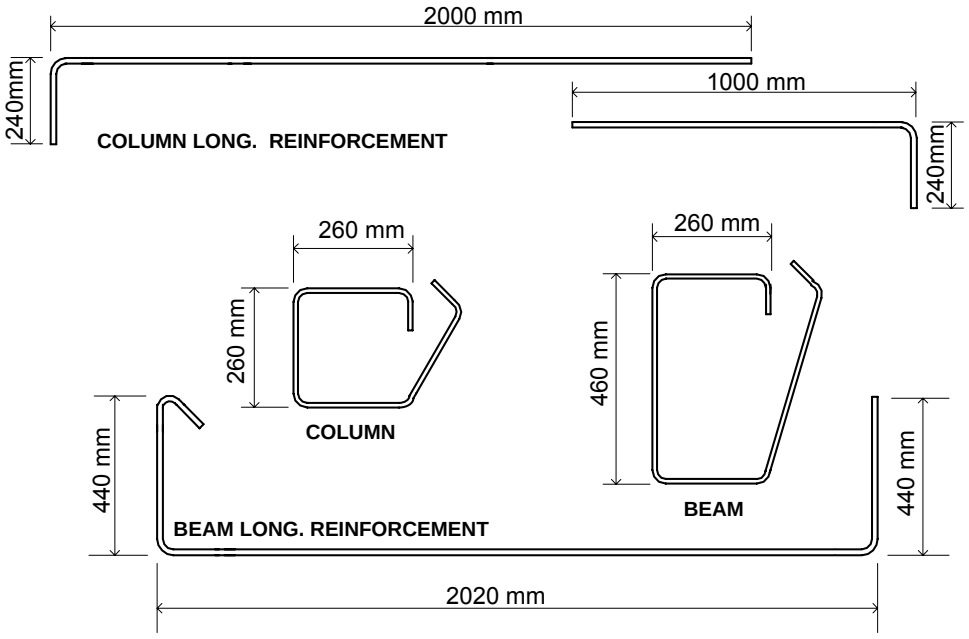


(b)

Figure 2.29. Reinforcement details for Specimen TR-5 Control

After testing of specimen TR-5 Control, all the damages were repaired with chemical epoxy matrix and epoxy injection method described in Section 2.7. After repairing procedure, the specimen was called as specimen TR-5-R.

Due to all deficiencies included by specimen TR-5 Control, it was selected as critical one and three identical specimens were produced. Different configuration of CFRP wrapping will be applied on these three specimens for obtaining effective strengthening methodology. The $28^{th}$ day cylindrical compressive strengths of the specimens are obtained from average strength of three samples for each test specimen and given in Table 2.12.

Table 2.12. Concrete compressive strengths

| Specimen | $f'_c$ (MPa) |
|---|---|
| TR-5-Control | 14.2 |
| TR-5-FRP-1 | 14.6 |
| TR-5-FRP-2 | 16.0 |
| TR-5-FRP-3 | 16.0 |
| TR-5-R | 14.2 |

### 2.8.6. Strengthening Method for Specimen TR-5-FRP-1

Step 1: Reinforcement of the specimen starts with wrapping the joint region diagonally. This orientation scheme is associated with cracks observed in control specimens which were caused because of the lack of the stirrups in the joint region and was designed to provide shear reinforcement for the joint region. The shear cracks observed in control specimens were started from one corner of joint panel and goes through to the opposite corner diagonally. Therefore, the slope of cracks, $\alpha$, was depending on the dimensions of joint panel.

Due to the CFRP was working as tension members, fibers should be placed perpendicular to the cracks for obtaining optimum solution. Therefore, the slope of CFRP fibers, $\gamma$, can be calculated by Eq (2.9). If the CFRP fibers placed vertical or horizontal, some shear forces exerted on CFRP which is unwanted situation.

$$\alpha + \gamma = 90^0 \quad , \quad \gamma = \arctan\left(b/h\right) \tag{2.9}$$

In all specimens, $b$=300 mm, $h$= 500 mm, and the slope of CFRP fiber orientation, $\gamma$, is found as 31°.

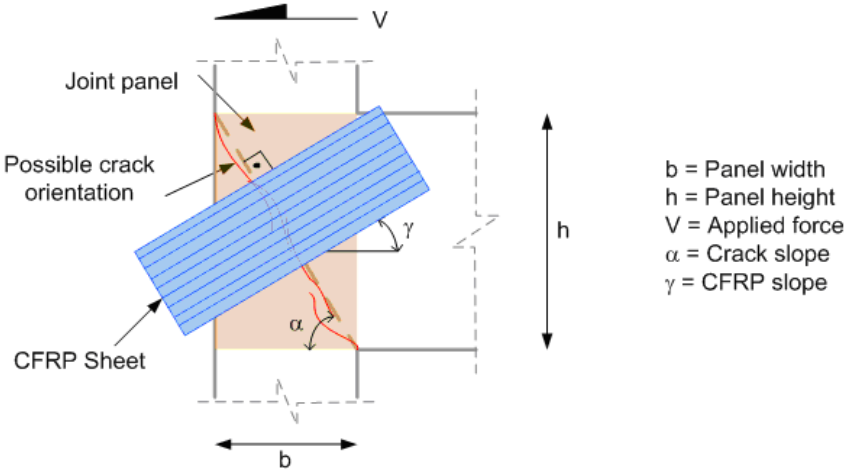


Figure 2.30. Slope of diagonal fibers

Figures 2.31 and 2.32 shows the application of externally bonded CFRP for the joint region. The diagonal CFRP sheets were installed perpendicular to possible crack orientation for push and pull direction of loading. Therefore, four corner of beam-column connection interface were wrapped with CFRP with the angle of 31°.

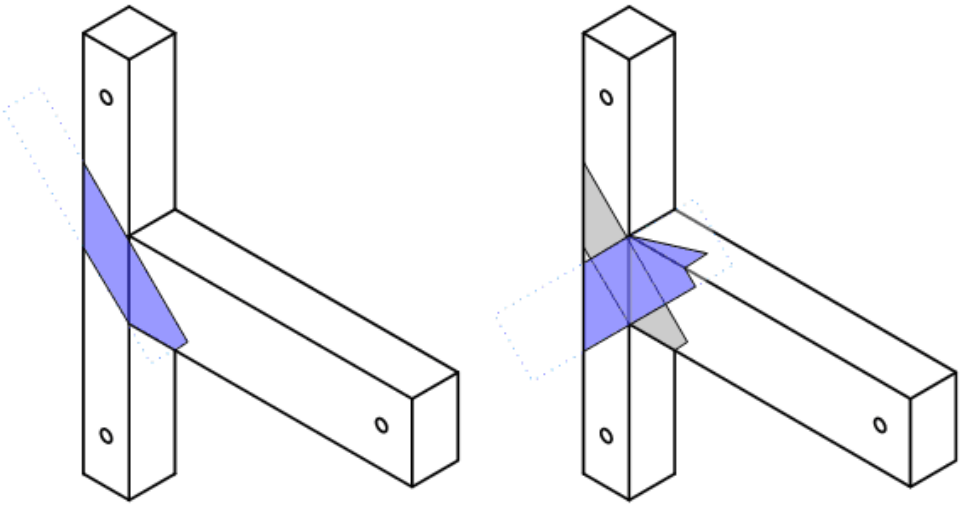

(a) $+\gamma$ diagonal fibers (b) $-\gamma$ diagonal fibers

Figure 2.31. Installation of diagonal fibers

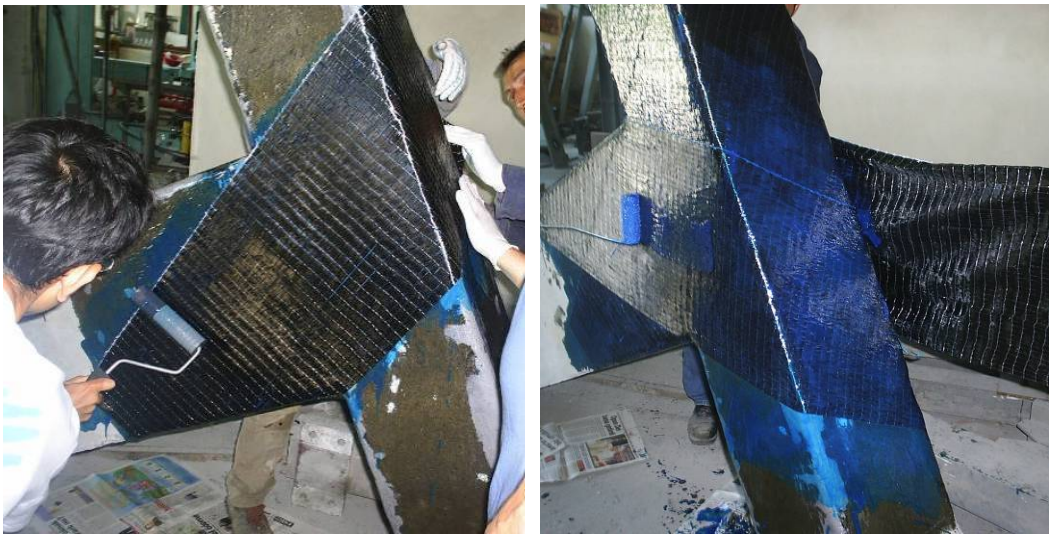

(a) (b)

Figure 2.32. CFRP application

Step 2: In order to prevent the debonding of CFRP on the beam, the anchorages were applied for the diagonal sheets at the beam. A 50 cm width of the single layer of CFRP sheet was wrapped around the beam (Figure 2.33). This application provided also some shear reinforcement to the beam in addition to its main purpose. In Figure 2.34 and Figure 2.35, photos from application were given.

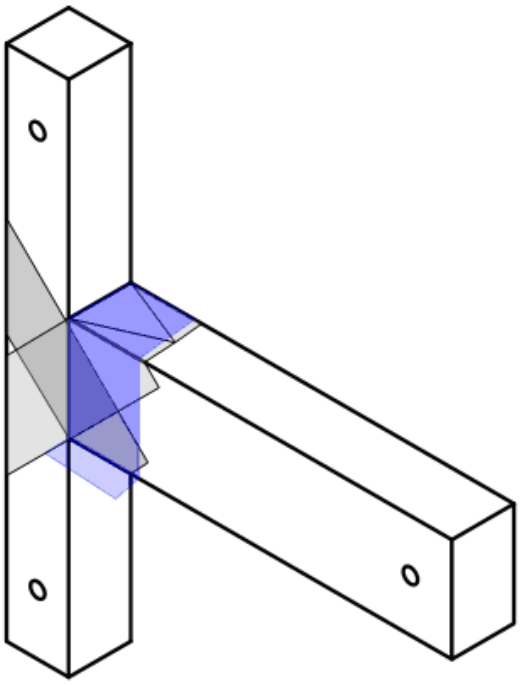

Figure 2.33. CFRP application of beam

Figure 2.34. Picture from application of diagonal CFRP

Figure 2.35. Final view of strengthened specimen.

### 2.8.7. Strengthening Method for Specimen TR-5-FRP-2

Step 1: One layer longitudinal CFRP sheet was applied to the back side of the column for eliminating lap splice effects. Also, one layer of "L Shape" CFRP sheets were introduced to the front side of the column for top and bottom. These L shapes was continued to 300 mm of the beam. The Figure 2.36 and Figure 2.37 indicate the application of longitudinal and L shapes CFRP of column.

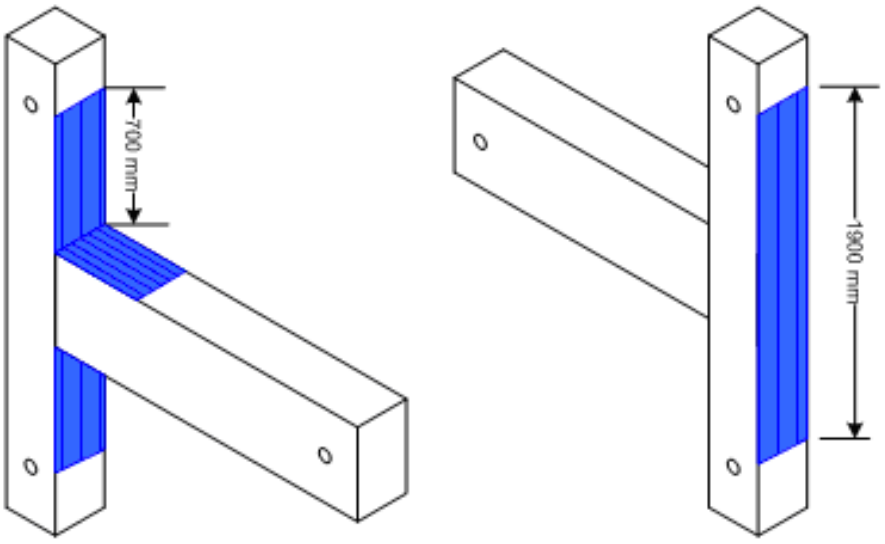


Figure 2.36. Installing longitudinal and L Shaped fibers

Figure 2.37. Application of L Shaped fibers

Step 2: Second step was similar to the first step of specimen TR-5-FRP-1. The CFRP fiber was placed perpendicular to the possible shear cracks at the joint region. Totally 4 sheets, one layer for each corner were applied (Figure 2.38 and Figure 2.39). This application provided shear and longitudinal reinforcement column, beam and joint region.

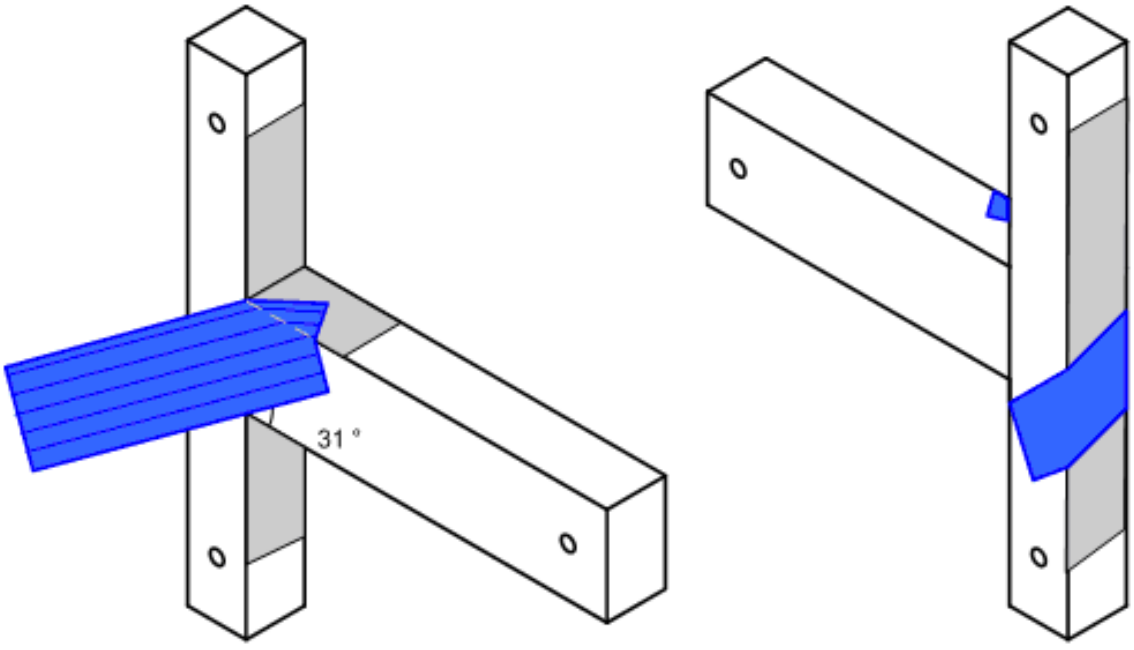


Figure 2.38. Installing diagonal fibers

Figure 2.39. Application of diagonal fibers

Step 3: Third step was the application of the anchorage for the diagonal sheets and L shapes at the top and bottom column portion. 300 mm part of the columns, near to the joint region, were wrapped with 2 layers of 300 mm wide CFRP sheets as shown in Figure 2.40. This application provided also some shear reinforcement to the columns and induced confinement effects for the lap spliced region.

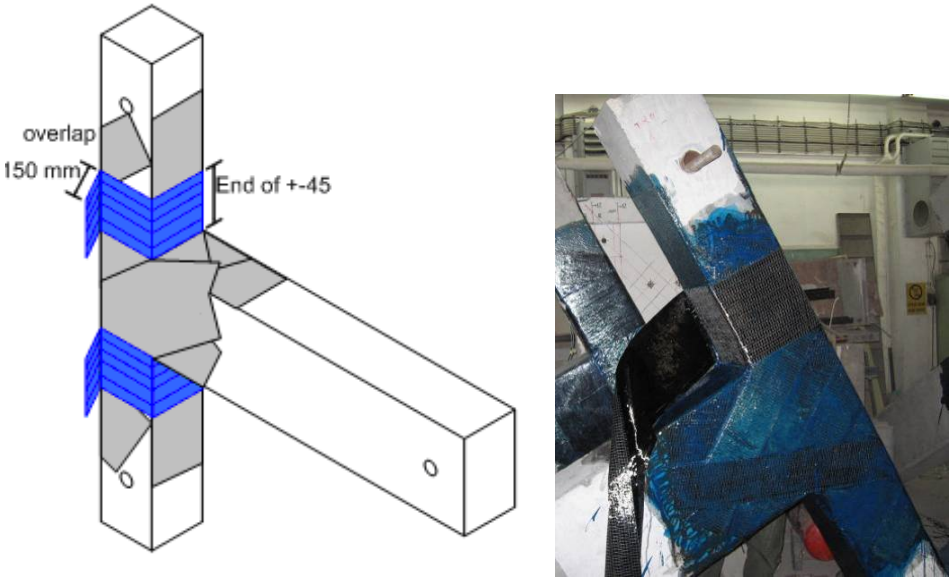


Figure 2.40. Column confinements

Step 4: Fourth step was the application of the anchorage for the diagonal sheets and L shapes at the beam. A 300 mm width of the CFRP sheet was wrapped around the beam with three layers as shown in Figure 2.41. In addition to anchorage this application provided also some shear resistance to the beam.

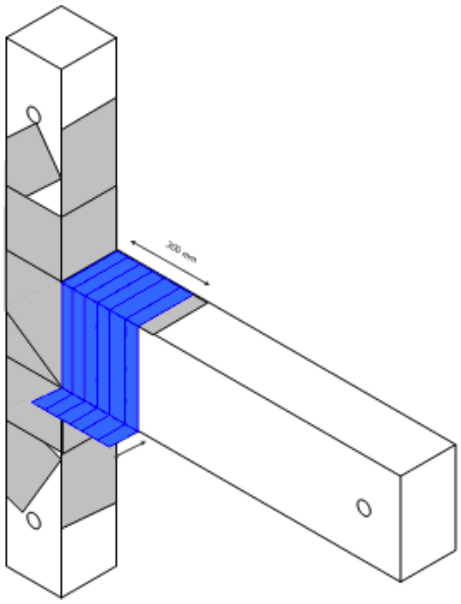

Figure 2.41. Beam confinements

### 2.8.8. Strengthening Method for Specimen TR-5-FRP-3

Step 1: In order to prevent the debonding of the CFRP sheets from the surface of the beam, 4 holes with 12 mm diameter were drilled in beam. The holes were drilled for the purpose of installing CFRP anchorages in the beam. Locations of the anchorage holes were illustrated in Figure 2.42.

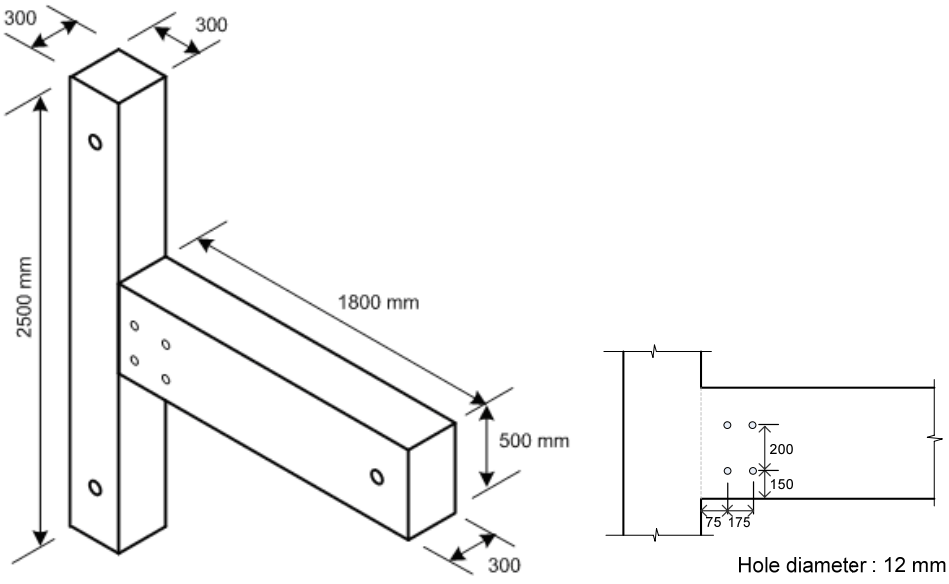


(a) (b)

Figure 2.42. Anchorage holes

Step 2: For increasing the flexural capacity of the column, one layer longitudinal CFRP sheet was applied to the west side of the column for eliminating lap splice effects. The length of the column flexural CFRP was 1900 mm. Also, one layer of "L Shaped" CFRP sheets were introduced to the east side of the column for upper and bottom portion. These L shapes was continued to 300 mm of the beam. The Figure 2.43 indicates the application of longitudinal and "L shaped" CFRP sheets.

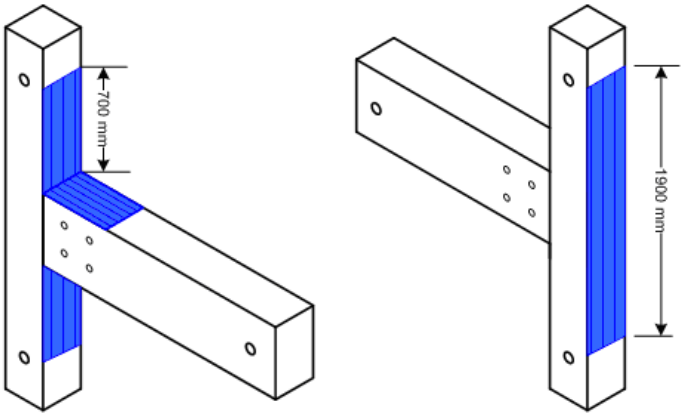


Figure 2.43. Installing longitudinal and L Shaped fibers

Step 3: Reinforcement of the specimen starts with wrapping the joint region diagonally similar application with the previous specimen. In addition to one layer diagonal fibers for each corners of joint panel, 3 -layers of CFRP patches, which have 150 mm depths, were installed on the diagonal fibers. Increasing the number of layers of CFRP at the corner of the joint region, prevents the initiating of the cracks at that location. Figure 2.44 illustrated the application of diagonal sheets and patches on the joint panel.

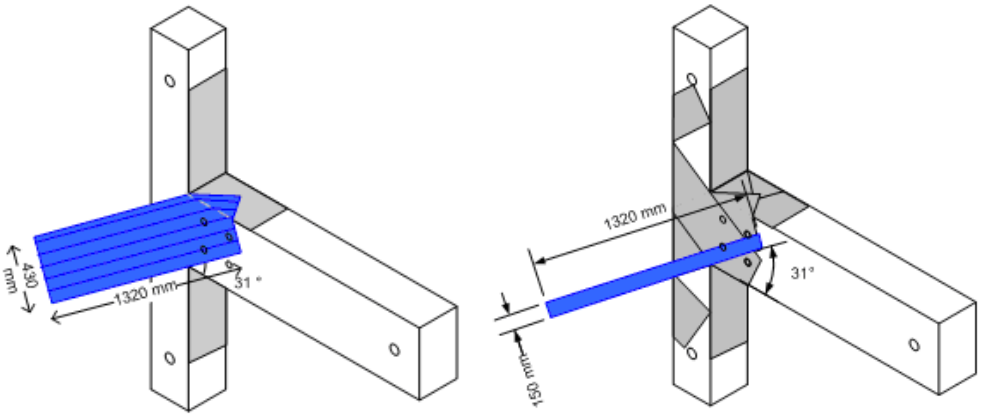


Figure 2.44. Installing diagonal fibers and patches

Step 4: Fourth step was the application of the anchorage for the diagonal sheets and L shapes at the top and bottom column. Two layers of CFRP sheet with 300 mm width was wrapped around the columns as shown in Figure 2.45.

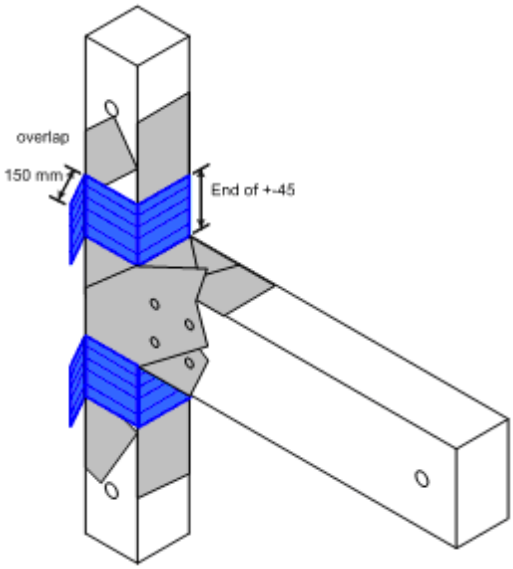


Figure 2.45. Column confinements

Step 5: Fifth step was the application of the anchorage for the diagonal sheets and L shapes at the beam. A 300 mm width of the CFRP sheet was wrapped around the beam with three layers as shown in Figure 2.46. In addition to anchorage, this application provided also some shear reinforcement to the column.

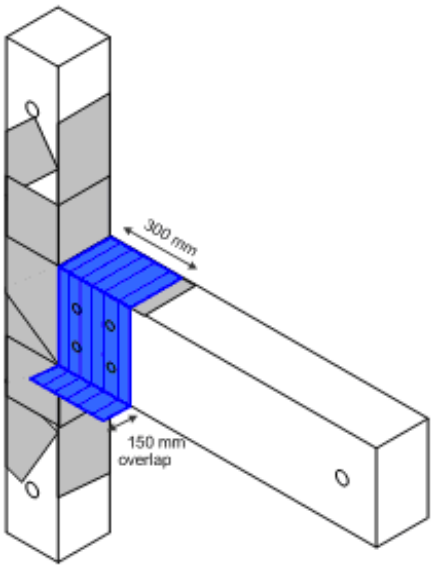


Figure 2.46. Beam confinements

Step 6: As a final stage, for preventing the debonding on the beam, CFRP sheets were anchored to the concrete by using the holes drilled in first step (Figure 2.47). 150 mm CFRP sheets were used as anchor material.

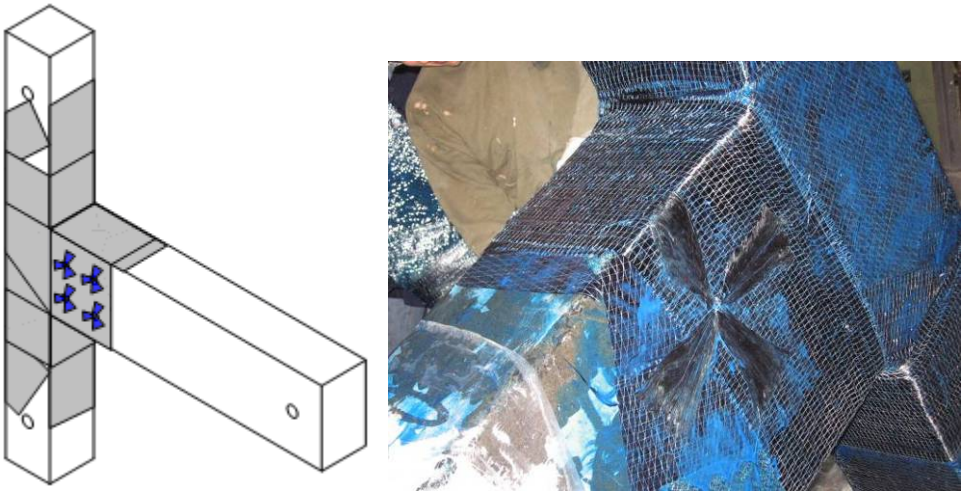

Figure 2.47. Anchorages

# 3. TEST RESULTS

## 3.1. Test Observations

An extensive experimental program was conducted to investigate the shear strength and seismic performance of beam-column joint specimens. In order to determine the effects of deficiencies on the behavior of the beam-column joint specimens, and also to see the possible crack patterns, experiments were carried out on non-strengthened, control specimens, TR-1 Control to TR-5 Control. CFRP sheets for strengthening were applied in such a way to either stop or delay the formation of cracks observed in control specimens. The observations of the tests and some pictures obtained during the tests were given in this section for the specimens. Also, detailed crack propagation such as locations, lengths and widths of the cracks with the applied lateral loads for each drift levels, were given in Appendix A.

Due to having inadequate shear reinforcements and the low quality concrete in the joint regions, diagonal shear cracks were formed within the joint of all control specimens. It is possible to say that pinching effects (all hysteresis loops passed near to the origin) occurred for all of the control specimens (TR-1 Control to TR-5 Control).

### 3.1.1. Specimen TR-1 Control

Specimen TR-1 Control fulfilled all requirements of TEC-75. Axial load on the column was 35% of the column axial load capacity (550 kN). Maximum applied lateral load was 50 kN at a drift level of 1.40%.

At the first drift level, which is 0.20%, a flexural crack initiated at the maximum moment region, at the top face of the beam when the specimen was forced with a peak force of 18.3 kN. An approximate moment value of 31 kNm, which was calculated using the load obtained from the data acquisition system, caused this initial crack. In the subsequent cycles having applied the load both in pull and push directions, additional

hairline flexural cracks developed both at top and the bottom faces of the beam (Figure 3.1).

The first crack in the joint region was formed at a drift level of 0.75%, and at a load level of 44 kN. This crack formed vertically just about 50 mm away from the column face. Also, the vertical cracks observed at the back side of the column when the specimen was pushed at this drift level. These cracks were the first indication of buckling or movement of the column longitudinal reinforcement. The cover concrete was pushed out by buckled reinforcing bars, Figure 3.2.

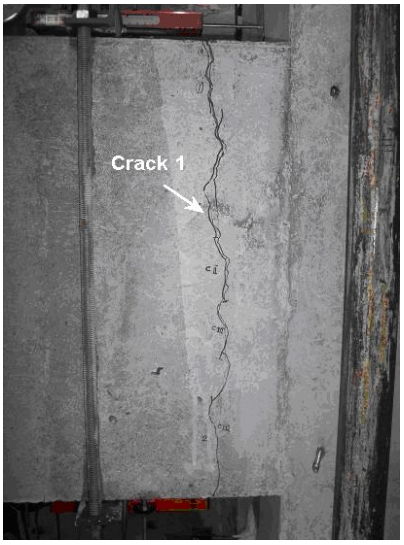


Figure 3.1. Flexural cracks up to the drift level of 0.50%

The first joint shear crack at the joint region was observed at a drift level of 1.00%., when the 48 kN lateral load applied in pull direction, the crack initiated from the bottom corner of the beam-column connection and extended into the joint core.

The maximum lateral load, measured as 50 kN, was obtained during loading to 1.40 % drift cycles in the pull and push direction of loading. Existing cracks elongated and widened and new flexural cracks were formed. Although the positive and negative moment capacities of beam were not same due to the amount of longitudinal reinforcements at the top and bottom of the beam, the load carrying capacity was almost same in experiment in push and pull direction of loading. It can be said that before the yielding of beam reinforcements, the joint shear was controlled the failure of specimen.

In the subsequent drift cycles, up to the 2.20% drift level, additional shear cracks formed at the joint region and no new cracks observed on the beam. Load carrying capacity was started to decrease due to the joint shear cracks.

At a drift level of 2.75%, the column longitudinal reinforcements buckled in a joint region, therefore, the cover concrete at the back side of the joint totally spalled. When the load carrying capacity of the specimen decreased up to 80% of maximum load, test was ended. Crack pattern at 2.20%, 2.75 % drift level and also at the end of the test can be seen in Figures 3.3 and 3.4, respectively. The detailed crack propagation tables were given in Table A.1 to A.4 in Appendix A.

Figure 3.2. The first crack in the joint region, (0.75% drift level)

Figure 3.3. Crack pattern at 2.20% and 2.75% drift level

Figure 3.4. Final damage in the joint region

Since the code provisions were fulfilled, Specimen TR-1 Control can carry the 50 kN lateral load which was the maximum carried lateral load among the control specimens. The lateral load capacities of other control specimens were less than that of TR-1 due to the deficiencies in the reinforcement details. Although the amount of longitudinal reinforcements were different in the top (5ϕ16) and the bottom (4ϕ16) of the beam, there was no significant difference between the lateral load capacities in pull and push direction of loadings. The reason for this, the failure was governed by the crushing of joint core concrete, which is joint shear failure, before the yielding of beam longitudinal reinforcements. Figure 3.5 illustrates the lateral load versus top displacement and drift relationships of specimen TR-1 Control.

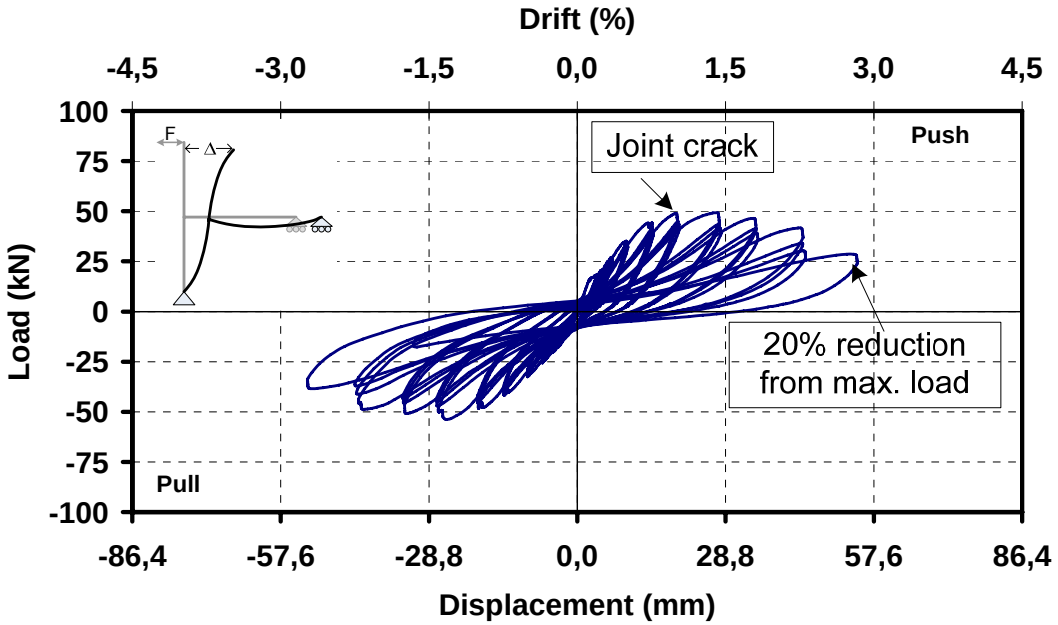


Figure 3.5. Lateral load versus top displacement for Specimen TR-1 Control

### 3.1.2. Specimen TR-1 R

The repaired specimen TR-1-R was the same specimen with the specimen TR-1 Control and tested in the same manner as specimen TR-1-Control. Maximum applied lateral load was 81 kN at a drift level of 2.20% in push direction of loading. Having high strength repairing materials instead of low quality concrete at the joint region, cause significant increase in lateral load capacity.

The first flexural crack was observed at the top face of the beam, when the applied load was 37.6 kN in the pull direction of 0.35% drift cycles. The location of the crack was 680 mm from the column surface. Second flexural crack, which was located about 300 mm from the column face, was observed at the same drift level when the applied load was 34.9 kN in push direction of loading.

During the 0.50% drift cycles, the first diagonal crack, which was flexural shear crack, observed on the beam. No cracks were observed at the joint region at this drift cycles. Up to the drift level of 1.00%, additional flexural cracks formed on the beam surface. It was noticed that all the cracks observed on the beam were 300 mm far away from the column face. No cracks appeared on repaired region.

At a drift level of 1.40%, existing cracks widened and elongated. The width of crack (crack 2), occurred at the top portion of the beam was reached 5 mm. The concrete was starting to crush and the longitudinal beam reinforcements were buckled. In other words, the hinging mechanism was observed on the beam where the repairing materials end. The ultimate load capacity, which was 70 kN for pull direction, was achieved during the testing of 1.40% drift level, whereas 81 kN for push direction at a drift level of 2.20% (Figure 3.6). The detailed crack propagations were given in Table A.5 to A.8 in Appendix A.

Figure 3.6. Final crack patterns of beam

It can be said that, applying the high strength repairing materials to the joint, prevents the occurrence of shear cracks. The failure mechanism shifted from the joint shear to the beam hinging. Having different number of re-bars at the top and the bottom of the beam, different load carrying capacities obtained for the push and pull direction of loading.

In specimen TR-1-R, by using repair material the joint behavior was improved significantly. Since the low quality concrete at the joint region was replaced with high strength repairing materials, shear cracks were formed at a higher drift levels at the beam-column joint region. Also, the hysteresis loops of repaired specimen became wider than that of control ones and no pinching effect was observed. Although the repaired specimen was pre-damaged; it reached higher load capacity and the ductility than the original one. The test was stopped at a drift level of 3.5% due to 20% strength degradation achieved. Figure 3.7 shows the load versus displacement and drift relationship of specimen TR-1-R.

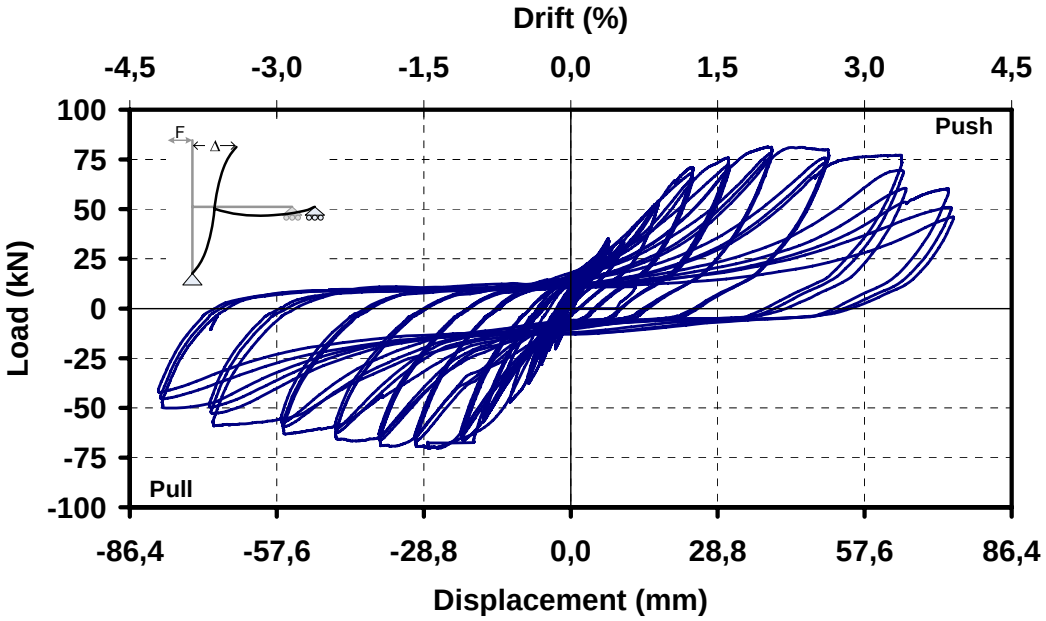


Figure 3.7. Lateral load versus top displacement for Specimen TR-1-R

### 3.1.3. Specimen TR-2 Control

Specimen TR-2 Control has deficiencies of insufficient transverse reinforcement in column and in beam and also, lack of transverse reinforcement at the joint region. Axial load on the column was 40% of the column axial load capacity (450 kN). Maximum applied lateral load was 40 kN at a drift level of 1.40%.

At the beginning of the test, at a 0.15% drift level, 15 kN loads were applied in both push and pull direction without any crack occurrence. In the next drift level, which is 0.20%, the first flexural hairline cracks were formed at the maximum moment region of the beam, when the specimen was pushed with the load of 19.5 kN. In pull direction the similar crack developed at the top side of the beam.

No new cracks were formed at the drift levels of 0.25% and 0.35%. Only existing cracks elongated and widened, such as the hairline crack mentioned above reached 0.2 mm width.

The first crack within the joint region was noticed at the first cycle of 0.50% drift level. This crack was formed vertically just 30-40 mm away from the column face when

the load level was about 34 kN. In the subsequent cycles of this drift level, diagonal cracks were formed at the joint core.

In addition to the elongation of existing cracks at a drift level of 0.75%, additional flexural cracks were formed at the beam. The width of the first crack was reached 1.2 mm at this drift level. The view of the test at 0.75% was seen in Figure 3.8.


Figure 3.8. Flexural cracks up to the drift level of 0.75%

At a drift level of 1.40%, the maximum load were observed in pull and push direction of loading which is about 40 kN. The width of crack formed at the intersection of beam-column connection was reached 2.5 mm during the testing of 1.75% drift level when the applied load was 34 kN. As in specimen TR-1 Control one, joint shear failure was governed the behavior of this specimen. Also, buckling of the longitudinal reinforcements of the column at the joint region observed due to lack of confinements. The cover concrete was crushed. In Figure 3.9 illustrates the final crack pattern of the specimen. Table A.9 to A.12 in Appendix A illustrates the detailed crack propagations.

Figure 3.9. Failure mechanism of the specimen

The lateral load versus top displacement and the drift relationships of specimen TR-2 Control was given in Figure 3.10. The pinching effect due to shear cracks in the joint was observed in the of load deformation hysteresis curve. Having no transverse reinforcements in the joint region caused the shear cracks in early drift levels. The load carrying capacities of both directions of loadings are almost same at about 37 kN. The failure was governed by the crushing of joint core concrete, before reaching the flexural capacities of the beam.

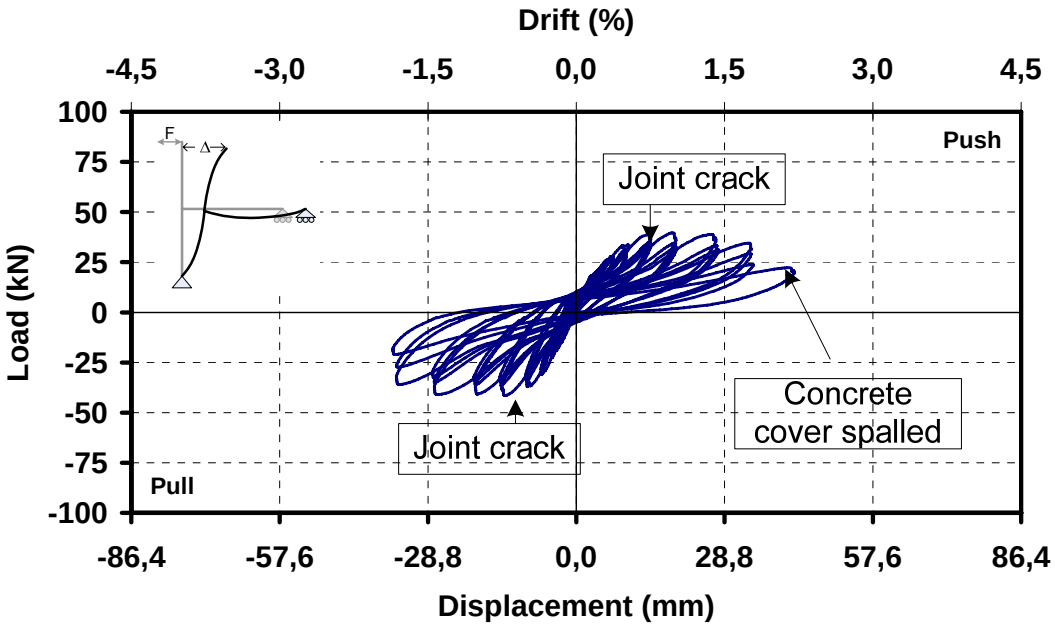


Figure 3.10. Lateral load versus top displacement for Specimen TR-2 Control

### 3.1.4. Specimen TR-2-R-FRP

The specimen TR-2-R-FRP was repaired and retrofitted as described in Section 2.8.7 and tested in the same manner with the specimen TR-2 Control. Due to the fact that the joint region was covered with CFRP material and the cracks developed at the joint region cannot be observed clearly. However, some other cracks were formed at the outside of the wrapped area. Maximum applied lateral load was 99 kN at a drift level of 1.40% in pull direction.

The observed first crack, which was flexural, was formed at the bottom side of the beam at the push cycles of 0.20% drift level, when the applied lateral load was 16 kN. It was located at 680 mm away from the column face. In pull direction of loading cycles of 0.25% drift level, flexural cracks were also observed. In the following cycles up to the 1.40% drift level, the cracks was dense on the beam, where the CFRP wrapped region ended as seen in Figure 3.11.

Figure 3.11. Cracks formed on the beam

During the 1.40% drift cycles, the maximum load (80 kN) in push direction and (99 kN) in pull direction were obtained. The reason of the difference in pull and push direction of loading was the amount of beam top and bottom reinforcements of the beam as seen in previous repaired specimens. This indicated that the shear failure of joint was prevented by using CFRP material. The failure was shifted from the joint shear to the beam hinging mechanism. Also, in this drift level, debonding was observed on the diagonal layer

of the CFRP installed on the beam, explained in Step 4 of strengthening method 3. However, the beam wrapping application, explained in Step 6, prevented the propagation of debonding failure. Debonded region was shown schematically in Figure 3.12.

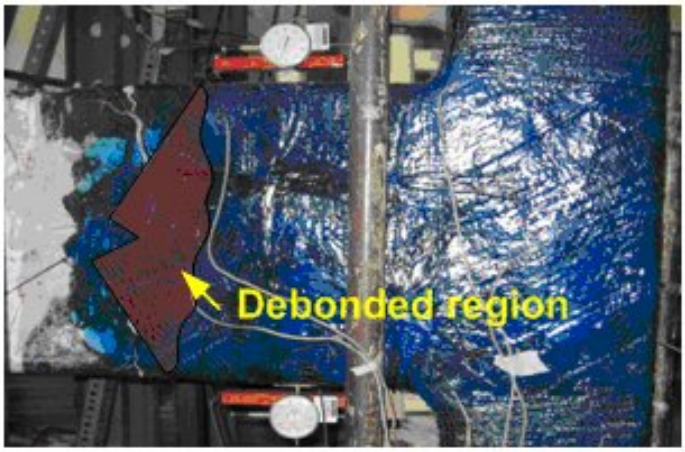


Figure 3.12. Debonded region

The hinge mechanism started to form at the beam where the CFRP wrapping ended. During the drift level of 2.75%, the cracks at the beam were reached 15 mm. Unlike Specimen TR-2 Control, repaired and retrofitted specimen lasted up to the drift level of 3.50%. The failure was governed by the yielding of the beam reinforcements. Crushing of the concrete and the buckling of the beam longitudinal reinforcement were observed. The detailed crack propagations were given in Table A.13 to A.15 in Appendix A.

Replacing the loose concrete of joint region with high strength repairing materials and also retrofitting the joint with CFRP strengthening technique described in Section 2.8.8, the performance of the specimen was improved significantly in the specimen TR-2-R-FRP. As seen from the load deformation diagrams, the yielding of the beam reinforcements was achieved. As a result the energy and the stiffness value of the specimen were increased. In Figure 3.13, lateral load versus top displacement and inter-story drift relationships of the specimen TR-2-R-FRP was illustrated.

The differences of the lateral load carrying capacities of push and pull direction of loading was due to the flexural capacity of beam cross-section. There were four reinforcing bars working in tension in push direction of loading (beam bottom reinforcements),

however, five reinforcing bars working in tension in pull direction of loading (beam top reinforcements).

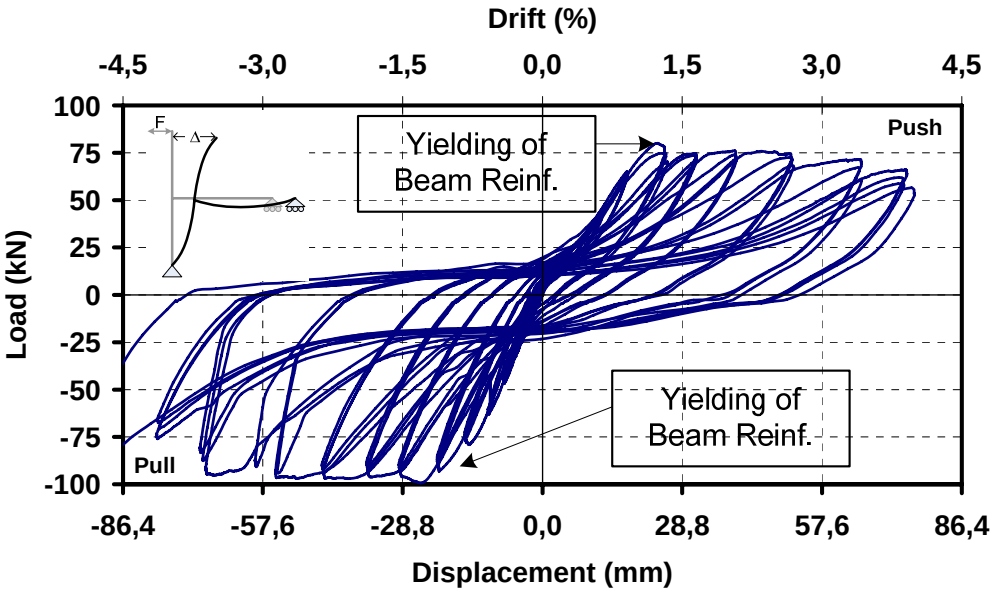


Figure 3.13. Lateral load versus top displacement for Specimen TR-2-R-FRP

### 3.1.5. Specimen TR-3 Control

Specimen TR-3 Control has a small cross-section of beam and column tested under 330 kN axial load which is 40% of the column axial load capacity. Maximum applied lateral load was 27 kN at a drift level of 0.75%.

At the first drift level, which is 0.15%, a flexural crack was formed at the maximum moment region coincides the top of the beam region in pull direction. In the following cycles of same drift, the second crack was formed at the bottom of the beam, in push direction. The maximum loads observed in this drift level were 14 kN in pull and 12 kN in push directions.

Flexural cracks were developed on the top and bottom of the beam during the 0.20% and 0.25% drift levels. The first diagonal shear crack at the joint region was observed at a drift level of 0.35% (Figure 3.14). When the load reached to 23 kN, in pull direction of loading, the crack initiated from the top corner of the beam-column connection and extended into the joint core.

Figure 3.14. Flexural cracks up to the drift level of 0.35%

After the 0.50% drift level, the more visible damages were observed at joint region. At the drift level of 0.75%, the maximum loads observed in pull and push directions were 27 kN and 24 kN, respectively.

In the subsequent drift cycles, up to the 1.75% drift level, additional shear cracks occurred at the joint region and load carrying capacity started to decrease. When the drift level of 1.75% was applied, the column longitudinal reinforcements started buckling, and thus, the cover concrete at the back side of the joint totally spalled-off. At the same time, the diagonal cracks widened. The test ended due to the load carrying capacity of the specimen decreased up to 80% of maximum load. The crack pattern at the end of the tests was illustrated in Figure 3.15. The detailed crack propagations were given in Table A.16 to A.18 in Appendix A.

Figure 3.15. The cracks occurred in the joint region at the end of the test

For the thinner specimen, TR-3 Control, relationships of load versus top displacement and drift were illustrated in Figure 3.16. Same as previous control specimen, lacking of transverse reinforcement in the joint region causes the diagonal shear cracking at the joint region, therefore, the hysteresis curves exhibited pinching effects. Also, it was obviously seen from the figure that the stiffness and the strength degradations were occurred during the repeated cycles of drift levels. The first joint shear crack of joint was formed at 1.00% drift level. After this drift level, the lateral load started to decrease. Before the yielding of beam longitudinal reinforcements, shear failure mechanism was formed at the beam-column joint region.

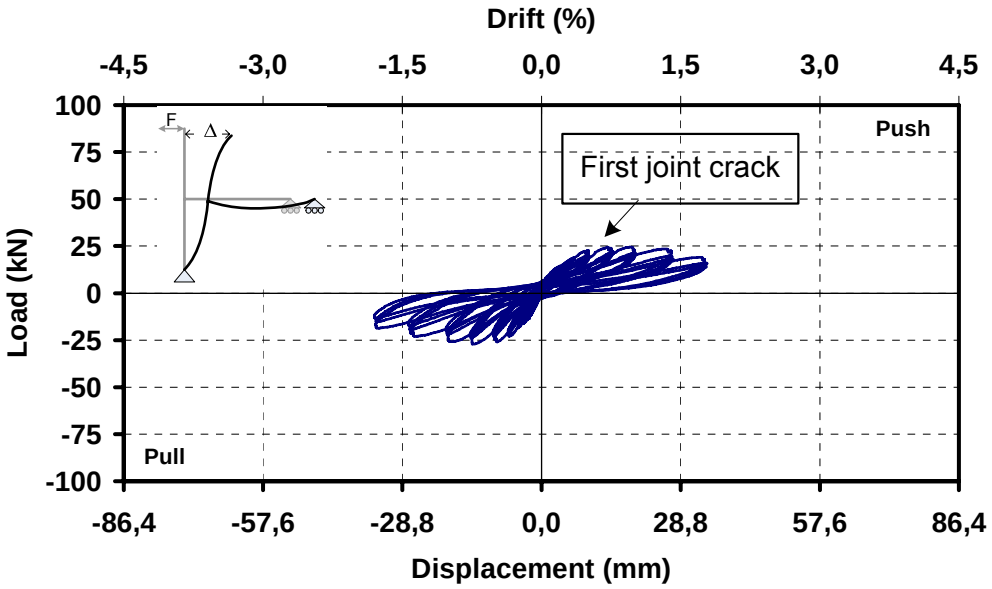


Figure 3.16. Lateral load versus top displacement for Specimen TR-3 Control

### 3.1.6. Specimen TR-3 R

The repaired specimen TR-3-R was tested in the same manner as specimen TR-3 Control. The first crack was observed at the top of the beam, 90 mm away from the column surface, in the pull cycles. The drift level was0.25% and the load carrying capacities were 16.5 kN and 24.1 kN for push and pull directions, respectively. Up to drift level of 0.75%, flexural crack occurred on the beam only.

During the 1.00% drift cycles, the first diagonal crack, started from the top corner of the beam-column joint region. The recorded loads were 45.3 kN and 63.2 kN for push and

pull directions, respectively. After this drift level, the load carrying capacities started to decrease. The first crack on the beam widened further to about 2.5 mm at the drift level of 1.40%. During this drift level, the vertical cracks were observed at the back side of the column at joint region. The reason of these cracks could be due to buckling of longitudinal reinforcements of column.

The test was ended at 2.75% drift level when the cover concrete at the back side of the column crushed completely and the column longitudinal bars buckled (Figure 3.17). The detailed crack propagations were given in Table A.19 to A.21 in Appendix A.

Figure 3.17. Cracking of joint region at the end of the test

As in previous repaired specimen, TR-1-R, the behavior of the specimen was improved significantly in TR-3-R, by using repairing materials. Forming of the joint shear cracking was delayed by replacing the low-quality, loose concrete with high strength repairing materials. Therefore, the load deformation hysteretic cycles became fat and no pinching effects observed (Figure 3.18). The test was stopped at drift level of 3.5% due to 20% strength degradation achieved.

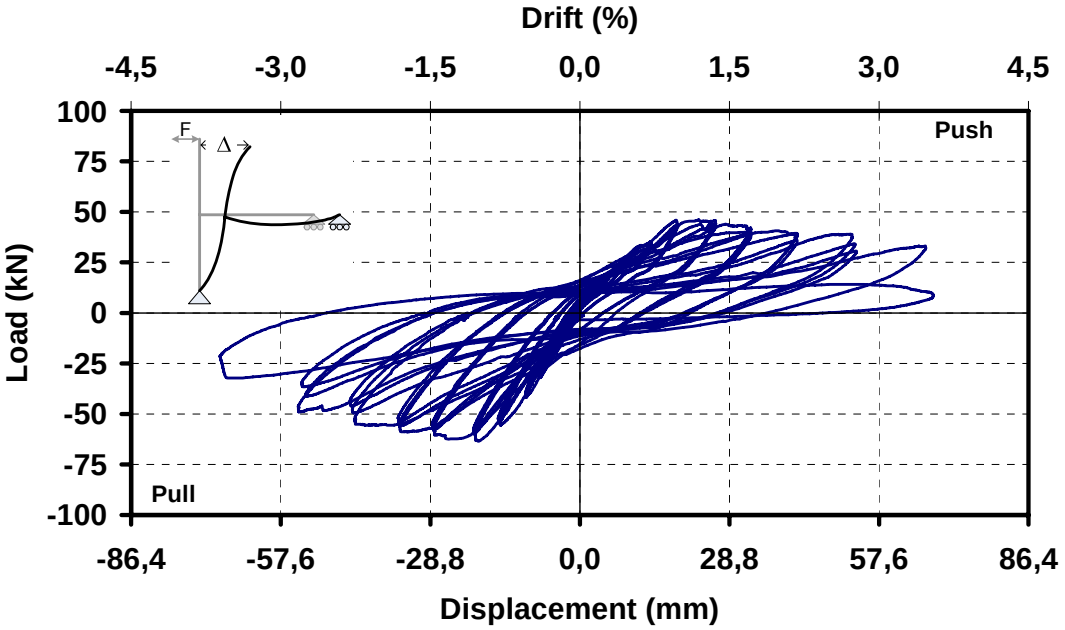


Figure 3.18. Lateral load versus top displacement for Specimen TR-3-R

### 3.1.7. Specimen TR-4 Control

Specimen TR-4 Control has deficiencies of lacking of transverse reinforcement at the joint region and short anchorages of longitudinal reinforcements coming from the beam. Axial load on the column was 40% of the column axial load capacity (450 kN). Maximum applied lateral load was 46 kN for push and pull direction of loading at a drift level of 1.00%.

The first flexural crack was appeared at the top of the beam, when the 18 kN load was applied in pull direction of loading, at 0.15% drift level. In the following drift levels, at a drift level of 0.20%, additional flexural cracks developed on the beam surfaces. The first crack at the joint region was formed during the testing of drift level of 0.25%. Vertical crack with the length of 90 mm observed at the center of the joint core. In the subsequent cycles of this drift level, that vertical crack extended diagonally (Figure 3.19). During the testing of 0.35% drift level, vertical cracks formed at the back side of the column in the joint region. One of the reasons for that vertical crack was the buckling of longitudinal reinforcements of column. The other reason was slipping of the beam longitudinal reinforcement.

Figure 3.19. The first shear crack in the joint

The maximum load which were 42 kN and 46 kN for push and pull direction were observed during the 1.00% drift level. The test was ended due to the load carrying capacity decreased under the 80% of maximum carried load at a drift level of 1.75%. At the end of the test, the column reinforcement was totally buckled (Figure 3.20). The diagonal crack formed at the back side of the column. The detailed crack propagations were given in Table A.22 to A.24 in Appendix A.

Figure 3.20. Buckling of column reinforcements

Figure 3.21 illustrates the lateral load versus top displacement and drift relationship of the specimen TR-4 Control. Having no shear reinforcements in the joint region, bring about the pinching effects in load deformation hysteretic curves. Degradation in load carrying capacities is started after 1.00% drift level due to the effects of shear deformations. The test was stopped at a drift level of 1.75%, when the lateral load capacity was decreased to 80% of the maximum lateral load.

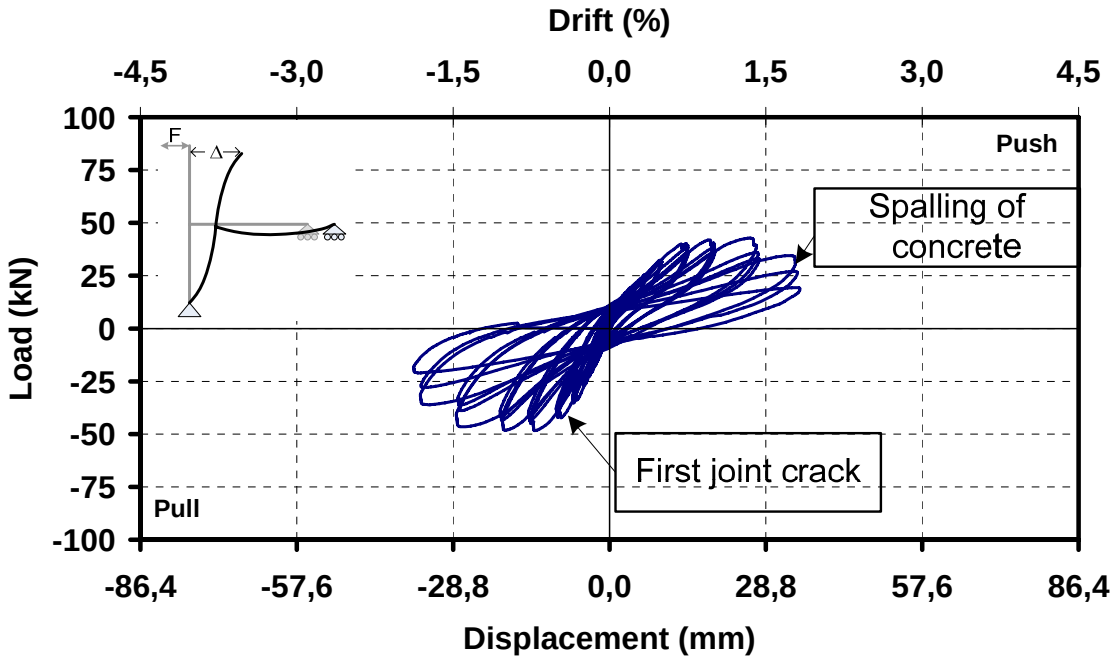


Figure 3.21. Lateral load versus top displacement for Specimen TR-4 Control

### 3.1.8. Specimen TR-4 R-FRP

The specimen TR-4-R-FRP was repaired and retrofitted as described in Section 2.7.8 and tested in the same manner as specimen TR-4 Control. Due to the fact that the joint region was covered with CFRP material, the cracks occurred at the joint region cannot be observed. However, some other cracks occurred at the outside of the wrapped area were noticed. The observed first crack, which was flexural crack, was occurred at the bottom side of the beam at the push cycles of drift level of 0.20%. It was located at 520 mm away from the column face. In pull cycles of 0.25% drift level, flexural cracks were also observed. In the following cycles up to the 1.40% drift level, the cracks was dense on the beam, where the CFRP wrapped region ends as seen in Figure 3.22.

Figure 3.22. Cracks on the beam

The maximum load which was 72.2 kN for push direction was obtained in 1.40% drift level. However in pull direction, the maximum load, 97.4 kN, was obtained in 1.00% drift level. The reason of the difference in pull and push direction of loading was the amount of top and bottom reinforcements of the beam. That means, shear failure of joint was prevented by using CFRP material. The failure was shifted to the beam. Debonding region can be seen in Figure 3.23.

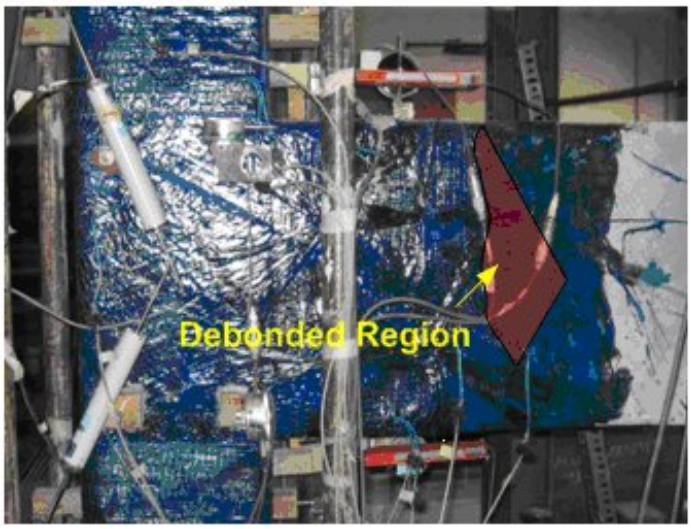


Figure 3.23. Debonded region

Unlike specimen TR-4 Control, repaired and retrofitted specimen lasted up to the drift level of 4.00%. The failure was governed by the flexure of the beam. Crushing of the

concrete and the buckling of the beam longitudinal reinforcement were observed. The detailed crack propagations were given in Table A.25 to A.27 in Appendix A.

The lateral load versus deformation relationship of the TR-4-R-FRP specimen is given in Figure 3.24. The performance of the specimen was improved significantly with using repairing materials and retrofitting the joint with the CFRP materials. As seen from the figure, the flexural capacity of the beam was achieved. Also, shear cracks were observed at the joint region at higher drift level. So the hysteretic loops became fat and no pinching effects observed.

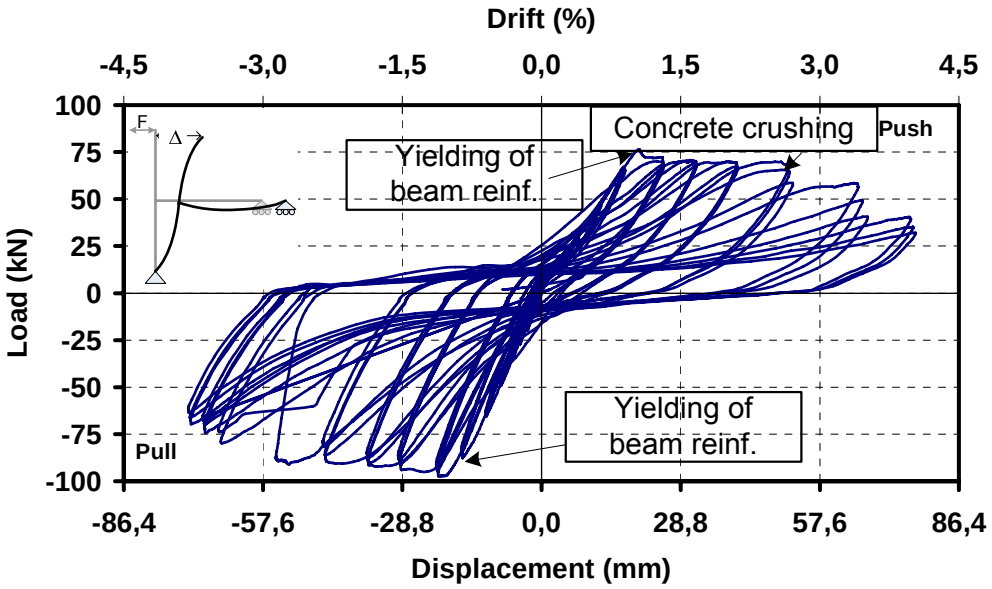


Figure 3.24. Lateral load versus top displacement for Specimen TR-4-R-FRP

### 3.1.9. Specimen TR-5 Control

Specimen TR-5 Control has deficiencies of lacking of transverse reinforcement, short anchorages of beam longitudinal reinforcement and lap splices at the top column. Axial load on the column was 40% of the column axial load capacity (510 kN). Maximum applied lateral load was 47 kN at a drift level of 0.75%.

In pull and push direction of loading, similar lateral load carrying capacities were obtained. The first crack, which is flexural crack with the length of 220 mm, appeared at the bottom side of the beam and approximately 100 mm away from the face of the column,

when the drift level was 0.20 %. And also at about 700 mm away from the column face, another 40 mm length-flexural crack occurred at the top side of the beam when the specimen was pushed. At the same drift level the similar flexural cracks formed at the bottom side of the beam for pull direction.

The first joint crack was initiated from the top corner of the beam-column joint region at the drift level of 0.35%. Up to 0.75% drift level, the cracks were observed only in the beam. After that drift level, cracks shifted in to the joint region. As observed in Figure 3.25 and 3.26, the wide cracks developed at the joint region at the end of the test. The crack pattern in the joint region propagates from one top corner of joint to bottom corner diagonally. Therefore the slope of the crack was not exactly 45°; it depends on the dimensions of the joint block.

When the loads were 32 kN and 47.0 kN maximum load was reached at the drift level of 0.75% for both push and pull direction. During the 0.75% drift level the vertical crack occurred at the east side of the column in the joint region. This can be due to the buckling of longitudinal reinforcement of column. The test ended at the drift level of 1.75%, when load carrying capacity decreased below the 80% of maximum load in the descending branch. The detailed crack propagations were given in Table A.28 to A.30 in Appendix A.

Figure 3.25. Final crack patterns of Specimen TR-5 Control


Figure 3.26. Final crack pattern of Specimen TR-5 Control

The lateral load versus top displacement relationship of the specimen TR-5 Control is given in Figure 3.27. Pinching effect was also seen in this specimen due to the diagonal shear cracking of joint region. Although the amount of reinforcement was different in top and bottom of the beam, there is no significant difference between the lateral loads in pull and push directions. The reason for this, the failure was governed by the crushing of joint core concrete, before the yielding of reinforcement.

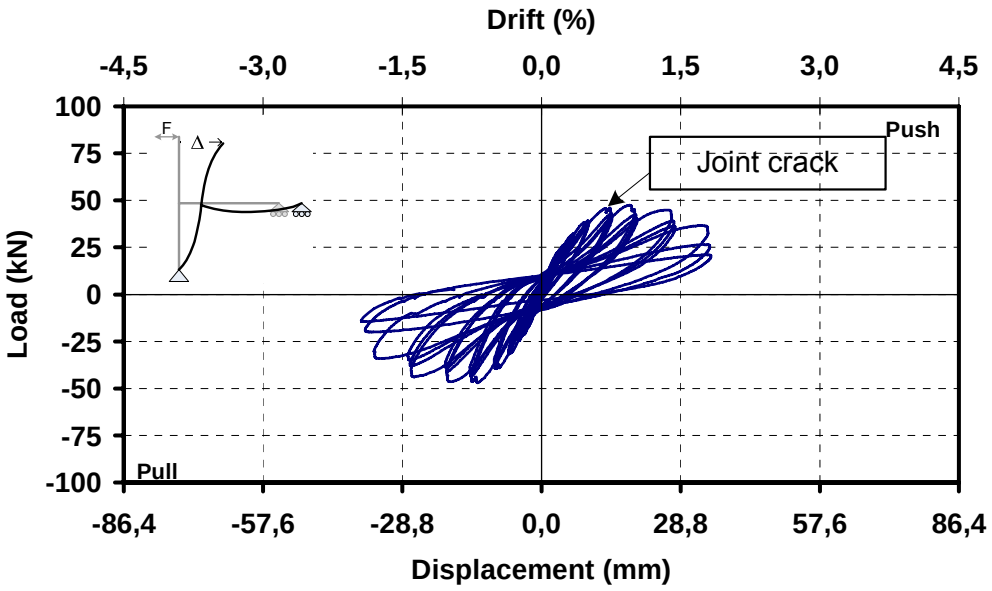


Figure 3.27. Lateral load versus top displacement for Specimen TR-5-Control

### 3.1.10. Specimen TR-5 FRP-1

This specimen was identical with the specimen TR-5 Control. According to the crack patterns occurred in control specimen, it was strengthened with CFRP described in Section 2.8.6. During the experiment the cracks occurred at the joint region cannot be traced due to the CFRP wrapping. Maximum applied lateral load was 80 kN at a drift level of 2.20%.

The first observed flexural crack appeared approximately 600 mm away from the face of the column and at the end of the wrapped region, at a drift level of 0.75% when the applied load was about 57 kN. When the drift was increased to 1.40%, on the back face of the column, at the top and the bottom face of the beam, and buckling was observed on the CFRP sheets (buckling length of approximately 20 mm). And 75.0 kN and 80.0 kN maximum load was reached at the drift level of 2.20% for push direction and pull direction respectively.

The ruptures of the CFRP layers were observed at the corner of beam-column connection at a drift level of 2.75%. The test ended at the drift level of 3.50%, when load carrying capacity decreased below the 80% of maximum load in the descending branch.

After removing the CFRP, the buckling of the longitudinal reinforcement of column at the west side was observed. The buckling level was exactly at the level of buckled CFRP. The concrete in the joint was totally crushed and the crack pattern was different from the control specimen (Figure 3.28). The detailed crack propagations were given in Table A.31 to A.33 in Appendix A.

The lateral load versus top displacement relationship of the specimen TR-5-FRP-1 is given in Figure 3.29. Using CFRP retrofitting materials at the joint, the performance of the specimen was improved significantly. As seen load deformation diagrams, the load carrying capacities are doubled.


Figure 3.28. Rupture of CFRP and crack pattern of Specimen TR-5-FRP-1

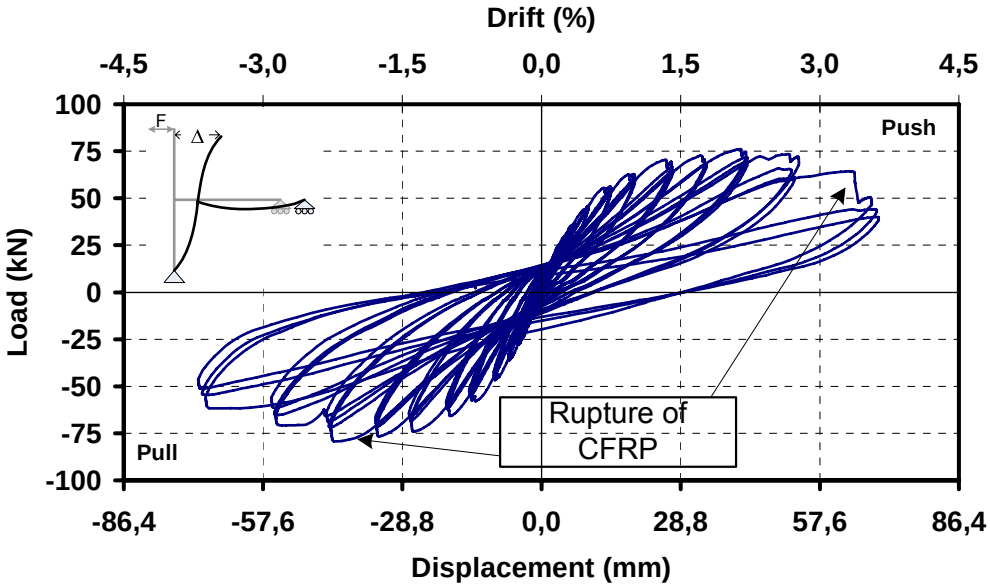


Figure 3.29. Lateral load versus top displacement for Specimen TR-5-FRP-1

### 3.1.11. Specimen TR-5 FRP-2

This specimen was also identical with specimen TR-5 Control. According to the damages and crack patterns developed in the first retrofitted specimen, it was strengthened with CFRP described in Section 2.8.7. Additional longitudinal CFRP were installed on columns and column confinement applied. During the experiment the cracks occurred at

the joint region cannot be traced due to the CFRP wrapping. Maximum applied lateral load was 95 kN at a drift level of 2.20%.

The first flexural crack was appeared at about 650 mm away from the face of the column during the drift level of 0.20%. And in subsequent cycles of the same drift, other two cracks were formed at the same region. At the drift level of 75%, some crackle sound came out when the load was 68 kN.

At the interface of beam-to-column connections, diagonal CFRP sheets were start to rupture at the drift level of 1.40%, however cracks could not be propagated due to four layers of CFRP sheets at those locations. During the 1.75% drift level, the tip of the diagonal fibers started to debond as seen in Figure 3.30. Also in this drift level, a diagonal cracks were formed on the beam at the end of beam CFRP wrapped region. At the drift level of 2.75%, when the applied lateral load was the maximum for push (71 kN) and pull (94 kN), CFRP sheets were debonded at the back side of the column due to the buckling of CFRP. And also, the cracks on the beam were widened and the concrete crushed. During the 3.50% drift level hinge mechanism occurred on the beam. The detailed crack propagations were given in Table A.34 to A.36 in Appendix A.

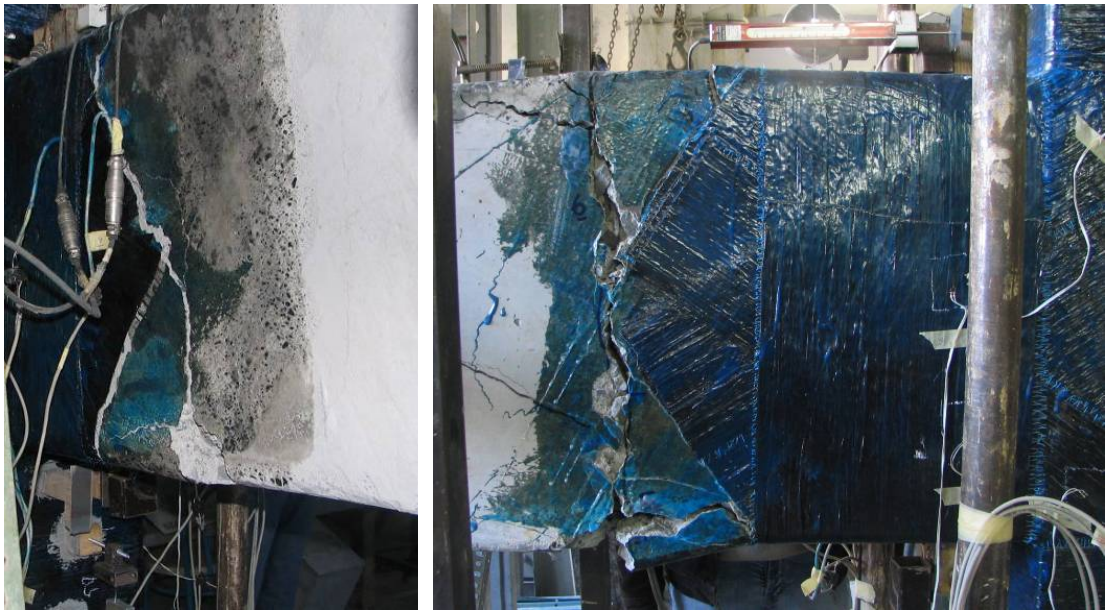

Figure 3.30. Debonding and beam hinging of Specimen TR-5-FRP-2

The lateral load versus top displacement relationship of the specimen TR-5-FRP-2 is given in Figure 3.31. The performance of the specimen was improved significantly with using repairing materials and retrofitting the joint with CFRP. As seen in load deformation diagram of specimen TR-5-FRP-2, the yielding of the beam longitudinal reinforcements was achieved.

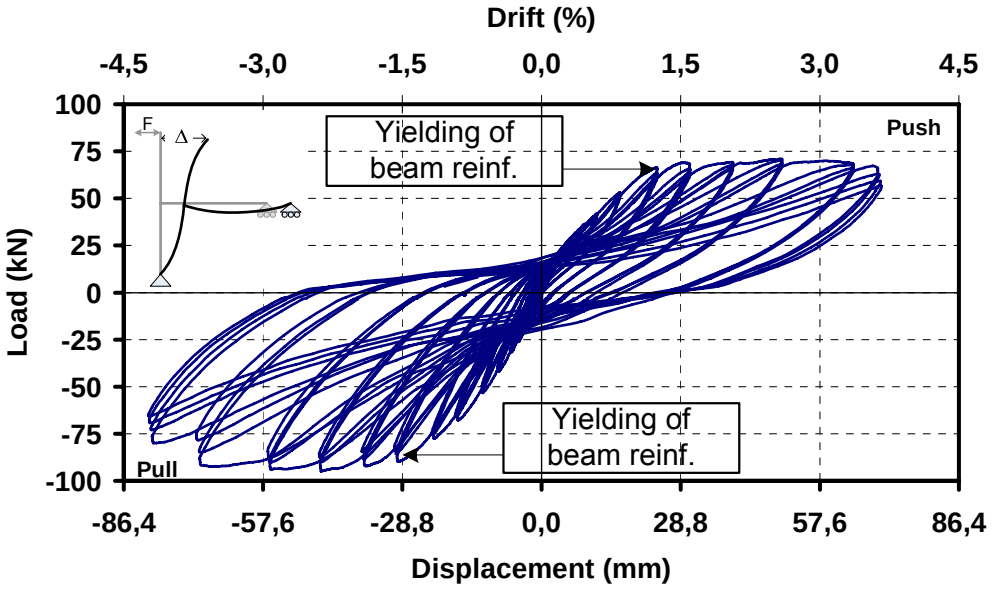


Figure 3.31. Lateral load versus top displacement for Specimen TR-5-FRP-2

### 3.1.12. Specimen TR-5 FRP-3

This specimen was also identical with specimen TR-5 Control. According to the damages and crack patterns occurred in the second retrofitted specimen, it was strengthened with CFRP described in Section 2.8.8. Additional diagonal patching and anchorages for debonding were applied. During the experiment, the cracks occurred at the joint region cannot be traced due to the CFRP wrapping.

The first flexural cracks were observed at a 0.20% drift level and at about 660 mm and 840 mm away from the face of the column. And in subsequent cycles of the same drift, other two cracks were formed. At the drift level of 35%, the flexural crack was formed at the location where the CFRP ended on the beam. The width of the crack which is the first crack was reached about 0.4 mm. The first shear cracks of the beam were occurred at the drift level of 1.40%. And the width of that crack was reached 1.2 mm at subsequent cycles.

At the interface of beam to column connections, diagonal CFRP sheets were start to rupture at the drift level of 2.20%, however cracks could not be propagated due to four layers of CFRP sheets at those locations. Also the concrete was crushed at the bottom side of the beam at this drift level. During the 2.75% drift level, the tip of the diagonal fibers started to debond as seen in Figure 3.32. The debonding cannot propagate due to the anchorages. At the drift level of 3.50%, the beam bottom reinforcements were buckled (Figure 3.32).

Figure 3.32. Debonding and beam hinging of Specimen TR-5-FRP-3

At the end of the tests, in order to see the damages at the joint region, CFRP materials were removed from the concrete. As seen in Figure 3.33, there were no significant damages observed at the joint region. The detailed crack propagations were given in Table A.37 to A.39 in Appendix A.

Figure 3.33. Final view of Specimen TR-5-FRP-3

The lateral load versus top displacement relationship of the specimen TR-5-FRP-3 is given in Figure 3.34. The performance of the specimen was improved significantly with using repairing materials and retrofitting the joint with CFRP. As in specimen TR-5-FRP-3, load deformation relationships, the yielding of the reinforcement was achieved. As a result the energy and stiffness value of the specimen were improved.

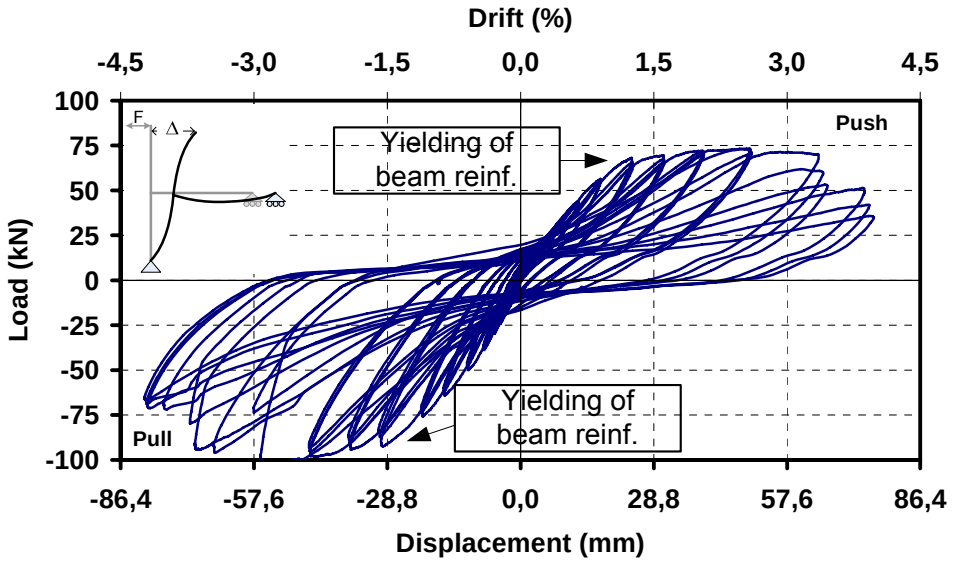


Figure 3.34. Lateral load versus top displacement for Specimen TR-5-FRP-3

### 3.1.13. Specimen TR-5 R

The repaired specimen TR-5-R was the same specimen with specimen TR-5 Control and tested in the same manner as specimen TR-5 Control. Maximum applied lateral load was 68 kN at a drift level of 1.00% in pull direction.

The first flexural crack was observed at about 500 mm and 700 mm away from the face of the column at a drift level of 0.20%, when the load was 22 kN. At the drift level of 0.50%, the first diagonal cracks occurred at the joint region in push direction. In the pull direction of same drift level, when the load was 50 kN, another diagonal crack occurred.

Some vertical cracks occurred at the joint and top column portion at a drift level of 1.00%. Also, the maximum load, 63 kN and 68 kN, were obtained in push and pull direction, respectively. The cover concrete were crushed and poured due to buckling of

column longitudinal reinforcement at the joint region as seen in Figures 3.35 and 3.36. The detailed crack propagations were given in Table A.40 to A.42 in Appendix A.

Figure 3.35. Damages of Specimen TR-5-R

The lateral load versus top displacement relationship of the specimen TR-5-R is given in Figure 3.37. The performance of the specimen was improved significantly with using repairing materials and retrofitting the joint with CFRP. As in specimen TR-5-FRP-2, load deformation relationships, the flexural capacity of the beam was reached.

Figure 3.36. Damages of Specimen TR-5-R

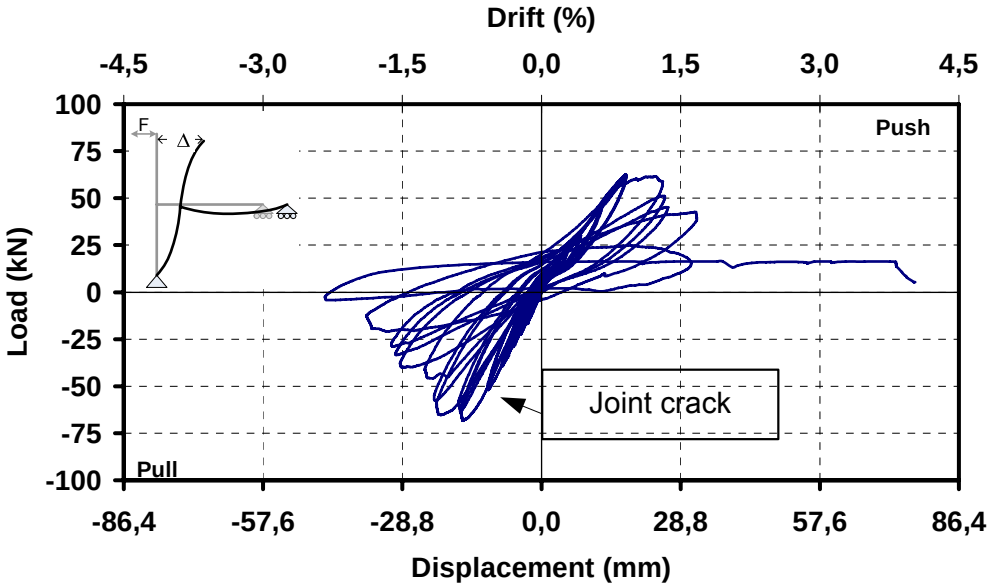


Figure 3.37. Lateral load versus top displacement for Specimen TR-5-R

## 3.2. Analysis of Test Results

This section includes all the experimental graphs such as Load-Drift envelopes, Moment-Curvature relationships of beam and columns, Shear deformation-Drift relationships and Shear deformation-Load relationships of the joint panel. Moreover, load versus drift envelope curves, stiffness degradation and some energy graphs were compared in this section.

### 3.2.1. Lateral Load versus Drift Relationships

The envelopes of hysteretic lateral load versus story drift responses for the control, strengthened, and repaired specimens were compared in Figure 3.38 to Figure 3.40. The effects of strengthening techniques can be seen obviously. Although all the CFRP strengthened specimens have the similar envelope, the failure modes are different.

As seen in Figure 3.38, specimen TR-1 Control carried the relatively high lateral load. Specimen TR-3 Control has less lateral load capacity due to its small cross-section. The remaining control specimens showed similar behavior, although they have different

deficiencies. The possible reason is, premature joint shear failures developed before the affects of deficiencies come to the picture.

Although specimen TR-5 Control behaved better than the specimen TR-2 Control and the specimen TR-4 Control, it was selected as a critical specimen that has to be strengthened, because it included all the deficiencies in itself. Once the joint shear was prevented, deficiencies have possible effects on behavior.

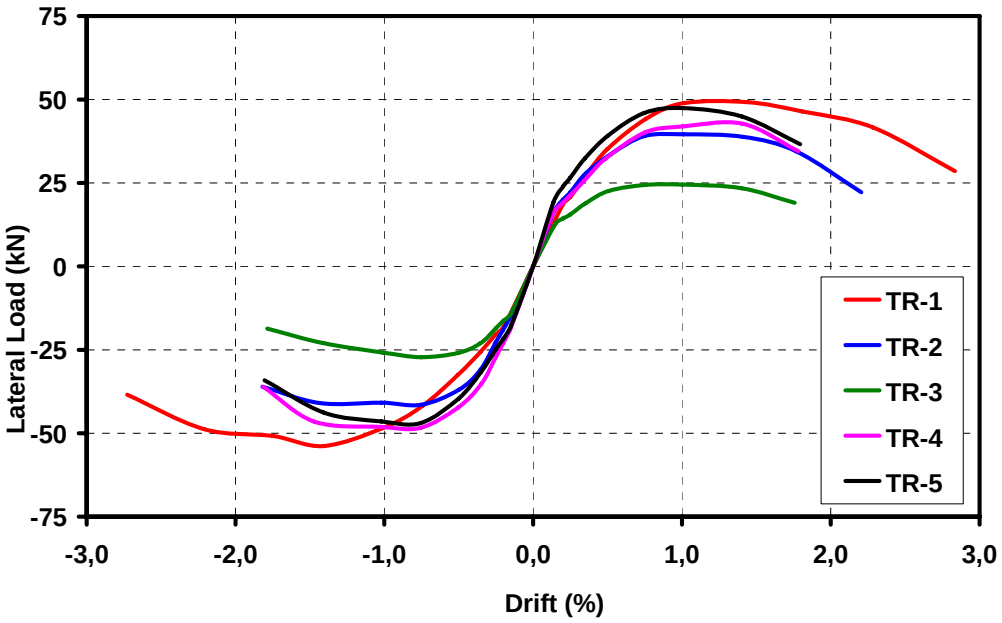


Figure 3.38. Backbone curve of control specimens

When the behavior of specimen TR-5 Control compared with CFRP strengthened specimens, it was obvious that CFRP improved the behavior much (Figure 3.39). The lateral load capacity increased 50% by proposed retrofitting techniques. However, in specimen TR-5-FRP-1, due to the insufficient wrapping and rupturing of CFRP layers, the shear failure observed at the joint region at a higher drift level.

Specimens TR-5-FRP-2 and TR-5-FRP-3 showed similar behavior. However, debonding of the CFRP layers from the beam was observed in TR-5-FRP-2. Therefore, four CFRP anchorages were used for the beam in TR-5-FRP-3.

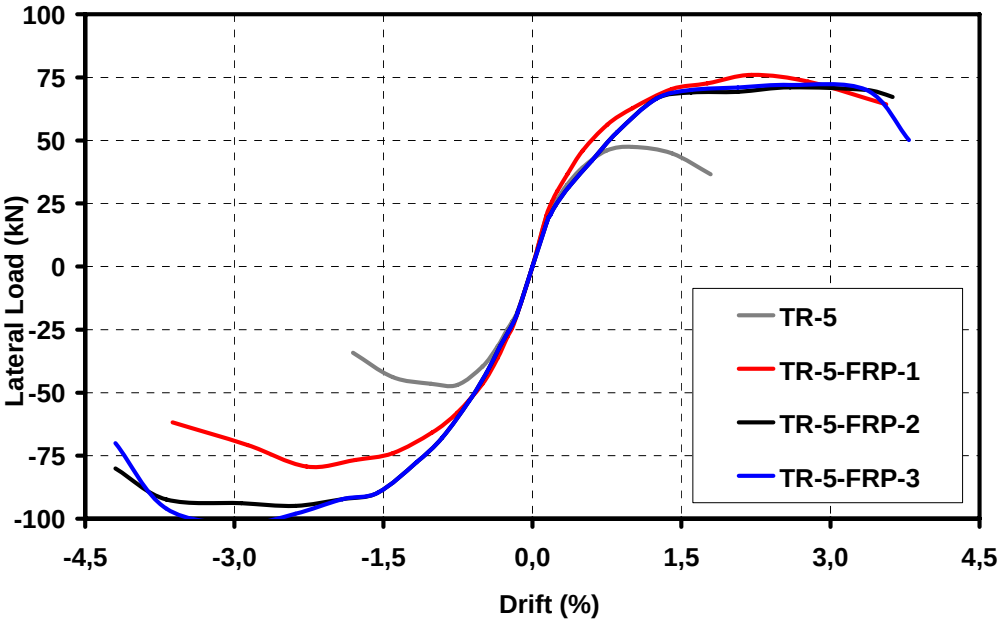


Figure 3.39. Backbone curve of strengthened specimens

Lateral load capacities of repaired only and repaired and retrofitted specimens improved significantly. Repairing materials delayed the shear cracking of the joints. However, repaired and retrofitted specimens (TR-2-R-FRP and TR-4-R-FRP) showed similar behavior with undamaged retrofitted specimens (Figure 3.40). Shear failure of joint was almost diminished.

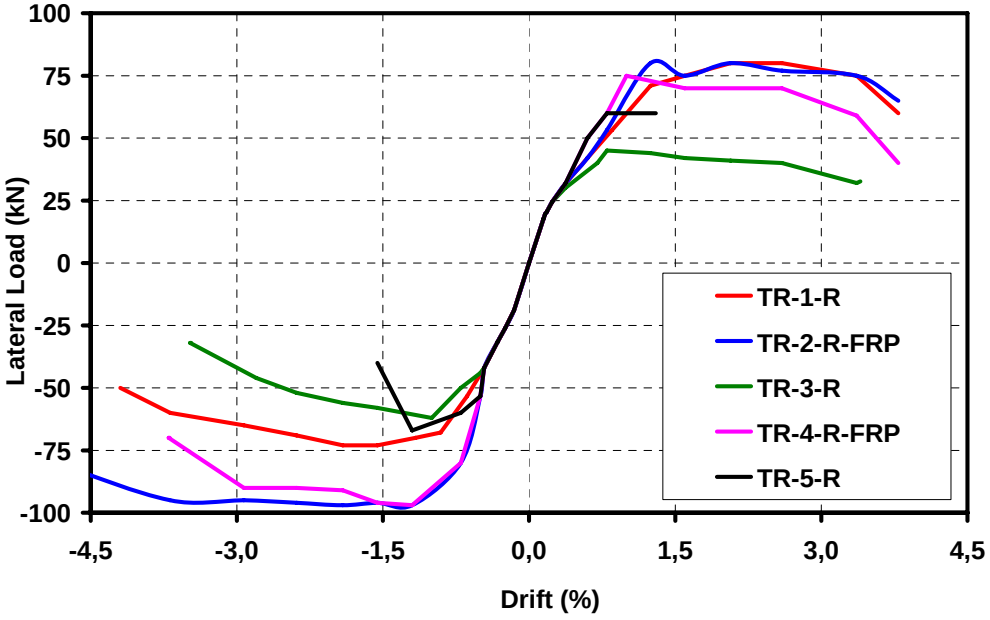


Figure 3.40. Backbone curve of repaired specimens

### 3.2.2. Moment Curvatures Relationships

As defined in Section (2.5.1) on instrumentation, average curvature readings were taken at four different locations on beam column specimen. The placement of displacement sensors close to the maximum tensile and compressive strain regions of the columns and beams allows an average curvature measurement along the gauge length of the sensors. The curvature measurement and instrumentation is described through Figures 3.41 and 3.42 and can be calculated by using Eq (3.1).

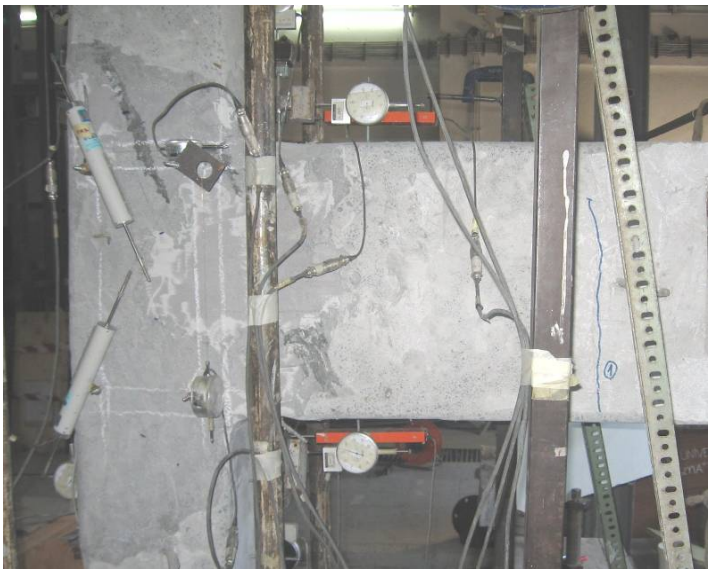

Figure 3.41. Beam curvature instrumentation

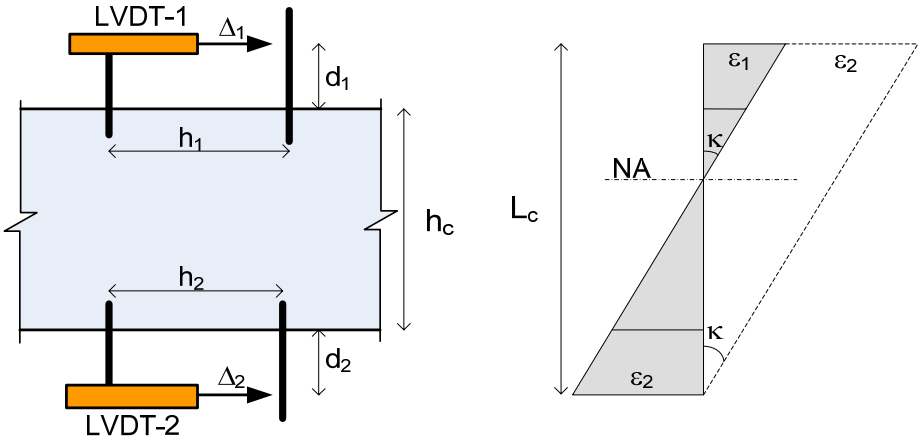


Figure 3.42. Curvature readings and calculations

$$\kappa = \frac{\Delta_1 / h_1 + \Delta_2 / h_2}{h_c + d_1 + d_2} = \frac{\varepsilon_1 + \varepsilon_2}{\sum L_c} \tag{3.1}$$

where; $\Delta_1$, $\Delta_2$ are relative longitudinal displacements readings taken from the displacement sensors, $h_1$ and $h_2$ are the gauge lengths of the displacement sensors, $h_c$ is the width of the member (column or beam), and $d_1$ and $d_2$ are the distances shown in Figure 3.42.

Experimental moment versus curvature relationships were obtained by using the above equation. This can be obtained at the possible plastic hinge region of the columns and the beam. The relationships are presented in Figures 3.43 to 3.81 for all specimens.

In all control specimens, the columns and the beam did not deform significantly under lateral loading. In both push and pull direction of loading, joint shear failure observed before the plastic hinge occurs within the structural members. And also, the effective height of the column is 710 mm which is the distance between the joint block and the loading level makes the curvature values small in columns. This indicates that the columns did not deform significantly under that lateral load. However, the curvature values of beam were much greater than column curvature values because of length of beam. In the specimens, since there is no slip problem in beam reinforcement, the difference between push and pull curvature values and moment values was due to only the differences in number of reinforcement in top and bottom of the cross-section of the beam.

The moment-curvature relationships of column (bottom portion and top portion) and beam for all specimens were shown in Figures 3.43 to 3.81.

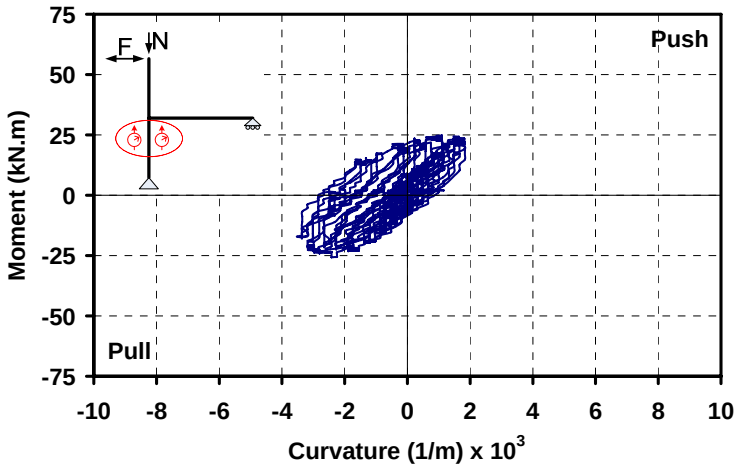


Figure 3.43. Moment versus curvature of column (bot.) for Specimen TR-1 Control

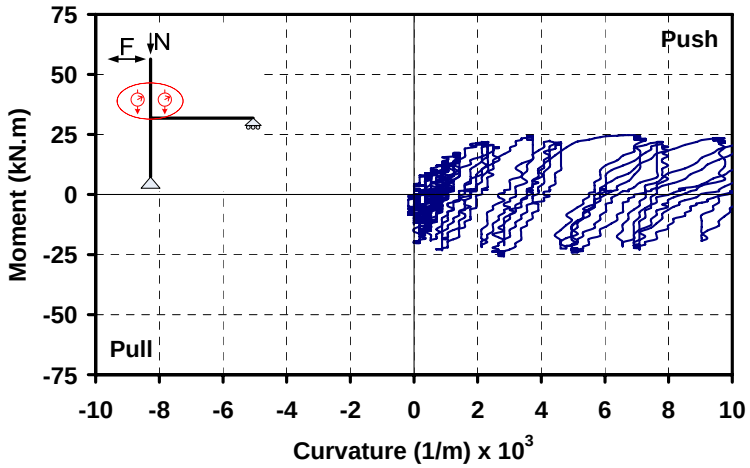


Figure 3.44. Moment versus curvature of column (top) for Specimen TR-1 Control

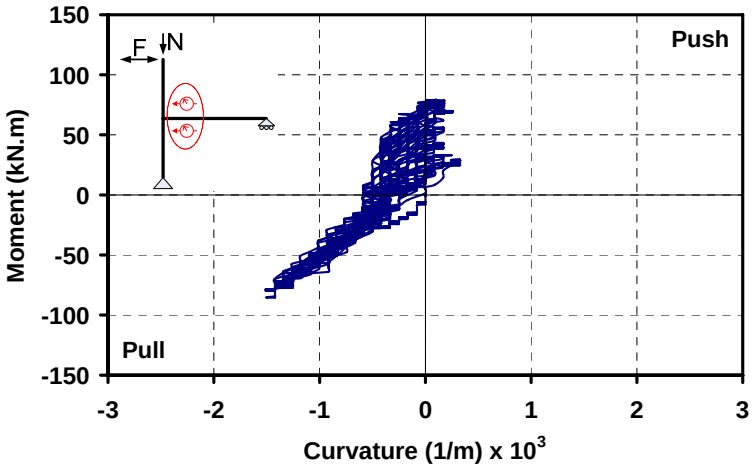


Figure 3.45. Moment versus curvature of beam for Specimen TR-1 Control

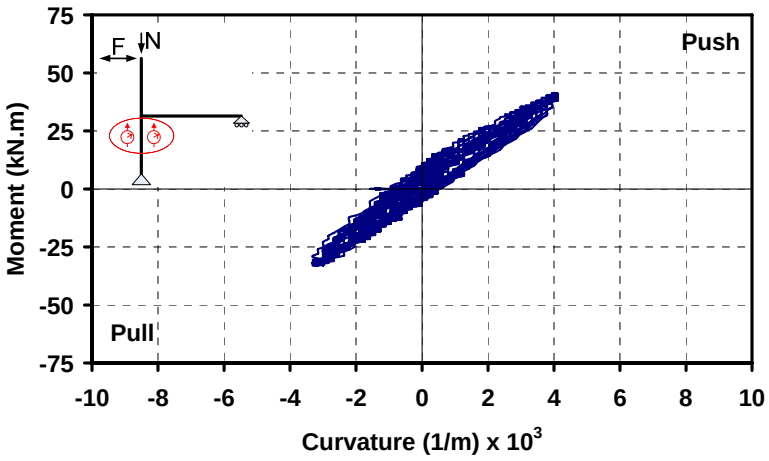


Figure 3.46. Moment versus curvature of column (bot.) for Specimen TR-1-R

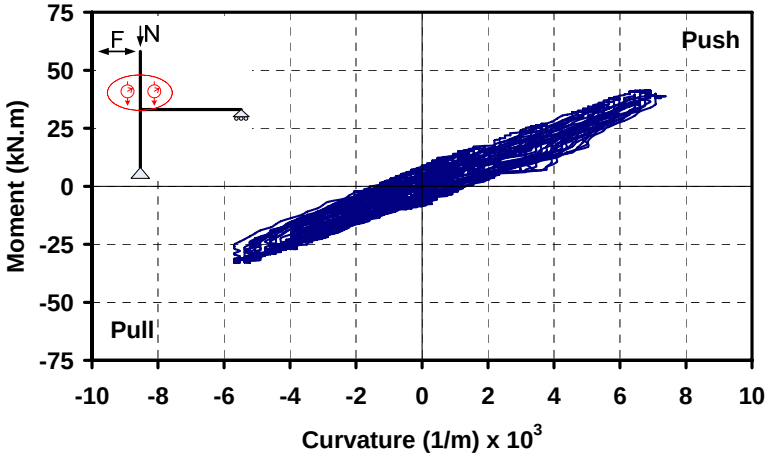


Figure 3.47. Moment versus curvature of column (top) for Specimen TR-1-R

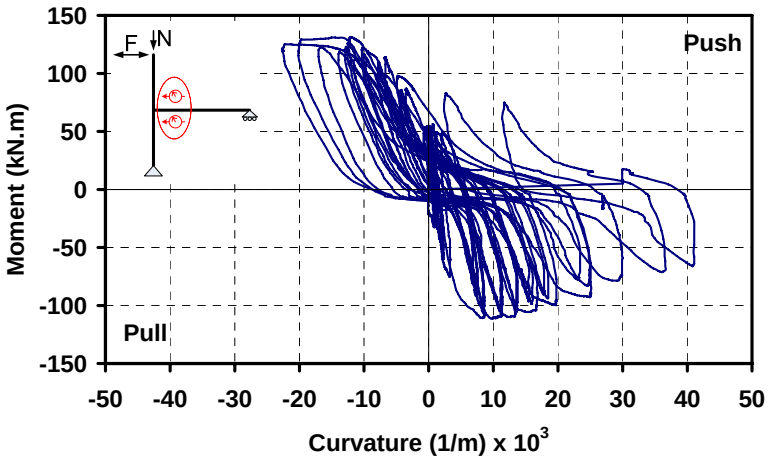


Figure 3.48. Moment versus curvature of beam for Specimen TR-1-R

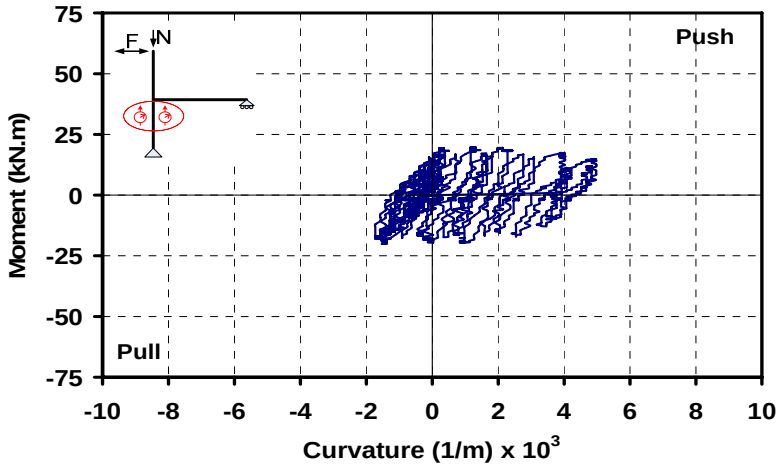


Figure 3.49. Moment versus curvature of column (bot.) for Specimen TR-2 Control

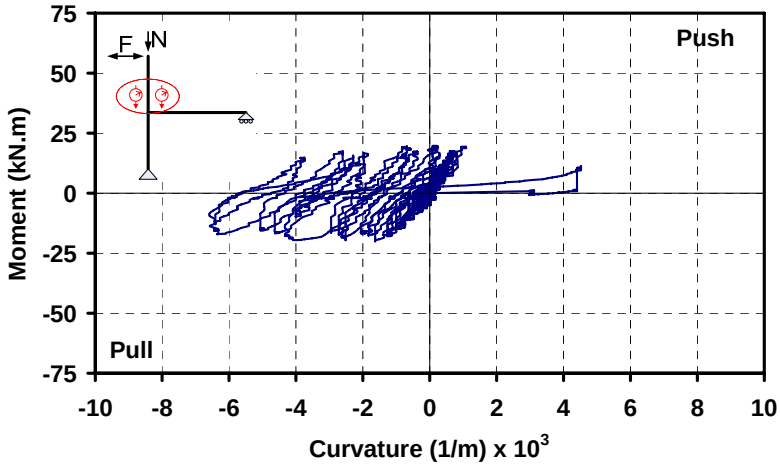


Figure 3.50. Moment versus curvature of column (top) for Specimen TR-2 Control

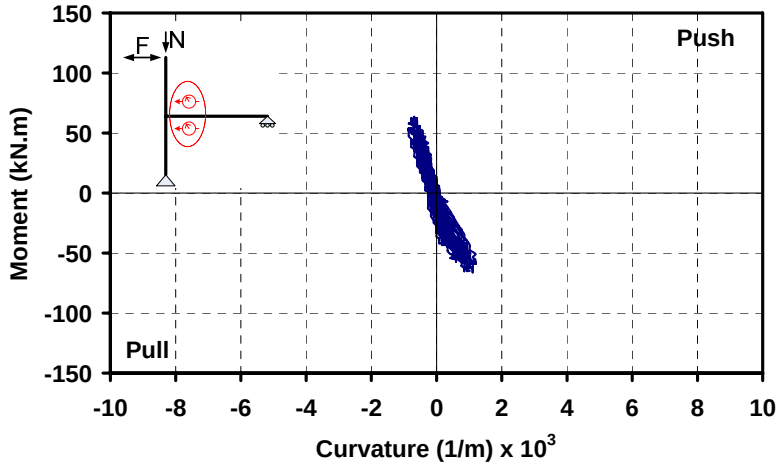


Figure 3.51. Moment versus curvature of beam for Specimen TR-2 Control

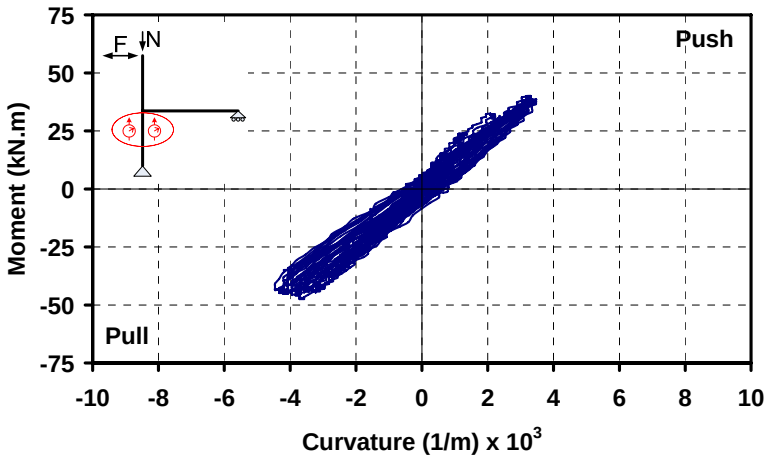


Figure 3.52. Moment versus curvature of column (bot.) for Specimen TR-2-R-FRP

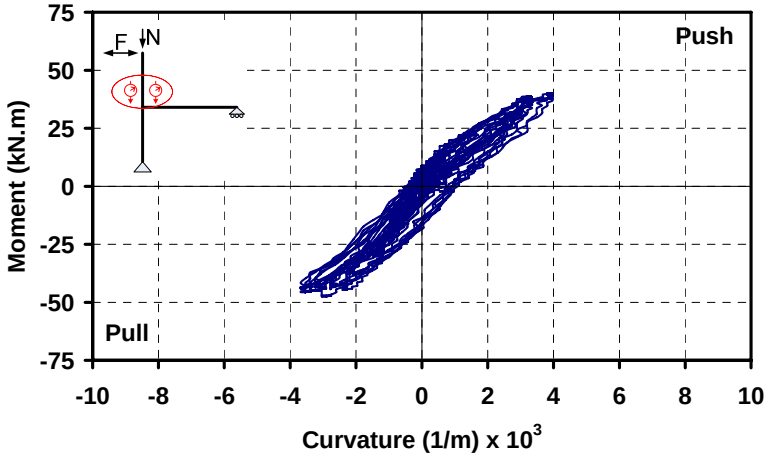


Figure 3.53. Moment versus curvature of column (top) for Specimen TR-2-R-FRP

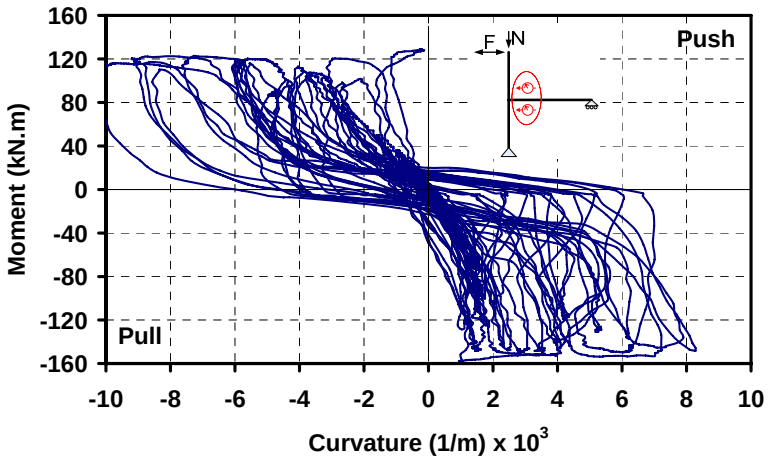


Figure 3.54. Moment versus curvature of beam for Specimen TR-2-R-FRP

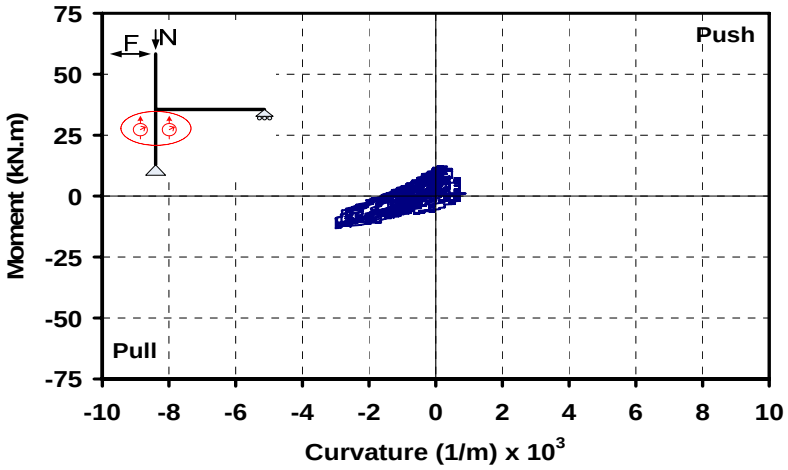


Figure 3.55. Moment versus curvature of column (bot.) for Specimen TR-3 Control

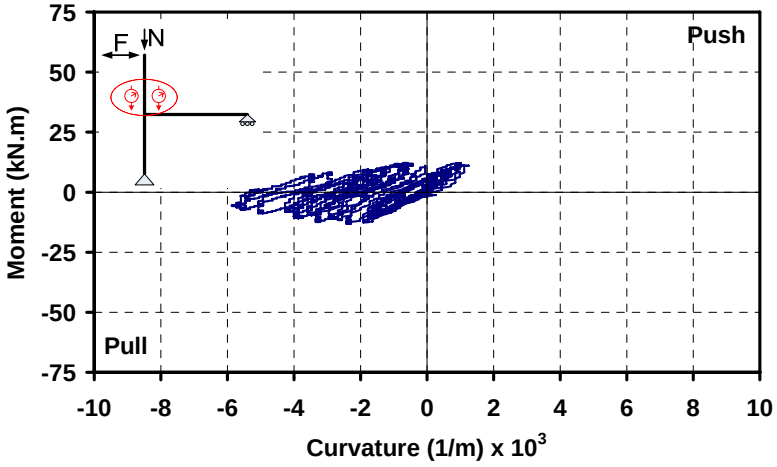


Figure 3.56. Moment versus curvature of column (top) for Specimen TR-3 Control

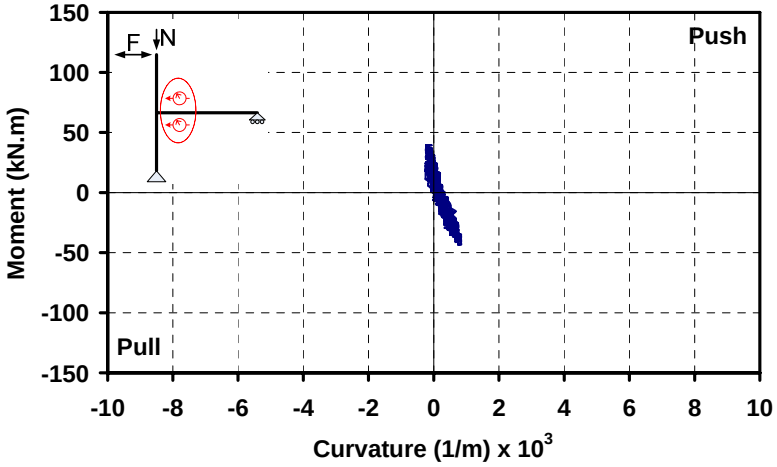


Figure 3.57. Moment versus curvature of beam for Specimen TR-3 Control

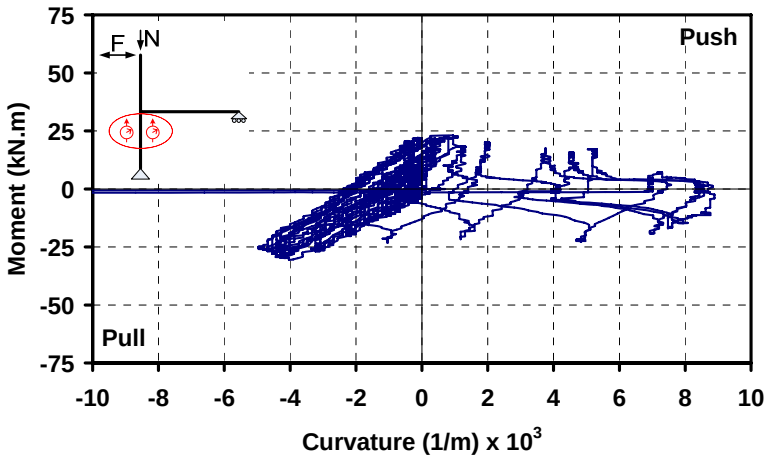


Figure 3.58. Moment versus curvature of column (bot.) for Specimen TR-3-R

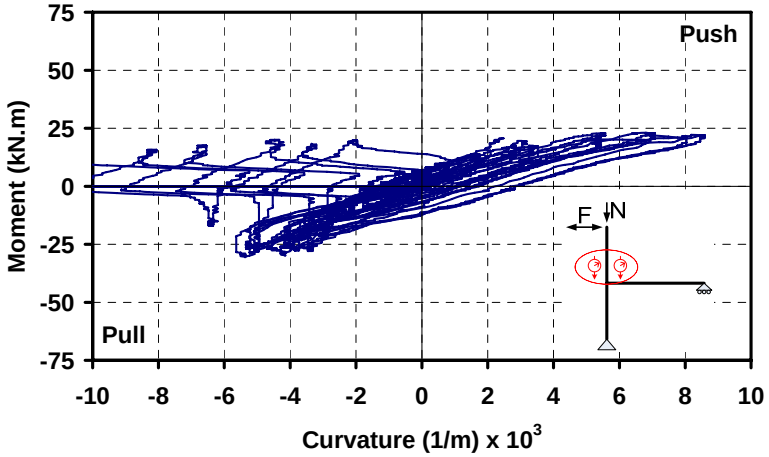


Figure 3.59. Moment versus curvature of column (top) for Specimen TR-3-R

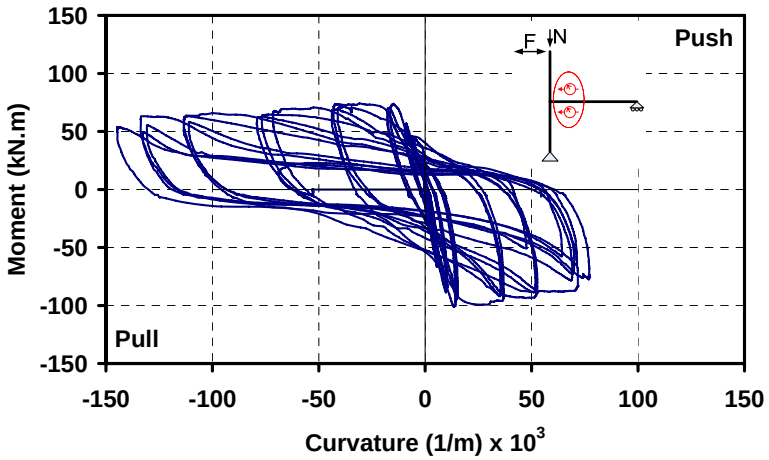


Figure 3.60. Moment versus curvature of beam for Specimen TR-3-R

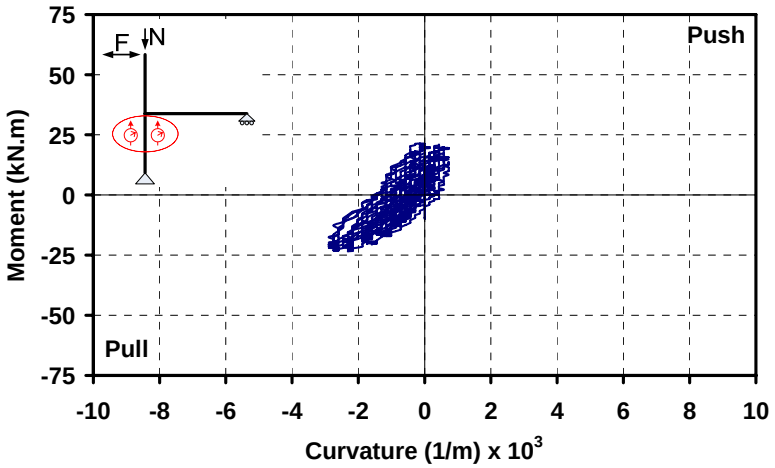


Figure 3.61. Moment versus curvature of column (bot.) for Specimen TR-4

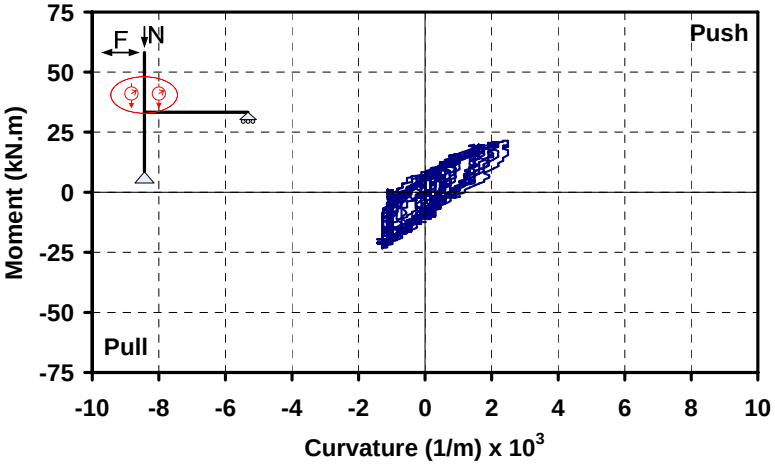


Figure 3.62. Moment versus curvature of column (top) for Specimen TR-4 Control

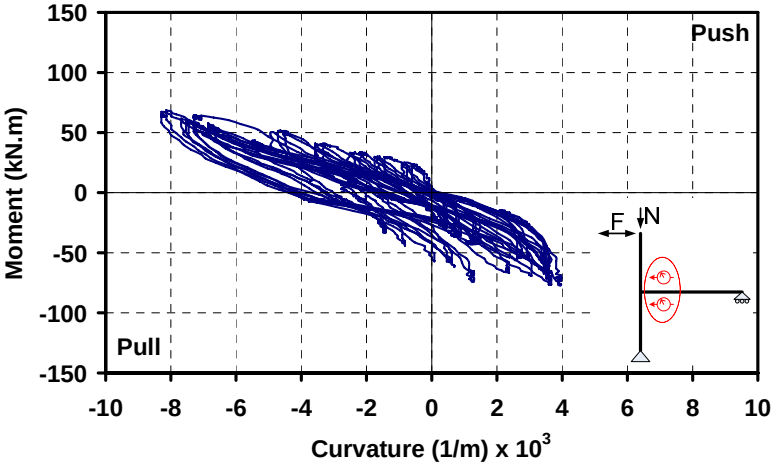


Figure 3.63. Moment versus curvature of beam for Specimen TR-4 Control

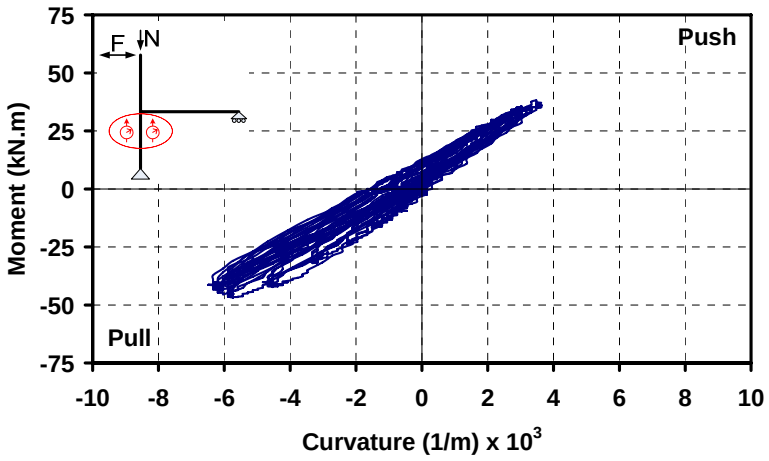


Figure 3.64. Moment versus curvature of column (bot.) for TR-4-R-FRP

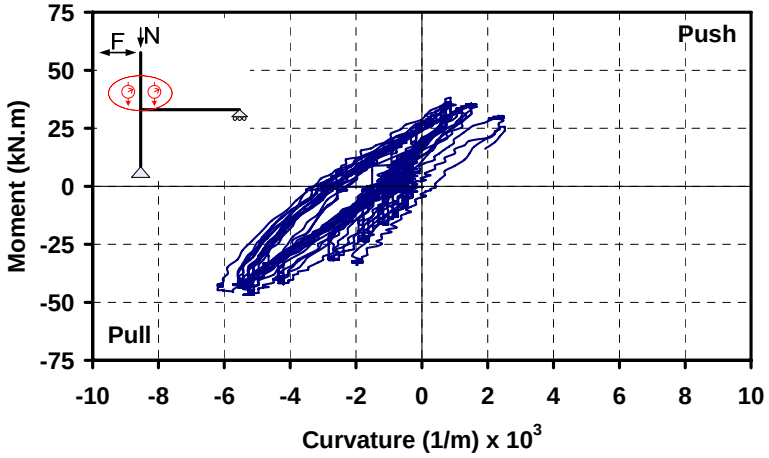


Figure 3.65. Moment versus curvature of column (top) for TR-4-R-FRP

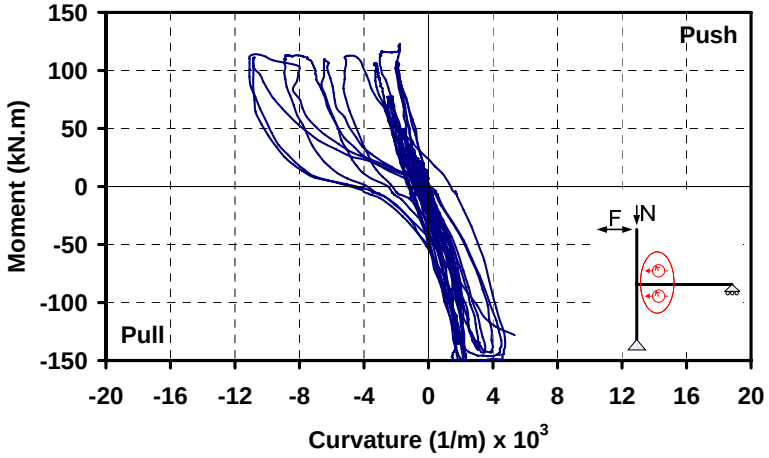


Figure 3.66. Moment versus curvature of beam for TR-4-R-FRP

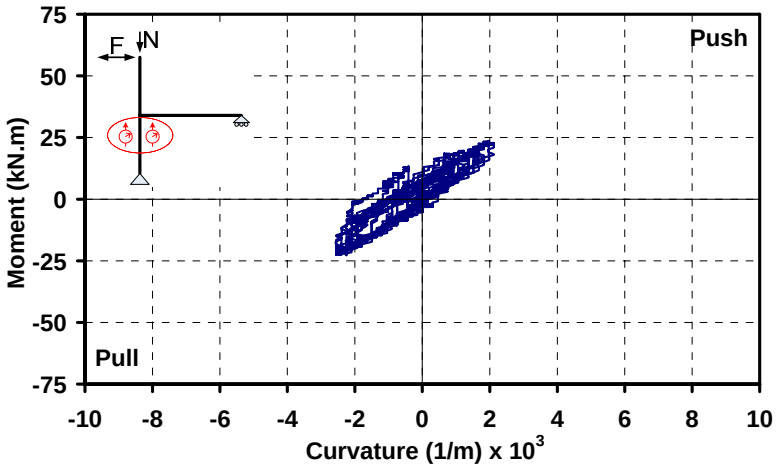


Figure 3.67. Moment versus curvature of column (bot.) for TR-5 Control

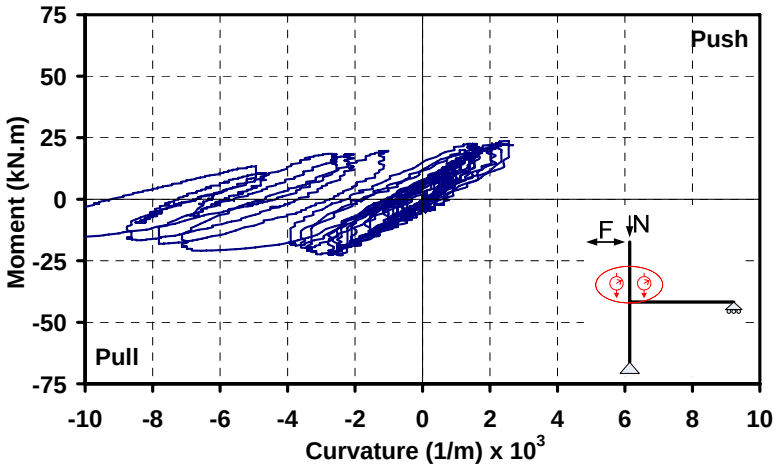


Figure 3.68. Moment versus curvature of column (top) for Specimen TR-5 Control

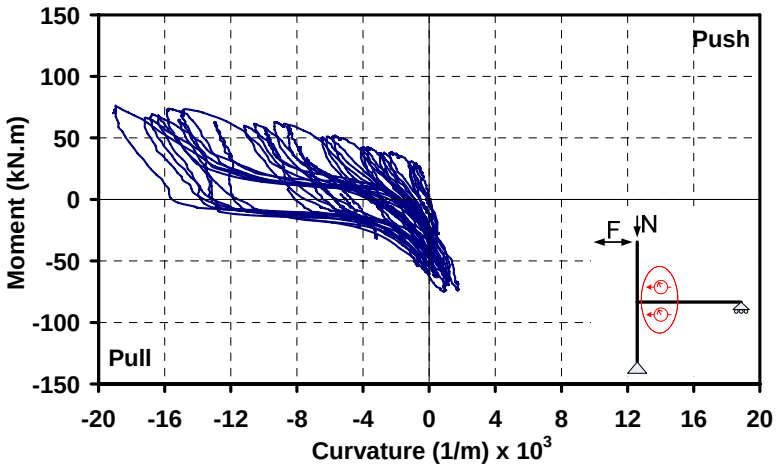


Figure 3.69. Moment versus curvature of beam for Specimen TR-5 Control

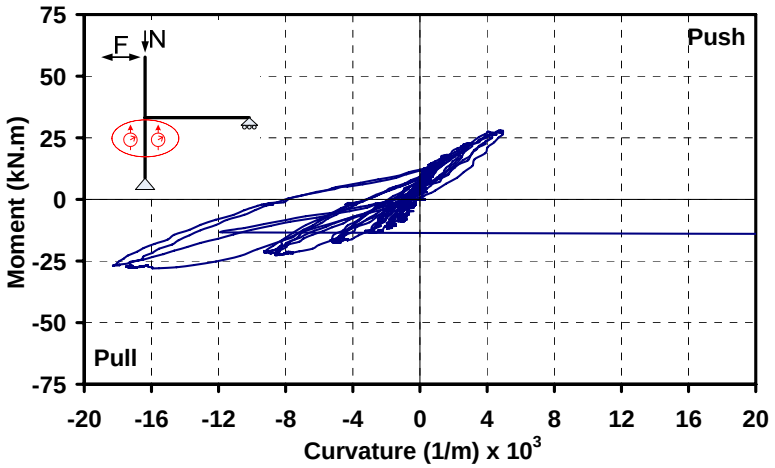


Figure 3.70. Moment versus curvature of column (bot.) for Specimen TR-5-FRP-1

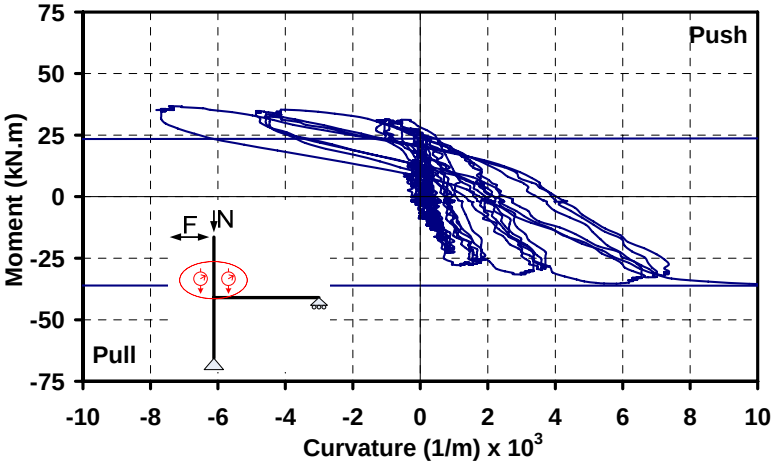


Figure 3.71. Moment versus curvature of column (top) for Specimen TR-5-FRP-1

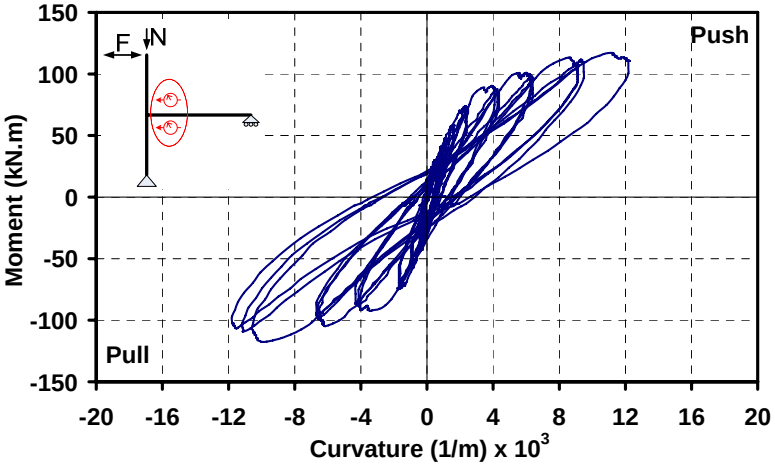


Figure 3.72. Moment versus curvature of beam for Specimen TR-5-FRP-1

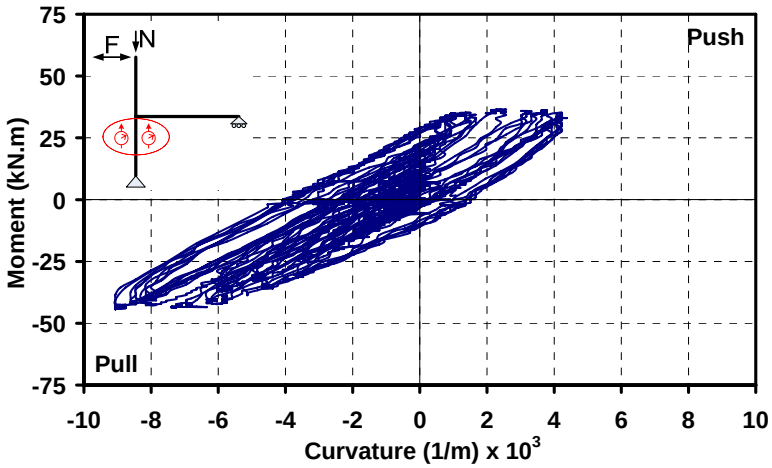


Figure 3.73. Moment versus curvature of column (bot.) for Specimen TR-5-FRP-2

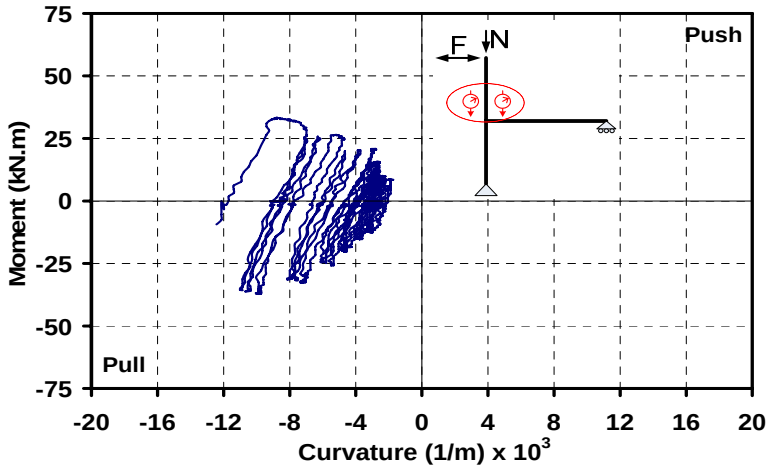


Figure 3.74. Moment versus curvature of column (top) for Specimen TR-5-FRP-2

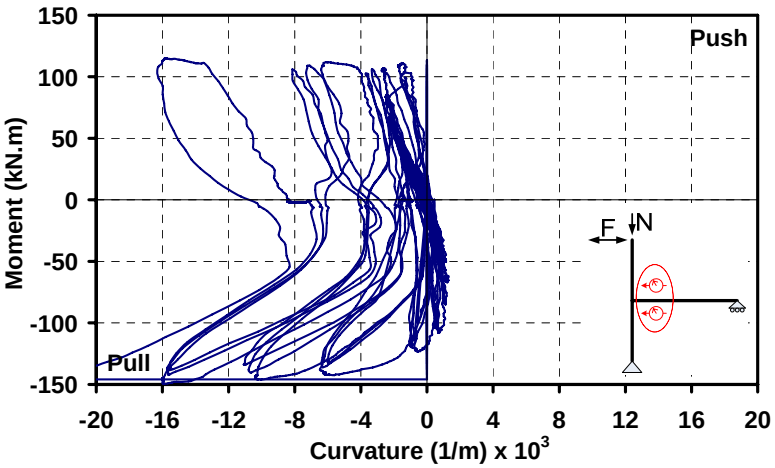


Figure 3.75. Moment versus curvature of beam for Specimen TR-5-FRP-2

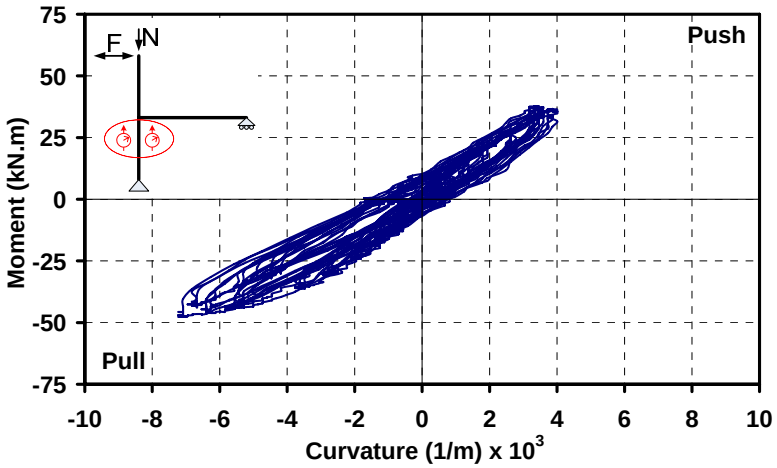


Figure 3.76. Moment versus curvature of column (bot.) for Specimen TR-5-FRP-3

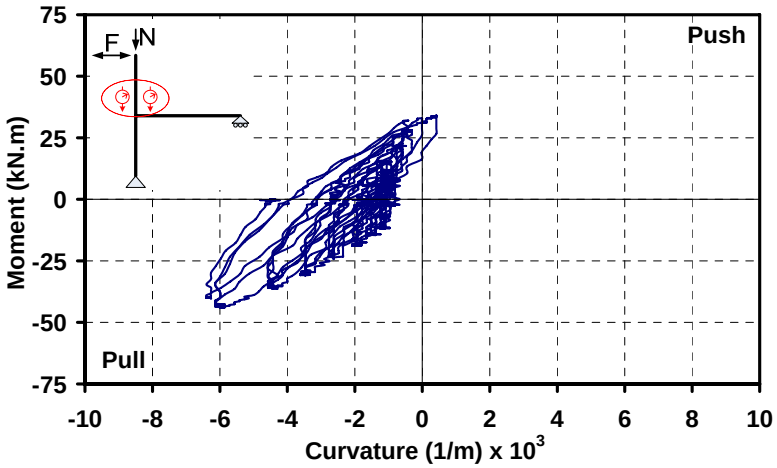


Figure 3.77. Moment versus curvature of column (top) for Specimen TR-5-FRP-3

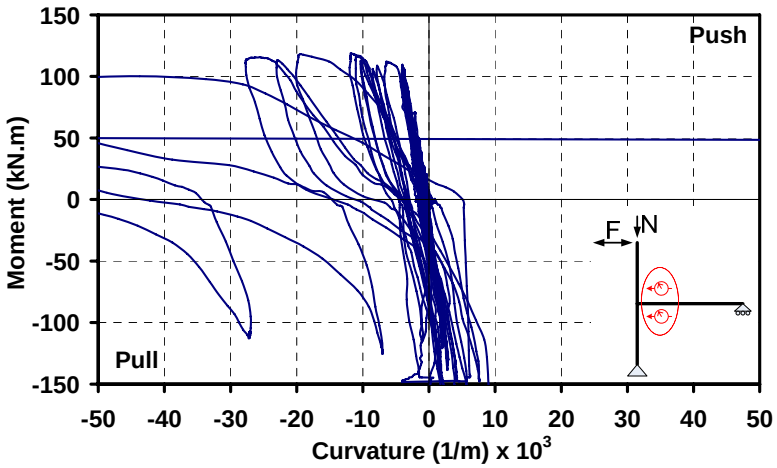


Figure 3.78. Moment versus curvature of beam for Specimen TR-5-FRP-3

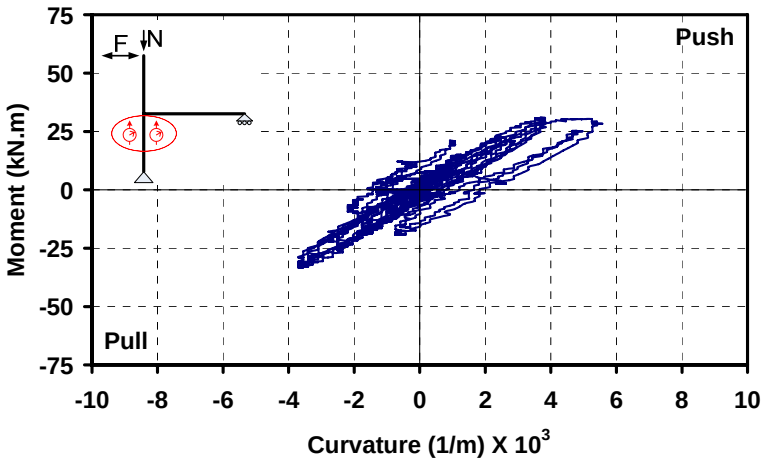


Figure 3.79. Moment versus curvature of column (bot.) for Specimen TR-5-R

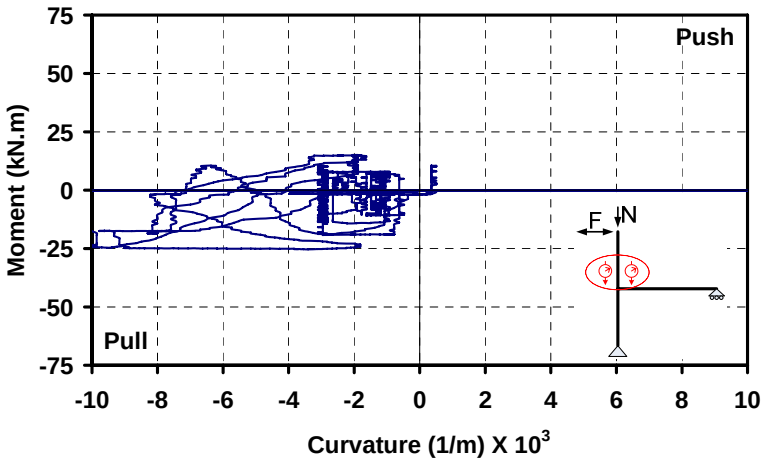


Figure 3.80. Moment versus curvature of column (top) for Specimen TR-5-R

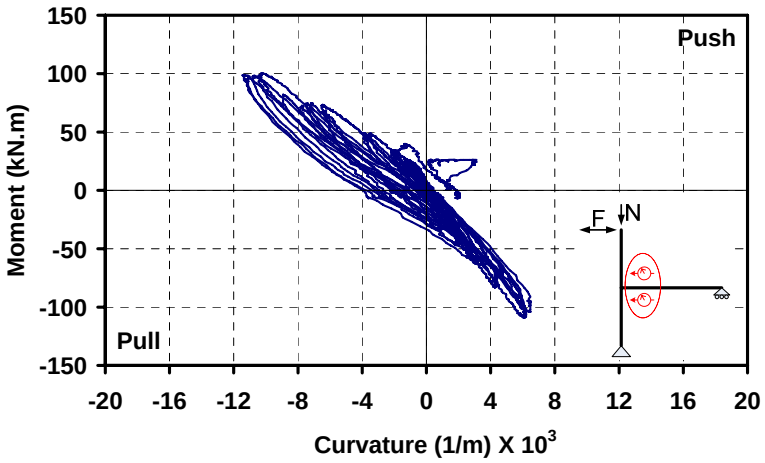


Figure 3.81. Moment versus curvature of beam for Specimen TR-5-R

In all experiment indicates that the curvature readings of the columns were relatively small than that of columns. Due to the shorter lever arm column has, the curvature readings were small.

### 3.2.3. Joint Shear deformations

For all specimens, shear deformations were also measured at the beam column joint panel region using two diagonal LVDTs installed as shown in Figure 3.82. Using the readings from these LVDTs, the shear deformation of the joints can be calculated according to Eq (3.2) (Figure 3.83).


Figure 3.82. Shear deformation readings

$$\gamma_s = \tan^{-1}\left(\frac{\sqrt{D_1^{\,2} - Y^2} - \sqrt{D_2^{\,2} - Y^2}}{2Y}\right) \tag{3.2}$$

where, $\gamma_s$ is shear deformation (rad); $D_1$ and $D_2$ are gauge lengths of diagonally placed LVDTs, and $X$ and $Y$ are the dimensions of undeformed joint panel. In this relationship, it is assumed that the height and the width of the shear panel do not change due to small shear deformations.

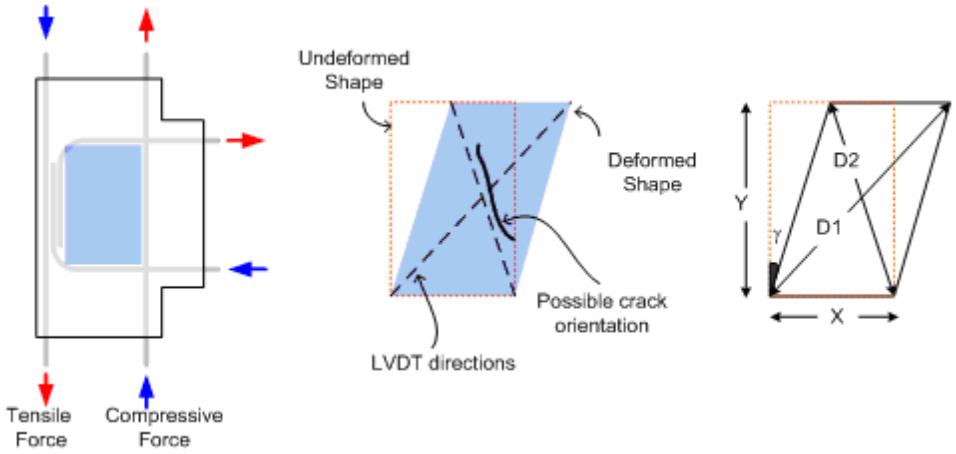


Figure 3.83. Shear deformation measurement

By using the given equation, lateral load versus shear deformation relationships of the joint panels were obtained. These relationships are presented for all specimens in Figures 3.84 to 3.109.

In all control specimens, lateral load level of push and pull direction is almost same. This also indicates that the load transferred to the joint was almost same and the shear deformation occurred in the joint core was almost same in push and pull direction. All the cracks were occurred symmetrically in push and pull direction.

In repaired and strengthened specimens, the joint shear failures were almost prevented. No or less damages occurred at the joint region.

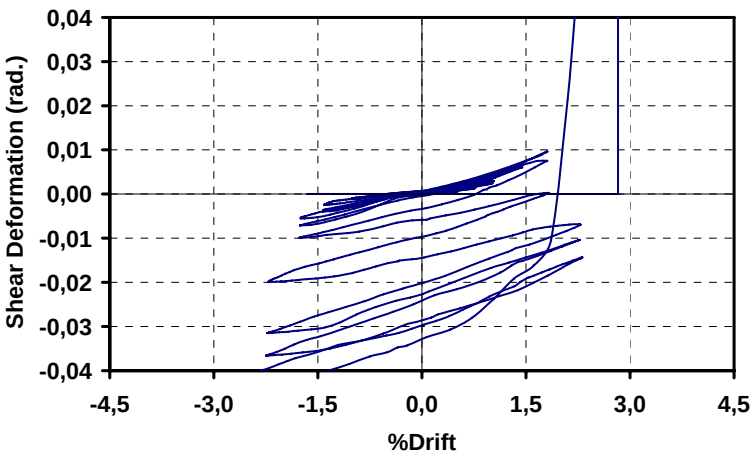


Figure 3.84. Shear deformation versus drift for Specimen TR-1 Control

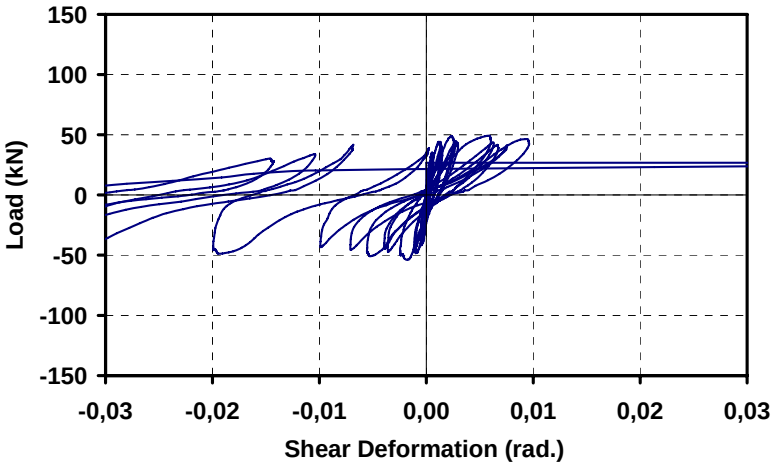


Figure 3.85. Shear deformation versus lateral load for Specimen TR-1 Control

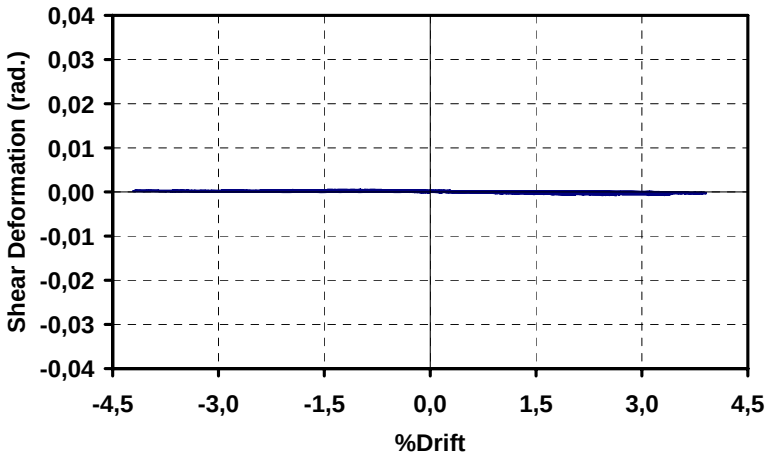


Figure 3.86. Shear deformation versus drift for Specimen TR-1-R

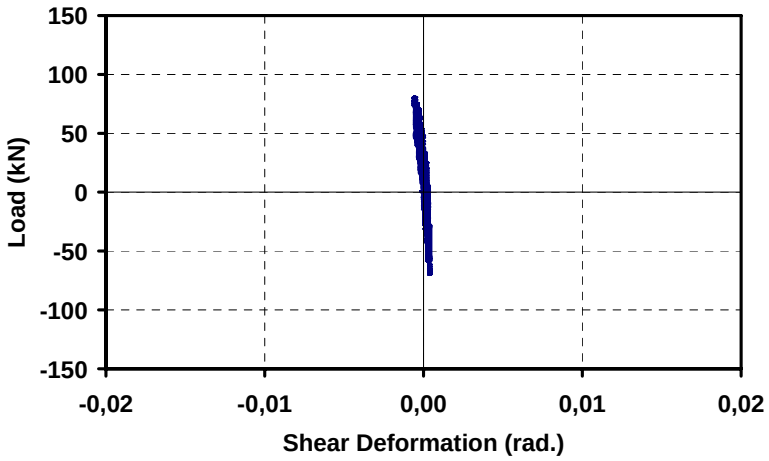


Figure 3.87. Shear deformation versus lateral load for Specimen TR-1-R

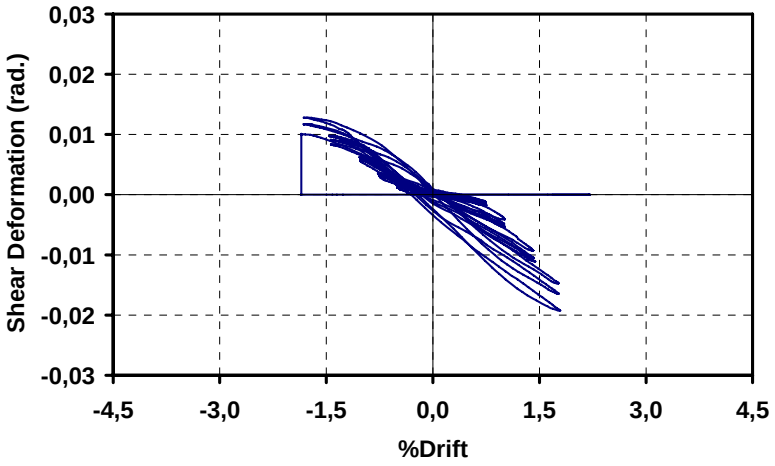


Figure 3.88. Shear deformation versus drift for Specimen TR-2 Control

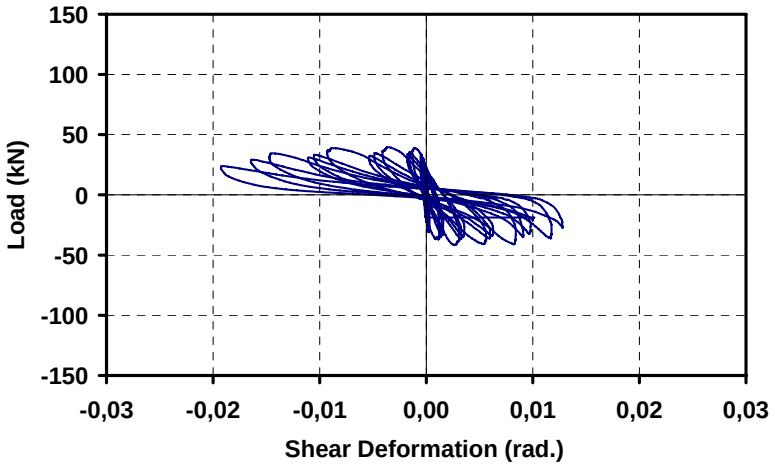


Figure 3.89. Shear deformation versus lateral load for Specimen TR-2 Control

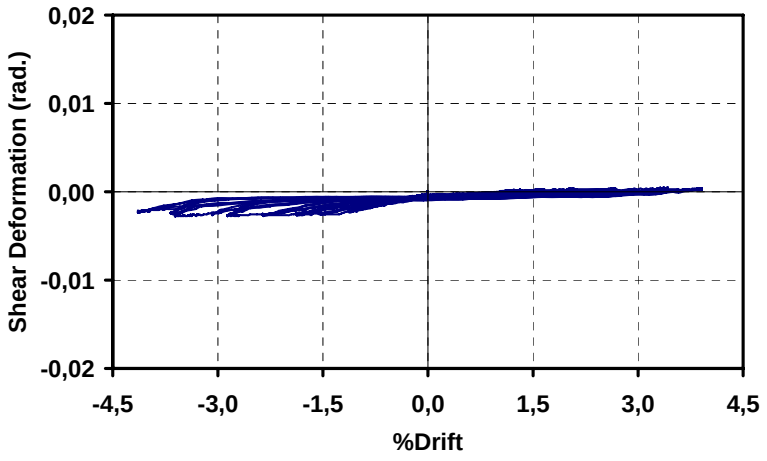


Figure 3.90. Shear deformation versus drift for Specimen TR-2-R-FRP

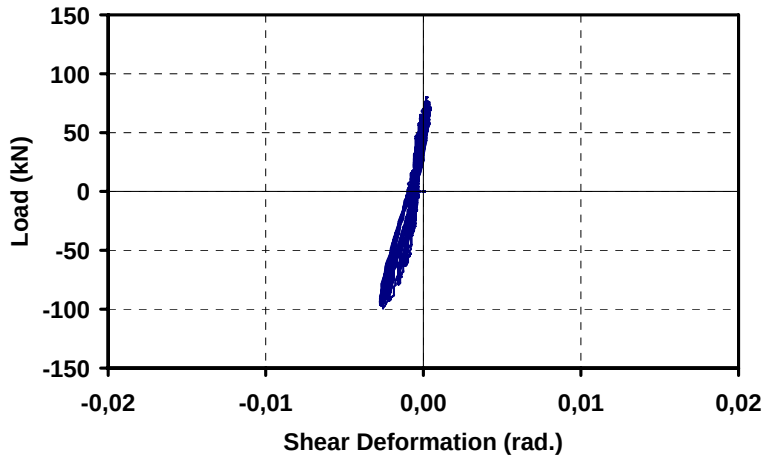


Figure 3.91. Shear deformation versus lateral load for Specimen TR-2-R-FRP

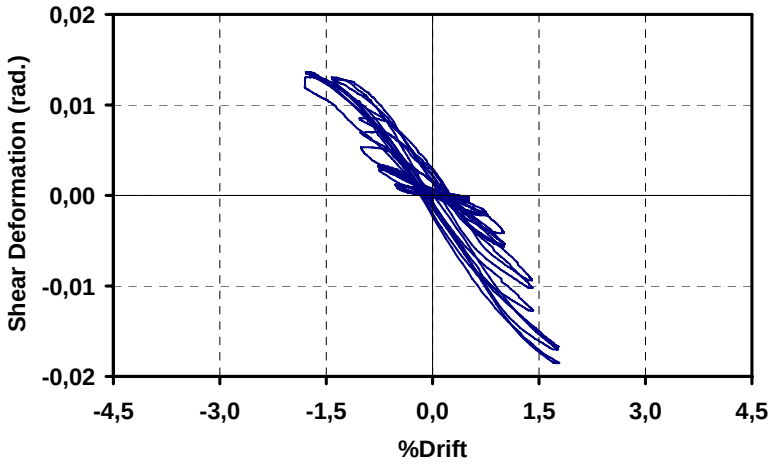


Figure 3.92. Shear deformation versus drift for Specimen TR-3 Control

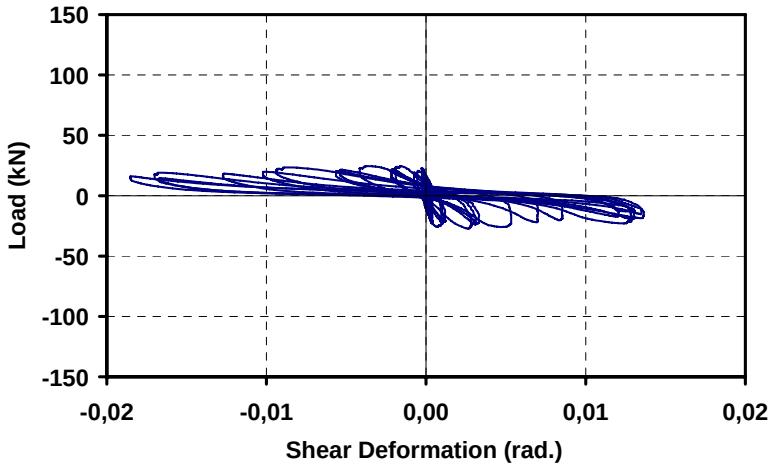


Figure 3.93. Shear deformation versus lateral load for Specimen TR-3 Control

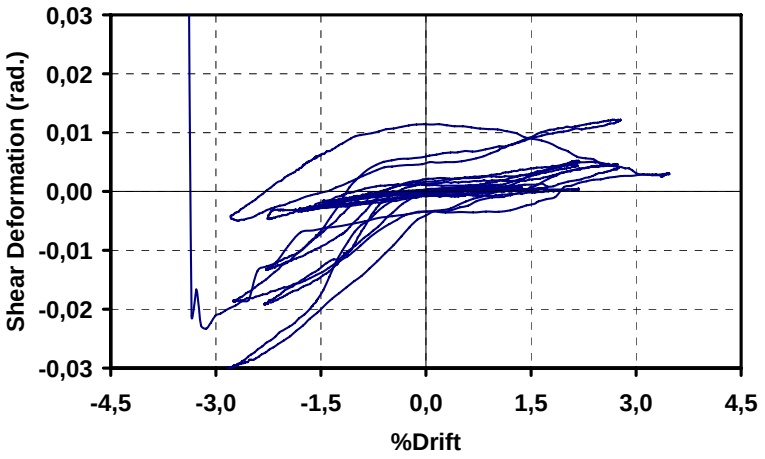


Figure 3.94. Shear deformation versus drift for Specimen TR-3-R

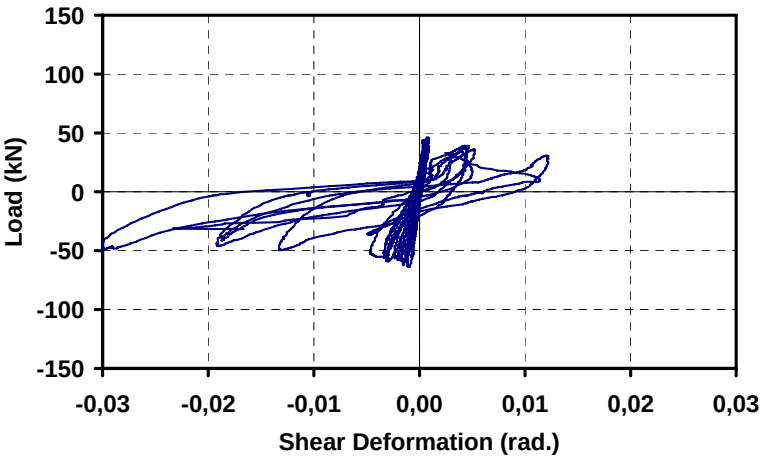


Figure 3.95. Shear deformation versus lateral load for Specimen TR-3-R

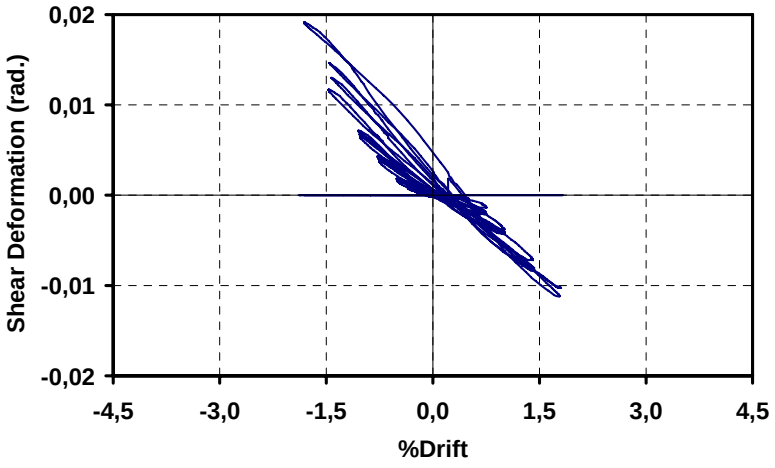


Figure 3.96. Shear deformation versus drift for Specimen TR-4 Control

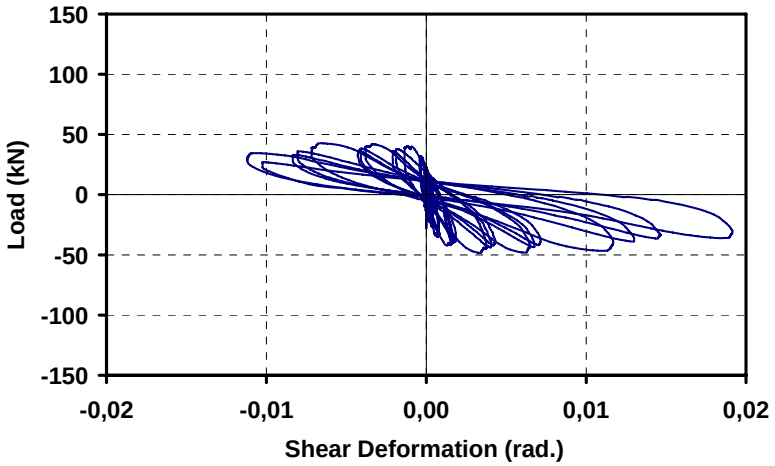


Figure 3.97. Shear deformation versus lateral load for TR-4 Control

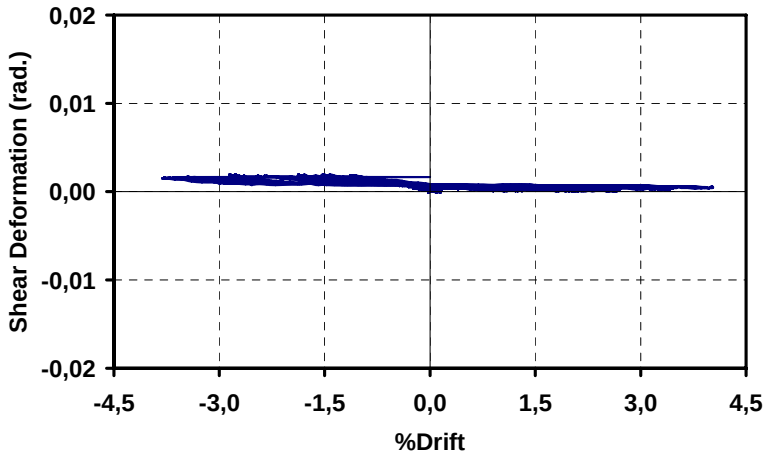


Figure 3.98. Shear deformation versus drift for Specimen TR-4-R-FRP

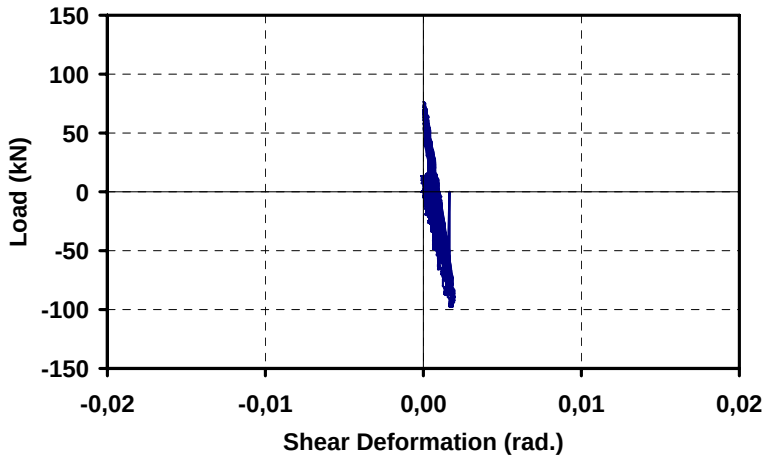


Figure 3.99. Shear deformation versus lateral load for Specimen TR-4-R-FRP

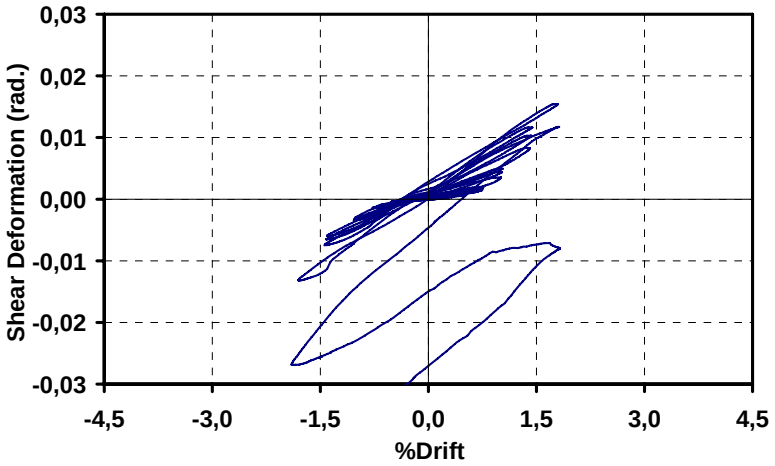


Figure 3.100. Shear deformation versus drift for Specimen TR-5 Control

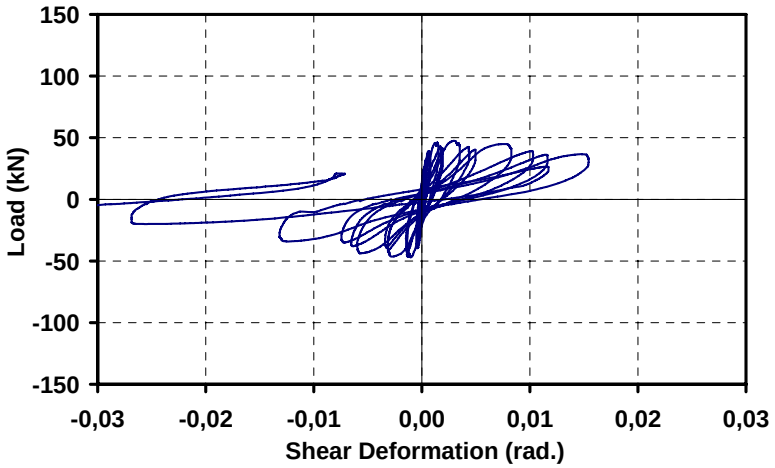


Figure 3.101. Shear deformation versus lateral load for Specimen TR-5 Control

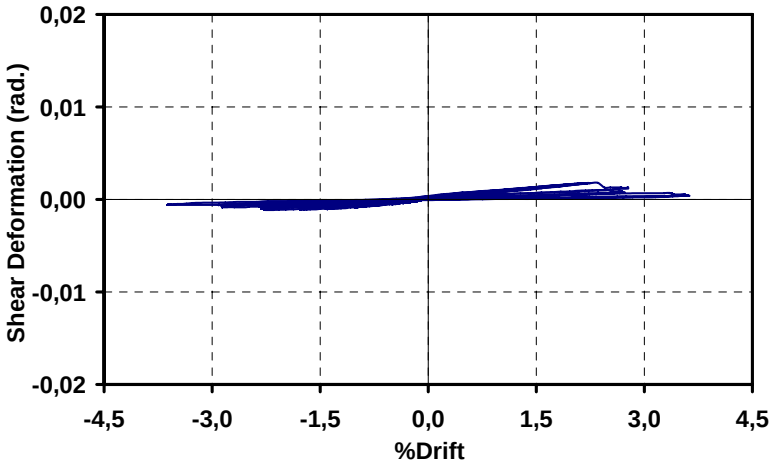


Figure 3.102. Shear deformation versus drift for Specimen TR-5-FRP-1

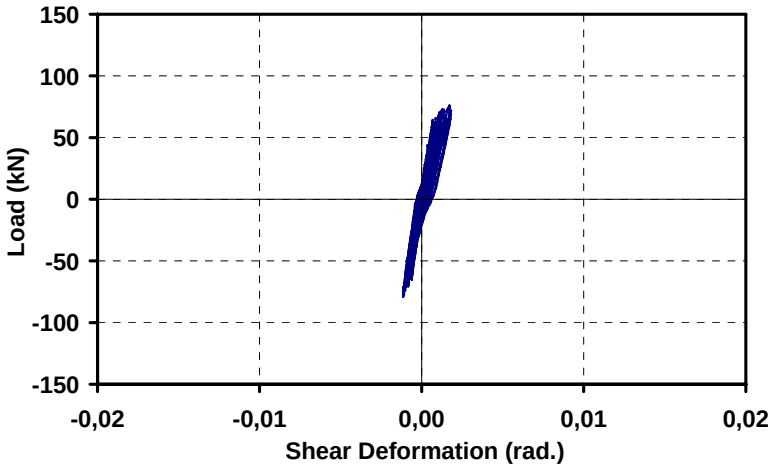


Figure 3.103. Shear deformation versus lateral load for Specimen TR-5-FRP-1

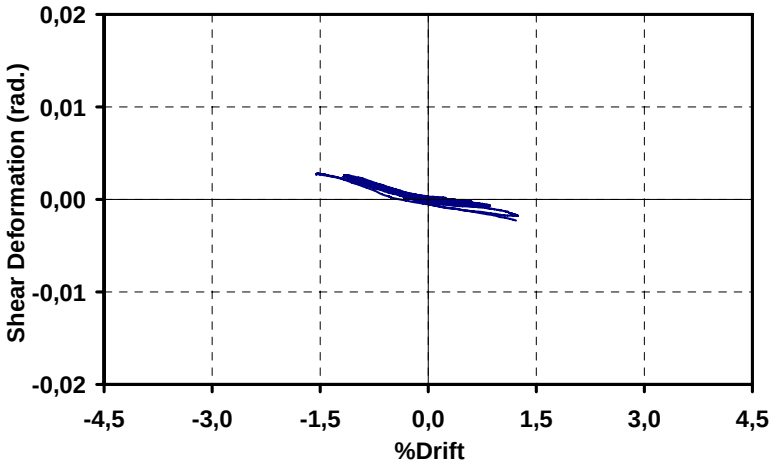


Figure 3.104. Shear deformation versus drift for Specimen TR-5-FRP-2

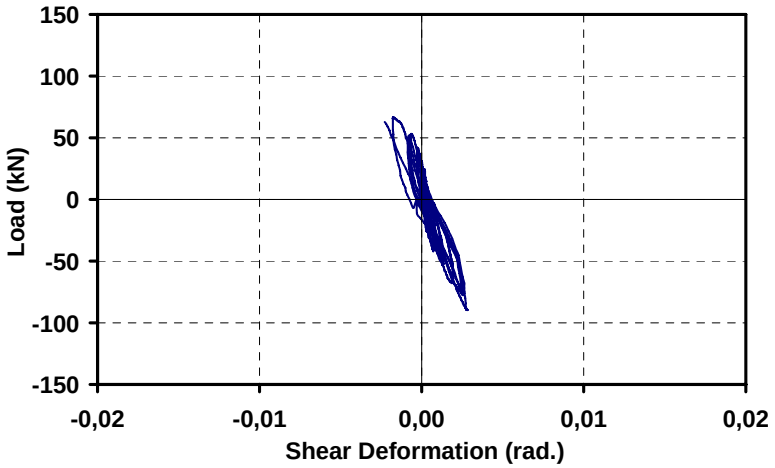


Figure 3.105. Shear deformation versus lateral load for Specimen TR-5-FRP-2

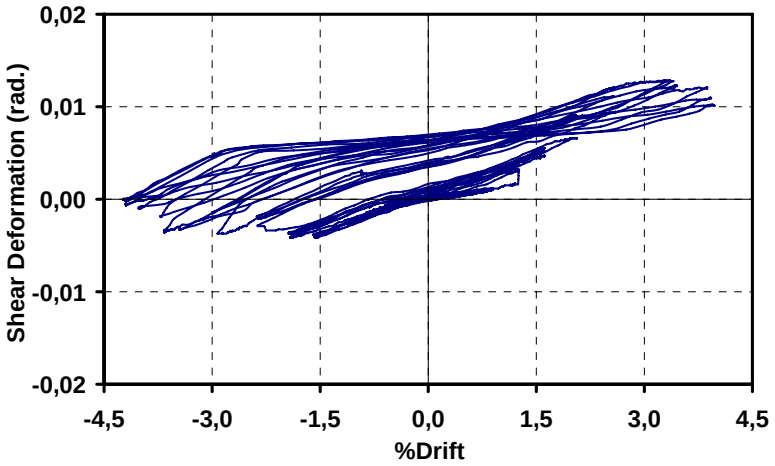


Figure 3.106. Shear deformation versus drift for Specimen TR-5-FRP-3

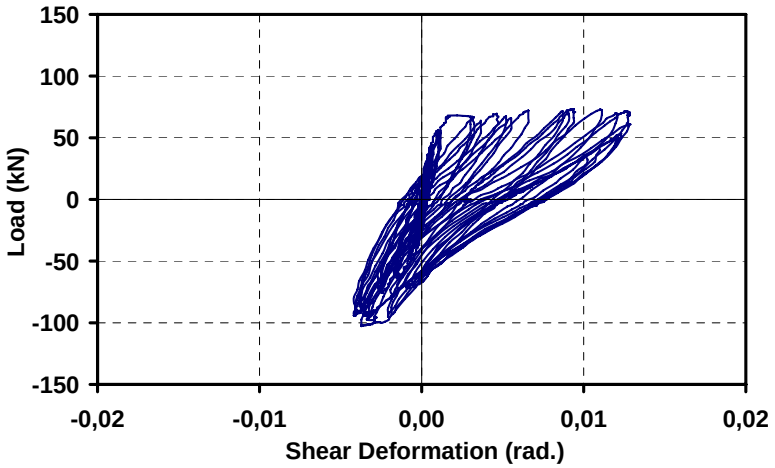


Figure 3.107. Shear deformation versus lateral load for Specimen TR-5-FRP-3

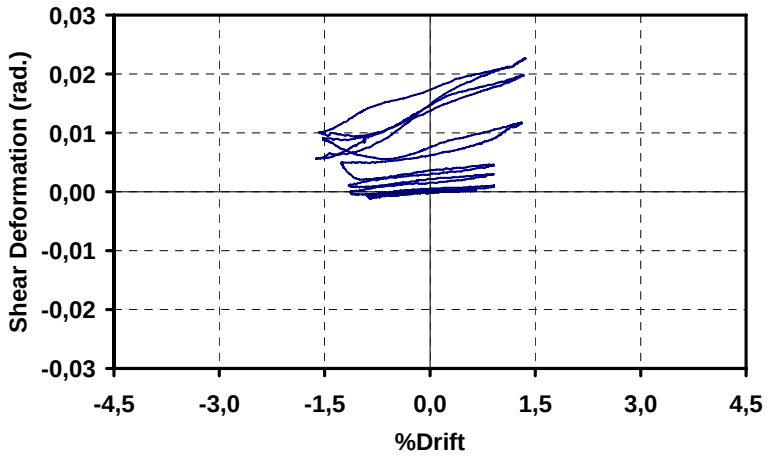


Figure 3.108. Shear deformation versus drift for Specimen TR-5-R

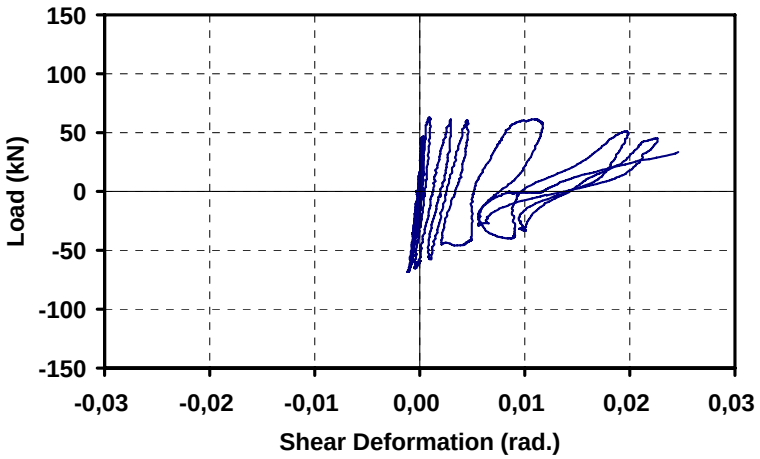


Figure 3.109. Shear deformation versus lateral load for Specimen TR-5-R

### 3.2.4. Stiffness Degradation

The secant stiffness of peak points of the measured lateral load versus top displacement response was also used for investigating the behavior of the specimens, in terms of stiffness degradation under cyclic lateral loads. The secant stiffness, *K*, is defined as the slope of the line that passes from the origin to a displacement reversal point of interest on the lateral load versus story drift loops. Figure 3.110 illustrates the definition of the secant stiffness. Measured story drift and stiffness degradation relationships for the control, strengthened and repaired specimens are shown in Figure 3.111 to 3.113. Since there is no confinement in joint region of control specimens, the brittle failure occurred and the rate of stiffness degradation was faster in the control specimen compared with the strengthened and repaired specimens.

Some degradation in stiffness values can be observed in the repeated cycles of same drift level. After the application of repairing and retrofitting materials, the joint behavior became more ductile, and the degradation of the stiffness values of each cycle decreased.

As mentioned before, all the strengthened specimens showed similar behavior in push direction of loading (positive drift levels) whereas TR-5-FRP-1 had less lateral load capacity than the other two strengthened specimens in pull direction of loading due to the rupturing of diagonal CFRP layers. Therefore, the rate of the stiffness degradation was higher in TR5-FRP-1 specimen in pull direction of loading (Figure 3.112).

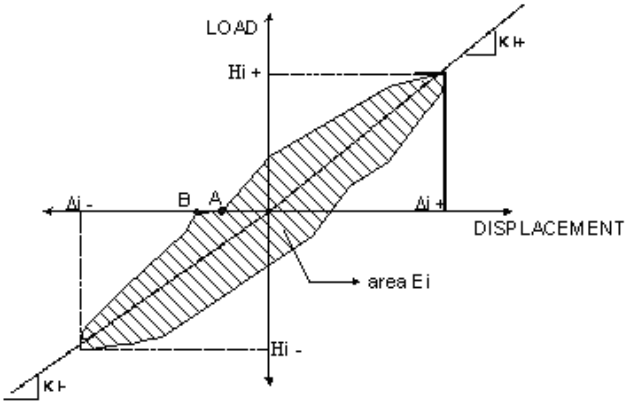


Figure 3.110. Stiffness and energy calculations

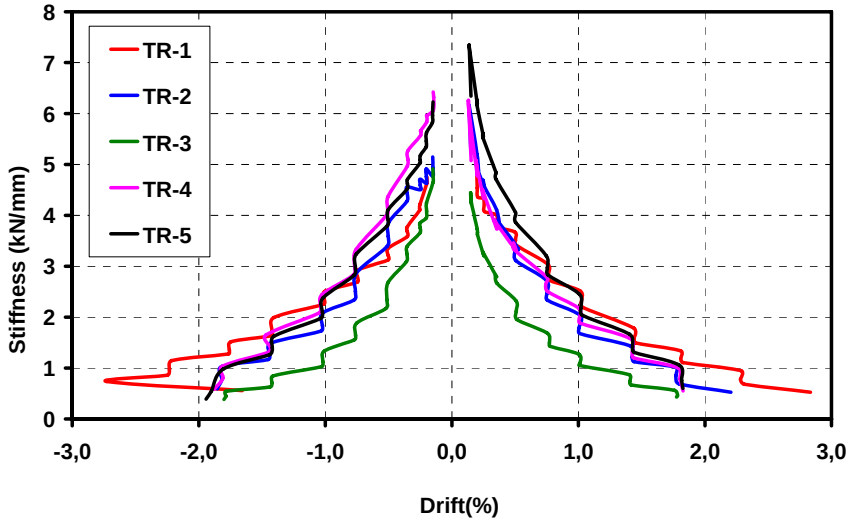


Figure 3.111. Stiffness degradation for control specimens

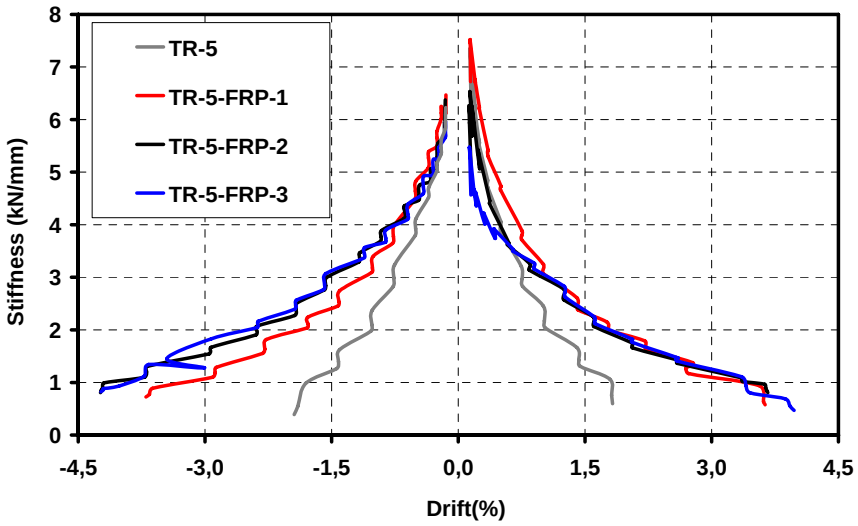


Figure 3.112. Stiffness degradation for strengthened specimens

Figure 3.113 clearly shows that repaired and strengthened specimens have higher stiffness values than only repaired specimens have.

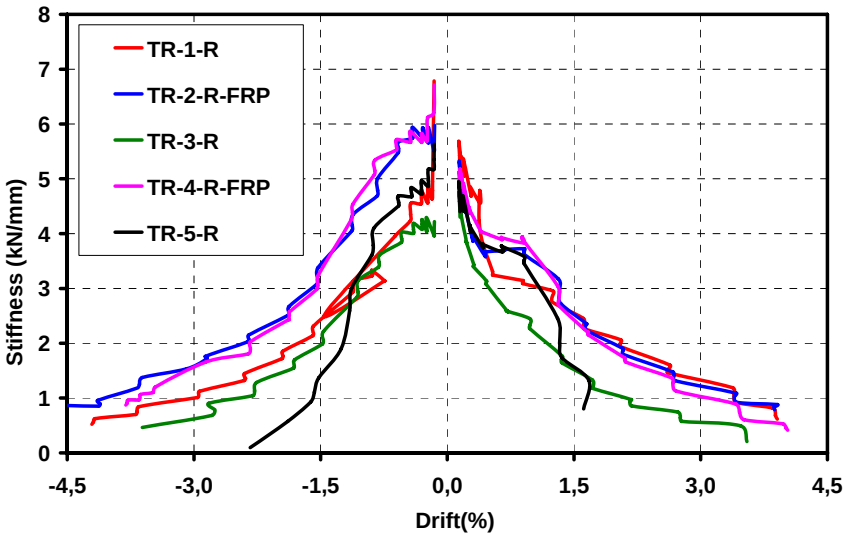


Figure 3.113. Stiffness degradation repaired specimens

### 3.2.5. Energy Dissipation

To characterize the response of the beam column specimens, one way to define the cumulative dissipated energy is the cumulative area under hysteresis loops of the lateral load versus top displacement response. Figure 3.110 illustrates the calculation of dissipated energy for one hysteresis loop.

Accordingly, the cumulative dissipated energy versus story drift relationships for control, strengthened and repaired specimens are presented in Figure 3.114 to 3.116. As observed from the Figure 3.114, the cumulative dissipated energy is highest in the Specimen TR-1 Control which was designed according to the provisions of TEC-75. And also, it was obvious from the Figure 3.114 that the TR-3 Control specimens showed poor energy dissipation capacity due to the lesser cross-section it has.

In TR-5-FRP specimens, by using the effective wrapping methodology, high energy dissipation capacities were achieved (Figure 3.115). In adequate wrapping was obviously seen from the specimen TR-5-FRP-1. Also, due to the repairing materials, the hysteretic cycles became fat in repaired and retrofitted specimens. Therefore, the area under the

hysteretic loops which shows the amount of dissipated energy increased in those specimens (Figure 3.116).

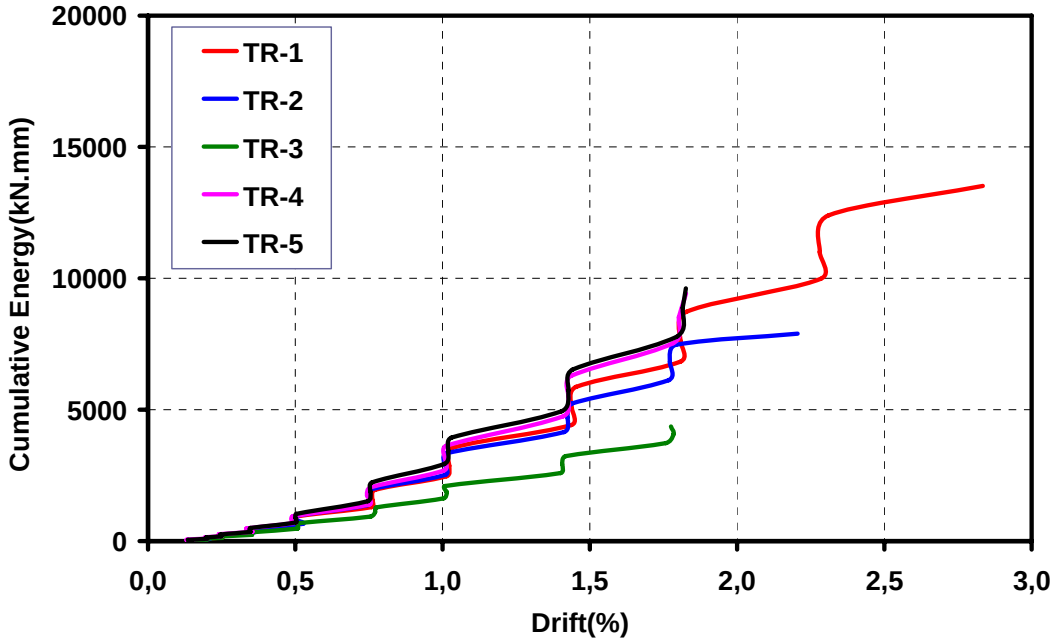


Figure 3.114. Cumulative dissipated energy for control specimens

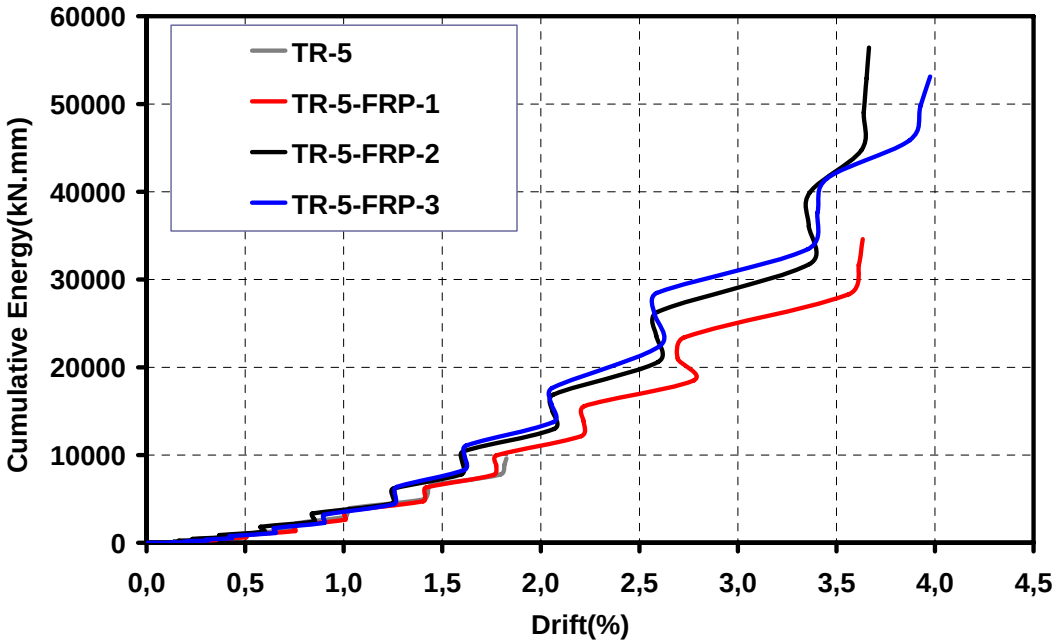


Figure 3.115. Cumulative dissipated energy for strengthened specimens

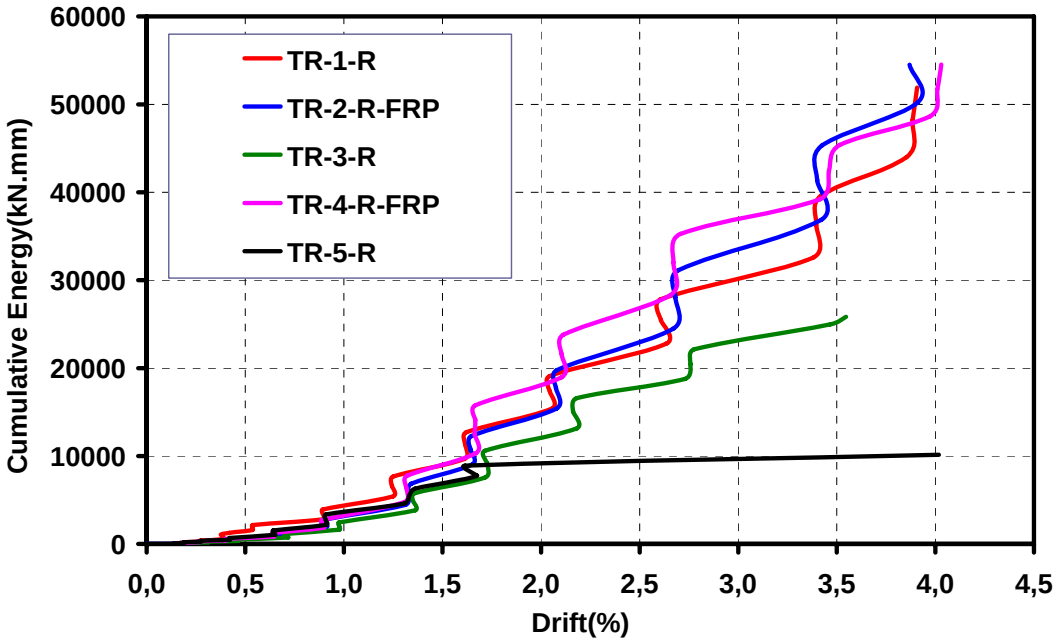


Figure 3.116. Cumulative dissipated energy for repaired specimens

Cumulative dissipated energy values were similar in all control specimens except TR-3 which has smaller cross-sectional dimension of beam and columns. After 1.40% drift level, the dissipated energy values of strengthened specimens started to increase due to subjected to high drift levels.

The repaired specimens (TR-1-R and TR-5-R) can carry 50% more lateral load than the control ones. However, the energy dissipation capacities show differences depending on existing transverse reinforcement at the joint region. For instance, specimen TR-1-R dissipated three times more energy than that of the specimen TR-1 Control, whereas no differences were observed in energy dissipation capacities of specimens TR-5-R and TR-5 Control

# 4. ANALYTICAL STUDY

## 4.1. Introduction

The analytical model was based on strut and tie model. Under incremental lateral loads, the proposed model mainly checks tensile and compressive stresses on possible failure locations. The lateral load capacity was obtained from the load when the first failure initiated.

From the background knowledge and experimental study, it can be summarized that there are 5 possible failure mechanisms can be developed in beam-column joint specimens which have flexural capacity ratio greater than 1.0. The first two mechanisms illustrated in Figure 4.1 can be observed in control specimens. The first mechanism is the joint shear failure. The second one is yielding of the beam reinforcements at the maximum moment region of the control specimens. The other three mechanisms can be observed in strengthened specimens as seen in Figure 4.2. The third mechanism is the rupture of $+\gamma$ diagonal CFRP layers. The tensile forces formed at the beam can cause the rupturing of $-\gamma$ diagonal CFRP at the maximum moment region of the beam. The forth one is the rupture of CFRP sheets in the joint panel due to the extreme joint shear stresses. And finally, the yielding of the beam reinforcement can cause a failure mechanism at the outside of the strengthened region.

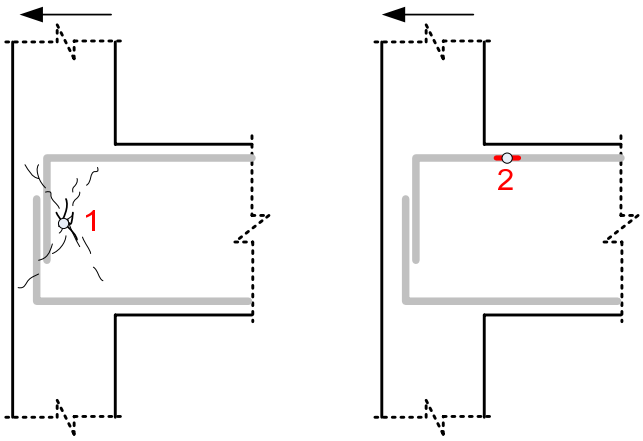


a) Joint shear failure b) Yielding of beam reinforcement

Figure 4.1. Possible failure mechanisms of control specimens

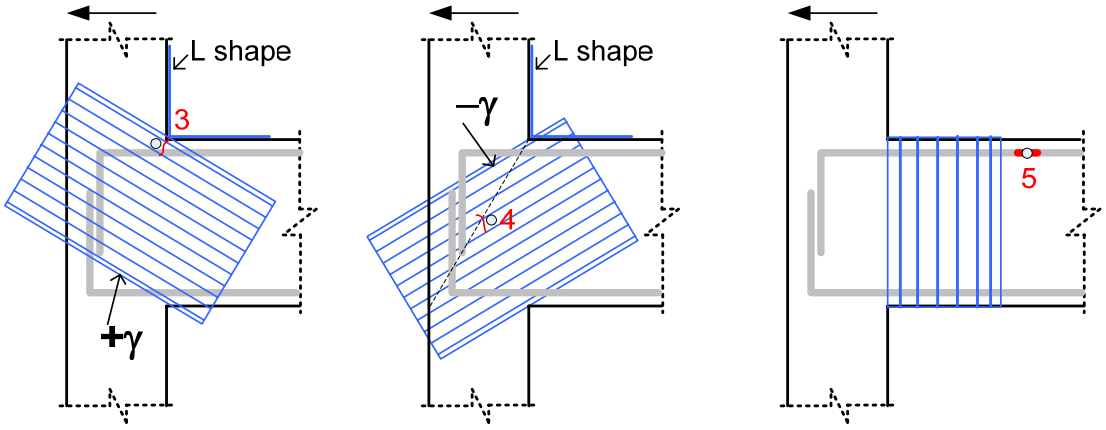


a) Tension failure b) Shear failure c) Beam failure

Figure 4.2. Possible failure mechanisms of strengthened specimens

## 4.2. Material Models

### 4.2.1. Concrete

The average concrete strength of the specimen was determined as $f'_c$ = 16 MPa from the compression test described in Section 2.4.1. Modulus of Elasticity of concrete, $E_c$, is calculated according to Eq (4.1) which is taken from ACI 318R-08 [69].

$$E_c = 57000\sqrt{f'}\ (\text{psi}) \rightarrow E_c = 4700\sqrt{f'} = 4700 \times \sqrt{16} = 18800\ \text{MPa} \tag{4.1}$$

The strain value at the maximum strength was calculated from Eq (4.2).

$$\varepsilon_o = 2\frac{f'_c}{E_c} = 2 \times \frac{16}{22000} = 0.00145 \tag{4.2}$$

The function of the pre-peak curve shown in Figure 4.3 was known as the Hognestad Curve and defined by Eq (4.3) and Eq (4.4) [70].

$$\sigma = f'_c\left[\left(2 \times \frac{\varepsilon}{\varepsilon_o}\right) - \left(\frac{\varepsilon}{\varepsilon_o}\right)^2\right] \tag{4.3}$$

The post-peak behavior of the concrete, as illustrated in Figure 4.3, was assumed as a linear behavior that 15% degradation in strength was accepted at the ultimate strain value [70].

$$\sigma = f_c' - f_c' \times (\varepsilon - \varepsilon_o) \times \left( \frac{0.15 \times f_c'}{\varepsilon_u - 2 \times \frac{f_c'}{E_c}} \right) \tag{4.4}$$

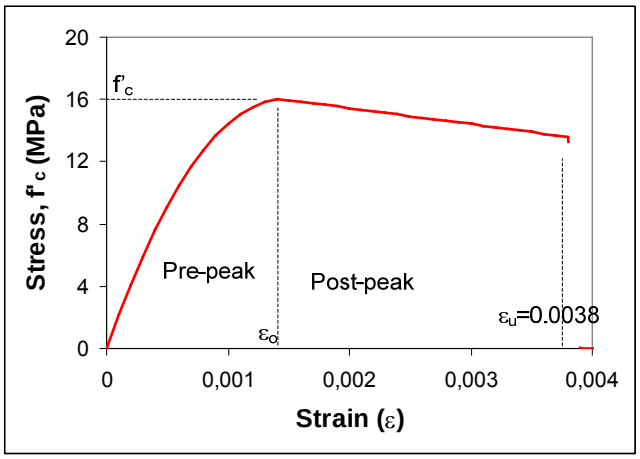


Figure 4.3. Concrete Model (Hognestad)

The tensile strength of concrete, $f_t$, was taken as the 8% of the compressive strength of concrete. In Figure 4.4, biaxial strength envelope of the concrete was illustrated [71]. This curve was used for the strength of concrete at the joint region subjected to compressive forces in one axis and tensile forces in other axis.

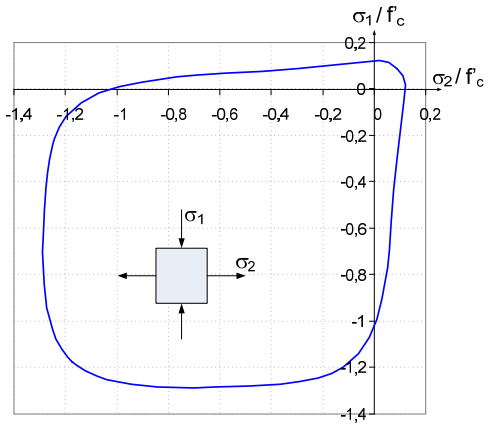


Figure 4.4. Biaxial strength envelope of concrete [71]

### 4.2.2. Steel

Tri-linear steel model was used. Yield strength of the reinforcements was determined as $f_y$ = 280 MPa by tensile tests as described in Section 2.4.2. The Modulus of Elasticity of the steel was taken as $E_s$ = 200000 MPa. Yield strain of the steel was determined by;

$$\varepsilon_y = \frac{f_y}{E_s} = \frac{280}{200000} = 0.0014 \tag{4.5}$$

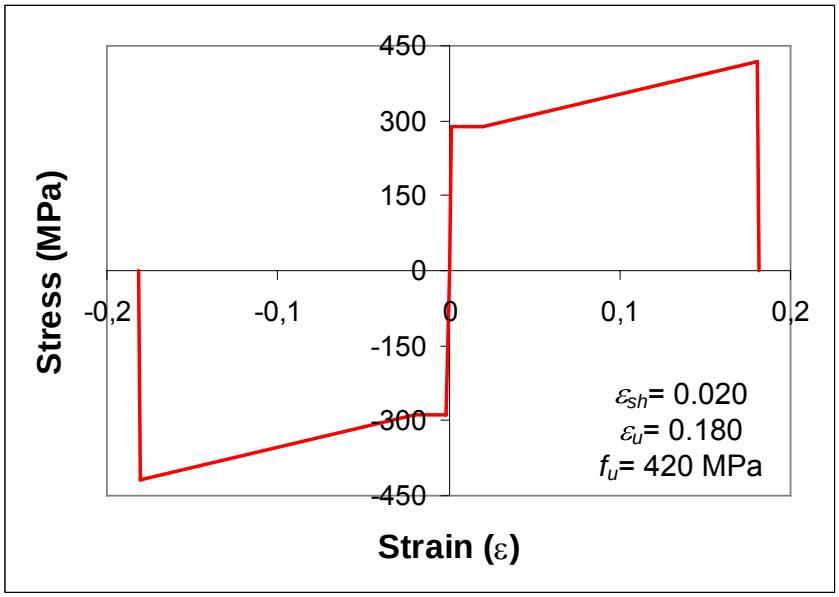


Figure 4.5. Tri-linear steel model

### 4.2.3. CFRP

The material properties of the CFRP fibers and adhesives were given in Section 2.4.3 and 2.4.5. When CFRP fibers and epoxy were combined, the ultimate strength and the Modulus of Elasticity of the matrix decrease significantly. From the CFRP strain values measured during the experiments and the observations, the ultimate strength of the matrix was taken as 70% of ultimate strength of fibers. Also, the modulus of Elasticity was taken as 200 GPa which was 20% less than the value given in manufacturers data.

## 4.3. Derivation of Analytical Model

The proposed model is based on the strut-and-tie concept. Usually, the strut-and-tie model applied to the joint region is considered to satisfy only the equilibrium conditions.

Before formulating a mathematical model, the forces around and within a joint should be identified. Figure 4.6 shows the earthquake-induced forces acting on an exterior joint. The horizontal joint shear force is estimated using the notation given in Figure 4.6 as

$$V_{jh} = T_b - V_{c1} \tag{4.6}$$

where $V_{jh}$ is the horizontal joint shear force; $T_b$ is the tensile force resulting from the steel of the beam; and $V_{c1}$ is the horizontal column shear above the joint.

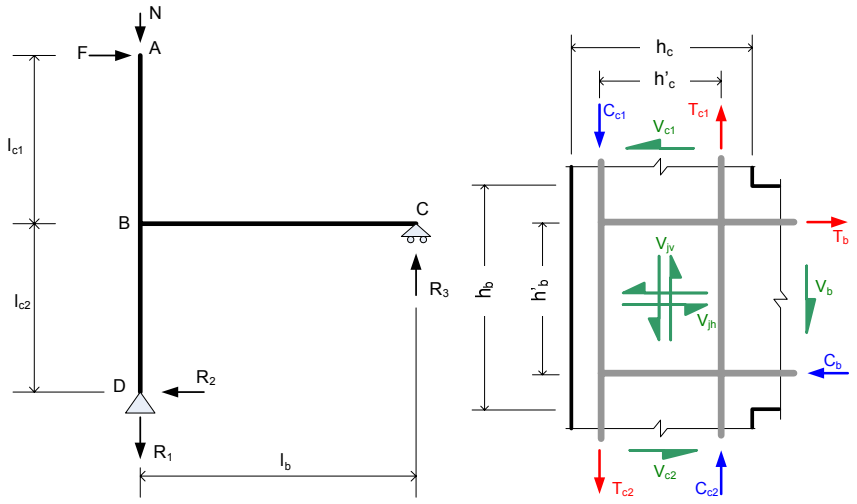


Figure 4.6. Macro-model for exterior joint

The derivation of the model was described step by step as the following:

Step 1. Calculations of reactions and internal forces: Under the axial load, $N$ and the incremental lateral load, $F$, the reactions, $R_1$, $R_2$ and $R_3$, can be calculated by using the equilibrium equations, as in Eq (4.7) to Eq (4.12).

$$\sum M_D = 0 \Rightarrow F \times \left(l_{c_1} + l_{c_2}\right) - R_3 \times (l_b) = 0 \tag{4.7}$$

$$R_3 = F \times \left( \frac{l_{c_1} + l_{c_2}}{l_b} \right) \tag{4.8}$$

$$\sum F_x = 0 \Rightarrow F - R_2 = 0 \tag{4.9}$$

$$R_2 = F \tag{4.10}$$

$$\sum F_y = 0 \Rightarrow -N - R_1 + R_3 = 0 \tag{4.11}$$

$$R_1 = -N + F \times \left( \frac{l_{c_1} + l_{c_2}}{l_b} \right) \tag{4.12}$$

By using the reactions calculated above, the moments at the joint region, coming from the columns and beam can be determined by statically as given in Eq (4.13) to Eq (4.18).

$$M_b = R_3 \times (l_b) \tag{4.13}$$

$$M_b = F \times \left( \frac{l_{c_1} + l_{c_2}}{l_b} \right) \times (l_b) = F \times (l_{c_1} + l_{c_2}) \tag{4.14}$$

$$M_{c_1} = F \times (l_{c_1}) \tag{4.15}$$

$$M_{c_2} = R_2 \times (l_{c_2}) = F \times (l_{c_2}) \tag{4.16}$$

$$M_{c_1} + M_{c_2} = M_b \tag{4.17}$$

$$F \times (l_{c_1}) + F \times (l_{c_2}) = F \times (l_{c_1} + l_{c_2}) \tag{4.18}$$

Step 2. Sectional Analysis: Applying a sectional analysis procedure to the beam and column section, the moment, $M$, and the curvature, $\kappa$, values can be determined. Also, for any lateral loads ($F$) of column, the corresponding moments, and accordingly extreme fiber compressive and tensile strain of the section ($\varepsilon_c$, $\varepsilon_t$), compression depths of columns and beam ($c_{c1}$, $c_{c2}$, $c_b$), and tensile forces of beam reinforcements ($T_b$) can be determined from back calculation of Sectional Analysis, as shown in Figure 4.7. The horizontal joint shear force ($V_{jh}$) can be found with the help of Eq (4.6).

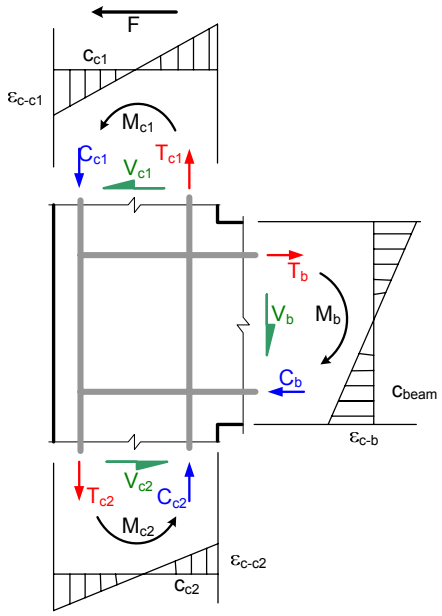


Figure 4.7. Moments and shear forces of joint region

Step 3. Calculation of effective area of concrete and CFRP: The forces, coming from the beam and the columns, were transferred into the joint region. The compression depths of the column and beam sections, calculated from the section analysis, define the compression strut area of the joint as shown in Figure 4.8a. The compressive strut area has no constant depth; it varies along the diagonal of the joint region. Therefore the effective depth should be determined for calculation of the effects of concrete on shear. The effective depth of compressive strut ($a_s$) can be determined from the depth of equivalent rectangular area along the diagonal axis of the joint region. The effective area of diagonal strut $A_{str}$ is defined as

$$A_{str} = a_s \times b_s \tag{4.19}$$

where $a_s$ is the effective depth of the diagonal strut, and the $b_s$ is the width of the diagonal strut.

For the CFRP strengthened specimens, the effective width of the CFRP sheets was defined as the width of CFRP sheets crossing the diagonal axis of the joint region (Figure 4.8b). The effective area of the CFRP sheets $A_{CFRP}$ is then calculated from Eq (4.20).

$$A_{CFRP} = b_{eff} \times n \times t \tag{4.20}$$

where $b_{eff}$ is the effective width of CFRP, $n$ is the number of the CFRP layers, and $t$ is the thickness of the one layer of CFRP sheets.

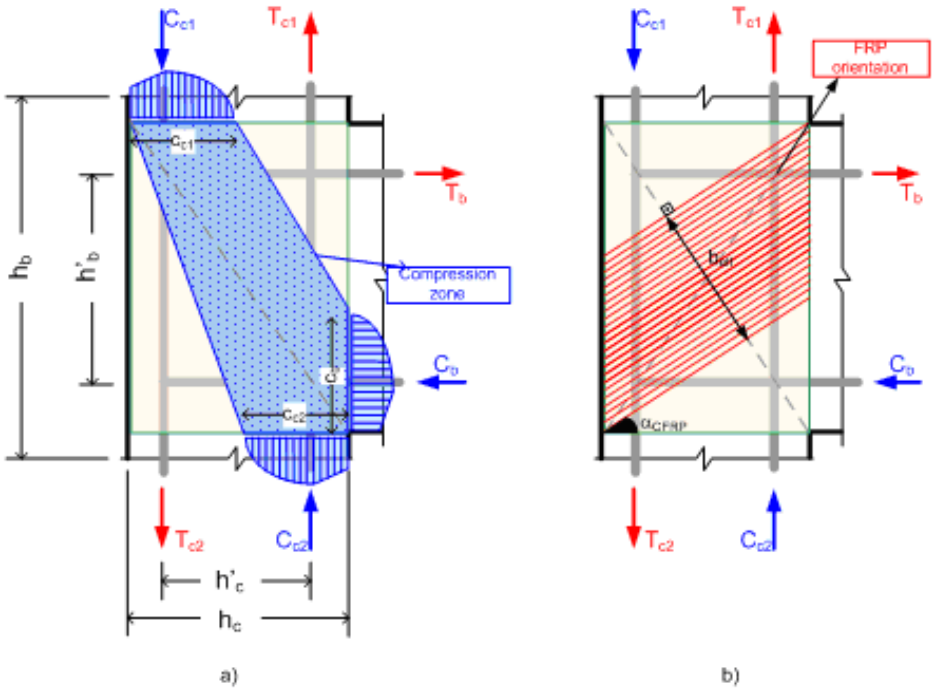


Figure 4.8. Forces acting on joint region and compression and tension struts

Step 4. Truss System: The mechanism of the joint region can be simplified as a truss system with compression and tension members as seen in Figure 4.9. The proposed truss model is a statically indeterminate system. By applying unit shear force to the top member of the truss (member 1), forces ($F_1$ to $F_6$) exerted on each truss member can be calculated from any structural analysis software or calculation procedures. Here, it was assumed that the outer members of the truss were more rigid than the braces. Thus, no elongation was

assumed in the outer members. The calculated forces exerted on each member of truss were illustrated in Figure 4.9.

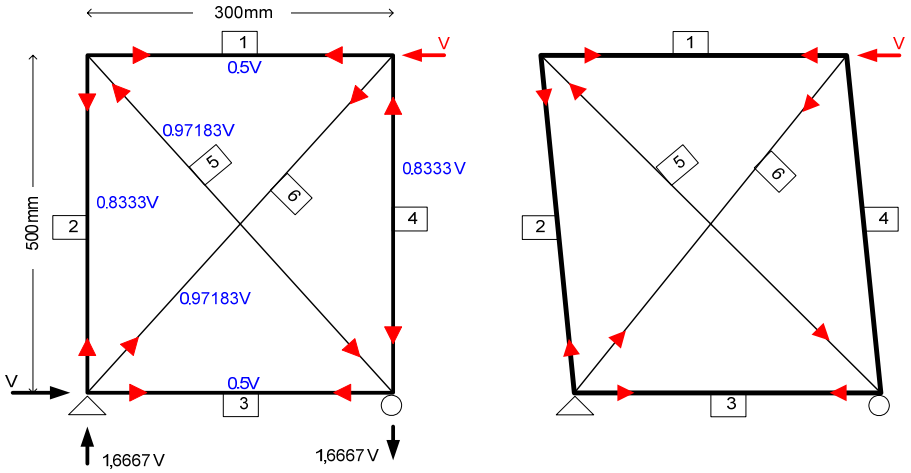


Figure 4.9. Forces acting on joint region and deformed shapes

Step 5. Calculation of stresses: As described in Figure 4.1, the first possible failure mechanism was crushing of concrete compression strut at the joint region of the control specimens. For each calculated $V_{jh}$ values, the compressive forces, $F_6$, and tensile forces, $F_5$, can determined by using above coefficients. The concrete compressive stresses due to $F_6$ compression force and concrete tensile stresses due to $F_5$ tensile force can be determined from Eq (4.21) and Eq (4.22) respectively.

$$f_{c-truss} = \frac{F_6}{A_{str}} \tag{4.21}$$

$$f_{t-truss} = \frac{F_5}{A_{diagonal}} \tag{4.22}$$

where $A_{diagonal}$ is the area of the diagonal cross-section of the joint and $A_{str}$ is the effective diagonal strut area. Since the concrete at the joint region was subjected to both tensile stresses in one axis and compressive stresses in the other axis, it should be checked that whether the point of ($f_{c\text{-}truss}$ , $f_{t\text{-}truss}$) is inside of the biaxial Kupfer envelope curve of the concrete given in Figure 4.4. Here, if there is no shear reinforcement used at the joint region, the envelope curve should be drawn by using unconfined concrete compressive

strength, $f'_c$. But if the joint has the shear reinforcements, confined concrete compressive strength should be used in envelope curve in order to take account the effects of shear reinforcements. Therefore, if the point of ($f_{c\text{-}truss}$ , $f_{t\text{-}truss}$) is inside of the Kupfer curve, the concrete can carry the stresses developed in the joint region. The lateral load which takes the point outside of the envelope curve is the maximum load that the joint can carry before the shear failure of the joint.

The second possible failure mechanism is the yielding of beam longitudinal reinforcements. The stresses of the beam longitudinal reinforcements ($f_s$) should be checked for yielding. If $f_s$ is greater than the yield stresses of reinforcement, $f_y$, the corresponding $F$ values is the maximum load that the specimen can carry before the beam hinging mechanism developed.

$$f_s = \frac{T_b}{A_s} \tag{4.23}$$

The maximum lateral load capacity of the control specimens is determined by the smallest of lateral load capacity calculated by using the biaxial envelope curve or by using the yielding of the beam longitudinal reinforcements.

The third possible failure mechanism as described in Figure 4.2 is the rupture of $+\gamma$ diagonal CFRP sheets for strengthened specimens. The axial force on the $+\gamma$ CFRP sheets is one of the components of tensile force of the beam. The stresses can be calculated from the Eq (4.24). Using the L-Shaped CFRP sheets decreases the stresses of $+\gamma$ CFRP sheets as calculated from Eq (4.25).

$$f_{CFRP+\gamma} = \frac{T_b \cdot \cos(\gamma)}{A_{CFRP}} \tag{4.24}$$

$$f_{CFRP+\gamma} = \frac{T_b \cdot \cos(\gamma)}{A_{CFRP} + A_{L-Shape} \cdot \cos(\gamma)} \tag{4.25}$$

$$A_{L-Shape} = n_L \cdot t \cdot b \tag{4.26}$$

where $\gamma$ is the slope of CFRP sheets ($\gamma$=31°) and $A_{L\text{-}Shape}$ is the cross-sectional area of the L-Shaped CFRP sheets (Figure 4.10), $n_L$ is the number of layer of L-shaped CFRP and $b$ is the width of the CFRP sheet. If $f_{CFRP+\gamma}$ is greater than the ultimate stress of fiber, $f_U$, the corresponding $F$ values is the maximum load that the specimen can carry before the $+\gamma$ CFRP ruptures.

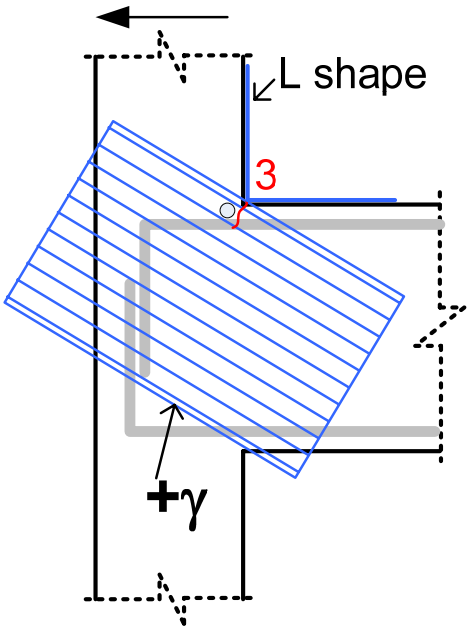


Figure 4.10. Stress calculation of $+\gamma$ CFRP sheets

The fourth possible failure mechanism is the rupture of $-\gamma$ diagonal CFRP sheets due to shear forces at the joint region. The tensile stresses of $-\gamma$ CFRP sheets can be found by dividing the tensile forces, $F_5$, to effective CFRP area. If $f_{CFRP\text{-}\gamma}$ is greater than the ultimate stress of fiber, $f_U$, the corresponding $F$ value is the maximum load that the specimen can carry before the $-\gamma$ CFRP ruptures.

$$f_{CFRP-\gamma} = \frac{F_5}{A_{CFRP}} \tag{4.27}$$

The fifth possible failure mechanism is the yielding of the beam reinforcement at the location where the beam wrapping ends as shown in Figure 4.2. The stresses of the reinforcement can be calculated from the equation given in Eq (4.23). However, in calculation of the $M_b$, the level arm should be taken from the beam support to possible yield location (Eq (4.13)). If calculated $f_s$ is greater than $f_y$, the corresponding $F$ value is the maximum load that the specimen can carry before the beam hinging mechanism developed.

The maximum lateral load capacity of the strengthened specimens is determined by the smallest lateral load capacity calculated by using the $f_{CFRP\text{-}\gamma}$, $f_{CFRP\text{-}\gamma}$ and $f_s$.

A set of solution procedure is proposed, as shown in the flowcharts in Figure 4.11. As a summary, in the Input part of the flowchart, dimensions of the column beam and the joint region were introduced. Then the amount of steel and CFRP materials, and the characteristic properties of the concrete, steel and CFRP materials were introduced. And finally a unit lateral load was applied. By using the equilibrium equations, all the reaction forces and moments at the joint regions were calculated in the second part of the flowchart.

The moment versus curvature relationships of beam and column cross-sections were obtained form the sectional analysis procedure. Thus, for each lateral load increments, moment can be calculated and the corresponding curvature values can be obtained. And accordingly, strain and stress distributions of beam and column sections and the forces of the reinforcements can be determined.

The geometry of the compression strut in the joint was determined by the compression depths of the beam and the column sections. Therefore, the forces exerted within the joint regions were obtained.

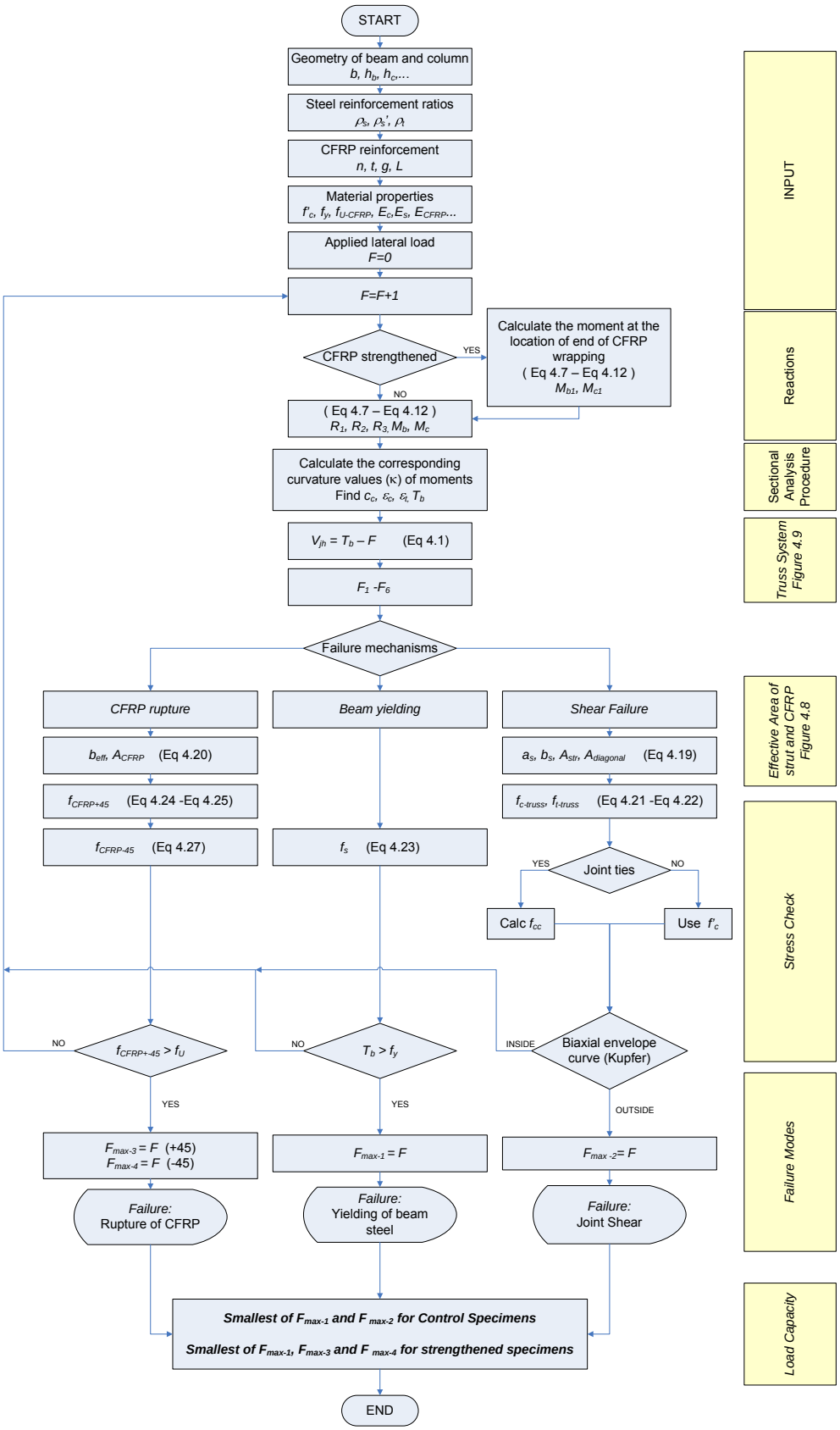


Figure 4.11. Flowchart

## 4.4. Experimental Verification

The proposed model was used to predict the lateral load capacity of the shear critical test specimens. Three of them had different reinforcement details and cross-section dimensions, and three of them were strengthened with CFRP. Table 4.1 illustrates the comparisons of experimental and analytical lateral load capacities.

Table 4.1. Experimental verification

| **Specimen ID** | $f'_c$ (MPa) | $f_y$ (MPa) | $N/A_g f'_c$ | $F_{col\text{-}test}$ *(push/ pull)* (kN) | **Failure Mode** | $F_{col\text{-}calc}$ *(push/ pull)* (kN) | $F_{col\text{-}test}/F_{col\text{-}calc}$ |
|---|---|---|---|---|---|---|---|
| TR-1 Control | 15.3 | 280 | 0.35 | 49.2 | Joint Shear | 46.5 | 1.06 |
| | | | | 53.8 | | 45.3 | 1.19 |
| TR-2 Control | 12.8 | 280 | 0.35 | 39.6 | Joint Shear | 36.3 | 1.09 |
| | | | | 41.5 | | 35.8 | 1.16 |
| TR-3 Control | 13.5 | 280 | 0.35 | 24.5 | Joint Shear | 24.7 | 0.99 |
| | | | | 27.2 | | 24.4 | 1.11 |
| TR-5 FRP-1 | 14.6 | 280 | 0.35 | 76.0 | Beam Yielding / Rupture of FRP | 77.7 | 0.98 |
| | | | | 79.3 | | 70.6 | 1.12 |
| TR-5 FRP-2 | 16.0 | 280 | 0.35 | 71.1 | Beam Yielding / Debonding | 77.7 | 0.92 |
| | | | | 94.9 | | 95.9 | 0.99 |
| TR-5 FRP-3 | 16.0 | 280 | 0.35 | 73.4 | Beam Yielding | 77.7 | 0.94 |
| | | | | 102.8 | | 95.9 | 1.07 |

Generally, the experimental lateral load capacities of the specimens were in good agreement with the capacities calculated from the analytical model. For the joint shear critical specimens, which are un-strengthened (TR-1 to TR-3), the model underestimated the load carrying capacity. There are two possible failure mechanisms were expected in these specimens as described in Figure 4.1. One of them is the joint shear failure the other one is the yielding of the beam reinforcement. Before the reaching the flexural capacities of beam the concrete was crushed at the joint region. For TR-1 and TR-2, when the lateral load was 55.0 and 66.9 for push and pull direction of loading, respectively, the beam longitudinal reinforcements were yield at the maximum moment region. For TR-3 specimen, due to the smaller cross-section it has, the load of 40.4 and 53.0 for push and

pull direction, respectively, yield the beam longitudinal reinforcements. However, the concrete at the joint region was crushed due to shear forces when the applied lateral load was less than the load mentioned above. Therefore, the joint shear forces govern the failure mechanisms of the specimens. Figure 4.12 to 4.14 indicated the predicted lateral load capacities and experimental backbone curve of the tests specimens.

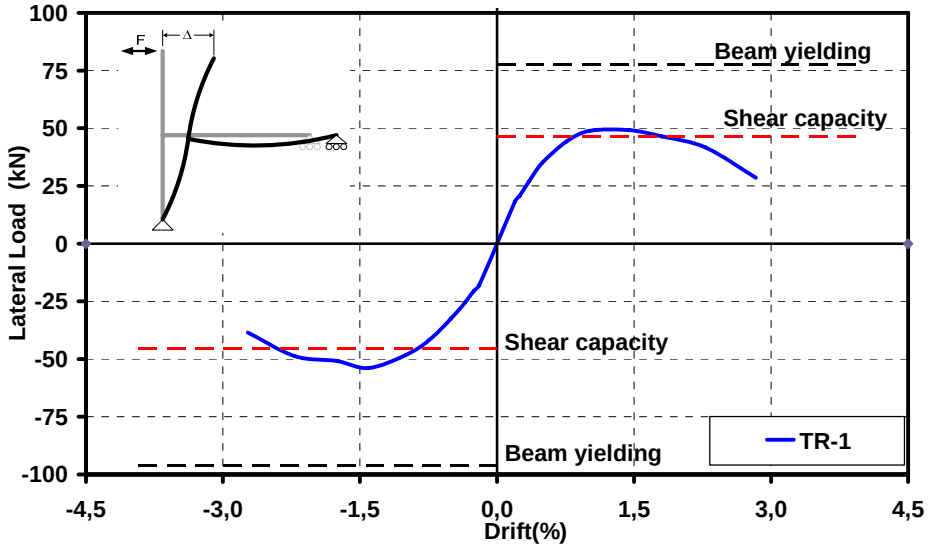


Figure 4.12. Prediction of strength of TR-1

For strengthened specimens, there are three possible failure mechanism expected as described in Figure 4.2. One of them is rupturing of +γ diagonal CFRP at the maximum moment region of the beam due to tensile forces on beam longitudinal reinforcements. The second one is rupturing of -$\gamma$ diagonal CFRP at the joint region due to shear forces and the last one is yielding of beam longitudinal reinforcements where the CFRP wrapping ended (500 mm away from the column surface).

The failure of the specimen was governed by the rupturing of +$\gamma$ diagonal CFRP in specimen TR-5-FRP-1. There was no “L Shaped” CFRP used in this specimen. Only the diagonal CFRP resist the tensile force of beam longitudinal reinforcement. The model estimates the lateral load as 70 kN, when the CFRP was ruptured.

However, in TR-5-FRP-2 and TR-5-FRP-3 specimens; the rupture of +$\gamma$ diagonal CFRP was prevented by using L shaped CFRP at the beam column intersections. When the

lateral loads were 77.7 and 95.9 for push and pull direction of loading respectively, the beam reached its flexural capacity at the un-strengthened region, before reaching the ultimate strength of diagonal CFRP sheets.

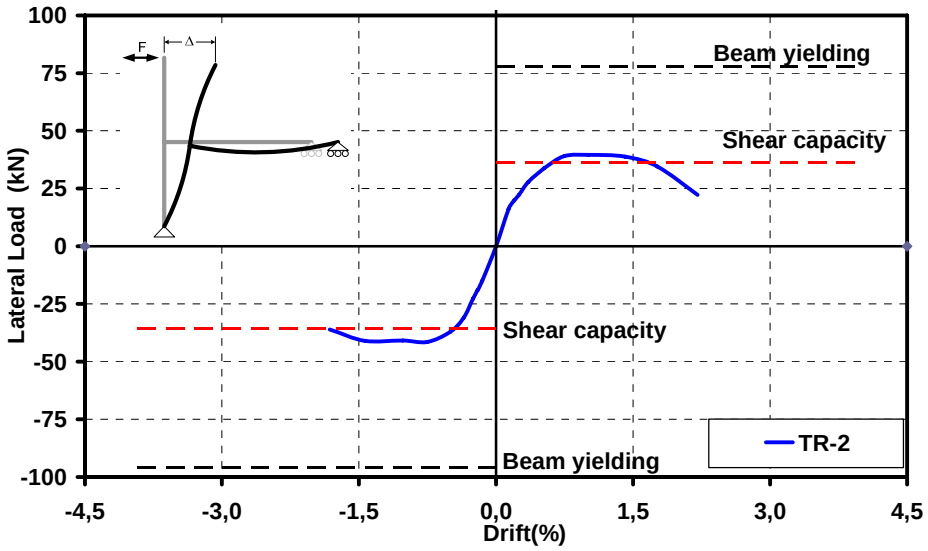


Figure 4.13. Prediction of strength of TR-2

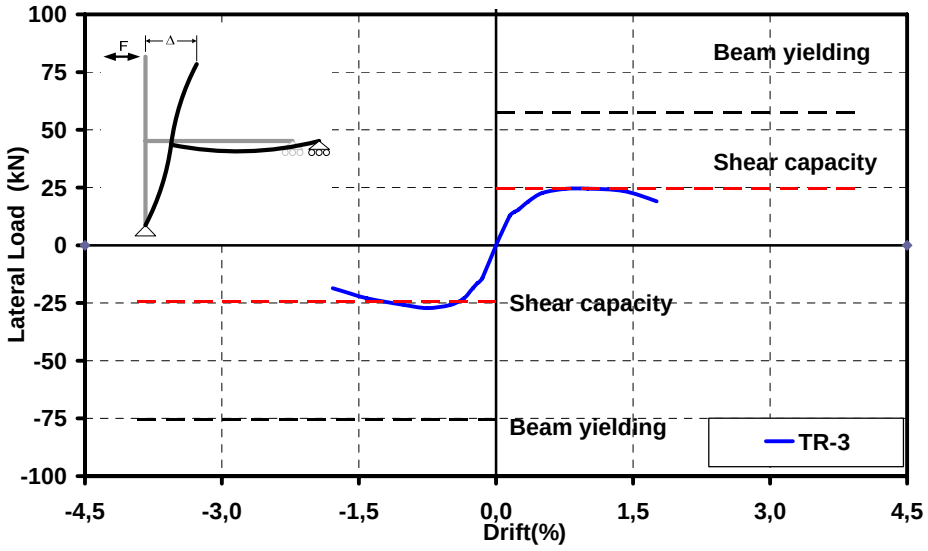


Figure 4.14. Prediction of strength of TR-3

The proposed model was used to calculate the lateral load capacity of 11 more test specimens (Table 4.2) described in the literature. All the specimens were exterior 2D beam column joints and failed in joint shear or beam yielding.

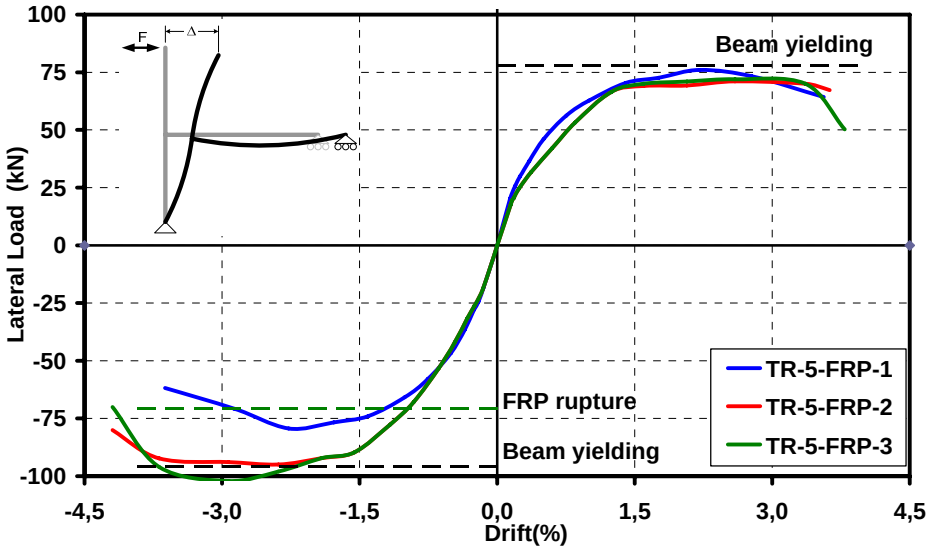


Figure 4.15. Prediction of strength of TR-5-FRP specimens

Table 4.2. Experimental verification (Literature)

| **Author** | **Specimen ID** | $f'_c$ (MPa) | $f_y$ (MPa) | $N/A_g f'_c$ | $F_{test}$ *(push/ pull)* (kN) | **Failure Mode** | $F_{calc}$ *(push/ pull)* (kN) | $F_{test}/F_{calc}$ |
|---|---|---|---|---|---|---|---|---|
| Altay [72] | US-1 | 24 | 450 | 0.30 | 60<br>74 | Joint shear | 61<br>61 | 0.98<br>1.21 |
| | US-1-FRP | 24 | 450 | 0.30 | 92<br>120 | B. yielding | 97<br>103 | 0.95<br>1.17 |
| Ehsani [11] | 1B | 33.6 | 340 | 0.09 | 142 | J. shear | 129.7 | 1.09 |
| | 2B | 35.0 | 350 | 0.07 | 135 | J. shear | 128.8 | 1.05 |
| | 3B | 40.9 | 350 | 0.06 | 178 | B. yielding | 161 | 1.11 |
| | 4B | 44.6 | 350 | 0.09 | 156 | B. yielding | 140 | 1.10 |
| | 6B | 39.8 | 340 | 0.07 | 156 | B. yielding | 163 | 0.96 |
| Ghobarah [3] | T0 | 30.6 | 425 | 0.20 | 86 | J. shear | 78 | 1.10 |
| Tsonos [29] | M1 | 34 | 500 | 0.2 | 52 | J. shear | 46.2 | 1.13 |
| | M2 | 33.5 | 500 | 0.2 | 45 | J. shear | 43.1 | 1.04 |
| Costas [1] | C1-C2 | 21.6 | 585 | 0.06 | 30 | J. shear | 20 | 1.50 |

# 5. CONCLUSIONS AND RECOMMENDATIONS

## 5.1. Summary

This study investigated the effects of common detailing deficiencies on the behavior and lateral load capacities of the exterior beam-column joint specimens. An experimental program was carried out at the Boğaziçi University's Structural Engineering Laboratory on thirteen large scale specimens subjected to reversed cyclic lateral loads. A strengthening technique using CFRP on the beam-column joint region was developed in order to increase the shear strength of the joint. Moreover, an analytical study was conducted to predict the shear strengths and failure modes of the beam-column joint specimens tested.

## 5.2. Conclusions

The main objectives of the research that are the seismic behavior of CFRP strengthened beam-column joints and investigation of shear strength has been attained. The following conclusions can be drawn on the basis of the results obtained from experimental and analytical study.

- In all control specimens, even specimen TR-1 Control, which was designed and detailed exactly according to the provisions of Turkish Earthquake Code (TEC-75), shear failure in the beam-column joint region, has occurred before the beam or column sections reached their ultimate flexural strength.

- The lateral load capacities of such beam-column joint specimens are susceptible to noticeable reductions due to the presence of deficiencies. In this study, having inadequate transverse reinforcements at the beam and at the column, and no transverse reinforcements at joint region reduced the lateral load capacities of the test specimens by 20 % compared to that of the specimen with adequate transverse reinforcements code required (TR-1). The hysteretic energy dissipation capacity (defined in this case as the cumulative area under the load-displacement response) was also reduced by 20 % compared to the specimen with shear reinforcements.

- The orientation of the joint shear cracks, observed in control specimens depended on the geometry of joint panel. The cracks were propagated diagonally from one corner to the other corner of the joint. In the CFRP strengthening technique, fibers were oriented perpendicular to the diagonal. Thus, Diagonal CFRP wrapping of the beam-column joints was more effective due to the fact that the orientation of the diagonal strips was closer to being parallel to the principal stresses in the joint core.

- The third CFRP-strengthening technique developed in this study significantly improved the behavior of deficient specimens. The lateral load capacities of the test specimens strengthened with the proposed methodology reached the flexural capacity of the beam. Strengthened specimens exhibited significantly increases strength and energy dissipation capacities as compared with those of original specimen. Elasto-plastic-shaped hystresis loops were observed with large energy dissipation capacity.

- Development of proposed joint shear strength model identified that along with the amount and location of CFRP, material properties of steel and concrete, joint transverse reinforcements and in-plane geometry can play an important role on determining joint shear capacity.

- The effects of deficiencies were examined in control specimens' tests. Three of the specimens were strengthened with CFRP materials, considering the effects of deficiencies in control specimens' tests. And the behavior of the strengthened specimens improved, such as the lateral load capacities increased at about 50% to 100%.

- Although the rate of the degradation of the stiffness was similar for all control specimens, the initial stiffness values of deficient specimens were less than TR-1. However, the rate of the degradation was decreased by using the proposed CFRP strengthening.

- Cumulative dissipated energy values were similar in all control specimens except TR-3 which has smaller cross-sectional dimension of beam and columns. After

1.40% drift level, the dissipated energy of strengthened specimens were started to increase significantly when compared to that of control specimens.

- The repaired specimens (TR-1-R and TR-5-R) can carry 50% more lateral load than the control ones. However, the energy dissipation capacities show differences depending on existing transverse reinforcement at the joint region. For instance, specimen TR-1-R dissipated three times more energy than that of the specimen TR-1 Control, whereas no differences were observed in energy dissipation capacities of specimens TR-5-R and TR-5 Control.

- The repaired and retrofitted specimens (TR-2-R-FRP and TR-4-R-FRP), which had a different reinforcement details and deficiencies, failed by plastic hinging of the beam. The lateral load and the dissipated energy capacities were almost same with the capacities of specimen TR-5-FRP-3.

- Specimen TR-5-FRP-3 behaved better than the other two strengthened specimens. Because the anchorages applied on to the beam prevented the debonding of CFRP. Therefore, plastic hinging has occurred on the beam. Design capacity of the beam was then reached.

- Capacity predictions were within the reasonable range with the experimental part of this study. For the shear critical specimens, the lateral load capacities were underestimated. The reason for this is the model estimates the lateral load at the first joint cracking.

- Lateral load capacity predictions provided by the analytical models were found in extremely good agreement with 11 experimental results found in the literature, thus adding confidence to the validity of the proposed equations.

## 5.3. Recommendations

- Further experimental research is necessary to investigate the seismic performance of beam-column joints which are detailed according to current code of practice.

- In the manufacturer data, only the characteristic properties of the CFRP material were given. Although it has no shear resistance alone, when combined with epoxy, it becomes more rigid and brittle. The ultimate strength and the shear strength of the CFRP matrix should be investigated.

- Additional tests should be coducted to calibrated the proposed model.

- The effects of CFRP debonding can also be included in the model.

# APPENDIX A. CRACK PATTERNS

## A1 Specimen TR-1-Control

Table A.1. Observations of Specimen TR-1 Control

| Drift (%) | Observations | Crack pattern |
|---|---|---|
| 0.20 | Max lateral load : (+)17.30 kN (Push)<br>: (-)18.30 kN (Pull)<br>**Crack-1:** In pull direction of loading, the flexural crack formed at the top of the beam, 90 mm away from the column face. The crack was 80 mm in length and 0.1 mm. in width. In the following cycles of that drift level the crack was elongated at about 135 mm. | 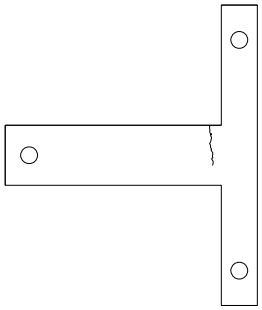 |
| 0.25 | Max lateral load : (+)20.40 kN (Push)<br>: (-)20.50 kN (Pull)<br>**Crack-2:** In push direction of loading, the flexural crack formed at the bottom face of the beam, 80 mm away from the column face.<br>**Crack-1 and Crack-2**: Both cracks were joined. All the beam section at about 80 mm away from the column face was cracked. | 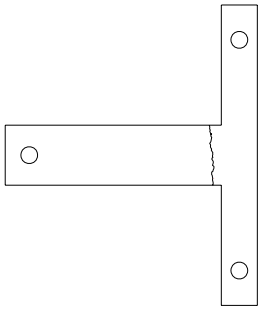 |
| 0.35 | Max lateral load : (+)25.60 kN (Push)<br>: (-) 27.00 kN (Pull)<br>**Crack-1:** The width of the crack was reached 0.6 mm. | 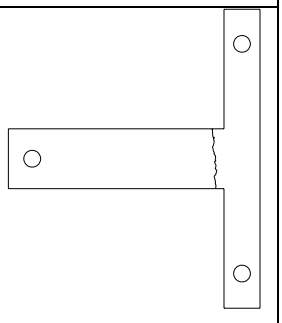 |
| 0.50 | Max lateral load : (+)32.30 kN (Push)<br>: (-) 35.10 kN (Pull)<br>**Crack-1:** The width of the crack was reached 1.0 mm. | 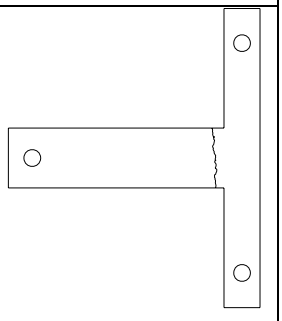 |

Table A.2. Observations of Specimen TR-1 Control (continued)

| Drift (%) | Observations | Crack patterns |
|---|---|---|
| 0.75 | Max lateral load : (+)41.00 kN (Push)<br>: (-)44.00 kN (Pull)<br>**Crack-1:** The crack width was reached 1.6 mm. Some flexural cracks developed at the column maximum moment regions.<br>**Crack-3, Crack-4 & Crack-5:** Shear (diagonal) cracks formed at the joint region panel.<br>**Crack-3:** Length of the crack was 140 mm<br>**Crack-4:** Length of the crack was 100 mm<br>**Crack-5:** Length of the crack was 75 mm<br>**Crack-3:** The crack was elongated<br>**Crack-6:** Vertical crack formed at the back of the column<br>**Crack-7:** Diagonal crack occurred at the back of the column | 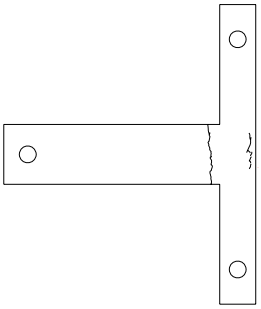 |
| 1.00 | Max lateral load : (+)48.20 kN (Push)<br>: (-)48.80 kN (Pull)<br>**Crack-6:** elongated.<br>**Crack-8:** Diagonal crack formed at the back side of the column.<br>**Crack-9:** Vertical crack formed at beam column intersection of the joint and extended towards the joint core.<br>**Crack-10:** the crack formed at top of the beam to the joint.<br>**Crack-3:** elongated upwards.<br>**Crack-6 and Crack-7:** elongated.<br>**Crack-3, Crack-4 and Crack-5:** crack width: 0.1-0.2 mm<br>**Crack-5:** Extended | 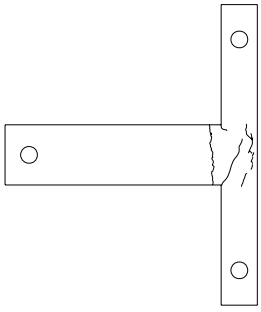 |

Table A.3. Observations of Specimen TR-1 Control (continued)

| Drift (%) | Observations | Crack patterns |
|---|---|---|
| 1.00 cont. | **Crack-11:** diagonal crack was formed at the front side of the column. Starts from bottom side of the column and goes into the column<br>**Crack-12:** Diagonal crack at the back side of the column | |
| 1.40 | Max lateral load : (+)50.00 kN (Push)<br>: (-)47.50 kN (Pull)<br>**Crack-9 :** extended horizontally at the joint core<br>**Crack-10:** Diagonal crack at the joint core<br>**Crack-5:** extended downward<br>**Crack-12:** extended.<br>**Crack-13:** Flexural crack occurred at the bottom of the beam, 630 mm away from the column. Length was 180 mm.<br>**Crack-14:** 100 mm Vertical crack occurred at the column 35 mm away from the corner.<br>**Crack-10:** Extended horizontally into the column<br>**Crack-11:** crack width: 0.6 mm<br>**Crack-15:** Vertical crack started from center of column and goes diagonally at the joint core<br>**Crack-3:** extended upward<br>**Crack-12:** extended towards the top of the column<br>**Crack-7:** Extended downward<br>**Crack-15 and Crack-10:** joined | 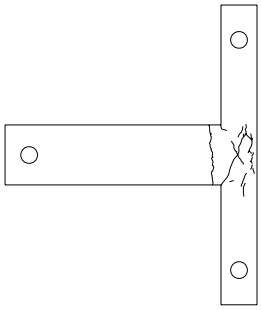 |
| 1.75 | Max lateral load : (+)50.00 kN (Push)<br>: (-)44.80 kN (Pull)<br>**Crack-13:** behaves as shear crack<br>**Crack-10:** extended downwards<br>**Crack-11:** width: 1.6 mm and doubled<br>**Crack-14 and Crack-10:** doubled at the joint core<br>**Crack-5:** extended vertically downwards<br>**Crack-12:** the corner of the column started to crush<br>**Crack-11:** width: 1.7 mm | 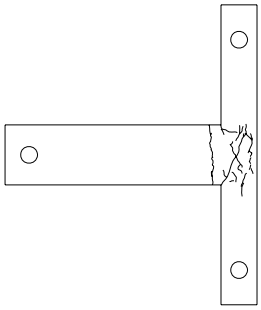 |

Table A.4. Observations of Specimen TR-1 Control (continued)

| Drift (%) | Observations | Crack patterns |
|---|---|---|
| 2.20 | Max lateral load :(+)45.40 kN (Push)<br>:(-)44.00 kN (Pull)<br>**Crack-6 :** crushing<br>**Crack-12 and Crack-7:** joined<br>**Crack-11:** crack with is 2.5 mm<br>Joint totally crushed | 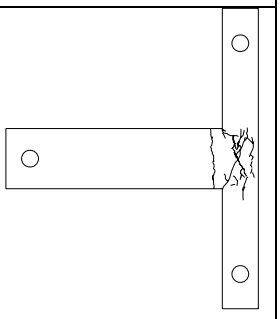 |
| 2.75 | Max lateral load : (+)38.50 kN (Push)<br>: (-)35.00 kN (Pull)<br>The concrete at the back of the column was crushed | 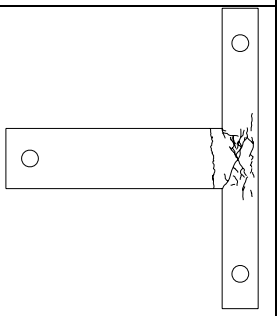 |

## A2 Specimen TR-1-R

Table A.5. Observations of Specimen TR-1-R

| Drift (%) | Observations | Crack Patterns |
|---|---|---|
| 0.15 | Max lateral load :(+)14.40 kN (Push)<br>:(-)16.20 kN (Pull)<br>No cracks observed | 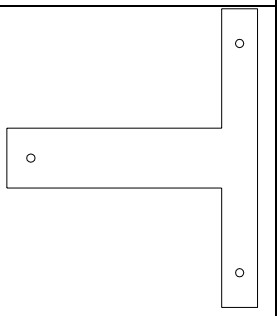 |
| 0.20 | Max lateral load :(+)17.30 kN (Push)<br>:(-)21.20 kN (Pull)<br>No cracks observed | 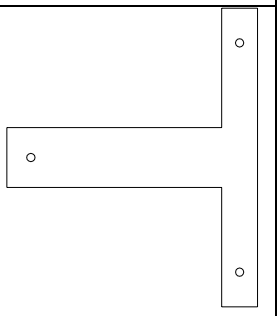 |
| 0.25 | Max lateral load :(+)19.40 kN (Push)<br>:(-)28.00 kN (Pull)<br>No cracks observed | 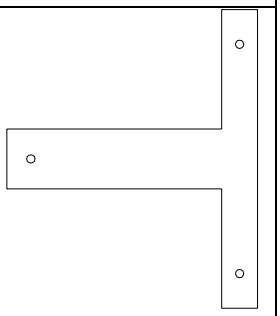 |
| 0.35 | Max lateral load :(+)20.60 kN (Push)<br>:(-)31.90 kN (Pull)<br>**Crack-1:** Flexural crack was formed at the bottom of the beam, 680 mm away from the column. Length was 400 mm.<br>**Crack-2:** Flexural crack was formed at the top of the beam, 300 mm away from the column. Length was 120 mm. | 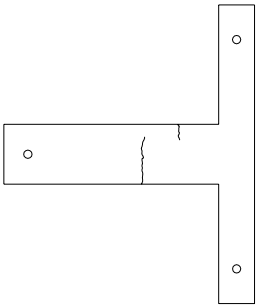 |

Table A.6. Observations of Specimen TR-1 R (continued)

| Drift (%) | Observations | Crack Patterns |
|---|---|---|
| 0.50 | Max lateral load :(+)33.70 kN (Push)<br>:(-)46.80 kN (Pull)<br>**Crack-3:** flexural + shear crack occurred at the top of the beam, 350 mm away from the column. the length of the crack was 370 mm. | 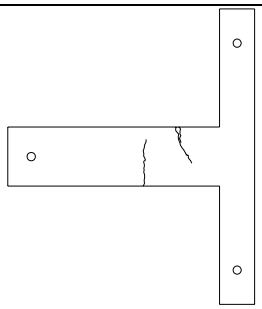 |
| 0.75 | Max lateral load :+)33.30 kN (Push)<br>:(-)56.20 kN (Pull)<br>No new cracks observed | 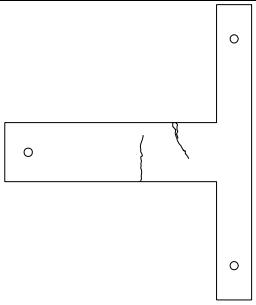 |
| 1.00 | Max lateral load :(+)54.16 kN (Push)<br>:(-)66.00 kN (Pull)<br>**Crack-3:** extended about 100 mm.<br>**Crack-4:** Flexural crack was formed at the bottom of the beam. It is located at about 290 mm away from the column face and its length was 100 mm.<br>**Crack-5:** Flexural crack developed at the bottom of the beam. It is located at about 290 mm away from the column face and its length was 100 mm. | 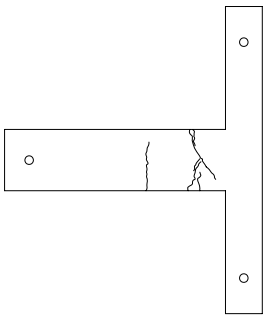 |
| 1.40 | Max lateral load :(+)70.08 kN (Push)<br>:(-)70.00 kN (Pull)<br>**Crack-3:** doubled at the top of the beam. And extended from the bottom.<br>**Crack-5:** doubled at the bottom.<br>**Crack-4** extended.<br>**Crack-2:** the width of the crack was reached 5 mm.<br>Spalling of concrete observed around **Crack 2 and Crack 3.** | 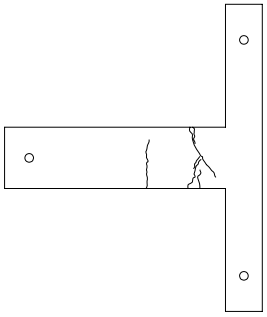 |

Table A.7. Observations of Specimen TR-1 R (continued)

| Drift (%) | Observations | Crack Patterns |
|---|---|---|
| 1.75 | Max lateral load :(+)75.85 kN (Push)<br>:(-)69.00 kN (Pull)<br>No new racks observed.<br>Existing cracks were extended. | 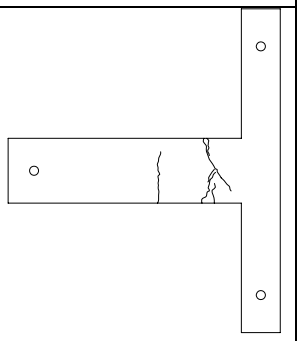 |
| 2.20 | Max lateral load :(+)81.00 kN (Push)<br>:(-)66.00 kN (Pull)<br>**Crack-6:** flexural crack was formed at the bottom, 920 mm away from the column face.<br>**Crack-7:** Flexural crack developed in push direction at the end of the beam, near to the roller support.<br>**Crack-5:** widened<br>**Crack-8:** Diagonal crack apperared at the top side of the beam, 500 mm away from the column. And joined with **Crack 3:** Concrete crushing observed near to the **Crack-7**<br>**Crack-3:** widened and the reinforcement can be seen from the crack | 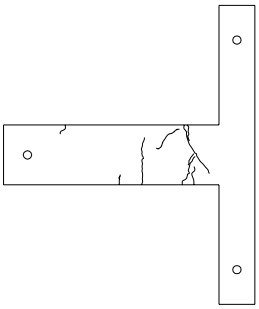 |
| 2.75 | Max lateral load :(+)80.00 kN (Push)<br>:(-)63.20 kN (Pull)<br>Repairing material was crushed at the joint region.<br>**Crack-3:** Doubled and extended towards joint. Width of crack was 3.5 mm.<br>**Crack-7:** Width of crack was 3 mm.<br>The spalling of cover concrete observed at the region of roller support.<br>**Crack-9:** Flexural crack occurred at bottom of the beam, 1020 mm away from the column. | 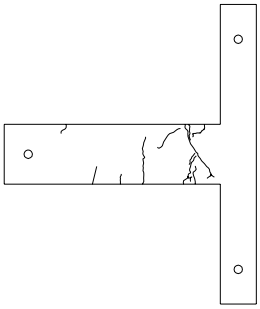 |

Table A.8. Observations of Specimen TR-1 R (continued)

| Drift (%) | Observations | Crack Patterns |
|---|---|---|
| 3.50 | Max lateral load :(+)76.00 kN (Push)<br>:(-)58.90 kN (Pull)<br>**Crack-3 and Crack 5:** doubled and alongated towards the joint.<br>**Crack-5:** Crack width about 2 mm.<br>**Crack-3:** Crack width about 2.5 mm. | 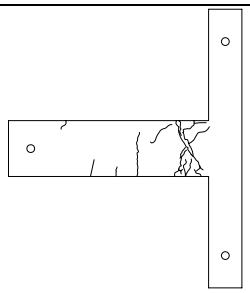 |
| 4.00 | Max lateral load :(+)60.30 kN (Push)<br>:(-)48.90 kN (Pull) | 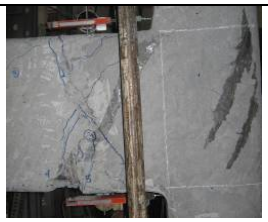 |

## A3 Specimen TR-2-Control

Table A.9. Observations of Specimen TR-2 Control

| Drift (%) | Observations | Crack patterns |
|---|---|---|
| 0.15 | Max lateral load : (+)15.00 kN (Push)<br>: (-)15.00 kN (Pull) | 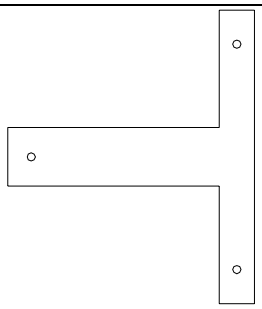 |
| 0.20 | Max lateral load : (+)19.80 kN (Push)<br>: (-)18.80 kN (Pull)<br>**Crack-1:** Flexural hairline crack was formed at the bottom of the beam, 45 mm away from the column. Length of crack is 120 mm.<br>**Crack-2:** Flexural crack developed at the upper side of the beam, 70 mm away from the column. Length of it is 75 mm.<br>**Crack-3:** Flexural crack formed at the upper side of the beam, 95 mm away from the column. Length of it is 55 mm.<br>**Crack-2:** elongated at about 20 mm | 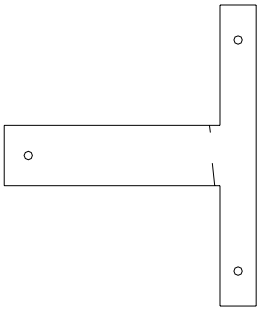 |
| 0.25 | Max lateral load :(+)22.20 kN (Push)<br>: (-)22.70 kN (Pull)<br>**Crack-3:** 50 mm extended<br>**Crack-2:** 35 mm extended<br>**Crack-3:** 60 mm extended<br>**Crack-2:** 40 mm extended<br>**Crack-1:** width :0.1 mm | 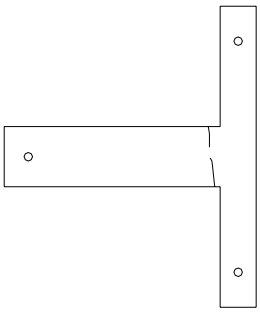 |
| 0.35 | Max lateral load :(+)27.60 kN (Push)<br>:(-)30.90 kN (Pull)<br>**Crack-1:** width :0.2 mm<br>**Crack-3&Crack-2:** joined<br>**Crack-3:** width :0.2 mm | 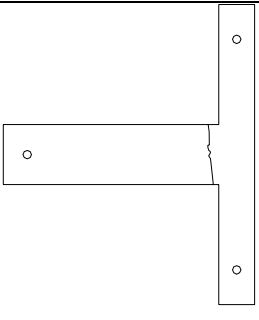 |

Table A.10. Observations of Specimen TR-2 Control (continued)

| Drift (%) | Observations | Crack patterns |
|---|---|---|
| 0.50 | Max lateral load :(+)33.60 kN (Push)<br>:(-)36.60 kN (Pull)<br>**Crack-1:** width :0.5 mm<br>**Crack-4:** Diagonal crack formed at the backside of column<br>**Crack-5**: 250 mm Vertical crack formed in the back side of column<br>**Crack-7:** doubled and 50 mm elongated to downwards<br>**Crack-8:** shear crack at the top corner of beam column intersection propagate into the joint 60 mm<br>**Crack-9:** shear crack at the bottom corner of beam column intersection propagate into the joint 60 mm<br>**Crack-4:** 110 mm elongated upward<br>**Crack-1:** crack width:0.6 mm<br>**Crack-6:** 200 mm extended downward with the angle of 75 degree<br>**Crack-4:** 45 mm extended upward | 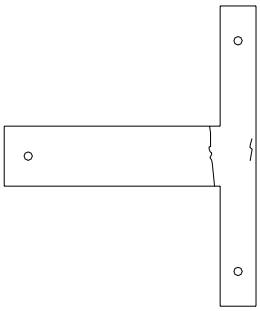 |
| 0.75 | Max lateral load :(+)37.20 kN (Push)<br>:(-)38.70 kN (Pull)<br>**Crack-6:** doubled<br>**Crack-10:** 50 mm shear crack at the joint core<br>**Crack-11:** Flexural crack occurred at the bottom of the beam, 450 mm away from the column. Length o crack is 220 mm.<br>**Crack-12:** shear crack in the joint (Parallel to Crack-10)<br>**Crack-13:** shear crack at the bottom corner of joint.<br>**Crack-7:** 60 mm extended<br>**Crack-14:** (similar to Crack-11) Flexural crack formed on the beam 450 mm away from the column. Length of the crack is 220 mm. | 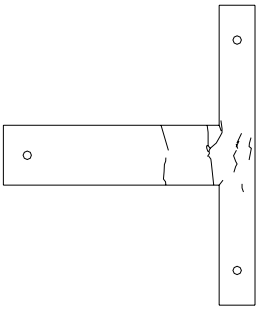 |

Table A.11. Observations of Specimen TR-2 Control (continued)

| Drift (%) | Observations | Crack patterns |
|---|---|---|
| 0.75 cont. | **Crack-15:** shear crack formed at the top side of the joint. 90 mm.<br>**Crack-16&-17:** shear crack formed at the bottom side of the joint.<br>**Crack9:** crack propagated on to the beam from the joint<br>**Crack-17 & Crack-13:** joined.<br>**Crack-8:** crack width: 0.4 mm<br>**Crack-9&Crack-12:** joined.<br>**Crack-1:** crack width: 1.0 mm<br>**Crack-5:** 40 mm elongated<br>**Crack-6:** 120 mm extended upward<br>**Crack-13:** All the sides of the beam column intersection were cracked<br>**Crack-9:** 90 mm extended<br>**Crack-17:** crack width at the joint core was 0.2 mm<br>**Crack-16:** 50 mm extended downward<br>**Crack-1:** crack width: 1.2 mm | 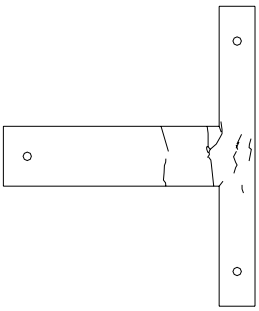 |
| 1.00 | Max lateral load :(+)38.00 kN (Push)<br>:(-)40.80 kN (Pull)<br>**Crack-6:** crack width: 0.7 mm.<br>**Crack-9:** doubled and extended 60 mm downward.<br>**Crack-17:** occurred at the joint core and joined with Crack-8**.**<br>**Crack-13:** doubled and extended 70 + 45 mm upward.<br>**Crack-12:** extended with 45 degree angle<br>**Crack-8:** crack width: 1.2 mm. the spilling of concrete cover was started<br>**Crack-16:** 40 mm extended downward<br>**Crack-15:** doubled and extended upward | 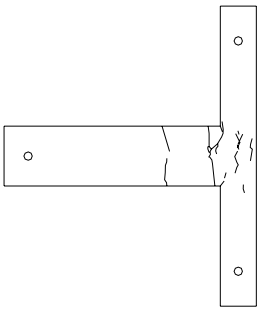 |

Table A.12. Observations of Specimen TR-2 Control (continued)

| Drift (%) | Observations | Crack patterns |
|---|---|---|
| 1.00 cont. | **Crack-16:** propagated diagonally to the column surface.<br>**Crack-4:** 30 mm extended<br>**Crack-15:** 50 mm elongated upward<br>**Crack-6:** crack width: 0.9 mm<br>**Crack-7:** 50 mm extended downward | 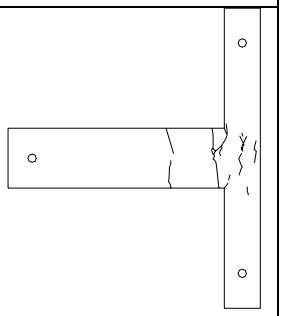 |
| 1.40 | Max lateral load :(+)37.00 kN (Push)<br>:(-)41.00 kN (Pull)<br>**Crack-8:** crack width is 1.2 mm<br>The width of crack at the core was 0.8 mm<br>**Crack-6:** crack width is 1.2 mm<br>The width of crack at the core was 1.2 mm<br>**Crack-13:** crack width is 1.6 mm.<br>**Crack-6:** crack width is 1.6 mm<br>**Crack-9:** 85 mm extended towards the joint core<br>**Crack-15:** extended 50 mm<br>Cover spilled at the joint core<br>**Crack-18:** formed at the right side of the column.<br>**Crack-13:** crack width: 1.8 mm.<br>**Crack-8:** crack width 1.6 mm. | 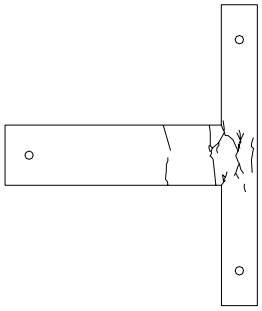 |
| 1.75 | Max lateral load :(+)33.80 kN (Push)<br>:(-)34.70 kN (Pull)<br>**Crack-6:** crack width: 2 mm.<br>**Crack-13:** crack width: 2.5 mm.<br>**Crack-19:** vertical crack formed at the joint core<br>**Crack-13:** doubled and extended 70 + 45 mm upward.<br>**Crack-6:** 150 mm extended upward<br>Concrete covers at the corner was spilled<br>**Crack-19 & Crack-12:** joined | 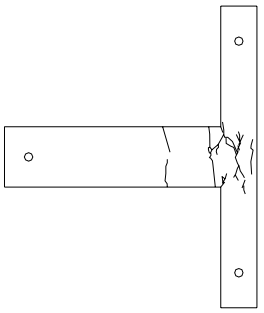 |

## A4 Specimen TR-2-R-FRP

Table A.13. Observations of Specimen TR-2-R-FRP

| Drift (%) | Observations | Crack Patterns |
|---|---|---|
| 0.15 | Max lateral load :(+)13.50 kN (Push)<br>:(-)17.30 kN (Pull) | |
| 0.20 | Max lateral load :(+)16.20 kN (Push)<br>:(-)25.00 kN (Pull)<br>**Crack-1:** Flexural crack was formed at the bottom of the beam, 680 mm away from the column. The length of the cracks is 140 mm. | 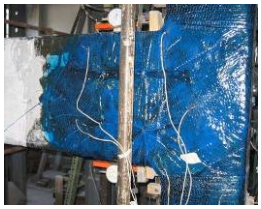 |
| 0.25 | Max lateral load :(+)18.10 kN (Push)<br>:(-)32.70 kN (Pull)<br>**Crack-2 and Crack 3:** Flexural cracks were formed at the top of the beam. They are located at 820 and 1050 mm away from the column face and the length of them are 90 mm and 100 mm respectively | 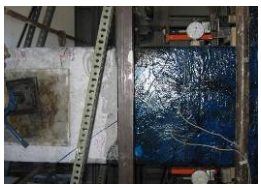 |
| 0.35 | Max lateral load :(+)22.40 kN (Push)<br>:(-)46.60 kN (Pull)<br>**Crack-4 and Crack 5:** Flexural cracks developed at the bottom of the beam, at about the end of the wrapped region. | |
| 0.50 | Max lateral load :(+)30.88 kN (Push)<br>:(-)62.90 kN (Pull)<br>**Crack-6 and Crack 7:** the flexural cracks occurred at the bottom side of the beam.<br>**Crack-8:** flexural crack occurred at the top of the beam. | |
| 0.75 | Max lateral load :(+)48.00 kN (Push)<br>:(-)78.20 kN (Pull)<br>**Crack-1, Crack-6 and Crack-7:** extended<br>**Crack-9:** diagonal crack occurred at the beam<br>**Crack-3 and Crack-1**: joined. |  |

Table A.14. Observations of Specimen TR-2-R-FRP (continued)

| Drift (%) | Observations | Crack Patterns |
|---|---|---|
| 1.00 | Max lateral load :(+)65.00 kN (Push)<br>:(-)93.20 kN (Pull)<br><br>Debonding occurred at the tip of the diagonal CFRP sheets. |  |
| 1.40 | Max lateral load :(+)78.40 kN (Push)<br>:(-)99.00 kN (Pull) | |
| 1.75 | Max lateral load :(+)74.60 kN (Push)<br>:(-)95.60 kN (Pull)<br>**Crack-4:** the width of the crack is 3 mm.<br>**Crack-9:** the length of the crack was elongated.<br>**Crack-4 and Crack 9:** joined<br>**Crack-10 and Crack-11:** occurred. |  |
| 2.20 | Max lateral load :(+)75.20 kN (Push)<br>:(-)96.70 kN (Pull)<br>**Crack-9:** extended laterally at the reinforcement level.<br>Crushing of concrete occurred at the **Crack-4**<br>**Crack-12 and Crack 13:** formed at the roller support | |
| 2.75 | Max lateral load :(+)74.40 kN (Push)<br>:(-)96.50 kN (Pull)<br>**Crack-5:** The width of the crack reached 15 mm.<br>**Crack-9:** The width of the crack reached 2.5 mm.<br>Dowel action observed at the beam bottom reinforcing bars. | 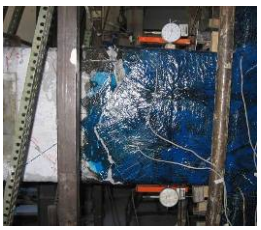 |

Table A.15. Observations of Specimen TR-2-R-FRP (continued)

| Drift (%) | Observations | Crack Patterns |
|---|---|---|
| 3.50 | Max lateral load :(+)71.30 kN (Push)<br>:(-)94.70 kN (Pull)<br>Spalling of concrete at the Crack |  |
| 4.00 | Max lateral load :(+)65.80 kN (Push)<br>:(-)76.40 kN (Pull)<br>Spalling of concrete at the Crack. |  |
| 4.50 | Max lateral load :(+)75.20 kN (Push)<br>:(-)96.70 kN (Pull) | |

## A5 Specimen TR-3-Control

Table A.16. Observations of Specimen TR-3 Control

| Drift (%) | Observations | Crack Patterns |
|---|---|---|
| 0.15 | Max lateral load : (+)12.30 kN (Push)<br>: (-)14.20 kN (Pull)<br>**Crack-1:** In pull direction, flexural crack was formed at the top of the beam, 55 mm away from the column. Length of crack is 60 mm. | 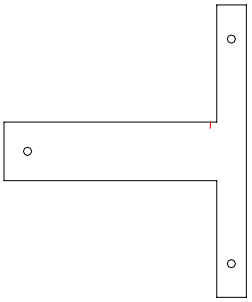 |
| 0.20 | Max lateral load :(+)14.30 kN (Push)<br>: (-)16.20 kN (Pull)<br>**Crack-2:** In push direction of loading, flexural crack formed at the bottom of the beam, 75 mm away from the column. Length of crack is 230 mm. crack width is 0.2 mm.<br>**Crack-3**: In pull direction, flexural crack developed at the top of the beam, 270 mm away from the column. Length of crack is 50 mm | 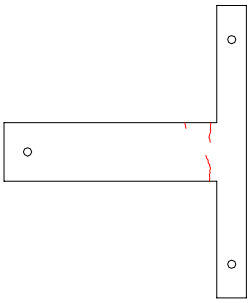 |
| 0.25 | Max lateral load :(+)15.50 kN (Push)<br>:(-) 18.50 kN (Pull)<br>**Crack-4:** In push direction, flexural crack occurred at the bottom of the beam, 450 mm away from the column. Length of crack is 50 mm.<br>**Crack-1:** Crack width 0.2 mm<br>**Crack-3:** elongated | 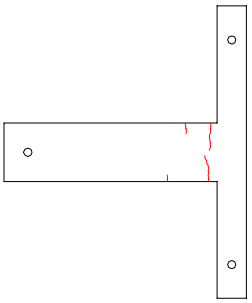 |
| 0.35 | Max lateral load :(+)18.80 kN (Push)<br>:(-)23.00 kN (Pull)<br>**Crack-2:** Extended 40 mm, crack width 0.4 mm.<br>**Crack-5:** the first diagonal crack at the joint region<br>**Crack-6:** flexural crack apperared at the top of the beam, 450 mm away from the column surface. Length of crack is 190 mm. | 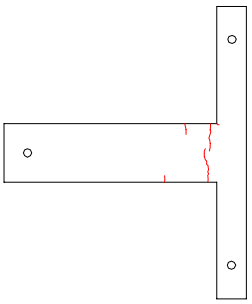 |

Table A.17. Observations of Specimen TR-3 Control (continued)

| Drift (%) | Observations | Crack Patterns |
|---|---|---|
| 0.50 | Max lateral load :(+)22.60 kN (Push)<br>:(-)24.90 kN (Pull)<br>**Crack-4:** extended 90 mm<br>**Crack-7:** Shear (diagonal) cracks developed at the joint region. Started from bottom corner and the length of crack is 30 mm.<br>**Crack-1 and Crack-2:** joined<br>**Crack-5:** extended through the joint core.<br>**Crack-8:** diagonal crack at he joint core<br>**Crack-9 , Crack-10 and Crack- 11:** vertical cracks formed at the surface of the column<br>**Crack-12:**<br>**Crack-13: Crack-8:** branched<br>**Crack-14:** Diagonal crack at the joint region and the level of bottom part of the beam.<br>**Crack-15:** started from outside of the joint region and extended to the top of column | 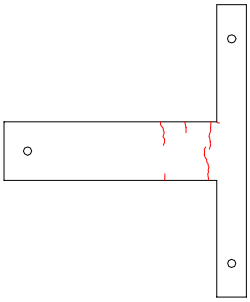 |
| 0.75 | Max lateral load :(+)24.00 kN (Push)<br>:(-)27.20 kN (Pull)<br>Spalling of cover concrete<br>**Crack-16 and Crack-17:** occurred at the joint core<br>**Crack-7:** Branched<br>The cracks at the joint region were extended | 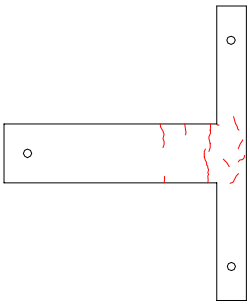 |
| 1.00 | Max lateral load : (+)23.80 kN (Push)<br>: (-)25.80 kN (Pull)<br>Spalling of cover concrete at the joint core<br>**Crack-15 and Crack-17:** branched<br>**Crack-16 , Crack-4 and Crack-7:** extended<br>**Crack-18 and Crack-19:** shear cracks occurred at the joint core | 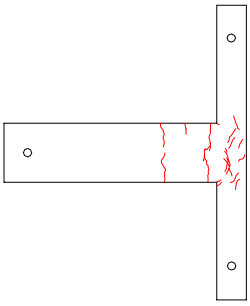 |

Table A.18. Observations of Specimen TR-3 Control (continued)

| Drift (%) | Observations | Crack Patterns |
|---|---|---|
| 1.40 | Max lateral load :(+)23.40 kN (Push)<br>:(-)21.70 kN (Pull)<br>Crack width at the joint is 1.2 mm<br>Cracks were extended at the joint region | 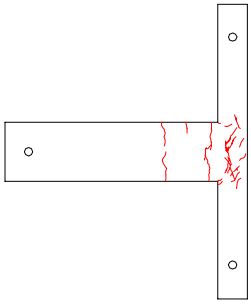 |
| 1.75 | Max lateral load :(+)19.00 kN (Push)<br>:(-)18.70 kN (Pull)<br>**Crack-8:** elongated | 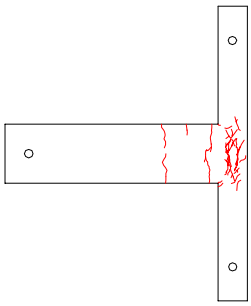 |

## A6 Specimen TR-3-R

Table A.19. Observations of Specimen TR-3 R

| Drift (%) | Observations | Crack Patterns |
|---|---|---|
| 0.15 | Max lateral load :(+)12.4 kN (Push)<br>:(-)12.1 kN (Pull)<br>The blue cracks indicated in the Figures are the cracks remaining from control specimen's tests. No new cracks observed at this drift level | 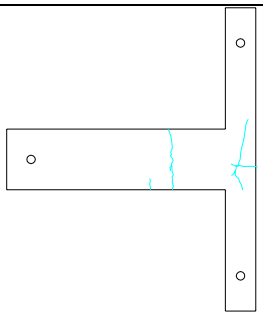 |
| 0.20 | Max lateral load :(+)13.80 kN (Push)<br>:(-)20.00 kN (Pull)<br>**Crack-1:** Flexural crack formed at the top of the beam. The length of the cracks is 90 mm. | 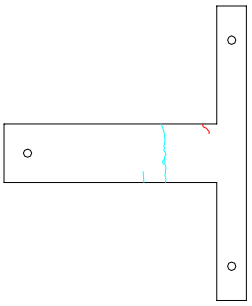 |
| 0.25 | Max lateral load :(+)16.50 kN (Push)<br>:(-)24.40 kN (Pull)<br>Existing cracks were widened | 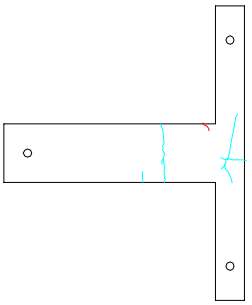 |
| 0.35 | Max lateral load :(+)20.60 kN (Push)<br>:(-)31.90 kN (Pull)<br>**Crack-1:** extended about 80 mm | 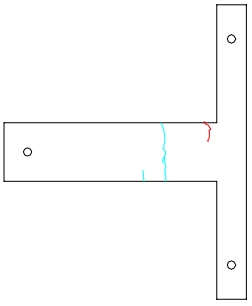 |

Table A.20. Observations of Specimen TR-3 R (continued)

| Drift (%) | Observations | Crack Patterns |
|---|---|---|
| 0.50 | Max lateral load :(+)27.90 kN (Push)<br>:(-)41.90 kN (Pull)<br><br>**Crack-2:** the flexural crack was formed at the bottom of the beam, 90 mm away from the column face.<br>**Crack-3:** flexural crack was formed at the top of the beam, 270 mm away from the column. the length of the crack was 90 mm. | 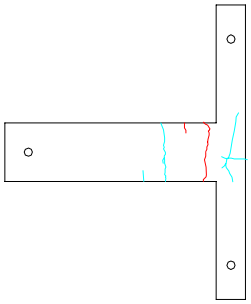 |
| 0.75 | Max lateral load :(+)35.75 kN (Push)<br>:(-)55.55 kN (Pull)<br>**Crack-2 and Crack-3:** joined | 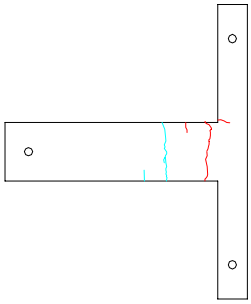 |
| 1.00 | Max lateral load :(+)45.4 kN (Push)<br>:(-)63.15 kN (Pull)<br>**Crack-4:** The first diagonal shear crack formed at the joint region. It started from top intersection of beam column connection.<br>**Crack-5:** Existing cracks were extended.<br>**Crack-6:** the flexural crack occurred at the bottom of the beam | 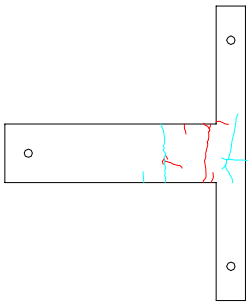 |
| 1.40 | Max lateral load :(+)45.40 kN (Push)<br>:(-)60.50 kN (Pull)<br>**Crack-1:** width 2.5 mm<br>**Crack-6:** Existing cracks were extended.<br>**Crack-7:** diagonal cracks developed at the side face of the column.<br>**Crack-8:** vertical cracks appeared at the back side of the column<br>**Crack-8 and Crack-7:** joined | 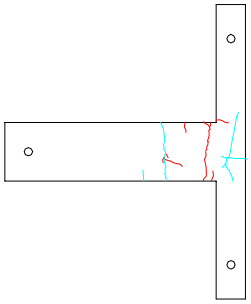 |

Table A.21. Observations of Specimen TR-3 R (continued)

| Drift (%) | Observations | Crack Patterns |
|---|---|---|
| 1.75 | Max lateral load :(+)42.00 kN (Push)<br>:(-)58.20 kN (Pull)<br>Existing cracks were elongated and widened. | 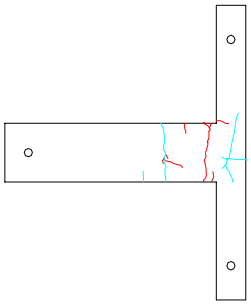 |
| 2.20 | Max lateral load :(+)40.00 kN (Push)<br>:(-)54.60 kN (Pull)<br>Small diagonal cracks developed at the joint region near to the maximum moment region of the beam. | 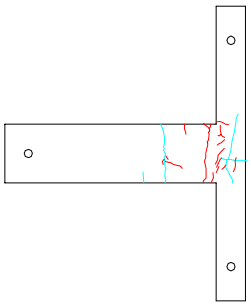 |
| 2.75 | Max lateral load :(+)39.00 kN (Push)<br>:(-)49.00 kN (Pull)<br>The spalling of cover concrete and buckling of column longitudinal reinforcement. |  |

## A7 Specimen TR-4-Control

Table A.22. Observations of Specimen TR-4 Control

| Drift (%) | Observations | Crack patterns |
|---|---|---|
| 0.15 | Max lateral load : (+)14.60 kN (Push)<br>: (-)18.2 kN (Pull)<br>**Crack-1:** Flexural crack formed at the top of the beam, 670 mm away from the column. Length of crack is 10 mm. | 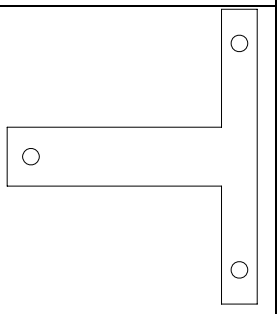 |
| 0.20 | Max lateral load : (+)18.40 kN (Push)<br>: (-)22.80 kN (Pull)<br>**Crack-2:** Flexural crack was formed at the bottom of the beam, 130 mm away from the column. Length of crack is 90 mm.<br>**Crack-3:** Flexural crack was formed at the upper side of the beam, 15 mm away from the column. Length of it is 10 mm.<br>**Crack-4:** Flexural crack formed at the top of the beam, 80 mm away from the column. Length of crack is 35 mm. | 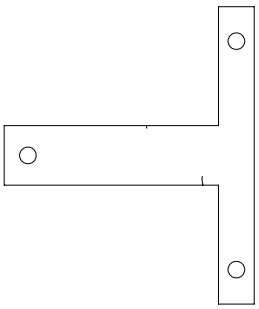 |
| 0.25 | Max lateral load :(+)20.80 kN (Push)<br>: (-)26.70 kN (Pull)<br>**Crack-5:** vertical shear crack occurred at the center of the joint core. Length is 90 mm<br>**Crack-2:** extended 70 mm<br>**Crack-6:** Flexural crack occurred 300 mm away from the column face at the bottom of the beam<br>**Crack-5:** extended to downward 100 mm | 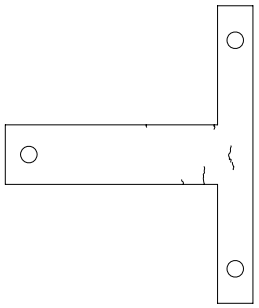 |

Table A.23. Observations of Specimen TR-4 Control (continued)

| Drift (%) | Observations | Crack patterns |
|---|---|---|
| 0.35 | Max lateral load :(+)25.40 kN (Push)<br>:(-) 34.80 kN (Pull)<br>**Crack-5:** extended to upward 110 mm<br>**Crack-4:** extended to downward 70 mm<br>**Crack-3:** extended to downward 40 mm<br>**Crack-7:** shear crack occurred as (Crack-5.)<br>**Crack-8:** Flexural crack was formed at the top of the beam, 340 mm away from the column. Length of crack is 140 mm<br>**Crack-9:** Flexural crack occurred at the top of the beam, 560 mm away from the column. Length of crack is 50 mm<br>**Crack-10:** Flexural crack occurred at the top of the beam, 210 mm away from the column. Length of crack is 50 mm<br>**Crack-11:** 100 mm-Vertical cracks occurred at back side of the column. | 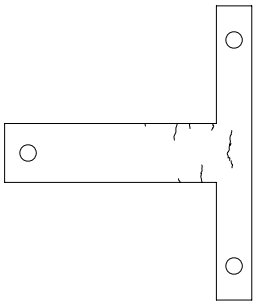 |
| 0.50 | Max lateral load :(+)31.70 kN (Push)<br>:(-)41.80 kN (Pull)<br>**Crack-12:** Flexural crack occurred at the top of the beam, 50 mm away from the column. Length of crack is 100 mm<br>**Crack-2:** 300 mm Extended<br>**Crack-6:** extended diagonally as shear crack<br>**Crack-5:** extended downward to the column<br>**Crack-13**: Flexural crack occurred at the beam, 55 mm away from the column. Length of crack is 100 mm<br>**Crack-5:** doubled and crack width reached 3 mm<br>**Crack-7:** reached to the top of intersection of the beam column & **Crack-5:** Joined<br>**Crack-5:** Extended<br>**Crack-14:** Shear crack occurred at the joint core | 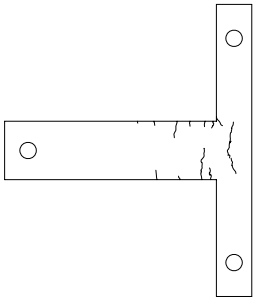 |

Table A.24. Observations of Specimen TR-4 Control (continued)

| Drift (%) | Observations | Crack pattern |
|---|---|---|
| 0.75 | Max lateral load :(+)39.30 kN (Push)<br>:(-)44.90 kN (Pull)<br>**Crack-12:** extended<br>**Crack-2:** elongated with 45 degree angle<br>**Crack-6:** extended upward<br>**Crack-15:** Shear crack was formedat the bottom part of the joint core<br>**Crack-11:** spalling<br>**Crack-7 & Crack-5:** joined<br>**Crack-5:** spalling<br>**Crack-16:** Vertical crack was formed at the back side of the column<br>**Crack-11:** elongated to upside of the column<br>**Crack-16:** extended downward | 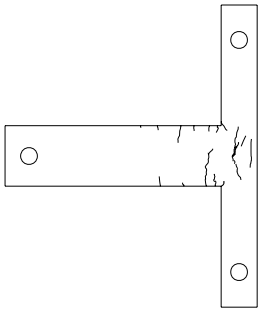 |
| 1.00 | Max lateral load :(+)40.50 kN (Push)<br>:(-)48.20 kN (Pull)<br>Existing cracks were elongated and widened | 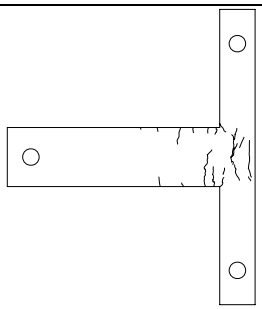 |
| 1.40 | Max lateral load : (+)40.00 kN (Push)<br>: (-)46.00 kN (Pull)<br>Existing cracks were elongated and widened | 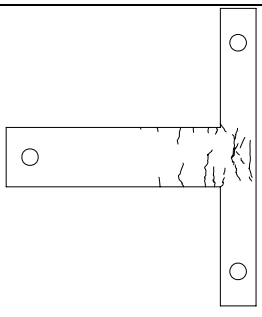 |
| 1.75 | Max lateral load : (+)34.40 kN (Push)<br>: (-)34.10 kN (Pull)<br>Spalling of cracked concrete | 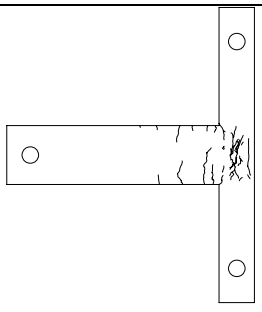 |

## A8 Specimen TR-4-R-FRP

Table A.25. Observations of Specimen TR-4-R-FRP

| Drift (%) | Observations | Crack Patterns |
|---|---|---|
| 0.15 | Max lateral load :(+)13.30 kN (Push)<br>:(-)19.74 kN (Pull)<br>No cracks observed | |
| 0.20 | Max lateral load :(+)15.40 kN (Push)<br>:(-)27.18 kN (Pull)<br>**Crack-1:** Flexural crack formed at the bottom of the beam, 500 mm away from the column face. The length of the cracks is 190 mm.<br>**Crack-2:** Flexural crack formed at the top of the beam, 500 mm away from the column face. The length of the cracks is 250 mm. | 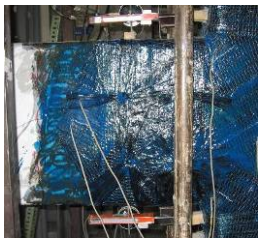 |
| 0.25 | Max lateral load :(+)18.50 kN (Push)<br>:(-)33.80 kN (Pull)<br>**Crack-3:** Flexural crack was developed at the bottom of the beam, 710 mm away from the column face. The length of the cracks is 230 mm.<br>**Crack-4:** Flexural crack was occurred at the top of the beam, 710 mm away from the column face. The length of the cracks is 140 mm. | |
| 0.35 | Max lateral load :(+)22.30 kN (Push)<br>:(-)48.66 kN (Pull)<br>**Crack-5:** Flexural crack was formed at the top of the beam, 930 mm away from the column face. The length of the cracks is 100 mm.<br>**Crack-6:** Flexural crack was appeared at the top of the beam, 1100 mm away from the column face. The length of the cracks is 100 mm<br>**Crack-2 and Crack-1:** joined |  |

Table A.26. Observations of Specimen TR-4-R-FRP (continued)

| Drift (%) | Observations | Crack Patterns |
|---|---|---|
| 0.50 | Max lateral load :(+)30.70 kN (Push)<br>:(-)65.70 kN (Pull)<br>**Crack-7:** the flexural crack apperaed at the bottom of the beam, 110 mm away from the column face. The length of the cracks is 100 mm | |
| 0.75 | Max lateral load :(+)48.00 kN (Push)<br>:(-)87.40 kN (Pull)<br>**Crack-8:** the flexural crack was formed at the bottom of the beam, 360 mm away from the column face. The length of the cracks is 90 mm. | 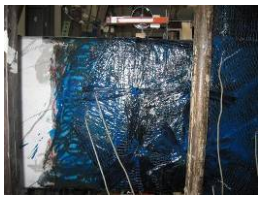 |
| 1.00 | Max lateral load :(+)65.85 kN (Push)<br>:(-)97.40 kN (Pull)<br>**Crack-9:** the flexural crack was developed at the bottom of the beam, 350 mm away from the column face. The length of the cracks is 60 mm.<br>**Crack-10:** the flexural crack was formed at the top of the beam, 370 mm away from the column face. The length of the cracks is 270 mm.<br>Debonding occurred at the end of the wrapped region. | 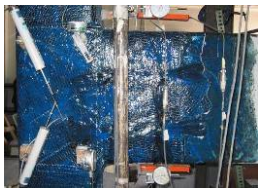 |
| 1.40 | Max lateral load :(+)72.20 kN (Push)<br>:(-)93.00 kN (Pull)<br>**Crack-10 and Crack-1:** joined | |
| 1.75 | Max lateral load :(+)70.12 kN (Push)<br>:(-)91.60 kN (Pull)<br>**Crack-1:** width of crack is 5 mm.<br>Cracks were formed at the roller support. | |
| 2.20 | Max lateral load :(+)69.50 kN (Push)<br>:(-)90.00 kN (Pull)<br>Concrete was crushed at the bottom of the beam, the beam reinforcements were buckled. |  |

Table A.27. Observations of Specimen TR-4-R-FRP (continued)

| Drift (%) | Observations | Crack Patterns |
|---|---|---|
| 2.75 | Max lateral load :(+)68.20 kN (Push)<br>:(-)90.40 kN (Pull)<br>The plastic hinging was occurred at the bottom of the beam. |  |
| 3.50 | Max lateral load :(+)58.12 kN (Push)<br>:(-)73.41 kN (Pull)<br>Cover concrete spalled |  |
| 4.00 | Max lateral load :(+)40.60 kN (Push)<br>:(-)68.90 kN (Pull) |  |

## A9 Specimen TR-5-Control

Table A.28. Observations of Specimen TR-5-Control

| Drift (%) | Observations | Crack patterns |
|---|---|---|
| 0.15 | Max lateral load : (+)18.20 kN (Push)<br>: (-)17.70 kN (Pull)<br>No cracks observed | |
| 0.20 | Max lateral load : (+)23.60 kN (Push)<br>: (-)21.60 kN (Pull)<br>**Crack-1:** Flexural crack formed at the bottom of the beam, 10 mm away from the column. Length of crack is 220 mm.<br>**Crack-2:** Flexural crack was formed at the bottom of the beam, 700 mm away from the column. Length of it is 40 mm.<br>**Crack-3:** Flexural crack was formed at the top of the beam, 80 mm away from the column. Length of crack is 90 mm.<br>**Crack-4:** Flexural crack was formed at the top of the beam, 300 mm away from the column. Length of it is 90 mm. |  |
| 0.25 | Max lateral load :(+)26.50 kN (Push)<br>: (-)24.60 kN (Pull)<br>**Crack-5:** Flexural crack developed at the bottom of the beam, 300 mm away from the column. Length of it is 60 mm.<br>**Crack-6:** Flexural crack appeared at the top of the beam, 530 mm away from the column. Length of it is 100 mm.<br>**Crack-1:** elongated.<br>**Crack-3:** extended.<br>**Crack-4:** length reached to 100 mm. | 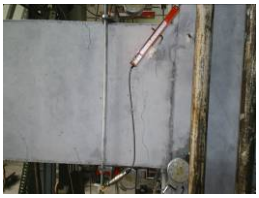 |

Table A.29. Observations of Specimen TR-5-Control (continued)

| Drift (%) | Observations | Crack patterns |
|---|---|---|
| 0.35 | Max lateral load :(+)32.20 kN (Push)<br>:(-)31.70 kN (Pull)<br>**Crack-1 & Crack-5 & Crack-6:** extended.<br>**Crack-1&Crack-3:** joined.<br>**Crack-7:** Flexural crack formed at the top of the beam, 500 mm away from the column. Length of it is 40 mm.<br>**Crack-8:** diagonal crack was formed at the top corner of the joint with the length of 10 mm.<br>**Crack-9:** vertical crack in the joint region (cover). |  |
| 0.50 | Max lateral load :(+)39.20 kN (Push)<br>:(-)39.40 kN (Pull)<br>**Crack-1:** doubled.<br>**Crack-10:** diagonal crack formed at the bottom corner of the joint with the length of 10 mm.<br>**Crack-9:** extended towards bottom and top (length: 400 mm).<br>**Crack-7:** extended diagonally<br>**Crack-3:** crushed (crack width= 0.35 mm)<br>**Crack-11:** A hairline diagonal crack occurred in the joint. Length: 110 mm<br>**Crack-6 and Crack-7:** joined and extended to bottom of the beam<br>**Crack-12:** Hairline crack at the back of column |  |
| 0.75 | Max lateral load :(+)45.40 kN (Push)<br>:(-)46.90 kN (Pull)<br>**Crack-12:** elongated.<br>**Crack-2:** elongated.<br>**Crack-1:** crack width : 0.6 mm<br>**Crack-8:** extended<br>**Crack-11:** extended diagonally |  |

Table A.30. Observations of Specimen TR-5-Control (continued)

| Drift (%) | Observations | Crack patterns |
|---|---|---|
| 1.00 | Max lateral load :(+)47.00 kN (Push)<br>:(-)46.70 kN (Pull)<br>**Crack-11, Crack-8 and Crack-10:** extended towards to the joint core<br>**Crack-13:** Flexural crack was formed at the top of the beam, 700 mm away from the column. Length of it is 300 mm |  |
| 1.40 | Max lateral load :(+) 44.20 kN (Push)<br>:(-) 43.80 kN (Pull)<br>**Crack 14:** Flexural crack was formed at the back face of column. |  |
| 1.75 | Max lateral load :(+) 36.50 kN (Push)<br>:(-) 33.80 kN (Pull) |  |

## A10 Specimen TR-5-FRP-1

Table A.31. Observations of Specimen TR-5-FRP-1

| Drift (%) | Observations | | Crack Patterns |
|---|---|---|---|
| 0.15 | Max lateral load | :(+)18.50 kN (Push)<br>:(-)18.00 kN (Pull) | 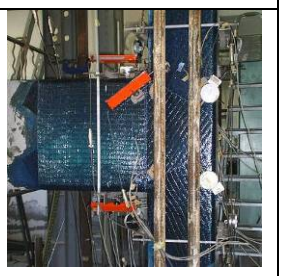 |
| 0.20 | Max lateral load | :(+)25.80 kN (Push)<br>:(-)24.20 kN (Pull) | |
| 0.25 | Max lateral load | :(+)29.50 kN (Push)<br>:(-)28.00 kN (Pull) |  |
| 0.35 | Max lateral load | :(+)36.60 kN (Push)<br>:(-)36.30 kN (Pull) |  |
| 0.50 | Max lateral load | :(+) 45.90 kN (Push)<br>:(-) 46.60 kN (Pull) |  |

Table A.32. Observations of Specimen TR-5-FRP-1 (continued)

| Drift (%) | Observations | Crack Patterns |
|---|---|---|
| 0.75 | Max lateral load :(+) 56.00 kN (Push)<br>:(-) 58.00 kN (Pull)<br>**Crack 1:** Flexural crack was formed at the top and bottom of the beam, at the end of CFRP wrapped region. |  |
| 1.00 | Max lateral load :(+) 62.70 kN (Push)<br>:(-) 65.00 kN (Pull) |  |
| 1.40 | Max lateral load :(+) 68.90 kN (Push)<br>:(-) 73.10 kN (Pull)<br>Cracks were widened on the beam |  |
| 1.75 | Max lateral load :(+) 72.00 kN (Push)<br>:(-) 76.10 kN (Pull) |  |

Table A.33. Observations of Specimen TR-5-FRP-1 (continued)

| Drift (%) | Observations | Crack Patterns |
|---|---|---|
| 2.20 | Max lateral load :(+) 75.90 kN (Push)<br>:(-) 79.50 kN (Pull)<br>Debonding occurs at the back side of the column in joint region due to buckling.<br>At the top and bottom corner of the beam column joint interface, CFRP sheets were elongated and ruptured. | 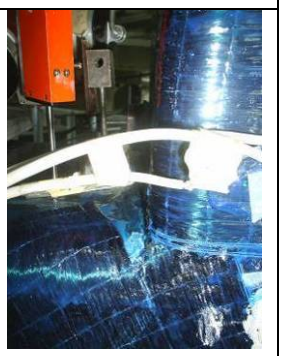 |
| 2.75 | Max lateral load :(+) 73.40 kN (Push)<br>:(-) 70.80 kN (Pull)<br>CFRP ruptured at the beam column joint corners. |  |
| 3.50 | Max lateral load :(+) 64.20 kN (Push)<br>:(-) 61.50 kN (Pull) | |

## A11 Specimen TR-5-FRP-2

Table A.34. Observations of Specimen TR-5-FRP-2

| Drift (%) | Observations | Pictures |
|---|---|---|
| 0.15 | Max lateral load :(+) 14.50 kN (Push)<br>:(-) 18.80 kN (Pull) | 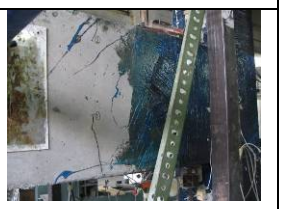 |
| 0.20 | Max lateral load :(+) 25.80 kN (Push)<br>:(-) 26.00 kN (Pull)<br>**Crack-1 and Crack-2:** Flexural crack was formed at the top and bottom of the beam, 650 mm away from the east face of the column. The length of the Crack-1 is 200 mm, Crack-2 is 90 mm.<br>**Crack-3:** Flexural crack was formed at the top of the beam, 860 mm away from the east face of the column. | 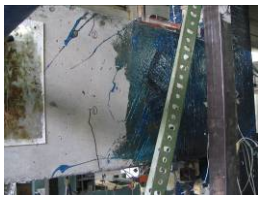 |
| 0.25 | Max lateral load :(+) 25.80 kN (Push)<br>:(-) 31.30 kN (Pull)<br>**Crack-4:** Flexural crack was formed at the bottom of the beam, 900 mm away from the east face of the column. Length is 50 mm | |
| 0.35 | Max lateral load :(+) 24.40 kN (Push)<br>:(-) 41.70 kN (Pull)<br>**Crack-1:** Extended 230 mm.<br>**Crack-5:** was formed at the top of the beam, 470 mm away from the column.<br>**Crack-6:** developed at the bottom of the beam as symmetrical of **Crack-5**.<br>And joined with **Crack-5**. | 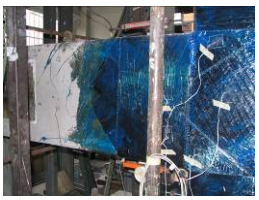 |
| 0.50 | Max lateral load :(+) 31.70 kN (Push)<br>:(-) 53.00 kN (Pull)<br>**Crack-7:** was formed at the top of the beam, 915 mm away from the column. |  |

Table A.35. Observations of Specimen TR-5-FRP-2 (continued)

| Drift (%) | Observations | Pictures |
|---|---|---|
| 0.75 | Max lateral load :(+) 42.00 kN (Push)<br>:(-) 67.70 kN (Pull)<br>**Crack-4:** 70 mm extended diagonally<br>**Crack-1:** widened at about 0.3 mm.<br>Some sounds came out from CFRP sheets |  |
| 1.00 | Max lateral load :(+) 53.00 kN (Push)<br>:(-) 77.40 kN (Pull)<br>The section was totally cracked at the region of **Crack-1.**<br>**Crack-8:** Diagonal crack was formed at the end of the wrapped region, starting from the top of beam. | |
| 1.40 | Max lateral load :(+) 89.40 kN (Push)<br>:(-) 66.50 kN (Pull)<br>FRP sheets at the top and bottom of the corners were under stress. |  |
| 1.75 | Max lateral load :(+) 69.00 kN (Push)<br>:(-) 91.70 kN (Pull)<br>Debonding of diagonal fibers at the end of wrapped area.<br>**Crack-1:** Diagonal cracks were formed at the bottom of the beam next to the **Crack-1**,<br>Diagonal cracks occurred between the **Crack 1 and Crack 5.**<br>**Crack-1 and Crack-8**: are joined. |  |
| 2.20 | Max lateral load :(+) 69.30 kN (Push)<br>:(-) 94.70 kN (Pull)<br>**Crack-5:** width of crack reached 3.5 mm.<br>CFRP sheets at the corner of the beam column interface were stressed. | 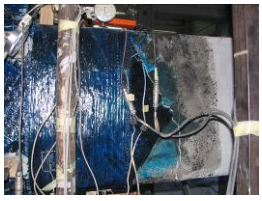 |

Table A.36. Observations of Specimen TR-5FRP-2 (continued)

| Drift (%) | Observations | Pictures |
|---|---|---|
| 2.75 | Max lateral load :(+) 71.00 kN (Push)<br>:(-) 94.00 kN (Pull)<br>**Crack-5:** width of the crack was 5 mm.<br>**Crack-6 and Crack-8:** widths of the cracks were 0.5 mm.<br>CFRP buckled and debonded at the backside of the column at the joint region.<br>Beam was hinged at the end of the wrapped section |  |
| 3.50 | Max lateral load :(+) 69.70 kN (Push)<br>:(-) 92.30 kN (Pull)<br>CFRP sheets were ruptured at the top corner of beam column interface<br>Concrete was totally crushed and beam bottom reinforcements were buckled at the hinged region. | 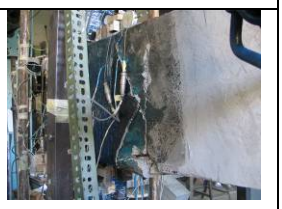 <br>  |
| 4.00 | Max lateral load :(+) 67.00 kN (Push)<br>:(-) 80.00 kN (Pull) |  <br>  |

## A12 Specimen TR-5-FRP-3

Table A.37. Observations of Specimen TR-5-FRP-3

| Drift (%) | Observations | Pictures |
|---|---|---|
| 0.20 | Max lateral load :(+) 16.70 kN (Push)<br>:(-) 24.50 kN (Pull)<br>**Crack-1, Crack-2 and Crack-3:** Flexural cracks were formed at the top and bottom of the beam, 660mm , 840 mm and 1000 mm away from the east face of the column. The length of the **Crack-**1 is 50 mm, Crack-2 is 50 mm.<br>**Crack-4 and Crack-5:** Flexural cracks were formed at the top f the beam, 680mm and 800 mm away from the east face of the column. |  |
| 0.25 | Max lateral load :(+) 17.80 kN (Push)<br>:(-) 29.80 kN (Pull)<br>**Crack-4 and Crack -1**.: joined | |
| 0.35 | Max lateral load :(+) 24.00 kN (Push)<br>:(-) 38.90 kN (Pull)<br>**Crack-6 and Crack -7**: Flexural cracks were formed at the top and bottom of the beam at the end of the CFRP wrapped region.<br>**Crack-8 and Crack -9**: Some cracks were appeared at the beam support region, due to slippage of beam longitudinal reinforcements |  |
| 0.50 | Max lateral load :(+) 31.00 kN (Push)<br>:(-) 49.70 kN (Pull)<br>**Crack-10**: Flexural cracks were formed at the top of the beam, 700 mm away from the column surface<br>All the other cracks were elongated | |

Table A.38. Observations of Specimen TR-5-FRP-3 (continued)

| Drift (%) | Observations | Pictures |
|---|---|---|
| 0.75 | Max lateral load :(+) 44.20 kN (Push)<br>:(-) 64.00 kN (Pull)<br>No new crack was formed<br>Existing cracks were widened and elongated | 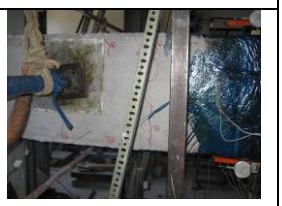 |
| 1.00 | Max lateral load :(+) 56.50 kN (Push)<br>:(-) 75.70 kN (Pull)<br>**Crack-7:** was formed at the top of the beam, 915 mm away from the column. | |
| 1.40 | Max lateral load :(+) 68.00 kN (Push)<br>:(-) 91.90 kN (Pull)<br>Some vertical cracks were formed at location of Crack-1 and Crack-4, The beam was started to hinged |  |
| 1.75 | Max lateral load :(+) 69.50 kN (Push)<br>:(-) 94.00 kN (Pull)<br>The cross-section of the beam where the CFRP wrapping ended were totally cracked |  |
| 2.20 | Max lateral load :(+) 71.90 kN (Push)<br>:(-) 98.00 kN (Pull)<br>The crack width was reached almost 4mm at the bottom of the beam (Crack 1)<br>The diagonal CFRP layers were started to rupture from the corner but due to patching they do not propogate. |  <br>  |

Table A.39. Observations of Specimen TR-5-FRP-3 (continued)

| Drift (%) | Observations | Pictures |
|---|---|---|
| 2.75 | Max lateral load :(+) 73.00 kN (Push)<br>:(-) 102.00 kN (Pull)<br>Concrete was crushed at the bottom of the beam |  |
| 3.50 | Max lateral load :(+) 71.00 kN (Push)<br>:(-) 94.10 kN (Pull)<br>The concrete was spalled and the reinforcement were buckled at the bottom of the beam. |  <br>  |
| 4.00 | Max lateral load :(+) 51.00 kN (Push)<br>:(-) 71.00 kN (Pull)<br>Beam was hinged |  |

## A13 Specimen TR-5-R

Table A.40. Observations of Specimen TR-5-R

| Drift (%) | Observations | Pictures |
|---|---|---|
| 0.15 | Max lateral load :(+) 12.70 kN (Push)<br>:(-) 18.80 kN (Pull)<br>No crack observed | |
| 0.20 | Max lateral load :(+) 14.60 kN (Push)<br>:(-) 22.20 kN (Pull)<br>**Crack-1:** Flexural crack was formed at the bottom of the beam, 500 mm away from the east face of the column. The length of the **Crack-1** is70 mm,<br>**Crack-2:** Flexural crack developed at the bottom of the beam, 700 mm away from the east face of the column. The length of the crack is 70 mm.<br>**Crack-3:** Flexural and shear crack was appeared at the top of the beam, 740 mm away from the east face of the column. The length of the crack is 250 mm.<br>**Crack-4:** Flexural a crack was formed at the top of the beam, 880 mm away from the east face of the column. The length of the crack is 80 mm. |  |
| 0.25 | Max lateral load :(+) 16.00 kN (Push)<br>:(-) 29.00 kN (Pull) | |
| 0.35 | Max lateral load :(+) 21.30 kN (Push)<br>:(-) 39.20 kN (Pull)<br>**Crack 5:** Flexural crack was formed at the top of the beam, 110 mm away from the east face of the column. The length of the **Crack-1** is 100 mm |  |

Table A.41. Observations of Specimen TR-5-R (continued)

| Drift (%) | Observations | Pictures |
|---|---|---|
| 0.50 | Max lateral load :(+) 30.40 kN (Push)<br>:(-) 51.70 kN (Pull)<br>**Crack 5':** Flexural crack was formed at the bottom of the beam, 160 mm away from the east face of the column. The length of the crack is 140 mm,<br>**Crack 6:** Diagonal shear crack appeared at the top portion of the joint shear panel. The length of the crack is 100 mm.<br>**Crack 7:** Diagonal shear crack developed at the bottom portion of the joint shear panel. |  |
| 0.75 | Max lateral load :(+) 45.60 kN (Push)<br>:(-) 68.20 kN (Pull)<br>**Crack 8:** vertical crack was formed at the top portion of the column The length of the crack is 100 mm. |  |
| 1.00 | Max lateral load :(+) 62.50 kN (Push)<br>:(-) 65.10 kN (Pull)<br>**Crack 10:** Flexural hairline crack was formed at the bottom of the beam, The length of the crack is 100 mm<br>**Crack 11:** 150 mm length, vertical crack at the back side of the column<br>**Crack 12:** 200 mm length, vertical crack at the north side of the column<br>**Crack 13:** 100 mm length, vertical crack at the north side of the column<br>**Crack 7:** elongated 100 mm upward, 70 mm downward. The width of the crack was 0.8 mm.<br>**Crack 14:** Diagonal crack occurred at the north side of the column when the specimen was pulled.<br>**Crack 3:** Kicking.<br>**Crack 8:** extended vertically to downward up to shear bottom. |  |

Table A.42. Observations of Specimen TR-5-R (continued)

| Drift (%) | Observations | Pictures |
|---|---|---|
| 1.00 cont. | **Crack 15:** occurred at the north side.<br>Bottom side of the top column was crushed.<br>**Crack 12 and Crack 6:** extended | |
| 1.40 | Max lateral load :(+) 37.20 kN (Push)<br>:(-) 39.80 kN (Pull)<br>**Crack 12:** elongated and doubled vertically.<br>**Crack 6:** 200 mm extended vertically downward.<br>**Crack 17:** 300 mm length -shear crack was formed.<br>**Crack 12:** Spalling of concrete observed at **Crack 12**.<br>**Crack 18:** Flexural crack was formed at the top of the beam. Length is 50 mm<br>**Crack 7 and Crack 8** joined<br>**Crack 19:** Horizontal crack which started from **Crack 8.**<br>**Crack 12:** crack width 2 mm.<br>**Crack 20:** vertical crack was formed at the side of the column. Spalling of concrete was observed<br>**Crack 21:**<br>**Crack 17 and Crack 12** joined at the bottom side.<br>**Crack 22:** horizontal crack occurred at the column , bottom side of the beam column connection region |  |
| 1.75 | Max lateral load :(+) 42.50 kN (Push)<br>:(-) 19.00 kN (Pull)<br>Reinforcements of the column were buckled at the joint region and concrete cover crushed. |  |

# REFERENCES


1. Antonopoulos, C. P. and T. C. Triantafillou, "Experimental Investigation of FRP-Strengthened RC Beam-Column Joints Analysis of FRP Strengthened RC Beam-Column Joints", *Journal of Composites. for Construction*, *ASCE*, Vol. 7, No. 1, pp. 39-49, February 2003.

2. Alcocer, S. and J. O. Jirsa, "Strength of Reinforced Concrete Frame Connections Rehabilitated by Jacketing", *ACI Structural Journal*, Vol. 90, No. 3, pp. 249-261, May 1993.

3. Ghobarah, A., T. S. Aziz and A. Biddah, "Rehabilitation of Reinforced Concrete Frame Connections Using Corrugated Steel Jacketing", *ACI Structural Journal*, Vol. 94, No. 3, pp. 282–294, May 1997.

4. Biddah, A., A. Ghobarah and T. S. Aziz, "Upgrading of Nonductile Reinforced Concrete Frame Connections", *Journal of Structural Engineering*, *ASCE*, Vol. 123, No. 8, pp. 1001-1010, August 1997.

5. Alcocer, S. M., "RC Frame Connections Rehabilitated by Jacketing", *Journal of Structural Engineering*, *ASCE*, Vol. 119, No. 5, pp. 1413-1431, May 1993.

6. Beres, A. B., *Experimental and Analytical Study of the Performance of Reinforced Concrete Frames with Non-Ductile Details*, Ph.D. Thesis, Cornel University, Ithaca, NY., 1994.

7. Hanson, N. W. and H. W. Connor, "Seismic Resistance of Reinforced Concrete Beam-Column Joints", *Proceedings, ASCE*, Vol. 93, No. ST5, pp. 533-560, October 1967.

8. Park, R. and T. Paulay, *Reinforced Concrete Structures*, John Wiley and Sons, New York, 1975.

9. Paulay, T. and R. Park, *Joints in Reinforced Concrete Frames Designed for Earthquake Resistance*, University of Canterbury, Christchurch, New Zealand, Report No.84-9, June 1984.

10. Paulay, T., R. Park and M. J. N. Priestley, "Reinforced Concrete Beam-Column Joints Under Seismic Actions", *ACI Journal*, No.75-60, pp. 585-593, November 1978.

11. Ehsani, M. R. and J. K. Wight, *Behavior of External Reinforced Concrete Beam to Column Connections Subjected to Earthquake Type Loading*, UMEE 82-R5, University of Michigan, July 1982.

12. Durrani, A. J. and J. K. Wight, "Behavior of Interior Beam to Column Connections under Earthquake Type Loading" *ACI Structural Journal*, Vol. 82, No. 3, pp. 343-349, May 1985.

13. Ehsani, M. R. and J. K. Wight, "Exterior Reinforced Concrete Beam-to-Column Connections Subjected to Earthquake-Type Loading", *ACI Journal*, Vol. 82, No. 4, pp. 492-499, July 1985.

14. Fujii, S. and S. Morita, "Comparison between Interior and Exterior RC Beam-Column Joint Behavior", *Design of Beam-Column Joints for Seismic Resistance (SP-123),* American Concrete Institute, Detroit, Vol. 123, pp. 145-166, January 1991.

15. Ehsani, M. R. and J. K. Wight, "Effect of Transverse Beams and Slab on Behavior of Reinforced Concrete Beam to Column Connections", *ACI Structural Journal*, Vol. 82, No. 2, pp. 188-195, March 1985.

16. Tsonos, A. G., I. A. Tegos and G. G. Penelis, "Seismic Resistance of Type 2 Exterior Beam Column joints Reinforced with Inclined Bars", *ACI Structural Journal*, Vol. 89, No. 1, pp. 3-12, January 1993.

17. Beres, A., R. N. White and P. Gergely, *Seismic Performance of Interior and Exterior Beam-to-Column Joints Related to Lightly Reinforced Concrete Frame Buildings: Detailed Experimental Result*s, Report No 92-7, Cornel University, Ithaca, NY., November 1992.

18. Beres, A. B., *Experimental and Analytical Study of the Performance of Reinforced Concrete Frames with Non-Ductile Details*, Ph.D. Thesis, Cornel University, Ithaca, NY., 1994.

19. Beres, A., S. P. Pessiki, R. N. White and P. Gergely, "Implications of Experiments on Seismic Behavior of Gravity Load Designed RC Beam to Column Connections", *Earthquake Spectra*, Vol. 12, No.2, pp. 185-198, May 1996.

20. Clyde, C., C. P. Pantelides and L. D. Reaveley, *Performance-Based Evaluation of Exterior Reinforced Concrete Building Joints for Seismic Excitation*, Pacific Earthquake Engineering Research Center, University of California, Berkeley, Report No. PEER 2000-5, July 2000.

21. Shannag, M. J., A. D. Nabeela and A. F. G. Ghazi, "Lateral Load Response of High Performance Fiber Reinforced Concrete Beam–Column Joints", *Journal of Construction and Building Materials*, *Elsevier*, Vol. 19, No. 7, pp. 500-508, September 2005.

22. LaFave J. M. and J. K. Wight, "Reinforced Concrete Exterior Wide Beam - Column Slab Connections Subjected to Lateral Earthquake Loading" *ACI Structural Journal*, Vol. 96, No. 4, pp. 577-585, July 1999.

23. Shin, M. and J. M LaFave, "Seismic Performance of Reinforced Concrete Eccentric Beam - Column Connections with Floor Slabs", *ACI Structural Journal*, Vol. 101, No. 3, pp. 403-412, May 2004.

24. Hatamoto H., S. Bessho and Y. Matsuzaki, “Reinforced Concrete Wide-Beam-to-Column Subassemblages Subjected to Lateral Load”, *Design of Beam-Column Joints for Seismic Resistance (SP-123)*, American Concrete Institute, Detroit, Vol. 123, pp. 291-316, January 1991.

25. Hakuto, S., R. Park and H. Tanaka, “Effect of Deterioration of Bond of Beam Bars Passing through Interior Beam-Column Joints on Flexural Strength and Ductility”, *ACI Structural Journal*, Vol. 96, No. 5, pp. 858-864, September 1999.

26. Engindeniz, M., F. K. Lawrence and A. Zureick, “Repair and Strengthening of Reinforced Concrete Beam-Column Joints: State of the Art”, *ACI Structural Journal*, Vol. 102, No. 2, pp. 1–14, March 2005.

27. Lee, L. N., J. K. Wight and R. D. Hanson, “Repaired Beam-Column Sub assemblages Subjected to Earthquake Type Loads”, *Fifth European Conference on Earthquake Engineering*, Istanbul, No. 95. September 1975.

28. Lee, L. N., J. K. Wight and R. D. Hanson, “RC Beam-Column Joints under Large Load Reversals”, *Journal of Structural Division*, *ASCE,* Vol. 103, No. 12, pp. 2337-2349, December 1977.

29. Tsonos, A. G., “Lateral Load Response of Strengthened Reinforced Concrete Beam-to-Column Joints”, *ACI Structural Journal*, Vol. 96, No. 1, pp. 46-56, January 1999.

30. Adin, M. A., D. Z. Yankelevsky and D. N. Farhey, “Cyclic Behavior of Epoxy-Repaired Reinforced Concrete Beam-Column Joints”, *ACI Structural Journal*, Vol. 90, No. 2, pp. 170-179, March 1993.

31. Amoury, T. and A. Ghobarah, “Seismic Rehabilitation of Beam–Column Joint Using GFRP Sheet”, *Engineering Structures*, *Elsevier*, Vol. 24, No. 11, pp. 1397–1407, November 2002.

32. Geng, Z., M. J. Chajes, T. Chou and Y. P. David, "The Retrofitting of Reinforced Concrete Column-to-Beam Connections", *Journal of Composites Science and Technology*, *Elsevier*, Vol. 58, No. 8, pp. 1297-1305, August 1998.

33. Prota, A., A. Nanni, G. Manfredi and E. Cosenaza, *Seismic Upgrade of Beam-Column Joints with FRP Reinforcement*, Industria Italiana del Cemento, November 2000.

34. Gergely, J., C. P. Pantelides and L. D. Reaveley, "Shear strengthening of RCT-Joints Using CFRP Composites", *Journal of Composites for Construction, ASCE*, Vol. 4, No.2, pp. 56-64, May 2000.

35. Ghobarah, A. and A. Said, "Shear Strengthening of Beam-Column Joints", *Engineering Structures, Elsevier,* Vol. 24, No. 7, pp. 881–888, July 2002.

36. Kaya, O., C. Yalcin, A. Parvin and S. Altay, "Repairing of shear-damaged RC joint panel zone using chemical epoxy injection methodology", *14th World Conference on Earthquake Engineering (14WCEE)*, Bejing, China, October 2008.

37. Saatcioglu, M., "Modeling and Hysteretic Force-Deformation Relationships for Reinforced Concrete Elements", *Earthquake Resistance Structures* (*SP 127-5)*, Vol. 127, pp.153-198, October 1991.

38. Popov, E. P., V. V. Bertero and S. Viwathanatepa, "Analytical and Experimental Hysteretic Loops for R/C Subassemlages", *Fifth European Conference on Earthquake Engineering*, Istanbul, No.89, September 1975.

39. Lowes, L. N., N. Mitra and A. Altoontash, *A Beam Column Joint Model for Simulating the Earthquake Response of Reinforced Concrete Frames*, Pacific Earthquake Engineering Research Center, University of California, Berkeley, Report No. PEER 2003-10, February 2004.

40. Fenwick, R. C. and H. M. Irvine, *Reinforced Concrete Beam-Column Joints for Seismic Loading*, School of Engineering Report No: 142, University of Auckland, Auckland, New Zealand, March 1977.

41. Scarpas, A. and T. Paulay, *The Inelastic Behavior of Earthquake Resistant Reinforced Concrete Exterior Beam-Column Joints*, University of Canterbury, Christchurch, New Zealand, Report No: 81-2, February 1981.

42. Durrani, A. J. and J. K. Wight, *Experimental and Analytical Study of Internal Beam to Column Connections Subjected to Reversed Cyclic Loading*, UMEE 82R3, University of Michigan, Ann Arbor, Michigan, July 1982.

43. Scot, R. H., "Intrinsic Mechanism in Reinforced Concrete Beam Column Connection Behavior", *ACI Structural Journal*, Vol. 93, No. 3, pp. 336-346, May 1996.

44. Gergely, I., C. P. Pantelides, R. J. Nuismer and L. D. Reaveley, "Bridge Pier Retrofit Using Fiber-Reinforced Plastic Composites", *Journal of Composites for Construction, ASCE,* Vol. 2, No. 4, pp. 165–174, November 1998.

45. Antonopoulos, C. P. and T. C. Triantafillou, "Analysis of FRP-Strengthened RC Beam-Column", *Journal of Composites for Construction*, *ASCE*, Vol. 6, No. 1, pp. 41-51, February 2002.

46. Granata, P. J. and A. Parvin, "An Experimental Study on Kevlar Strengthening of Beam-Column Connections", *Composite Structures*, *Elsevier*, Vol. 53, No. 2, pp. 163-171, August 2001.

47. Parvin, A. and P. J. Granata, "Investigation on the Effects of Fiber Composites at Concrete Joints" *Composites Part B: Engineering Journal*, Vol. 31B, No. 6-7, pp. 499-509, November 2000.

48. Parvin, A. and S. Wu, "Evaluation of Wrap Thickness in CFRP-Strengthened Concrete T-Joints", *Proceedings of the Second International Conference on FRP*

*Composites in Civil Engineering, CICE 2004*, Adelaide, Australia, pp. 643-646, December 2004.

49. Hwang, S. J. and H. Lee, "Analytical Model for Predicting Shear Strengths of Exterior Reinforced Concrete Beam-Column Joints for Seismic Resistance", *ACI Structural Journal*, Vol. 96, No. 5, pp. 846-858, September-October 1999.

50. Hwang, S. J. and H. Lee, "Analytical Model for Predicting Shear Strengths of Interior Reinforced Concrete Beam-Column Joints for Seismic Resistance" *ACI Structural Journal*, Vol. 97, No. 1, pp. 35-44, January 2000.

51. Hwang, S. J. and H. Lee, "Strength Prediction for Discontinuity Regions by Softened Strut-and-Tie Model", *Journal of Structural Engineering*, *ASCE*, Vol. 128, No. 12, pp. 1519-1526, December 2002.

52. Bakir, P. G. and H. M. Boduroglu, "A New Design Equation for Predicting the Joint Shear Strength of Monotonically Loaded Exterior Beam-Column Joints", *Engineering Structures*, *Elsevier*, Vol. 24, No. 8, pp. 1105–1117, August 2002.

53. Lowes, L. N. and A. Altoontash, "Modeling Reinforced-Concrete Beam Column Joints Subjected to Cyclic Loading", J*ournal of Structural Engineering*, *ASCE*, Vol. 129, No. 12, pp. 1686-1694, December 2003.

54. Fleury, F., J. M. Reynouard and O. Merabet, "Multicomponent Model of Reinforced Concrete Joints for Cyclic Loading", *Journal of Engineering Mechanics*, *ASCE*, Vol. 126, No. 8, pp. 804-811, August 2000.

55. Shiohara, H., "New Model for Shear Failure of RC Interior Beam Column Connections", *Journal of Structural Engineering*, *ASCE,* Vol. 127, No. 2, pp. 152-160, February 2001.

56. Pantelides, C. P., J. Hansen, J. Nadauld and L. D. Reaveley, *Assessment of Reinforced Concrete Building Exterior Joints with Substandard Details,* Pacific

Earthquake Engineering Research Center, University of California, Berkeley, Report No. PEER 2002-18, May 2002.

57. Attaalla, S., "General Analytical Model for Nominal Shear Stress of Type 2 Normal and High strength Concrete Beam-Column Joints", *ACI Structural Journal*, Vol. 101, No. 1, pp. 65-75, January 2004.

58. Pantazopoulou, S. and J. Bonacci, "Consideration of Questions about Beam Column Joints", *ACI Structural Journal*, Vol. 89, No. 1, pp. 27-36, January 1993.

59. Wang, Y. C. and K. Hsu, "Shear Strength of RC Jacketed Interior Beam- Column Joints without Horizontal Shear Reinforcement", *ACI Structural Journal*, Vol. 106, No. 2, pp. 222-232, March-April 2009.

60. Specification for Structures to be Built in Disaster Areas, (TEC-1975), 1975.

61. Response-2000: Reinforced Concrete Sectional Analysis Software, University of Toronto.

62. American Society for Testing Materials, ASTM C39-96, *Standard Test Method for Compressive Strength of Cylindrical Concrete Specimens*, Annual Book of ASTM Standards, Vol. 04.02, West Conshohocken, Pennsylvania, 1996.

63. American Society for Testing Materials, ASTM A7096/A706M-06a, *Standard Specification for Low-Alloy Steel Deformed and Plain Bars for Concrete Reinforcement*, Annual Book of ASTM Standards, West Conshohocken, Pennsylvania, 2006.

64. ACI T1.1-01, *Acceptance Criteria for Moment Frames Based on Structural Testing*, American Concrete Institute, 2001.

65. Seible, F., M. J. N. Priestley, G. A. Hegemier and D. Innamorato, "Seismic Retrofit of RC Columns with Continuous Carbon Fiber Jackets", *Journal of Composites for Construction*, *ASCE*, Vol. 1, No. 2, pp. 52-62, May 1997.

66. Xiao, Y. and R. Ma "Seismic Retrofit of RC Circular Columns Using Prefabricated Composite Jacketing", *Journal of Structural Engineering*, Vol. 123, No. 10, pp. 1357-1364, October 1997.

67. Rochette, P. and P. Labossiere, "Axial Testing of Rectangular Column Models Confined with Composites", *Journal of Composites for Construction*, *ASCE*, Vol. 4, No. 3, pp. 129-136, August 2000.

68. ACI-ASCE Committee 352, *Recommendations for Design of Beam-Column Joints in Monolithic Reinforced Concrete Structures (ACI 352R-02),* American Concrete Institute, 2002.

69. ACI 318.08 Committee 318, *Building Code Requirements for Structural Concrete and Commentary,* American Concrete Institute, Farmington Hills, 2008.

70. Hognestad, E., "A Study of Combined Bending and Axial Load in Reinforced Concrete Members", *University of Illinois Engineering Exp. Station*, Bulletin No. 1, Vol. 49, No. 22, November 1951.

71. Kupfer, H., Hilsdorf, H. K., and Rüsh, H., "Behavior of Concrete under Biaxial Stresses", *Journal of the American Concrete Institute*, Vol. 66, No. 8, pp. 656-666, August 1969.

72. Altay, S., *Experimental Investigation and 3D Cyclic Finite Element Simulation of R/C Exterior Beam-Column Joints Retrofitted with CFRP Composites*, Ph.D. Thesis, Boğaziçi University, Istanbul, Turkey, 2009.